8-2022

Soil Genesis Across A Climo-Lithosequence of Western Haleakalā, Maui

Ryan C. Hodges
Utah State University

SOIL GENESIS ACROSS A CLIMO-LITHOSEQUENCE OF WESTERN HALEAKALĀ, MAUI

by

Ryan C. Hodges

A dissertation submitted in partial fulfillment
of the requirements for the degree

of

DOCTOR OF PHILOSOPHY

in

Soil Science

Approved:

Janis L. Boettinger, Ph.D. Major Professor	Grant E. Cardon, Ph.D. Committee Member
Astrid R. Jacobson, Ph.D. Committee Member	Dennis L. Newell, Ph.D. Committee Member
Jonathan L. Deenik, Ph.D. Committee Member	D. Richard Cutler, Ph.D. Vice Provost of Graduate Studies

UTAH STATE UNIVERSITY
Logan, Utah

2022

ABSTRACT

Soil Genesis Across a Climo-lithosequence of Western Haleakalā, Maui

by

Ryan C. Hodges, Doctor of Philosophy

Utah State University, 2022

Major Professor: Dr. Janis L. Boettinger
Department: Plants, Soils, and Climate

Assuming soils are formed in basalt, the broad soil diversity of western Haleakalā, Maui is likely influenced by climate (200-4000 mm mean annual precipitation (MAP) and 13-24 °C mean annual temperature (MAT)). However, the deposition of volcanic ash over basalt likely also affects soil development and makes mapping soils challenging.

The main goals of this research were to 1) examine soil properties with MAP and elevation to address how soil property-process-factor relationships vary across western Haleakalā; 2) use soil weathering indices derived from soil and rock elemental analysis data to identify trends and pedogenic thresholds across climosequences to observe the influence of volcanic ash on weathering direction; and 3) use environmental data rasters in multiple linear regression models to predict the spatial variation of soil properties used in classifying andic soils.

We sampled 16 soils formed in Kula Volcanics on northwest-facing slopes <5% from 7 to 1362 m in elevation ranging from 283 to 2768 mm MAP. Soils were described and sampled by genetic horizon to 1-m depth or a root restricting layer, and chemical,

physical, and mineralogical properties were determined in the laboratory. We applied and developed indices to help us assess degree of chemical weathering and soil age. Using climate raster and andic property data for sampled soils, we created and validated multiple linear regression models to predict the areal extent of andic soils in the study area.

A pedogenic threshold occurs at 1500 mm MAP for pH and base saturation. Crystalline Fe begins to reduce and mobilize at 2000 mm MAP due to perpetually wet soils, even when well-drained. Pedogenic thresholds for SiO_2/TiO_2 were identified at 500 mm indicating more weathered soils in Kahului and Kihei, and at 1300 mm, indicating intense leaching with higher MAP. Trends in Fe, SiO_2/TiO_2, and MnO/TiO_2 suggest lowland soils are likely older than soils closer to the summit and that upland soils are more influenced by volcanic ash. Soil property predictions using data to 1-m, over 60-cm and 75-cm, not only improves classification accuracy, but best accounts for the influence of ash across the landscape and the prediction of andic soils.

(215 pages)

PUBLIC ABSTRACT

Soil Genesis Across a Climo-lithosequence of Western Haleakalā, Maui

Ryan C. Hodges

The soils of western Haleakalā are incredibly diverse due to two primary reasons: 1) they receive varying levels of rainfall based on location relative to Haleakalā, and 2) volcanic vents upwind of the area indicate that volcanic ash has blanketed much of western Haleakalā in the past. Ash can weather to form short-range-order materials, which contribute to the classification of andic soil properties. Due to their structure, short-range-order materials impart soil behavior that creates benefits and challenges in land management. Therefore, an understanding of how these soils formed and differ, and where andic soils occur is crucial.

The objectives of this study were to observe soil properties to determine how they vary across the precipitation gradients of the study area and how they relate to soil formation and diversity; and to utilize spatial statistics to predict where andic soils may occur to improve soil mapping.

Sixteen soils were sampled on the same mapped substrate of northwest-facing slopes < 5% across gradients in elevation (7-1362 m) and mean annual precipitation (283-2768 mm MAP). Soils were described by horizon to at least 1-m depth, or a root-restricting layer, and rock fragments at the base of each soil pit were sampled. Soil chemical, physical, and mineralogical properties were performed, and soil data across depth and location were compared. Using climate raster data and soil property data used

to classify andic soils for the 16 soils sampled, we created and validated models to predict the areal extent of andic soils in the study area.

Soil organic carbon increased with increasing precipitation before decreasing at 2300 mm MAP. Base saturation and pH remain high until a threshold at 1500 mm MAP before decreasing abruptly. The degree of mineral weathering and soil development increased with increasing MAP. The lowland soils of central Maui are likely much older than soils of upcountry Maui. Ash-influenced soils of upcountry Maui were less developed, more likely to have andic soil properties, and had disrupted pedogenic thresholds for pH and base saturation. Spatial predictions of soil properties used to classify andic soils accurately classified Natural Resources Conservation Service soils to 88.9%.

ACKNOWLEDGMENTS

I could not have accomplished such an endeavor without the help and support of many. I would not be attending Utah State University in the first place if it were not for one of my best friends, J. Parker Christiansen, planting the seed of USU in my mind. A native of Ogden, UT, Parker and I deployed together aboard the USS Michael Murphy. He knew I wanted to attend graduate school in Soil Science and he told me I MUST attend USU. The rest is history. Rest in peace, brother. The fact that I even considered graduate school in soil science is due to the influence of one of my committee members, to which appreciation is due, Dr. Jonathan Deenik. He taught my first course in soil science at the University of Hawaii. It was both the hardest and most interesting course I took as an undergrad. Also, mahalo e Jonathan for your assistance in the field. If it were not for another committee member, Dr. Grant Cardon, I would not have even been admitted to the School of Graduate Studies at USU. As my major advisor for my master's program, Dr. Grant Cardon took a chance with an unconventional student. Thank you, Grant.

Throughout my research, many hands have helped in various ways. Thank you to some of Hawaii's NRCS staff: Jacky Vega, Soil Scientist; Kahana Stone, Soil Conservationist; and Amy Koch, State Soil Scientist, for your knowledge, your help accessing soil data, and for connecting me with landowners to attain property access for soil sampling. Thank you to the entire team at Haleakalā Ranch. Mahalo e Jordan Jokiel for taking the time to work with my team and allowing us to dig and sample soil on Ranch property and lending me Kalaʻi Pokini for multiple days. And mahalo e Kalaʻi for helping me dig soil pits during both research excursions. It was not easy work. Thank

you, University of Hawaii's Cooperative Extension Service in Kula, for lending me a generator for my field work.

To my major advisor, Dr. Janis Boettinger, there is a lot to thank you for. You happily, and so willingly, accepting me as your protégé. She probably did not expect me to suggest research in Hawaii when she tasked me with developing my own research project. So, thank you for allowing me to undertake such a project without hesitation. While my scientific writing certainly has room for improvement, I have seen it transform dramatically over the course of the past three plus years, thanks to you. Thank you for your patience, persistence, advice, and mentorship.

Lastly and most importantly, I want to thank my family. Without the support of my wife, Maria, as my rock, this endeavor would have crumbled. Thank you for being understanding as I informed you a doctoral program will take three years (while I knew it could potentially take 4-5 years). Thankfully, we were able to meet halfway. To my two kiddos, Wyatt and Marin, thank you for distracting me from work when I was home. Providing you with a future of greater opportunities is a big reason why I pursued this degree. While now, you know no other way of life, I thank you for your sacrifice.

Ryan C. Hodges

CONTENTS

Page

LIST OF TABLES

Page

LIST OF FIGURES

Page

I. INTRODUCTION

Climate has long been understood as a factor of soil genesis of which there are two components: precipitation and temperature (Jenny, 1941; Dixon et al., 2016). Climate influences soil processes, which are reflected by soil properties (Dahlgren et al., 1997), and soil scientists have long observed changes in soil properties across the landscape. By investigating soil properties, interpretations can be made about the type and rate of soil processes. To better understand the effects of climate on soil genesis is to study soils across climosequences, or sequences of soils in which climate is the main variable influencing soil formation. Climosequences are most often studied in mountainous areas, or along an elevational transect, where the temperature decreases at a rate of 6 °C per 1000 meters of elevation (Petterson, 1941), and atmospheric precipitation usually increases concurrently (Buol et al., 2011). This concurrent increase in precipitation with elevation against a mountainous landform can be explained by orographic climate effect—where a mountain landform forces approaching moist air to higher altitudes, reducing the partial pressure of water vapor, which causes it to cool rapidly. If air cools to dew point temperature, water vapor condenses and precipitation forms.

On an elevational transect (200 to 2865 m) of soils formed in residuum weathered from granitic rock (granodiorite and tonalite) on the western slopes of the central Sierra Nevada, CA (~38° latitude), mean annual precipitation (MAP) increased from 33 to 127 cm while mean annual temperature (MAT) decreased from 17 to 4 °C (Dahlgren et al., 1997). Soil pH and base saturation generally decreased with increasing elevation, while

organic carbon concentration increased, indicating increasing leaching and plant primary productivity with increased precipitation. Whole pedon concentrations of clay and secondary iron oxides increased with increasing elevation until reaching maximum levels (536 kg m^{-3} and 24 kg m^{-3}, respectively) at mid-elevation (1390 m; MAP (91 cm) and MAT (11.1 °C)), then decreased gradually. There was also an increase in hydroxy-Al interlayering of 2:1 silicate clay and gibbsite concentration with increasing elevation, especially at high elevations (1800-2865 m). This threshold-type change at about 1600 m coincided with the present-day average effective winter snowline, indicating a strong relationship between soil properties, processes, and climatic conditions. The relatively high precipitation falling as rain and relatively warm temperatures facilitated the greatest degree of mineral weathering in Alfisols just below the snowline, whereas the colder temperatures and higher precipitation falling as snow reduced mineral weathering and increased leaching and desilication in Inceptisols (Dahlgren et al., 1997).

In another elevational transect (150 m to 2800 m) on the western slopes of the Sierra Nevada (Rasmussen et al., 2007), soils formed in andesitic lahar (23 to 2.6 Ma) with minimal inputs of volcanic ash and eolian deposits were similar to that of Dahlgren et al. (1997), with a major threshold in soil development occurring at the winter snowline. Clay and secondary iron concentrations increased with elevation, reaching a maximum just below the winter snowline (1590 m), then dramatically dropped and remained low with increasing elevation. The concentration of short-range-order (SRO) aluminosilicates was highest above the winter snowline at 1700 and 2150 m, then decreased at the highest elevations of 2450 and 2700 m. (Rasmussen et al., 2007). In the snowfall-dominated zone, soil development was at a minimum at the highest elevations with the greatest

precipitation and coldest temperature (Inceptisols) and the clay fraction was dominated by SRO materials just above the winter snowline (Andisols). In contrast, soils at lower elevations dominated by rainfall showed less soil development in the driest and warmest climate (Mollisol), and greater soil development and clay fractions dominated by kaolins with increasing rainfall (Alfisol and Ultisol).

Further north in the Cascade Range (~40° latitude), an elevational transect (280 to 2300 m) of soils formed in mid to late Pleistocene basalt flows (~129 kyr) with varying inputs of late-Pleistocene and Holocene volcanic ash exhibited maximum soil development just below the winter snowline (~1200 m) (Rasmussen et al., 2010). Similar in climate to that described in Rasmussen et al. (2007) and Dahlgren et al. (1997), they found soils dominated by kaolinite and dehydrated halloysite, crystalline Fe-oxyhydroxides, and clay accumulation below the winter snowline, and significantly less weathering and soil development in soils in higher snow-dominated elevations. Alexander et al. (1993) also observed that with an increase in elevation (280 m to 2300 m) there was an increase in organic carbon, and that the clay mineralogy followed sequentially: smectite, kaolinite, halloysite, hydrated halloysite, and allophane, which is in general agreement with Rasmussen et al. (2007, 2010).

In Cameroon, Sieffermann and Millot (1969) studied clay mineralogy of “recent” (Tertiary) basalts in three climate zones across a precipitation gradient: 1) 10 m MAP and 29 °C MAT without a dry season, 2) 2.5 to 6 m MAP and 27-29 °C MAT with a moderate, 3-month dry season, and 3) 1.5 m MAP and 23 °C MAT with a 5-month dry season. They observed the direct genesis of gibbsite from allophane, without transitioning through halloysite, in Zone 1 in a desaturated, humid environment. The

formation of halloysite was observed to occur only in Zones 2 and 3 and occurred rapidly enough to keep allophane quantities to a minimum. In the surface horizons of these two zones, metahalloysite was formed at the expense of halloysite. In both Cameroon (Sieffermann and Millot, 1969) and the Cascade Range (Rasmussen et al., 2010), the destruction of allophane and formation of halloysite is due to seasonal wet/dry regimes and reduced silica leaching, which was also observed in New Zealand by Parfitt et al. (1983).

The Hawaiian Islands are a chain of basaltic volcanic islands more than 3,200 km (2,000 mi) from North America. This isolation, and the variation in climate between islands, has induced a large variety of endemic plant and animal life. The Hawaiian Islands vary in geologic age and illustrate a chronosequence of soils formed in basalt lava flows (Vitousek et al., 1997). Intra-island climate diversity over short distances has also influenced soil development, presenting a unique opportunity for pedologic study. The Hawaiian Islands provide ideal opportunities to study pedogenic thresholds and soil weathering processes due to similar basalt substrate across the island chain, rapid weathering of primary minerals, persistence of secondary minerals and oxyhydroxides (Vitousek and Chadwick, 2013), high density of climate stations and availability of broad climate data (Giambelluca et al., 2013), and a clear presence of orographic climate effect on its five major islands of Hawai‘i, Maui, Moloka‘i, O‘ahu, and Kauai. Yet, considering these environmental characteristics and the ability to constrain one or more external soil forming factors due to the sharp regional to local variation in each (Bates, 1962), there have been few climosequence studies in Hawaii.

Along the Kohala Peninsula of the Big Island, Hawaii, where parent material was constrained to basalt and uninfluenced by ash deposition, the degree of weathering and decrease in pH and base saturation occurred nonlinearly with rainfall (Chadwick et al., 2003). A leaching index of 1 (soil pore space completely filled annually) occurred at about 1400 mm MAP. At index values >1—implying intense leaching conditions due to pore water replacement—dramatic increase in long-term element loss, decrease in base cation saturation of the exchange complex, and decrease in pH occurred. This is supported by a companion study that used strontium (Sr) isotopic ratios as a passive tracer for cation sources to calculate weathering rates as a function of MAP (Stewart et al., 2001). The radiogenic isotope ^{87}Sr is produced, in part, from the decay of ^{87}Rb and is present in the parent basalt, precipitation, and far-traveled eolian dust. Up to 1400 mm MAP, the $^{87}Sr/^{86}Sr$ of labile base cations was near basalt values, then increased steadily to rainwater values by 3000 mm MAP, indicating the depletion of weatherable minerals and the supply of base cations exclusively from rainfall. The calculated weathering rate increased gradually with increasing rainfall up to 1400 mm MAP, at which point the weathering rate increased by more than an order of magnitude with increasing MAP (Stewart et al., 2001). Base saturation averaged about 50% up to around 1100 mm MAP before declining to 20% at about 2100 mm MAP. Thereafter it remained low to the observed MAP maximum of 3500 mm. At 1700 mm MAP, aluminum mobilized rapidly with increasing precipitation which coincides with a fall in pH below 6 (Vitousek and Chadwick, 2013). Cation exchange capacity increased with precipitation, but effective cation exchange capacity increased then began to decrease with increasing precipitation at the 1400 mm MAP threshold (Chadwick et al., 2003). Updates to the Rainfall Atlas of

Hawaii (Giambelluca et al., 2013) shifted the transition threshold described on the Island of Hawaii from 1400 mm to about 1700 mm MAP (Vitousek and Chadwick, 2013).

On Kauai, a comparable threshold to the 2100 mm MAP that occurred on the Kohala Peninsula, where base saturation is at a minimum, occurred near 900 mm MAP (Vitousek and Chadwick, 2013). Kauai substrate is considerably older (~4.1 Ma) than the Hawi substrate (~0.15 Ma)—both basalt-derived—though the Kauai pedogenic threshold occurs at a considerably lower MAP. This threshold along both gradients signifies an end to weathering rejuvenation, detectable biological uplift, and Al loss. At higher levels of precipitation, another pedogenic threshold at ~2500 mm MAP occurs on Kauai where Al:Fe (measured by total elemental analysis) increased to as high as 6 (Vitousek and Chadwick, 2013).

Like transitional precipitation thresholds seen with the dynamic soil properties of pH and base saturation across a climosequence, elemental leaching loss directly reflects the degree of leaching intensity over time by comparing element content of the fine-earth fraction to that of its parent material within a pedon (Chadwick et al., 2003, Birkeland, 1999). On the Kohala Peninsula, with basalt substrate age at 170 ka, silica and soluble base cations were leached to near completion at about 1400 mm MAP (1700 mm MAP in Vitousek and Chadwick, 2013), while about 40% of the less mobile aluminum remained in the soil (Chadwick et al., 2003). Above 2100 mm MAP on the Hawi substrate (900 mm MAP on Kauai), which marks a new domain of little change in the surface soil (<30 cm), elemental concentrations are low except for iron. Biological uplift and mineral weathering are unsustainable, and aluminum no longer declines rapidly (Vitousek and Chadwick, 2013).

On the other hand, along a high precipitation gradient (2200 to >5000 mm MAP) of East Maui, noncrystalline minerals were observed to decrease with increasing precipitation (Schuur et al., 2001), with amorphous Al values generally higher than amorphous Fe along the gradient (Miller et al, 2001). An observable increase in crystalline Fe occurred at ~2450 mm MAP, reaching 1.5 mol kg^{-1} at 2750 mm MAP, before decreasing to very low values as precipitation increased (Miller et al, 2001; Chadwick et al., 2003). However, on the Island of Hawaii, non-crystalline Fe- and Al-hydroxides were major weathering products under higher rainfall conditions (4000 mm MAP) (Wada, 1987). This may be due to the Island of Hawaii's younger substrate.

The island of Maui, and specifically, the western slope of Haleakalā, demonstrates a much wider range in soil development (eight soil orders) over a similar climate gradient to that of the Kohala Peninsula and has been little investigated with respect to the causes and influences of its soil diversity. From sea level to the mountain's peak (3,055 m), the western slope of Haleakalā spans a mean annual precipitation (MAP) range of 300-6000 mm (12-236 in.) (Giambelluca et al., 2013), creating a large gradient across a relatively small area. This precipitation gradient results from the shape and size of Haleakalā and the moist oceanic trade winds. Haleakalā's orographic climate effect has created this large precipitation gradient, covering a distance of about 20 km. As this weather wraps around Haleakalā to the leeward side, MAP decreases. This is evidenced by cooler montane and forest climates of the windward side, and a much warmer and drier climate of the leeward side.

The Kula Volcanics basalt formation covers a large area of East Maui and ranges in age from 0.15 Ma to 0.78 Ma—a 630 kyr interval. There has been nearly no

geochronological dating of the Kula Volcanics down the western face of Haleakalā and into central Maui (Sherrod et al., 2007, and Sherrod et al., 2003). Precipitation varies greatly across the western slope of Haleakala and all soils theoretically occur on the same parent material—Kula Volcanics basalt—thus making this area an ideal location to study the effects of climate on mineral weathering and soil development.

Currently available Natural Resources Conservation Service (NRCS) soil survey data (viewed using SoilWeb; https://casoilresource.lawr.ucdavis.edu/gmap/) show soils on Kula Volcanics in East Maui varying from Oxisols (e.g., Molokai series) and Aridisols (e.g., Keahua series) formed in material weathered from basic igneous rock, to Mollisols formed in volcanic ash overlying ‘a‘a lava (e.g., Kamaole series), to Inceptisols formed in material weathered from volcanic ash overlying basalt (e.g., Haliimaile series), to Andisols formed in volcanic ash overlying basalt (e.g., Olinda and Pane series). Much of this soil diversity is influenced by climate. However, such soil variation may also indicate variability in the age and type of soil parent materials (basalt vs. volcanic ash).

While climate is a clear factor influencing soil variability across the study area, the presence of surficial volcanic ash over basic igneous rock likely affects mineral weathering and soil development across western Haleakalā. Volcanic ash provides a rapidly weatherable source of base cations and silica, and can promote the subsequent formation of SRO aluminosilicates. These rejuvenating effects of volcanic ash may disrupt pedogenesis of some of these soils, eventually forming dissimilar soils adjacent to one another. What is not transparent is the extent of ash deposition, the intensity of past ejecta events, their composition, and frequency across western Haleakalā.

Variability in the presence of volcanic ash across western Haleakalā adds to the complexity of how soil properties vary across a climosequence, which makes mapping soils more challenging. Intermediately weathered soils formed in volcanic parent materials, particularly volcanic ash, typically develop andic soil properties (Buol et al. 2011). Andic soil properties include relatively high concentrations of SRO materials, high phosphate retention, and low bulk density—all of which can affect land use and management. Digital soil mapping may help refine the mapping of soils with andic properties. Environmental covariates used to quantitatively predict a soil class or attribute in digital soil mapping include spatially explicit data used to represent soil, climate, organisms, relief, parent material, age, and spatial location (McBratney et al., 2003).

The diversity of soils on the western slope of Haleakala in East Maui provides the unique opportunity to investigate how climate and volcanic ash deposition influence soil development on basalt. There are effectively two climosequences of soils: one that spans a large precipitation gradient (283-2768 mm MAP) with minimal change in temperature (22-23 °C MAT), and a second that spans an elevational transect with a slightly narrower precipitation gradient (283-2267 mm) but a significantly larger temperature gradient (13-24 °C MAT). The main goals of this research are 1) to examine soil chemical, physical, and mineralogical properties across climosequences, and to identify pedogenic thresholds that represent distinct changes in soil processes, 2) to identify volcanic ash deposits and understand their influence on soil development, particularly with respect to the development of andic soil properties, and 3) to refine the mapping of soils with andic properties using digital soil mapping techniques.

Research Questions

1) Are there pedogenic thresholds in soil chemical and physical properties across climosequences of these soils?
2) How do precipitation and temperature gradients contribute to nonlinear changes in soil chemical and physical properties, and may there be different thresholds across the two climosequences?
3) What soil properties along the climatic gradient indicate climate vs. parent material change? How might variation in parent material and time affect soil forming processes and the presence and importance of pedogenic thresholds?
4) Can elemental loss calculated from total elemental analysis indicate weathering intensity and/or the influence of a more recent volcanic ash deposit?
5) Can the answers to these questions above facilitate the mapping of these soils?

Objectives

1) Examine soil chemical and physical properties with mean annual precipitation (MAP) and elevation to address how soil property-process-factor relationships vary across western Haleakalā;
2) Use soil weathering indices derived from soil and rock elemental analysis data, and chemical data to identify trends and pedogenic thresholds across climosequences to observe the influence of volcanic ash on weathering direction; and

3) Use climate data and various environmental data rasters in multiple linear regression models to predict the spatial variation of soil properties used in classifying andic soils.

REFERENCES

Alexander, E. B., Mallory, J. I., & Colwell, W. L. (1993). Soil-elevation relationships on a volcanic plateau in the southern Cascade Range, northern California, USA. *Catena*, *20*(1-2), 113-128.

Bates, T. F. (1962). Halloysite and gibbsite formation in Hawaii. In *Clays and Clay Minerals* (pp. 315-328). Pergamon.

Birkeland, P. W. (1999). *Soils and Geomorphology*. 3rd edition. Oxford University Press, Inc.

Buol, S. W., Southard, R. J., Graham, R. C., & McDaniel, P. A. (2011). *Soil genesis and classification*. John Wiley & Sons.

Chadwick, O. A., Gavenda, R. T., Kelly, E. F., Zeigler, K., Olson, C. G., Elliot, W. C., & Hendricks, D. M. (2003). The impact of climate on the biogeochemical functioning of volcanic soils. *Chemical Geology 202*, 195-223.

Dahlgren, R. A., Boettinger, J. L., Huntington, G. L., & Amundson, R. G. (1997). Soil development along an elevational transect in the western Sierra Nevada, California. *Geoderma*, *78*(3-4), 207-236.

Dixon, J. L., Chadwick, O. A., & Vitousek, P. M. (2016). Climate-driven thresholds for chemical weathering in postglacial soils of New Zealand. *Journal of Geophysical Research: Earth Surface*, *121*(9), 1619-1634.

Giambelluca, T. W., Chen, Q., Frazier, A. G., Price, J. P., Chen, Y. L., Chu, P. S., Eischeid, J. K., & Delparte, D. M. (2013). Online Rainfall Atlas of Hawai'i. *Bulletin of the American Meteorological Society* 94, 313-316, doi: 10.1175/BAMS-D-11-00228.1.

Jenny, H. (1941). *Factors of Soil Formation: A System of Pedology*. McGraw-Hill book Company, Incorporated, New York.

McBratney, A. B., Santos, M. M., & Minasny, B. (2003). On digital soil mapping. *Geoderma*, *117*(1-2), 3-52.

Miller, A. J., Schuur, E. A., & Chadwick, O. A. (2001). Redox control of phosphorus pools in Hawaiian montane forest soils. *Geoderma*, *102*(3-4), 219-237.

Parfitt, R. L., Russell, M., & Orbell, G. E. (1983). Weathering sequence of soils from volcanic ash involving allophane and halloysite, New Zealand. *Geoderma*, *29*(1), 41-57.

Petterson, S. (1941). *Introduction to Meteorology*. New York, London: McGraw-Hills Book Company.

Rasmussen, C., Matsuyama, N., Dahlgren, R. A., Southard, R. J., & Brauer, N. (2007). Soil genesis and mineral transformation across an environmental gradient on andesitic lahar. *Soil Science Society of America Journal*, *71*(1), 225-237.

Rasmussen, C., Dahlgren, R. A., & Southard, R. J. (2010). Basalt weathering and pedogenesis across an environmental gradient in the southern Cascade Range, California, USA. *Geoderma*, *154*(3-4), 473-485.

Schuur, E. A., Chadwick, O. A., & Matson, P. A. (2001). Carbon cycling and soil carbon storage in mesic to wet Hawaiian montane forests. *Ecology*, *82*(11), 3182-3196.

Sherrod, D. R., Nishimitsu, Y., & Tagami, T. (2003). New K-Ar ages and the geologic evidence against rejuvenated-stage volcanism at Haleakala, East Maui, a postshield-stage volcano of the Hawaiian island chain. *Geological Society of America Bulletin*, *115*(6), 683-694.

Sherrod, D. R., Sinton, J. M., Watkins, S. E. & Blunt, K. M. (2007). *Geologic Map of the State of Hawaii*. US Department of the Interior. USGS.

Sieffermann, G., & Millot, G. (1969). Equatorial and tropical weathering of recent basalts from Cameroon: allophanes, halloysite, metahalloysite, kaolinite, and gibbsite. *Proceedings of the International Clay Conference*. Tokyo, Vol. 1.

Stewart, B. W., Capo, R. C., & Chadwick, O. A. (2001). Effects of rainfall on weathering rate, base cation provenance, and Sr isotope composition of Hawaiian soils. *Geochimica et Cosmochimica Acta*, *65*(7), 1087-1099.

Vitousek, P. M., Chadwick, O. A., Crews, T. E., Fownes, J. H., Hendricks, D. M., & Herbert, D. (1997). Soil and ecosystem development across the Hawaiian Islands. *GSA Today*, *7*(9), 1-8.

Vitousek, P. M., & Chadwick, O. A. (2013). Pedogenic thresholds and soil process domains in basalt-derived soils. *Ecosystems*, *16*(8), 1379-1395.

Wada, K. (1987). Minerals formed and mineral formation from volcanic ash by weathering. *Chemical Geology*, *60*(1-4), 17-28.

II. VARIABILITY IN SOIL CHEMICAL AND PHYSICAL PROPERTIES ACROSS ASH-INFLUENCED CLIMOSEQUENCES OF EAST MAUI

ABSTRACT

The western slope of Haleakalā, East Maui, demonstrates a wide range in soil development (eight soil orders) thus providing a unique opportunity to investigate how climate and volcanic ash deposition influence soil development on basalt. The objective of this study is to examine soil chemical and physical properties with mean annual precipitation (MAP) and elevation to address how soil property-process-factor relationships vary across western Haleakalā.

Sixteen soil pedons were sampled and described to 1-meter depth, or a root-restricting layer, across the study area, and were analyzed for a suite of chemical and physical soil properties. All pedons were observed before breaking them up into two climosequences: one low-elevation coastal climosequence uninfluenced by volcanic ash, and an elevational climosequence of pedons variably influenced by volcanic ash.

A clear pedogenic threshold occurs at 1500 mm MAP for dynamic soil properties, pH and base saturation, for all pedons and along the coastal climosequence. The dilation of amorphous Fe and Al and collapse of crystalline Fe in elevational climosequence indicate that pedons closer to the summit are influenced by volcanic ash. Furthermore, higher crystalline Fe in the coastal climosequence pedons, as well as pedons near Kihei, indicates that lower elevation landforms and soils more distant from the summit across western Haleakalā are likely older.

INTRODUCTION

Climate has long been understood as a factor of soil genesis of which there are two components: precipitation and temperature (Jenny, 1941; Dixon et al., 2016). Climate influences soil processes, which are reflected by soil properties (Dahlgren et al., 1997), and soil scientists have long observed changes in soil properties across the landscape. By investigating soil properties, interpretations can be made about the type and rate of soil processes. To better understand the effects of climate on soil genesis is to study soils across climosequences, or sequences of soils in which climate is the main variable influencing soil formation. Climosequences are most often studied in mountainous areas, or along an elevational transect, where the temperature decreases at a rate of 6 °C per 1000 meters of elevation (Petterson, 1941), and atmospheric precipitation usually increases concurrently (Buol et al., 2011). This concurrent increase in precipitation with elevation against a mountainous landform can be explained by orographic climate effect—where a mountain landform forces approaching moist air to higher altitudes, reducing its partial pressure, which causes it to cool rapidly. If air cools to dew point temperature, water vapor condenses and precipitation forms.

On an elevational transect (200 to 2865 m) of soils formed in residuum weathered from granitic rock (granodiorite and tonalite) on the western slopes of the central Sierra Nevada, CA (~38° latitude), mean annual precipitation (MAP) increased from 33 to 127 cm while mean annual temperature (MAT) decreased from 17 to 4 °C (Dahlgren et al., 1997). Soil pH and base saturation generally decreased with increasing elevation, while organic carbon concentration increased, indicating increasing leaching and plant primary productivity with increased precipitation. Whole pedon concentrations of clay and

secondary iron oxides increased with increasing elevation until reaching maximum levels (536 kg/m^3 and 24 kg/m^3, respectively) at mid-elevation (1390 m; MAP (91 cm) and MAT (11.1 °C)), then decreased gradually. There was also an increase in hydroxy-Al interlayering of 2:1 clay and gibbsite concentration with increasing elevation, especially at high elevations (1800-2865 m). This threshold-type change at about 1600 m coincided with the present-day average effective winter snow-line, indicating a strong relationship between soil properties, processes and climatic conditions. The relatively high precipitation falling as rain and relatively warm temperatures facilitated the greatest degree of mineral weathering in Alfisols just below the snowline, whereas the colder temperatures and higher precipitation falling as snow reduced mineral weathering and increased leaching and desilication in Inceptisols (Dahlgren et al., 1997).

In another elevational transect (150 m to 2800 m) on the western slopes of the Sierra Nevada (Rasmussen et al., 2007), soils formed in andesitic lahar (23 to 2.6 Ma) with minimal inputs of volcanic ash and eolian deposits were similar to that of Dahlgren et al. (1997), with a major threshold in soil development occurring at the winter snowline. Clay and secondary Fe concentrations increased with elevation, reaching a maximum just below the winter snowline (1590 m), then dramatically dropped and remained low with increasing elevation. The concentration of short-range-order (SRO) aluminosilicates was highest above the winter snowline at 1700 and 2150 m, then decreased at the highest elevations of 2450 and 2700 m. (Rasmussen et al., 2007). In the snowfall-dominated zone, soil development was at a minimum at the highest elevations with the greatest precipitation and coldest temperature (Inceptisols) and the clay fraction was dominated by SRO materials just above the winter snowline (Andisols). In contrast, soils at lower

elevations dominated by rainfall showed less soil development in the driest and warmest climate (Mollisol), and greater soil development and clay fractions dominated by kaolins with increasing rainfall (Alfisol and Ultisol).

Further north in the Cascade Range (~40° latitude), an elevational transect (280 to 2300 m) of soils formed in mid to late Pleistocene basalt flows (~129 kyr) with varying inputs of late-Pleistocene and Holocene volcanic ash exhibited maximum soil development just below the winter snowline (~1200 m) (Rasmussen et al., 2010). Similar climate to Rasmussen et al. (2007) and Dahlgren et al. (1997), they found soils dominated by kaolinite and dehydrated halloysite, crystalline Fe-oxyhydroxides, and clay accumulation below the winter snowline, and significantly less weathering and soil development in soils in higher snow-dominated elevations. Alexander et al. (1993) also observed that with an increase in elevation (280 m to 2300 m) there was an increase in organic carbon, and that the clay mineralogy followed sequentially: smectite, kaolinite, halloysite, hydrated halloysite, and allophane, which is in general agreement with Rasmussen et al. (2007, 2010).

The Hawaiian Islands are a chain of basaltic volcanic islands more than 3,200 km (2,000 mi) from North America. This isolation, and the variation in climate between islands, has induced a large variety of endemic plant and animal life. The Hawaiian Islands vary in geologic age and illustrate a chronosequence of soils formed in basalt lava flows (Vitousek et al., 1997). Intra-island climate diversity over short distances has also influenced soil development, presenting a unique opportunity for pedologic study. The Hawaiian Islands provide ideal opportunities to study pedogenic thresholds and soil weathering processes due to similar basalt substrate across the island chain, rapid

weathering of primary minerals, persistence of secondary minerals and oxyhydroxides (Vitousek and Chadwick, 2013), high density of climate stations and availability of broad climate data (Giambelluca et al., 2013), and a clear presence of orographic climate effect on its five major islands of Hawai‘i, Maui, Moloka‘i, O‘ahu, and Kauai. Yet, considering these environmental characteristics and the ability to constrain one or more external soil forming factors due to the sharp regional to local variation in each (Bates, 1962), there have been few climosequence studies in Hawaii.

Along the Kohala Peninsula of the Big Island, Hawaii, where parent material was constrained to basalt and uninfluenced by ash deposition, the degree of weathering and leaching of soil properties, including pH and base saturation, occurred nonlinearly with rainfall (Chadwick et al., 2003). A leaching index of 1 (soil pore space completely filled annually) occurred at about 1400 mm MAP. At index values > 1, dramatic increase in long-term element loss, decrease in base cation saturation of the exchange complex, and decrease in pH occurred, implying intense leaching conditions due to pore water replacement. This is supported by a companion study that used strontium (Sr) isotopic ratios as a passive tracer for cation sources to calculate weathering rates as a function of MAP (Stewart et al., 2001). The radiogenic isotope ^{87}Sr is produced, in part, from the decay of ^{87}Rb and is present in the parent basalt, precipitation, and far-traveled eolian dust. Up to 1400 mm MAP, the $^{87}Sr/^{86}Sr$ of labile base cations was near basalt values, then increased steadily to rainwater values by 3000 mm MAP, indicating the depletion of weatherable minerals and the supply of base cations exclusively from rainfall. The calculated weathering rate increased gradually with increasing rainfall up to 1400 mm MAP, at which point the weathering rate increased by more than an order of magnitude

with increasing MAP (Stewart et al., 2001). Base saturation averaged about 50% up to around 1400 mm MAP before declining to 20% at about 2100 mm MAP. Thereafter it remained low to the observed MAP maximum of 3500 mm. At 1700 mm MAP, aluminum mobilized rapidly with increasing precipitation which coincides with a fall in pH below 6 (Vitousek and Chadwick, 2013). Cation exchange capacity increased with precipitation, but effective cation exchange capacity increased then began to decrease with increasing precipitation at the 1400 mm MAP threshold (Chadwick et al., 2003). Updates to the Rainfall Atlas of Hawaii (Giambelluca et al., 2013) shifted the transition threshold described on the Island of Hawaii to about 1700 mm MAP (Vitousek and Chadwick, 2013).

On Kauai, a comparable threshold to the 2100 mm MAP that occurred on the Kohala Peninsula, where base saturation is at a minimum, occurred near 900 mm MAP (Vitousek and Chadwick, 2013). Kauai substrate is considerably older (~4.1 Ma) than the Hawi substrate (~0.15 Ma)—both basalt-derived—though the Kauai pedogenic threshold occurs at a considerably lower MAP. This threshold along both gradients signifies an end to weathering rejuvenation, detectable biological uplift, and Al loss. At higher levels of precipitation, another pedogenic threshold at ~2500 mm MAP occurs on Kauai where Al:Fe (measured by total elemental analysis) increased to as high as 6 (Vitousek and Chadwick, 2013).

The island of Maui, and specifically, the western slope of Haleakalā, demonstrates a wide range in soil development (eight soil orders) and has been little investigated with respect to the causes and influences of its soil diversity. From sea level to the mountain's peak (3,055 m), the western slope of Haleakalā spans a MAP range of 300-6000 mm (12-

236 in.) (Giambelluca et al., 2013), creating a large gradient across a relatively small area. This precipitation gradient results from the shape and size of Haleakalā and the moist oceanic trade winds. Haleakalā's orographic climate effect has created this large precipitation gradient, covering a distance of about 20 km. As this weather wraps around Haleakalā to the leeward side, MAP decreases. This is evidenced by cooler montane and forest climates of the windward side, and a much warmer and drier climate of the leeward side.

The Kula Volcanics basalt formation covers a large area of East Maui and ranges in age from 0.15 Ma to 0.78 Ma—a 630 kyr interval. There has been nearly no geochronological dating of the Kula Volcanics down the western face of Haleakalā and into central Maui (Sherrod et al., 2007, and Sherrod et al., 2003). Precipitation varies greatly across the western slope of Haleakala and all soils theoretically occur on the same parent material—Kula Volcanics basalt—thus making this area an ideal location to study the effects of climate on mineral weathering and soil development.

Currently available Natural Resources Conservation Service (NRCS) soil survey data (viewed using SoilWeb; https://casoilresource.lawr.ucdavis.edu/gmap/) show soils on Kula Volcanics in East Maui varying from Oxisols (e.g., Molokai series) and Aridisols (e.g., Keahua series) formed in material weathered from basic igneous rock, to Mollisols formed in volcanic ash overlying ‘a‘a lava (e.g., Kamaole series), to Inceptisols formed in material weathered from volcanic ash overlying basalt (e.g., Haliimaile series), to Andisols formed in volcanic ash overlying basalt (e.g., Olinda and Pane series). Much of this soil diversity is influenced by climate. However, such soil variation may also indicate variability in the age and type of soil parent materials (basalt vs. volcanic ash).

The diversity of soils on the western slope of Haleakalā in East Maui provides a unique opportunity to investigate how climate and volcanic ash deposition influence soil development on basalt. As mentioned, western Haleakalā spans a broad climosequence consisting of both ranges in precipitation and temperature. The study area is large enough that, within the climosequence of western Haleakalā, there are effectively two climosequences of soils: a coastal climosequence that spans a large precipitation gradient (461-2768 mm MAP) with minimal change in temperature (22-23 °C MAT) consisting of pedons that are not influenced by volcanic ash, and an elevational climosequence which is an elevational gradient of pedons (7-1362 m) variably influenced by precipitation (283-2267 mm MAP), temperature (13-24 °C MAT), and volcanic ash. Observing soil properties across the study area and among both the coastal and elevation climosequences will help to elucidate trends in property-process relationships.

We pose three research questions: (i) Are there pedogenic thresholds in soil chemical and physical properties across climosequences of these soils? (ii) How do precipitation and temperature/elevation gradients contribute to nonlinear changes in soil chemical and physical properties? (iii) How do more recent deposits of volcanic ash affect soil properties across these climosequences? To answer these questions, the objective of this study is to examine soil chemical and physical properties with MAP and MAT to address how soil property-process-factor relationships vary across western Haleakalā.

MATERIALS AND METHODS

Study Area

Geology

The Hawaiian Island chain formed due to hot spot magmatism as the Pacific Plate moved northwest with respect to a stationary mantle plume. The plume likely originates deep in the mantle, rises to the base of the lithosphere, and partial melting at the base of the lithosphere leads to the creation of crustal magma chambers. These chambers feed volcanism and are rejuvenated by additions of rising melts. As magma emerges above the sea surface, it forms a volcanic shield composed of tholeiitic basalt with the youngest volcanoes and islands near the position of the hot spot (Price and Elliott-Fisk, 2004). Maui was not always its own island but was once part of a larger island called the "Maui Nui" complex, which also included neighboring islands Molokaʻi, Lānaʻi, and Kahoʻolawe. It was composed of seven volcanoes which completed shield building between 2.2 Ma and 1.1 Ma (Chen et al., 1991).

After main shield building occurred, more viscous and explosive alkalic lava formed a distinct alkalic cap (Stearns and MacDonald, 1942), growing the once existing summit another 1300 m. This cap formed about 0.4 Ma, after which volcanic activity slowed dramatically (Sherrod et al., 2003). On the outer slopes, lavas were deposited as recently as 0.15 Ma (Price and Elliott-Fisk, 2004). The majority of the landscape is covered by lava flows of Pleistocene Kula Volcanics (Figure 2-1).

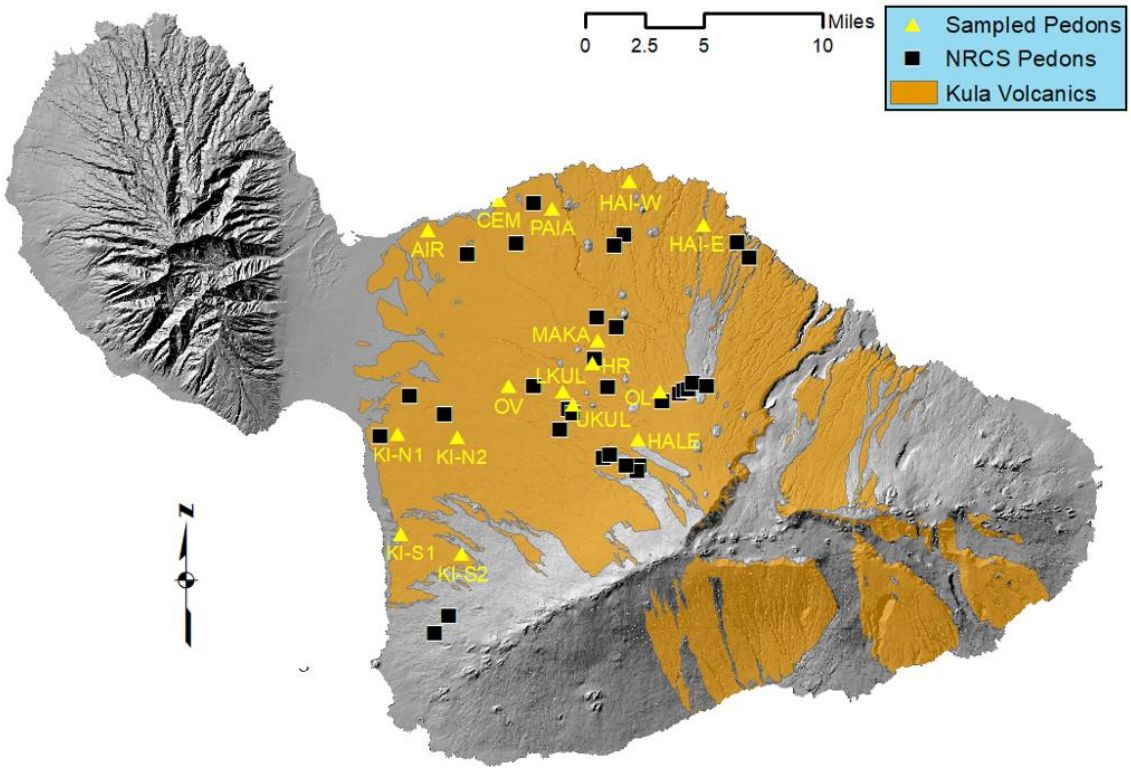

Figure. 2-1. Pleistocene Kula Volcanics geological map of Maui. Data Source: Sherrod et al., 2007.

The Kula Volcanics are alkalic and are predominantly ʻaʻā lava flows (Sherrod et al., 2007). The basalt rocks range in composition from basanite to mugearite and likely comprise tens of thousands of individual eruptive units (personal communication with John Sinton, University of Hawaii (UH), Mānoa). The majority of the radiocarbon and K-Ar dating of volcanic deposits occurred at the summit of Haleakalā, along Haleakalā's southwest and east rift zones, and on the younger Hāna Volcanics formation (Sherrod et al., 2007, and Sherrod et al., 2003). Kula Volcanics occurring near the summit were K-Ar dated at 0.113 ± 0.006 Ma (sample 7) and 0.234 ± 0.007 Ma (sample 20) (Sherrod et al., 2003). Samples of west-flank tephra were radiocarbon dated at 2,530 ^{14}C a B.P. (sample 27; sampled within a crater vent) and 26,800 ^{14}C a B.P. (sample 83) (Sherrod et

al., 2006). Geochronology of the Kula Volcanics was not done westward into the broader expanse of the formation of western Haleakalā (personal communication with John Sinton, UH Mānoa). It is possible that the Kula Volcanics were not extensively sampled because the boundary between the older Honomanū Basalt and Kula Volcanics is quite transparent, with the former characterized as being thin-bedded and porphyritic, while the latter is massive, thick, and aphyric (Chen et al., 1991).

When considering the possibility of island uplift and subsidence, evidence suggests that between one-half and two-thirds of the upbuilding of the Hawaiian Ridge is offset by subsidence (Moore, 1987). After subsidence, 90% of Maui Nui's area was below 1000 m during low sea stands of recent glacial periods, as compared to 85% at present (Price and Elliott-Fisk, 2004). Therefore, at no point has the currently exposed land mass of Maui been submerged in the past.

Climate

The Maui Nui complex at its maximum extent, when it had more lowland area, probably had more land area in warmer temperature regimes than the current island of Hawaii (Price and Elliott-Fisk, 2004). Glacial periods were also likely cooler and wetter than at present (Gavenda, 1992), but much like the modern Island of Hawaii, Maui Nui likely had a larger orographic climate effect.

What further contributes to the stark climatic differences across East Maui is the presence of an inversion layer. On the leeward side, dry air descends and warms, creating a rain shadow effect (Figure 2-2) (Minyard et al., 1994). In East Maui (Haleakalā), this

inversion layer exists at an elevation of about 2000 meters (Riehl et al., 1951), and acts as a barrier to the

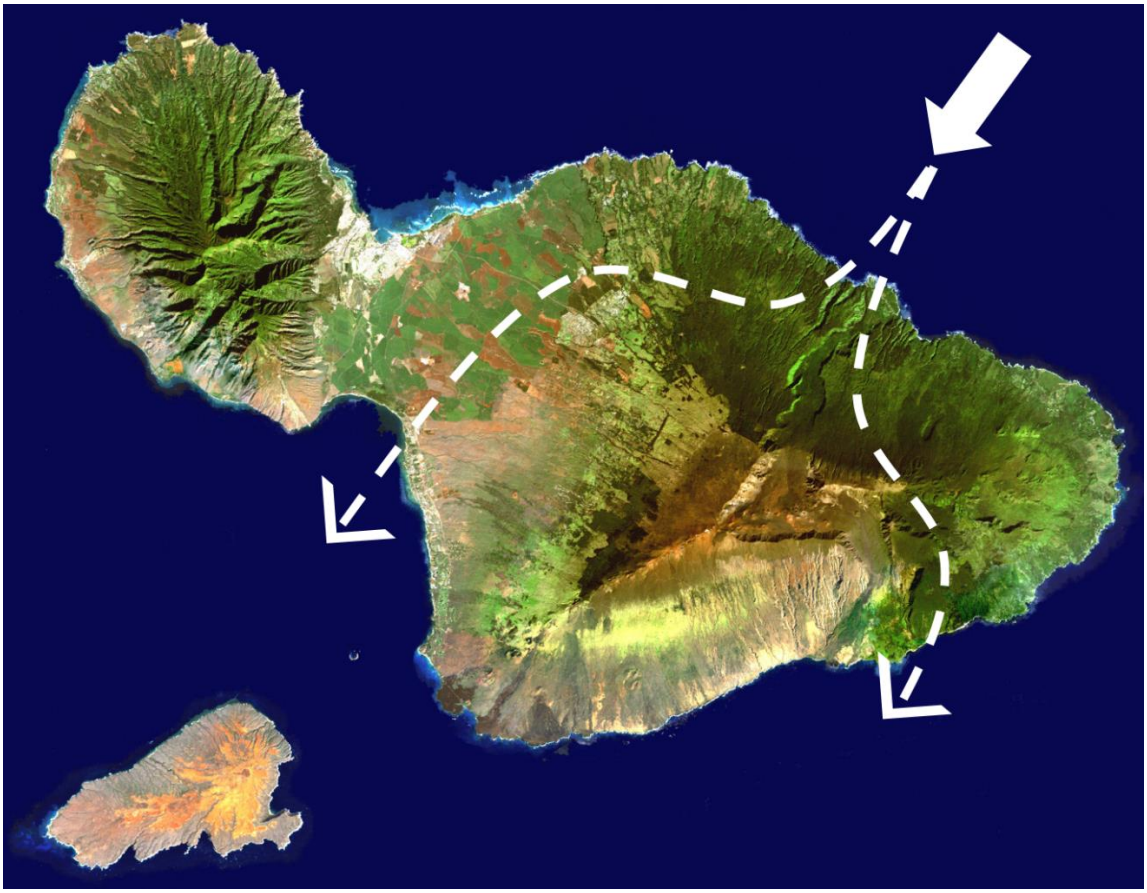

Figure 2-2. Wind pattern circumventing Haleakalā, Maui, caused by the mountain's inversion layer and resulting rain shadow effect.

upward movement of clouds. This causes weather above the inversion layer to be drier as elevation increases (Minyard et al., 1994). Below this, an increase in elevation towards the cloud layer and to the windward side is associated with an increase in rainfall and cooler temperatures. These factors contribute to East Maui's range in MAP from 300 to 6000 mm. Nearly all the moisture received by the leeward side of the Hawaiian Islands is deposited by sporadic high-level cyclonic storms passing through from the southwest,

contributing to their arid ecosystem (Giambelluca and Schroeder, 1998). Precipitation and air temperature data are sourced from Giambelluca et al. (2013).

Vegetation and Land Use

With variation in precipitation over any landscape comes a large diversity in plant ecology. Native vegetation of western Haleakalā is quite diverse and because the study area spans such large precipitation and elevation gradients, organisms as a soil forming factor will vary naturally across the climosequence.

Current and primary alien vegetation is composed of grasses (buffelgrass, feather fingergrass, etc.), weeds (sugarcane, ilima, uhaloa, Spanish Needle, lantana, and zinnia, etc.), and trees such as kiawe, eucalyptus, koa, and guava. Trees and forest vegetation become more prominent as precipitation and elevation increase to the cloud layer dominating the landscape of the windward side of East Maui, which encounters island trade winds and oceanic moisture. While there are still thousands of acres that are home to native vegetation on Maui, much of the island that receives up to 1400 mm in MAP has been altered for various reasons, mainly for production agriculture, cattle grazing, and koa tree harvest.

Sample Site Selection

The western Haleakalā study area encompasses approximately 465 km^2 (180 mi^2) of prime agricultural farmlands, rangelands, and residential and urban property. Site selection was done remotely with the assistance of ArcMap and various data layers, and NRCS soil survey information:

1. The Kula Volcanics polygon provided by gSSURGO was used to define the extent of the study area (Figure 2-1), which was designed to sample soils occurring on the Kula Volcanics but may include locations exposed to ash deposition.
2. Four classes of MAP were defined based on the range in MAP of the western facing aspect of Haleakalā, the premise that the main pedogenic transitional threshold occurred at 1400 mm MAP for the climosequence on Hawaii Island (Chadwick et al, 2003; Chorover et al., 2004), and to provide spatial balance for sampling across the study area: 271-400 mm, 401-700 mm, 701-1400 mm, and 1401-10271 mm (Figure 2-3). There were at least 3 sites per MAP class, and, to accommodate for variability in temperature due to elevation, sites were distributed across an elevation gradient to the best extent possible.

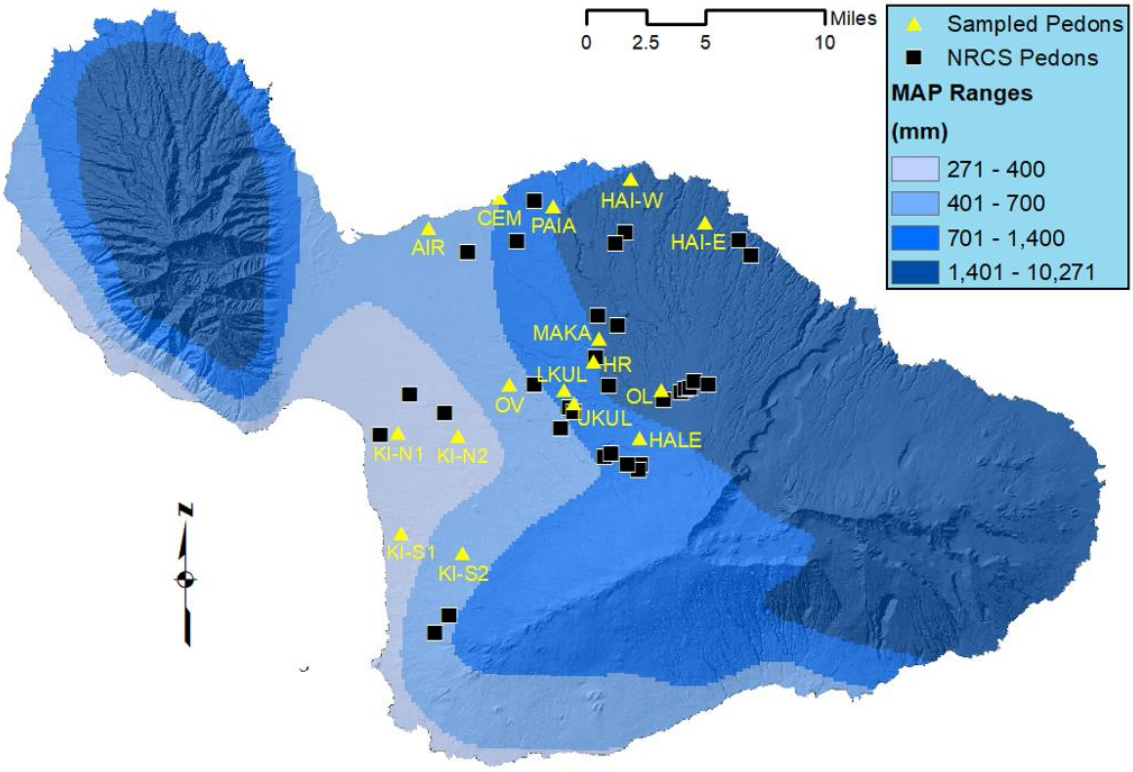

Figure 2-3. Sample sites in the four MAP classes of Maui: 271-400 mm, 401-700 mm, 701-1400 mm, and 1401-10271 mm. Triangles indicate the study soil sampling locations, and black squares indicate NRCS sampled soils. MAP: mean annual precipitation. MAP data source: Giambelluca et al. (2013).

3. All sites were located on slopes with gradients < 5%, westward facing aspect.
4. As much of central Maui is dedicated to agricultural use, priority was given to locations with native vegetation or on land that had not been cultivated within the past five years.
5. Areas prone to or which showed evidence of accelerated erosion were avoided. Google Earth was used in conjunction with slope data to exclude areas potentially affected by erosion such as shoulder- or foot-slopes. The variability in soil orders across the study area created an additional layer for site selection (Figure 2-4).

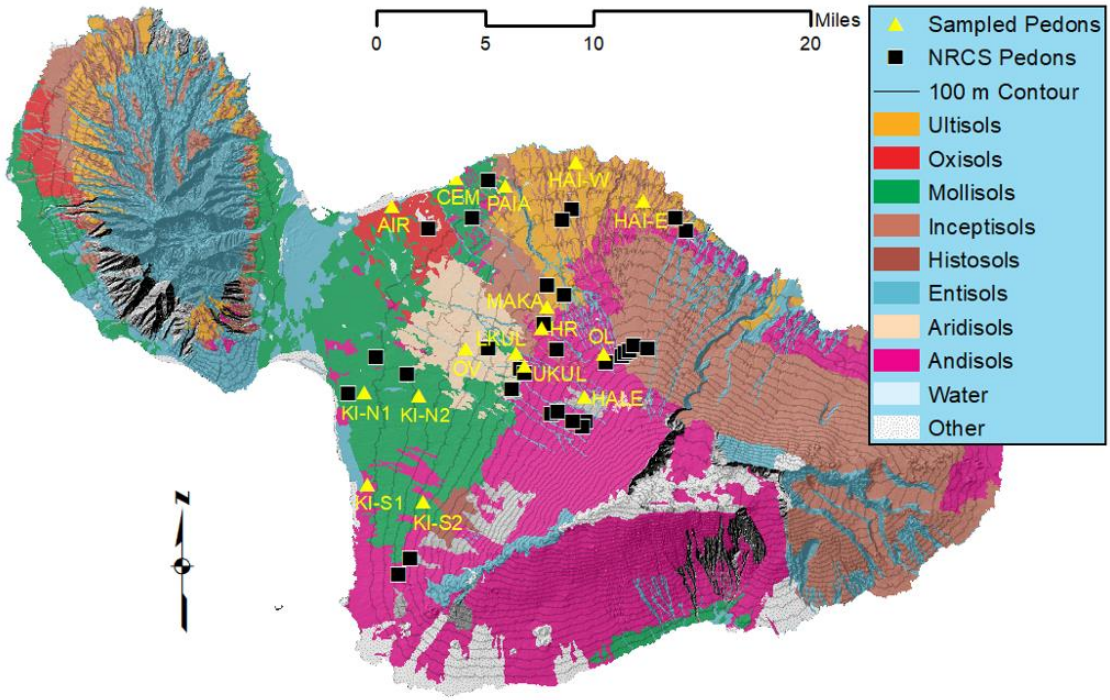

Figure 2-4. Soil Order map of the island of Maui. Triangles indicate the study soil sampling locations, and black squares indicate NRCS sampled soils. Soil Order data source: Gridded Soil Survey Geographic (gSSURGO).

6. The remaining limiting factor for site selection was property access. Areas classified as residential were avoided as much as possible.

Spatial data fitting the criteria above were delineated and sampling was initially random, selecting 3 sites in each MAP class with variation in elevation, MAP, and MAT. The locations of 16 pedons were selected and sampled in 2019 (7) and 2020 (9). Pedons were named based on their general location: north Kihei (KI-N1 and KI-N2), south Kihei/Makena (KI-S1 and KI-S2), Ocean Vodka Organic Farm and Distillery (OV), lower Kula (LKUL) and upper Kula (UKUL), the closest pedon to Haleakalā summit (HALE), Haleakalā Ranch (HR), Olinda (OL), Makawao (MAKA), Kahului Airport (AIR), Paia cemetery (CEM), Paia area (PAIA), west Haiku (HAI-W), and east Haiku (HAI-E) (Figures 2-3, 2-4).

Field Methods

At each selected location, observations of surface features including microtopography, surface rocks, aspect, and vegetation were made to determine if our initial site selections adequately met our spatial data limitations (slope % and hillslope position). Some sampling locations were shifted slightly (within 100 m) as needed. Nine pedons were on land which had not been tilled within the last eight years, and the remaining seven pedons were on uncultivated soils. Soils were manually excavated to at least 1-meter depth or to a root limiting layer, if shallower. Soil morphology and landscape characteristics were described according to Schoeneberger et al. (2012), and soils were sampled by genetic horizon. Bulk density samples were extracted using the hammer-driven corer method (Soil Survey Staff, 2014b) unless restricted due to high coarse fragment content. Presence of SRO aluminosilicates was determined using 1M sodium fluoride (NaF) and a pH stick (Soil Survey Staff, 2014a).

Chemical, Physical, and Mineralogical Analyses

All lab analyses were performed on the air-dried fine-earth fraction (< 2-mm) of soil from each genetic horizon of all pedons, unless otherwise noted. All analytical protocols followed the Soil Survey Field and Laboratory Methods Manual (SSIR 51) (Soil Survey Staff, 2014b) and the Kellogg Soil Survey Laboratory Methods Manual (SSIR 42) (Soil Survey Staff, 2014c), unless otherwise noted.

Particle size analysis was performed on the < 2-mm fraction using the PARIO instrument (METER Group). First, removal and quantification of organic matter of pretest samples were required (DIN, 2002; Gee and Or, 2002). Measurement samples were first chemically (Gee and Or, 2002) and physically (DIN, 2002) dispersed, followed

by sonication (800-1000 J mL^{-1}; Silva et al., 2015) before analysis. Sands were subsequently fractionated by wet sieving (DIN 2002; DIN 2011). Oven-dry bulk density was measured using the hammer-driven core samples. Water retention at -1500 kPa was measured using the WP4C Dewpoint PotentiaMeter (METER Group).

Total (TC) and inorganic carbon (IC) were analyzed using the Skalar Total Carbon Analyzer, and organic carbon (OC) was determined by difference (TC – IC = OC). Above a pH of 5.5, effective cation exchange capacity (ECEC) is considered relatively equal to CEC (Buol et al., 2011). Therefore, extractable Al by 1 N KCl was analyzed on samples with pH < 5.5 for determining ECEC. Extractable base cations, cation exchange capacity (CEC), and base saturation (BS) were measured by extraction with ammonium acetate (NH_4OAc at pH 7) (CEC_7 and BS_7) and by the compulsive exchange (CE) method with barium chloride ($BaCl_2$) (CEC_{CE} and BS_{CE}) (Gillman, 1979; Gillman and Sumpter, 1986). Data from BS_7 and CEC_7 are used for classifying soils according to Soil Taxonomy (Soil Survey Staff, 2014a), while $BaCl_2$ extraction is designed to accurately measure base cations, BS_{CE} and cation exchange CEC_{CE} for soils containing variable charge clays. Phosphate retention was measured using the New Zealand method. The pH and electrical conductivity (EC; dS/m) were measured using the 1:5 soil:water ratio method, and during the CE experiment.

Operationally defined selective dissolution extractions were performed non-sequentially. Organo-bound Fe and Al were extracted using sodium pyrophosphate (PY) (McKeague, 1967). Noncrystalline inorganic and organically complexed Fe, Al, and Si were extracted using acid ammonium oxalate (AO) at pH 3 following a modified method of Shang and Zelanzy (2008). While the AO extraction method is used to quantify

amorphous Fe and Al and is used as criteria for classifying andic soil properties according to Soil Taxonomy, AO is known to extract other materials. These other extractables include magnetite (6.6-7.9%), maghemite, some goethite and hematite (if small and poorly crystalline) (< 1%), and may even solubilize Fe and Al in organic associations (Rennert, 2018; Chao and Zhou, 1983). The hydroxylamine hydrochloride-hydrochloric acid (HH) extraction dissolves also < 1% of the Fe contained in hematite and goethite, but < 1% of magnetite (Chao and Zhou, 1983). Because the AO method dissolves a substantial amount of the crystalline Fe oxide magnetite (Algoe et al., 2012; Rhoton et al., 1981; Walker, 1983), which is common in Hawaiian volcanic soils (Silva et al., 2015), and the HH method dissolves virtually no magnetite (Ross et al., 1985; Chao and Zhou, 1983), the HH method was performed in addition to the AO method. Lastly, free (total) Fe oxides (organically bound, noncrystalline, and crystalline) were extracted by sodium citrate-dithionite (CD) in the dark.

Following oven-drying of the wet-sieved very fine sand fraction, the proportion of volcanic glass in the very fine sand fraction of selected soil horizons was determined by counting grains with a petrographic microscope (Thomas et al., 2008). For each sample, a few drops of oil with a refractive index of 1.54 was applied to a petrographic slide, and a small amount of very fine sand was placed in the sitting oil before being stirred and spread across the slide. At least 300 grains were counted and classified to attain a percent glass value of each sample.

The clay fraction of selected samples was analyzed with X-ray diffraction (XRD) according to Harris and White (2008). Preparation of clay samples for XRD followed the methods of Whittig and Allardice (1986). To fractionate clay samples, soil samples were

first dispersed using Na-hexametaphosphate and were shaken overnight. Following dispersion, samples were wet-sieved to remove the sand fraction, and the silt and clay suspension was transferred to a 1-L graduated cylinder where it was left to settle for 24 hours. The clay suspension was then aspirated from the column and stored at 4 °C. Samples were either saturated with 1M KCl or 1M MgCl prior to filtering through a < 0.45 µm filter and vacuum flask. Filtered clay samples were placed on petrographic slides and air-dried. K-saturated clay samples were analyzed with XRD three times sequentially following air-drying, oven drying to 110 °C for four hours, and oven drying to 300 °C for four hours. Mg-saturated samples were analyzed with XRD twice sequentially following air-drying, and following air-equilibration with glycerol in a desiccator for at least 7 days. Scan settings for XRD were set to continuous between 3-35 °2θ, and generator settings were 30 mA and 40 kV.

Data Analysis

All soil chemical and physical properties were calculated on a depth-weighted average to 1-m or to a root-restricting layer, if shallower, for each pedon. The quantity of Al + ½Fe (AO), required for determination of andic soil properties and classification of Andisols and Andic intergrades of other soil orders (Algoe et al., 2012; Soil Survey Staff, 2014a) was calculated. Other soil properties derived from selective dissolution results were calculated, including amorphous Fe (AO-PY) and Al (AO-PY), crystalline Fe (CD-AO) (Chao and Zhou, 1983; Rennert, 2018; Walker, 1983), and Fe (AO-HH). All soils were classified to order, suborder, great group, and subgroup using Soil Taxonomy (Soil Survey Staff, 2014).

RESULTS AND DISCUSSION

All Pedons

The classification of the 16 pedons described, sampled, and analyzed in this study included Mollisols, Inceptisols, Andisols, and Ultisols (Table 2-1).

Base saturation, regardless of the method, were close or equal to 100% in soils at

Table 2-1. Sampled pedon name, elevation, mean annual precipitation (MAP), mean annual temperature (MAT), soil order and subgroup classification of western Haleakalā, Maui.

Pedon	Elevation	MAP[a]	MAT[b]	Soil Order	Subgroup
	m	mm	°C		
KI-N1	73	283	24	Mollisol	Torroxic Haplustolls
KI-N2	224	329	24	Mollisol	Aridic Haplustolls
KI-S1	56	335	24	Mollisol	Aridic Argiustolls
AIR	15	461	23	Mollisol	Typic Haplustolls
KI-S2	457	527	24	Mollisol	Aridic Lithic Haplustolls
OV	325	568	23	Mollisol	Andic Haplustolls
CEM	7	709	23	Inceptisol	Oxic Haplustepts
LKUL	624	821	21	Mollisol	Andic Haplustolls
UKUL	715	826	19	Mollisol	Typic Argiustolls
HALE	1362	1082	13	Andisol	Pachic Haplustands
PAIA	113	1240	23	Mollisol	Oxic Haplustolls
HR	684	1336	19	Andisol	Humic Haplustands
MAKA	586	1542	22	Andisol	Humic Haplustands
HAI-W	101	1551	22	Ultisol	Typic Sombrihumults
OL	1226	2267	14	Inceptisol	Andic Dystrustepts
HAI-E	197	2768	22	Ultisol	Typic Haplohumults

[a] MAP, mean annual precipitation; mm, millimeters.
[b] MAT, mean annual temperature; °C, degrees Celsius.

or below about 1500 mm MAP and dropped sharply above 1500 mm MAP (Figure 2-5a). Soil pH decreased linearly with increasing MAP (Figure 2-5b). Surface OC concentration was lowest in the driest soils, generally increased as precipitation increased to about 1300 mm, then decreased with higher MAP (Figure 2-5c). Pedon LKUL had high subsurface

OC accumulation due to recent deposits of volcanic ash at this location, thereby inflating

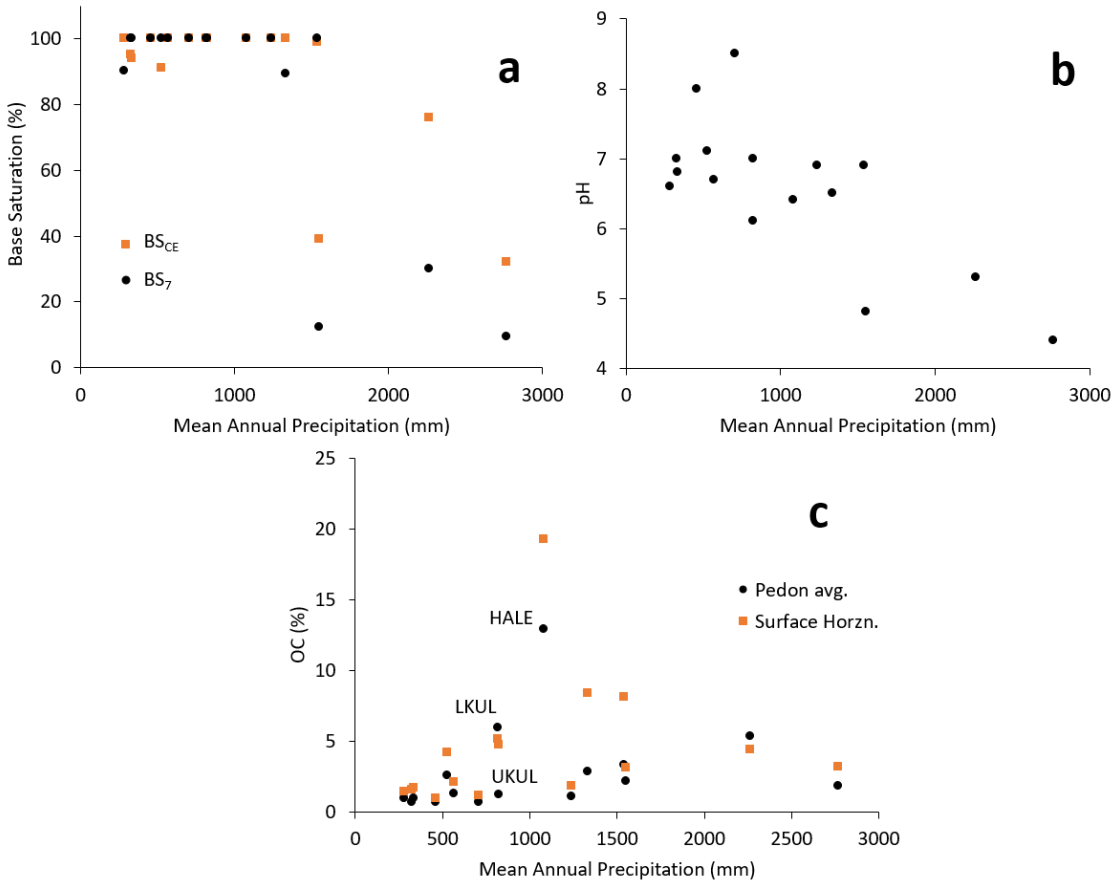

Figure 2-5. Depth-weighted pedon average of (a) base saturation (black circles are for BS_7 and orange squares are for BS_{CE}), (b) pH, and (c) organic carbon concentration (black circles are for pedon average and orange squares are for surface horizons) plotted against mean annual precipitation for the study area of western Haleakalā, Maui. BS_7, base saturation using NH_4OAc at pH 7; BS_{CE}, base saturation using the compulsive exchange method; OC, organic carbon.

pedon average OC compared to the relatively near UKUL pedon. On the Kohala Peninsula of the Big Island, Chadwick et al. (2003) noted an abrupt decrease in BS and pH as precipitation increased above 1400 mm (1700 mm – Vitousek and Chadwick, 2013). On Kauai (Vitousek and Chadwick, 2013), the decrease in BS and pH occurred

above 900 mm MAP. Organic carbon in soils on the Big Island followed a similar trend with increasing precipitation as in this study (Chadwick et al., 2003).

The difference in Fe extracted by AO and HH generally increased with increasing MAP (Figure 2-6), which may indicate increased weathering of the basalt substrate with increasing precipitation.

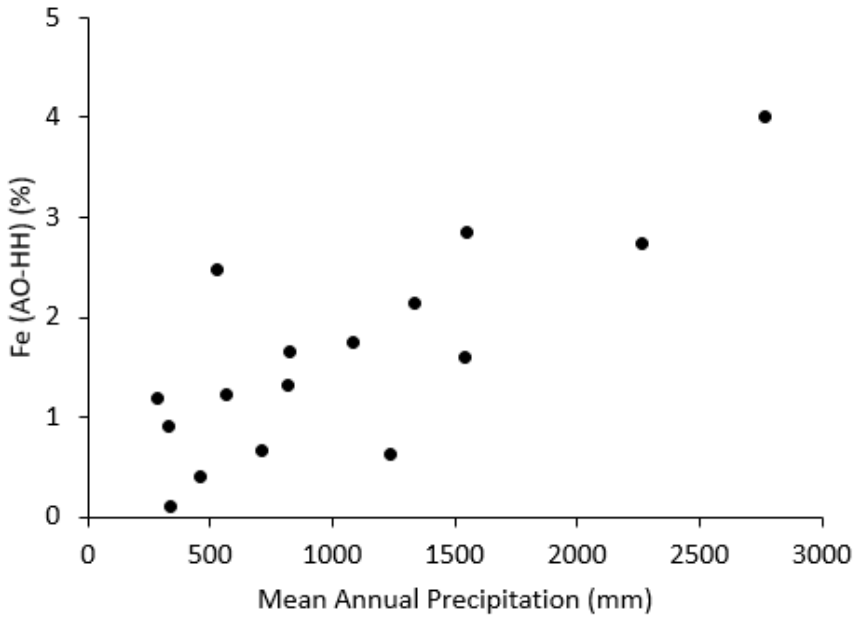

Figure 2-6. Depth-weighted average pedon values of Fe (AO-HH) plotted against mean annual precipitation (MAP) for the study area of western Haleakalā, Maui. AO, ammonium oxalate; HH, hydroxylamine hydrochloride-hydrochloric acid.

There was no clear trend in amorphous Fe across all pedons with increasing MAP until it decreased to 0% at about 1550 mm MAP (Figures 2-7a). Amorphous Al was highly variable with MAP (Figure 2-7c) and at higher elevations and cooler MAT below 22°C, and was low (< 2%) above 22°C (Figure 2-7d). Pedons UKUL, LKUL, HR, and MAKA occurred within 129 m in elevation of each other with similar MAT (19-22°C),

yet spanned a distance of 4600 m across upcountry Maui and a MAP gradient of 700 mm. Pedons LKUL (821 mm MAP) and

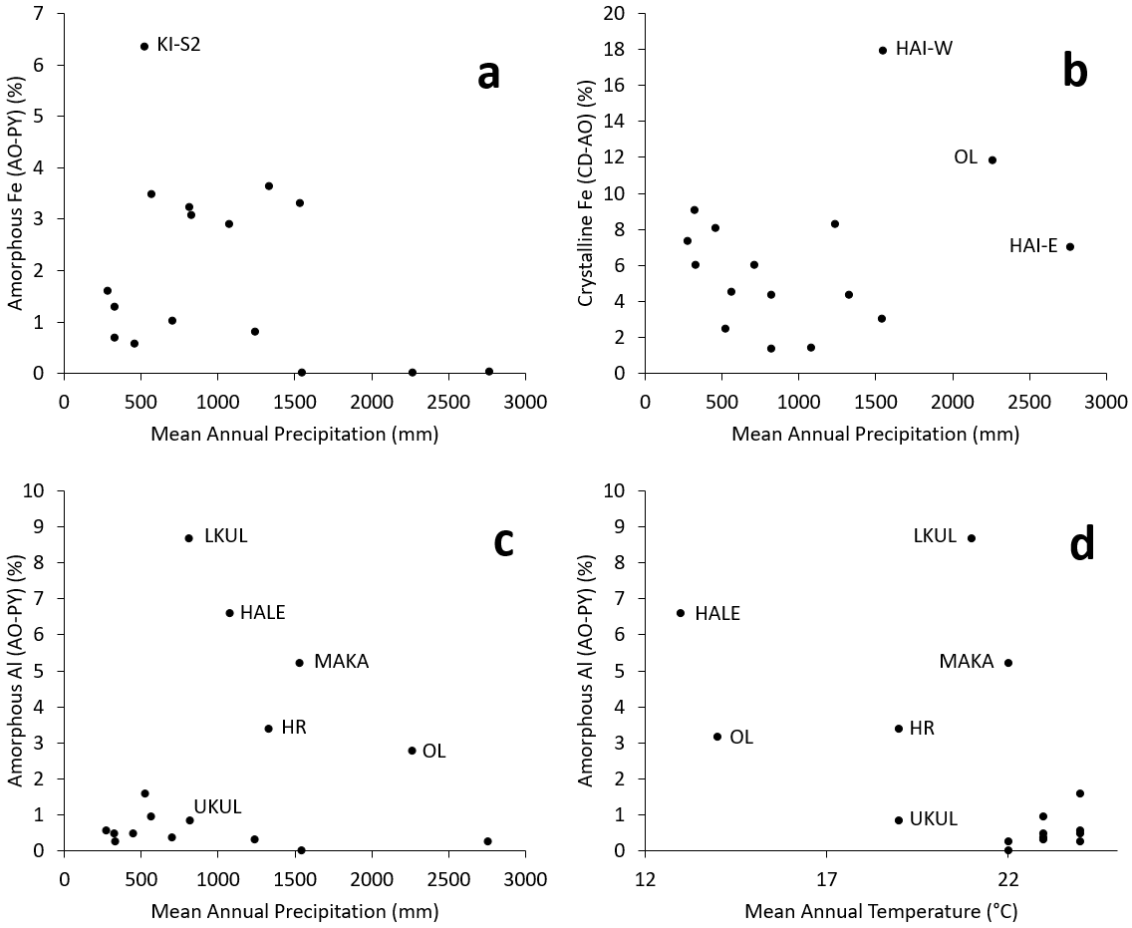

Figure 2-7. Depth-weighted average pedon values of amorphous Al and Fe and crystalline Fe plotted against mean annual precipitation (MAP), and amorphous Al plotted against mean annual temperature (MAT) for the study area of western Haleakalā, Maui. AO, ammonium oxalate; CD, citrate dithionite; PY, sodium pyrophosphate.

UKUL (826 mm MAP) (Figure 2-7c) occurred within 1-km of each other, yet LKUL had about 8% more amorphous Al. Pedons UKUL, LKUL, HR, and MAKA occurred downwind of volcanic vents (see Chapter 4, Figure 4-3) and the varying concentrations of

amorphous Al (Figures 2-7c and d) demonstrated the varying influence of volcanic ash deposits independent of MAT.

There were no clear trends in crystalline Fe (CD-AO) (Figure 2-7b), which contradicts trends found in climosequences of the Sierra Nevada, where crystalline Fe increased with elevation (increasing MAP and decreasing MAT) below the winter snowline (Dahlgren et al., 1997; Rasmussen et al. 2007, 2010). This ambiguity may also indicate the potential influence of volcanic ash on the weathering sequences of the soils of western Haleakalā.

Coastal Climosequence

Five of the sampled pedons (AIR, CEM, PAIA, HAI-W, HAI-E), were located on the north coast of East Maui between Kahului and Haiku, and spanned a precipitation gradient of > 2 m MAP (461-2768 mm MAP). These pedons occurred at less than 224 m in elevation and had mean annual temperature between 22 and 24 °C, effectively providing a climosequence where precipitation varied and temperature was relatively constant. Soil classification varied from Mollisols and Inceptisols, to Ultisols with increasing MAP (Table 2-1).

Base saturation was 100% for both surface horizons and pedon averages, then decreased to less than 50% in surface horizons and to less than 20% for pedon averages above about 1500 mm MAP (Figure 2-8a). Pedon weighted average pH was alkaline in the driest soils and decreased with increasing MAP, plunging to strongly acid with MAP greater than about 1500 mm (Figure 2-8b). Organic carbon (Figure 2-8c), similar to the trend with all pedons, increased with increasing MAP to about 1600 mm (versus 1300 mm for all pedons) before decreasing with pedon HAI-E. These trends of increasing

followed by decreasing OC were like those reported for the Kohala peninsula on the Big Island (Vitousek and Chadwick, 2013; Chadwick et al. 2003).

The five pedons in this coastal climosequence did not include Andisols or andic soils. One reason is that this area, along the north coast—upwind of volcanic vents of the northwest rift zone—was little influenced by volcanic ash. The three drier pedons (AIR, CEM, PAIA) had some volcanic glass, but their Al + ½Fe (AO) content was below 0.85%. Due to their lower levels of precipitation, the volcanic glass had not weathered sufficiently to form high concentrations of noncrystalline materials, including SRO aluminosilicates. Short-range-order aluminosilicates are high in aluminum, which has a strong electronegativity with oxygen, thus giving andic soils the capability to adhere to and accumulate organic carbon (Strawn et al., 2015). This phenomenon explains the low organic carbon in the coastal sequence pedons (Figure 2-8c; Table 2-5a). Pedons HAI-W and HAI-E were well-drained soils with relatively high MAP. However, like the study-wide pedon analysis of OC (Figure 2-5c), with increasing precipitation, there was a threshold where OC begins to decrease slightly. Pedons AIR and CEM have pH values above 8.0 for two unique reasons. The area of pedon AIR was once used in agriculture and its abnormally high pH may reflect a combination of factors including 1) the likelihood of liming in the area, 2) high calcium content in the surface horizons (AIR: 45.9 $cmol_c\ kg^{-1}$, CEM: 65.7 $cmol_c\ kg^{-1}$), and 3) dry climate. Pedon CEM was within 20 meters of the ocean and was likely influenced by sea spray. Both have high BS_7 (pedon 4: 100%; pedon 7: 100%) due to their low CEC_7, 12.0 $cmol_c\ kg^{-1}$ and 10.6 $cmol_c\ kg^{-1}$, respectively, and high calcium content.

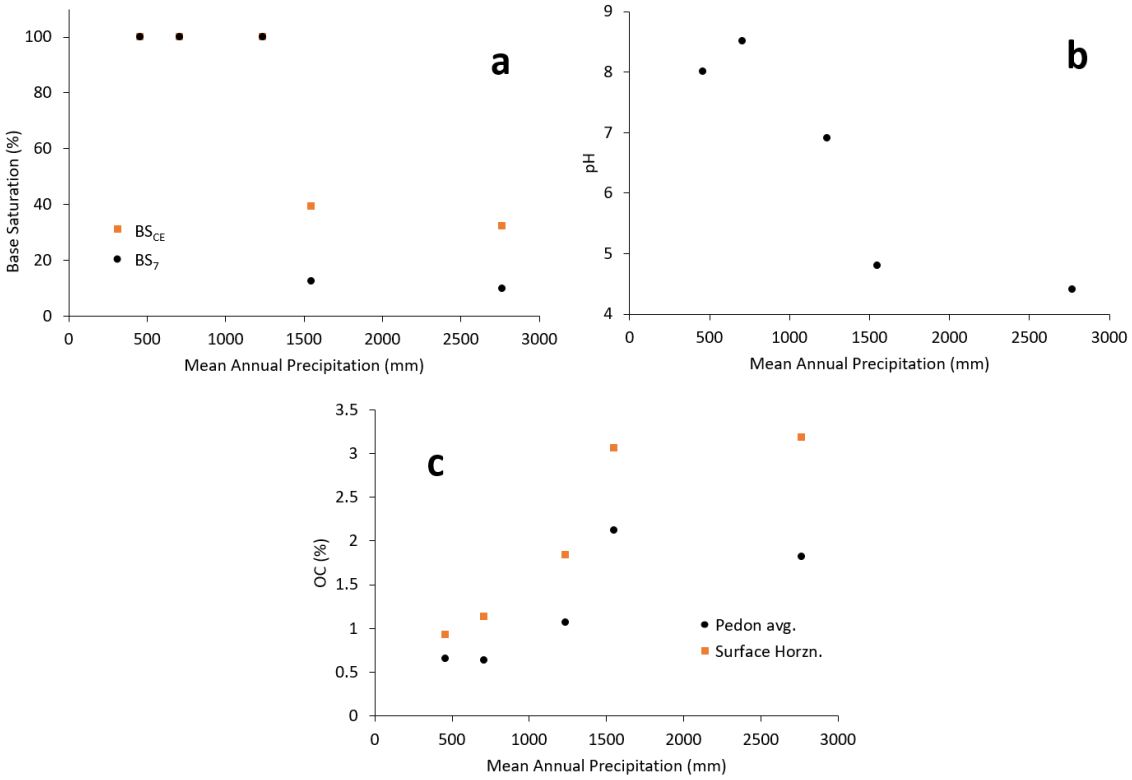

Figure 2-8. Depth-weighted pedon average (black circles) and surface horizon (orange squares) values of base saturation (a), pH (b), and organic carbon (c) as functions of mean annual precipitation for pedons AIR, CEM, PAIA, HAI-W, and HAI-E of western Haleakalā, Maui. BS_7, base saturation using NH_4OAc at pH 7; BS_{CE}, base saturation using the compulsive exchange method; OC, organic carbon.

The difference in Fe extracted by AO and HH, like all pedons, increased with increasing precipitation (Figure 2-9).

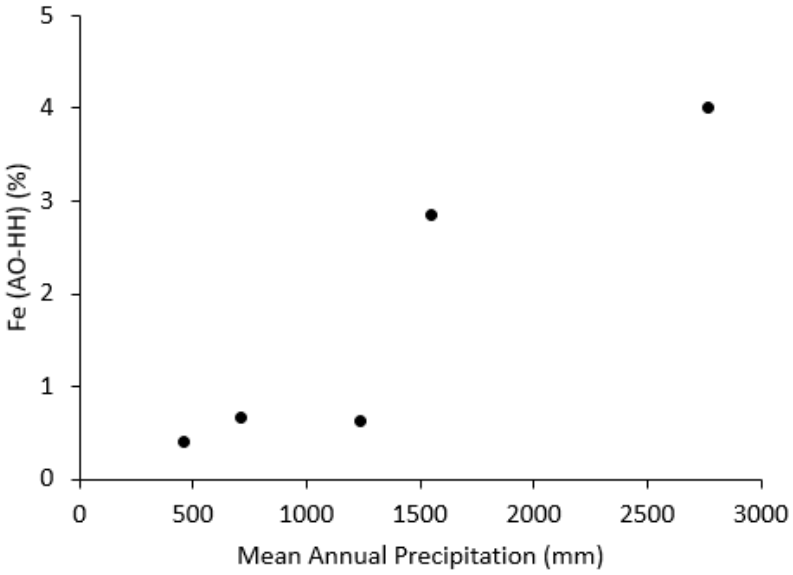

Figure 2-9. Depth-weighted average pedon values of Fe (AO-HH) as a function of mean annual precipitation (MAP) for pedons AIR, CEM, PAIA, HAI-W, and HAI-E of western Haleakalā, Maui. AO, ammonium oxalate; HH, hydroxylamine hydrochloride hydrochloric acid.

The coastal climosequence showed variability in amorphous Fe until 1550 mm MAP. Any positive correlation between amorphous Fe and MAP across the study area (Figure 2-7a) was temporary as MAP increased. Because HAI-E received so much rainfall and was persistently moist, it is likely that some non-organo associated Fe was reduced and leached from the profile at higher rainfall locations (Miller et al., 2001). Amorphous Fe and amorphous Al did not rise above 1% and 0.5% (Figures 2-10a and c) respectively, whereas amorphous Fe and Al for the "all pedons" sequence got above 6% and 8%, respectively. The low relative amorphous Fe and Al for the coastal pedons indicate how little influenced they were by volcanic ash.

Unlike the climosequence of all pedons (Figure 2-7b), the trend of crystalline Fe content (CD-AO) increased with increasing precipitation (Figures 2-10b and 2-11) then decreased dramatically > 1600 mm MAP, supporting the hypothesis that reducing

conditions cause Fe^{3+} to reduce to Fe^{2+} and leach in extremely wet environments, regardless of proper drainage. This trend of crystalline Fe with increasing precipitation follows a similar trend as a climosequence of soils of near the town of Olinda (Miller et al., 2001), where crystalline Fe decreased at the wettest sites. The threshold where

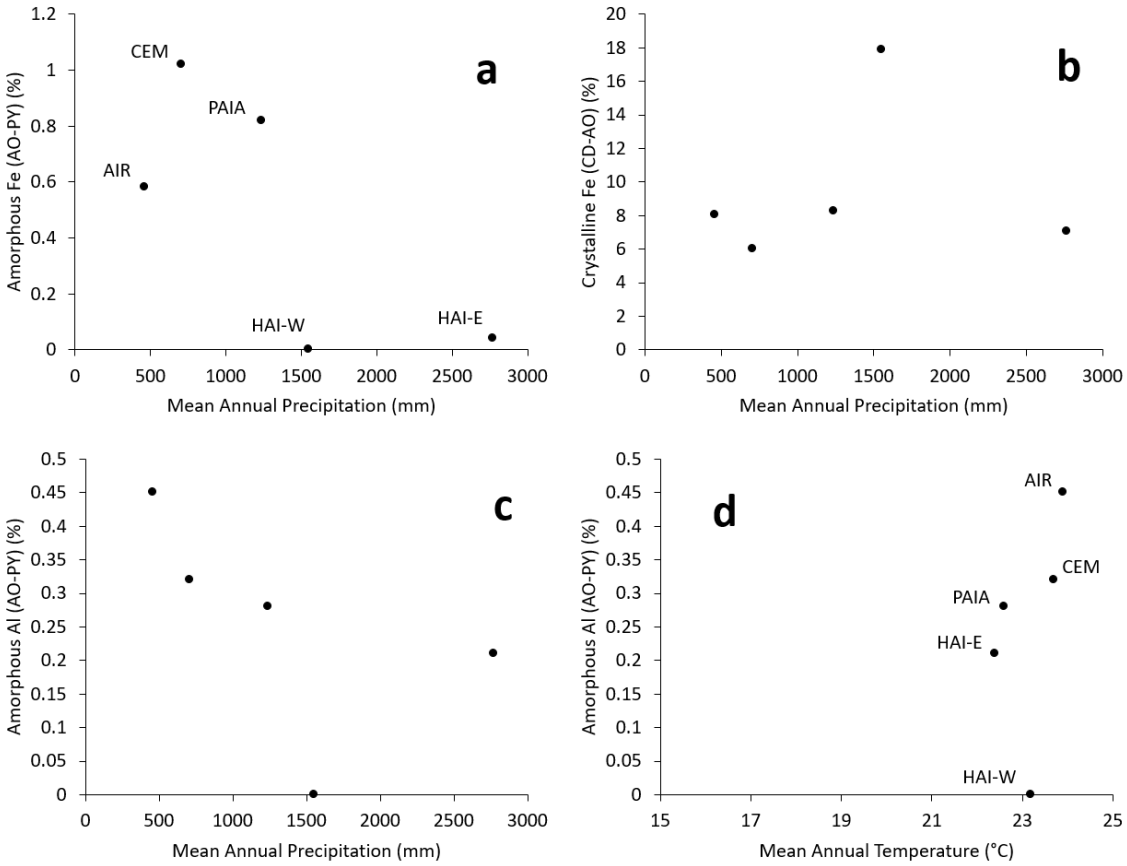

Figure 2-10. Depth-weighted average pedon values of various selective dissolution properties as a function of mean annual precipitation (MAP) (a-c) and mean annual temperature (d) for pedons AIR, CEM, PAIA, HAI-W, and HAI-E of western Haleakalā, Maui. AO, ammonium oxalate; CD, citrate dithionite; PY, sodium pyrophosphate.

crystalline Fe decreases in Miller et al. (2001) occurred at a higher MAP (> 2750 mm) than in the coastal climosequence, but MAT was much lower (16-17 °C). However, it is clear that reducing conditions can develop even though soils are well drained.

The increase in crystalline Fe (CD-AO) with depth in pedon HAI-W (Figure 2-11) followed a concomitant increase in clay content with depth to 92% in the deepest horizon (see Appendix).

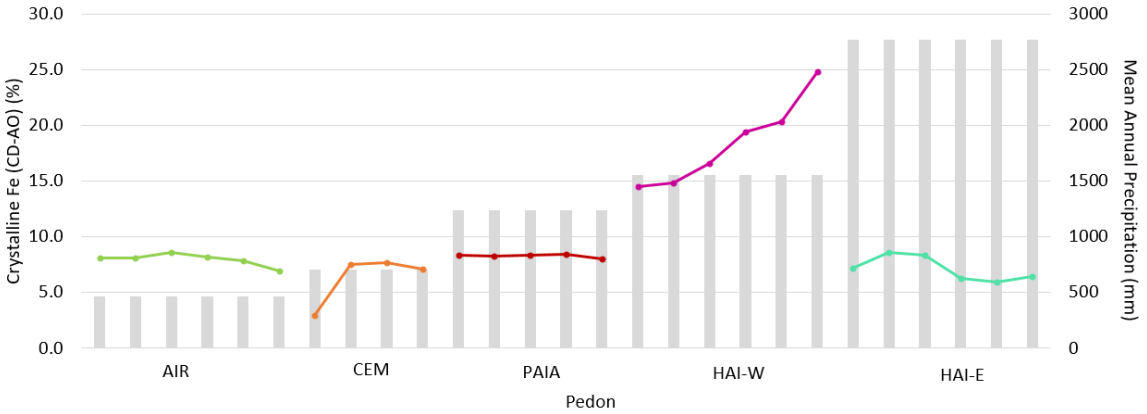

Figure 2-11. Crystalline Fe (CD-AO) by horizon for all sampled pedons of western Haleakalā, Maui. Soil horizon data are plotted from surface downward from left to right. Secondary y-axis (grey bars) indicates mean annual precipitation for each pedon.

Elevational Climosequence

Nine pedons (KI-N1, KI-N2, OV, LKUL, UKUL, HR, MAKA, OL, HALE) transect the precipitation gradient (283-2267 mm MAP) of western Haleakalā perpendicularly from the lowland coastal town of Kihei to the upcountry town of Olinda. Soils ranged from Mollisols, to Andisols, to an Inceptisol with increasing elevation. This climosequence provides the opportunity to observe the influence of climate and volcanic ash on soil development. Much like the coastal climosequence, base saturation and pH remained high with increasing MAP before reaching a pedogenic threshold above 1500 mm MAP where they dramatically decreased (Figure 2-12). While difficult to pinpoint due to a lack of data between 1542 mm and 2267 mm MAP, the threshold appears to be at a higher MAP than the coastal climosequence, which may be influenced by the cooler

MAT. Whole pedon OC generally increases with increasing MAP, except for an outlier (HALE). The elevation of pedon HALE exposes it to lower precipitation levels (1082 mm MAP), but its position in the cloud layer causes this area to be perpetually wet from condensation on vegetation. This combination of environmental conditions limits leaching, reduces microbial decomposition, and promotes the accumulation of organic matter and SRO aluminosilicates.

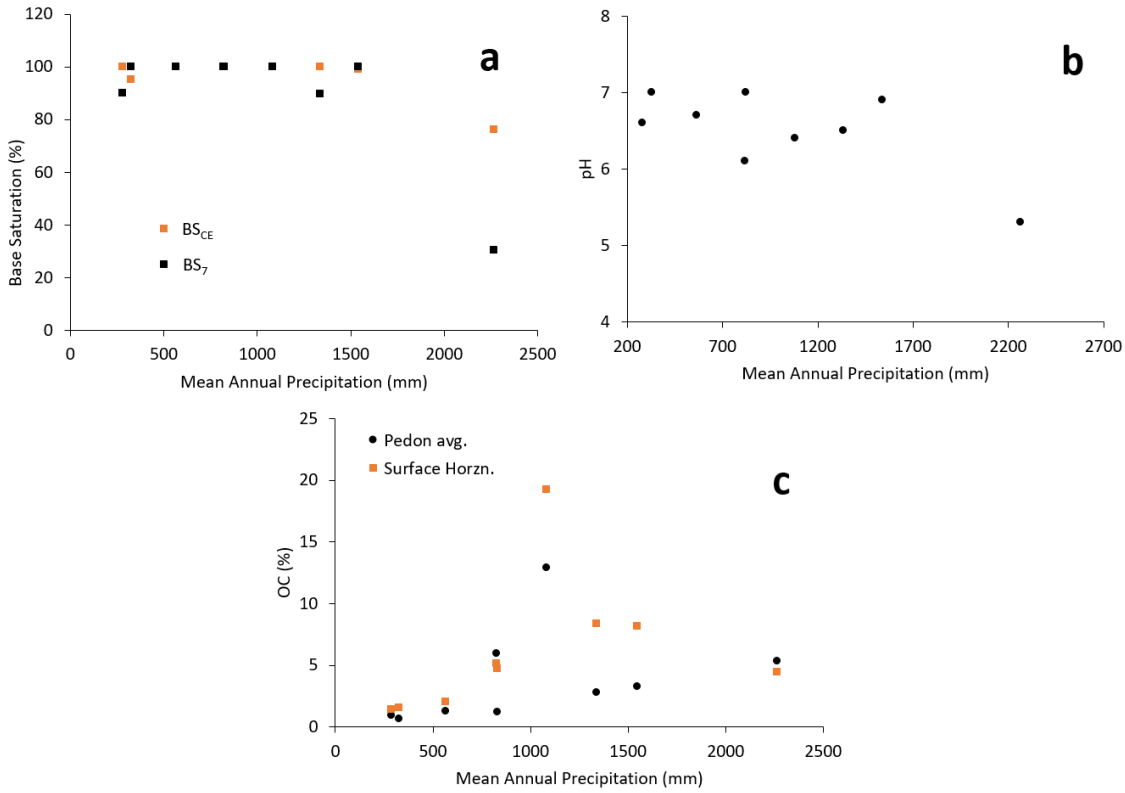

Figure 2-12. Depth-weighted pedon average (black circles) and surface horizon (orange squares) values of base saturation (a), pH (b), and organic carbon (c) as functions of mean annual precipitation for pedons KI-N1, KI-N2, OV, LKUL, UKUL, HR, MAKA, OL, and HALE of western Haleakalā, Maui. BS_7, base saturation using NH_4OAc at pH 7; BS_{CE}, base saturation using the compulsive exchange method; OC, organic carbon.

Figures 2-13 through 2-16 plot selected soil properties and MAP for the nine pedons of this sequence with increasing elevation from left to right. It is clear that

precipitation does not necessarily increase with increasing elevation, but, rather, that MAP is a function of location, windward or leeward, relative to Haleakalā. Pedons HR, MAKA, and OL increase in precipitation and are situated leeward to windward of Haleakalā. Additionally, all pedons in this sequence, with exception of HALE (with OL just above the lower limit of the cloud layer), occur below the cloud layer. HALE is more leeward of HR, and MAKA, but occurs well within the cloud layer.

Amorphous Fe increased sharply between about 300 mm and 500 mm MAP, remained high through 1500 mm MAP, and was low to absent at about 2300 mm MAP (Figure 2-13a), which follows a very different trend with increasing rainfall than the

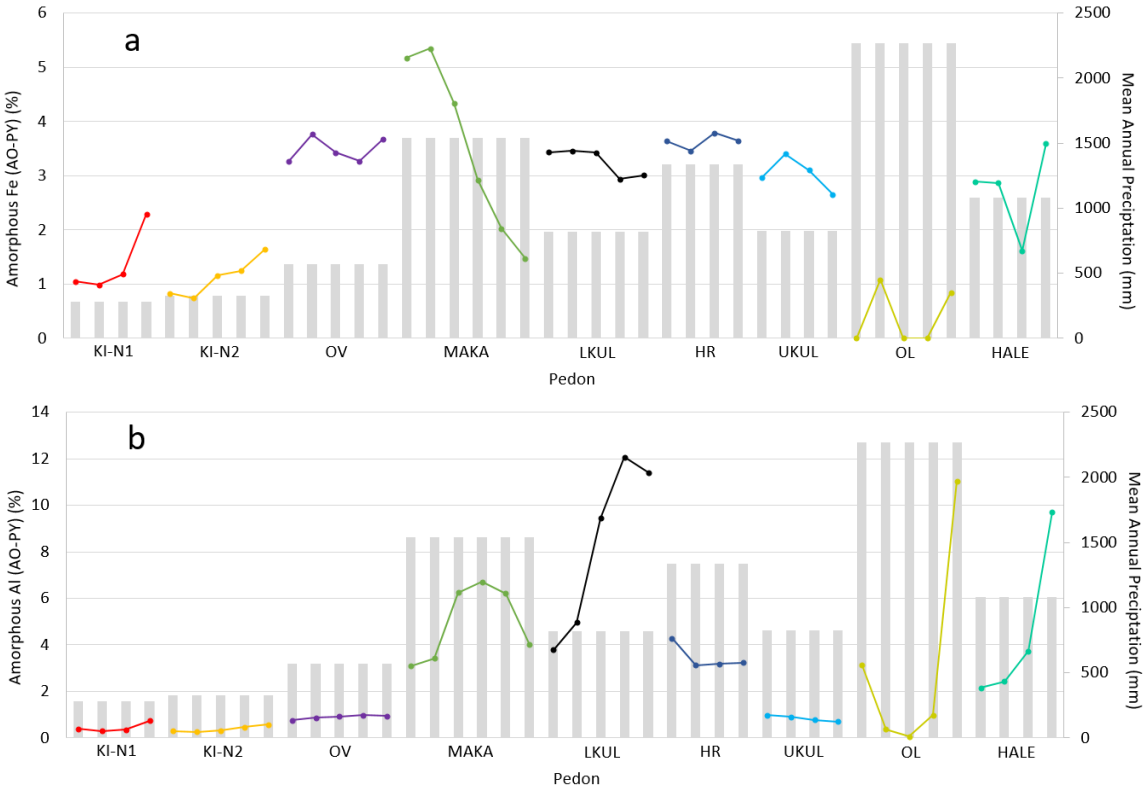

Figure 2-13. Amorphous Fe (AO-PY; a) and Al (AO-PY; b) values of genetic horizons for select pedons of western Haleakalā, Maui. Pedons are arranged by increasing elevation from left to right. Soil horizon data are plotted from the surface downward from left to right. Secondary y-axis (grey bars) indicates mean annual precipitation for each pedon. AO, ammonium oxalate; PY, sodium pyrophosphate.

coastal climosequence (Figure 2-11). Amorphous Al remained low for the three driest pedons and UKUL of the elevational climosequence (Figure 2-13), which were little influenced by volcanic ash. Pedon averages of amorphous Al for MAKA, LKUL, HR, and OL were higher, and these pedons sufficiently meet the requirements for andic soil properties to classify as Andisols (MAKA and HR) and as andic intergrades (LKUL and OL). Both amorphous Al and Al + ½Fe (AO) increased with depth for pedon LKUL. The high amorphous Al concentrations of the surface and deepest horizon of pedon OL also reflects the accumulation of Al + ½Fe (AO) in these two horizons.

Pedons KI-N1 and KI-N2 stand out with their high crystalline Fe values and low MAP (Figure 2-14), which is stark contrast to the increase in crystalline Fe (CD-AO) with increasing precipitation to about 2000 mm MAP before decreasing again (Figure 2-11). Considering how little MAP KI-N1 and KI-N2 received, and how high their crystalline Fe values were, these soils may occur on older landforms than the other pedons of this sequence, with the exception of maybe pedon OL. Pedon OL has a buried A horizon (deepest horizon). Because the middle three horizons are so high in crystalline Fe, it is likely that highly weathered soil material high in crystalline Fe was eroded from uphill and deposited in the area of pedon OL. Subsequently, the landform stabilized and formed a well-developed surface A horizon. Since crystalline Fe did not follow any particular trend with increasing elevation (Figure 2-14), it may better reflect soil weathering as a function of age.

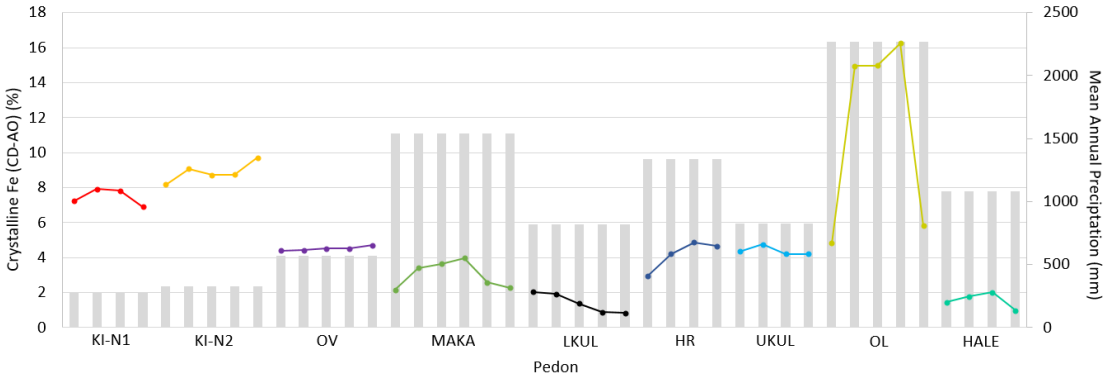

Figure 2-14. Crystalline Fe (CD-AO) values of genetic horizons for select pedons of western Haleakalā, Maui. Pedons are arranged by increasing elevation from left to right. Soil horizon data are plotted from the surface downward from left to right. Secondary y-axis (grey bars) indicates mean annual precipitation for each pedon. AO, ammonium oxalate; CD, citrate dithionite.

Iron associates well associated with organic matter and allophane/imogolite by forming complexes and chelates. Younger ash-rich parent material weathered to SRO materials and complexed with Fe. This is reflected by the relatively high concentrations of amorphous Fe (Figure 2-13a) in the elevational sequence, rather than higher crystalline Fe (Figure 2-14). The greater organic matter accumulation in pedons of the elevational climosequence is also enhanced, in part, by the lower MAT in upcountry Maui, which reduces microbial decomposition.

The distribution of Al + ½Fe (AO) in the elevational climosequence demonstrates the variable influence of volcanic ash on a soil, regardless of elevation (Figure 2-15). As KI-N1, KI-N2, and OV are the most distant soils from upwind sources of volcanic ash, coupled with their low precipitation, regardless of soil age, these soils did not develop substantial amounts of SRO aluminosilicates from volcanic ash weathering. Pedons LKUL and UKUL occur about 1 km from each other and had relatively equal amounts of MAP, but had dramatically different quantities of Al + ½Fe (AO), thus illustrating the

influence of volcanic ash on LKUL. Both soils are downwind from volcanic vents, but likely received different amounts of more recently deposited volcanic ash.

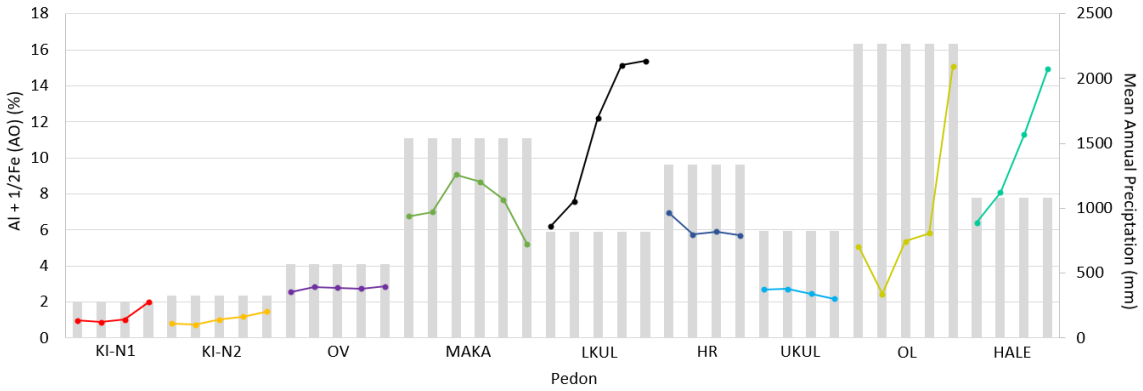

Figure 2-15. Al + 1/2Fe (AO) values of genetic horizons for select pedons of western Haleakalā, Maui. Pedons are arranged by increasing elevation from left to right. Soil horizon data are plotted from the surface downward from left to right. Secondary y-axis (grey bars) indicates mean annual precipitation for each pedon. AO, ammonium oxalate.

The variability in volcanic ash on soil development is well reflected in the phyllosilicate clay mineralogy of select soil pedons across the elevational climosequence. Figures 2-16 to 2-20 are X-Ray Diffractograms of select pedons along the elevational climosequence including KI-N2, LKUL, UKUL, OL, and HALE. The phyllosilicate clay fraction of KI-N2 (Figure 2-16) is dominated by kaolinite (7.1-7.3 Å in all treatments, to be verified with heating K300 samples to 550 °C), indicating it was likely little affected by deposition of volcanic ash. The presence of kaolinite in KI-N2 also supports the hypothesis that this soil occurs on a much older landform than upcountry Maui soils.

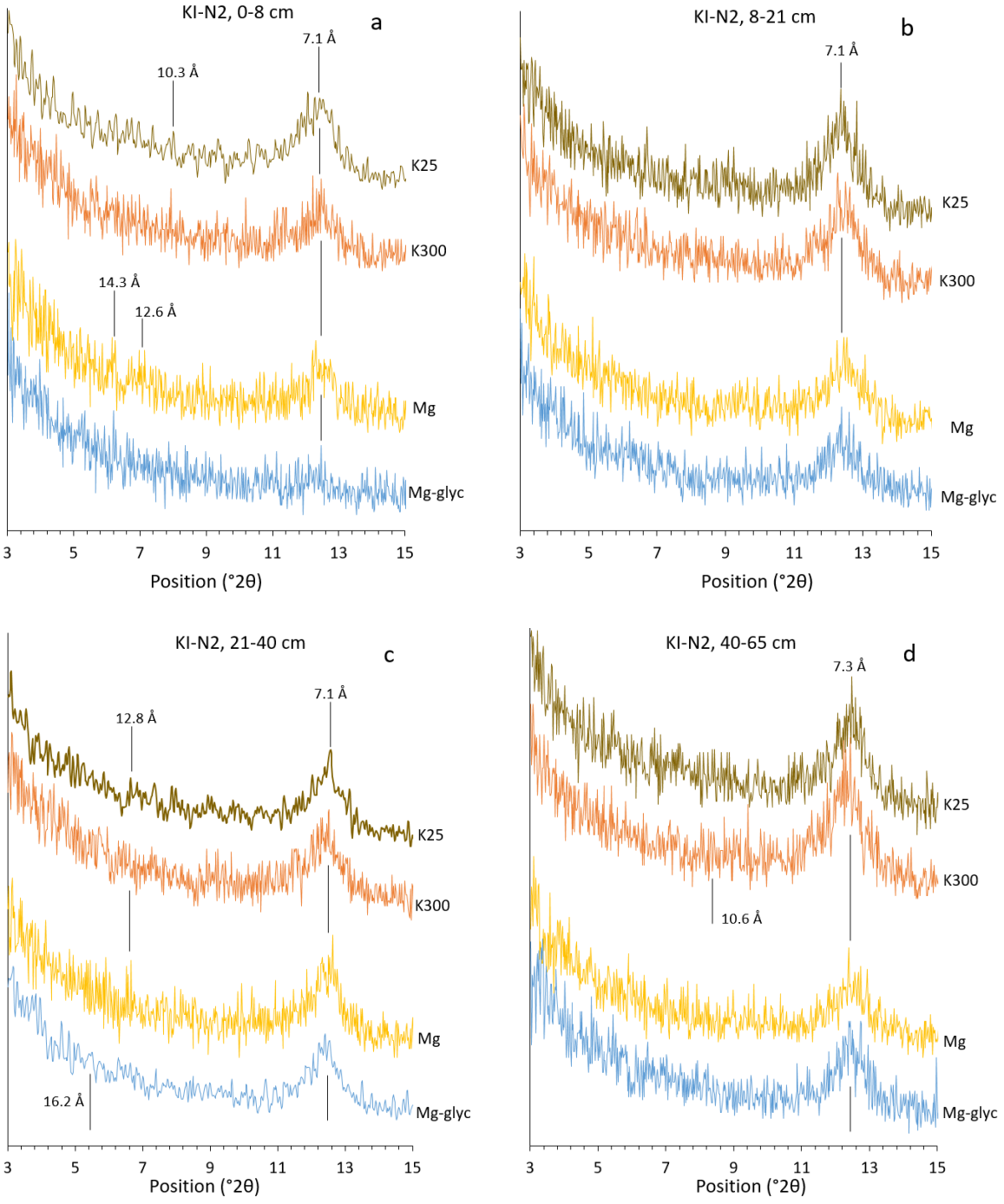
KI-N2, 0-8 cm
a
7.1 Å
10.3 Å
K25
K300
14.3 Å
12.6 Å
Mg
Mg-glyc
3 5 7 9 11 13 15
Position (°2θ)
KI-N2, 8-21 cm
b
7.1 Å
K25
K300
Mg
Mg-glyc
3 5 7 9 11 13 15
Position (°2θ)
KI-N2, 21-40 cm
c
7.1 Å
12.8 Å
K25
K300
Mg
16.2 Å
Mg-glyc
3 5 7 9 11 13 15
Position (°2θ)
KI-N2, 40-65 cm
d
7.3 Å
K25
K300
10.6 Å
Mg
Mg-glyc
3 5 7 9 11 13 15
Position (°2θ)

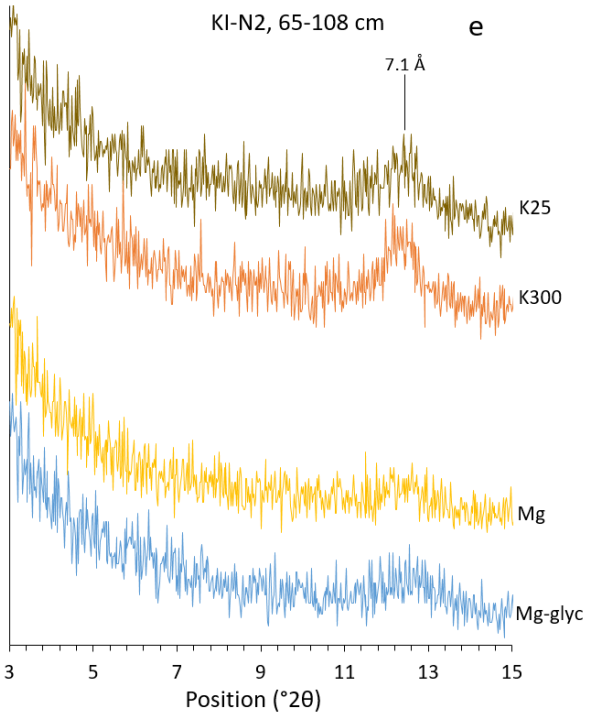

Figure 2-16. X-Ray Diffractogram data for pedon KI-N2 by genetic horizon (a-e). Peaks are marked with d-spacing. Å, angstrom; K25, K saturated sample at 25 °C; K300, K saturated sample at 300 °C; Mg, Mg saturated sample; Mg-glyc, Mg saturated sampled treated with glycerin.

Pedon UKUL shows weak peaks at 9.6 Å and 7.2 Å at K25 (Figure 2-17). When heated to 300 °C (K300), halloysite dehydrates and the 9.6 Å peak collapse to 7 Å, strengthening the kaolinite peak at 7.2 Å. Pedons LKUL and UKUL occurred 1 kilometer apart with nearly identical MAP and similar elevation, yet their crystalline mineralogy differs greatly. The LKUL pedon shows weak crystallinity at 7.1-7.3 Å at the surface with increasing amorphous signatures with depth. This is supported by the increase in amorphous Al and Al + ½Fe (AO) with depth in pedon LKUL (Figure 2-13b and Figure 15). Further investigation is warranted to determine the presence of halloysite. The crystalline clay minerals in UKUL indicate this soil is likely older and less affected by ash deposition than LKUL, which, except for the upper two horizons, lacks crystalline

phyllosilicate clay minerals. Higher crystallinity in the surface two horizons of LKUL with weaker peaks compared to UKUL demonstrates the limited soil weathering that has taken place with depth since the deposition of ash at pedon LKUL.

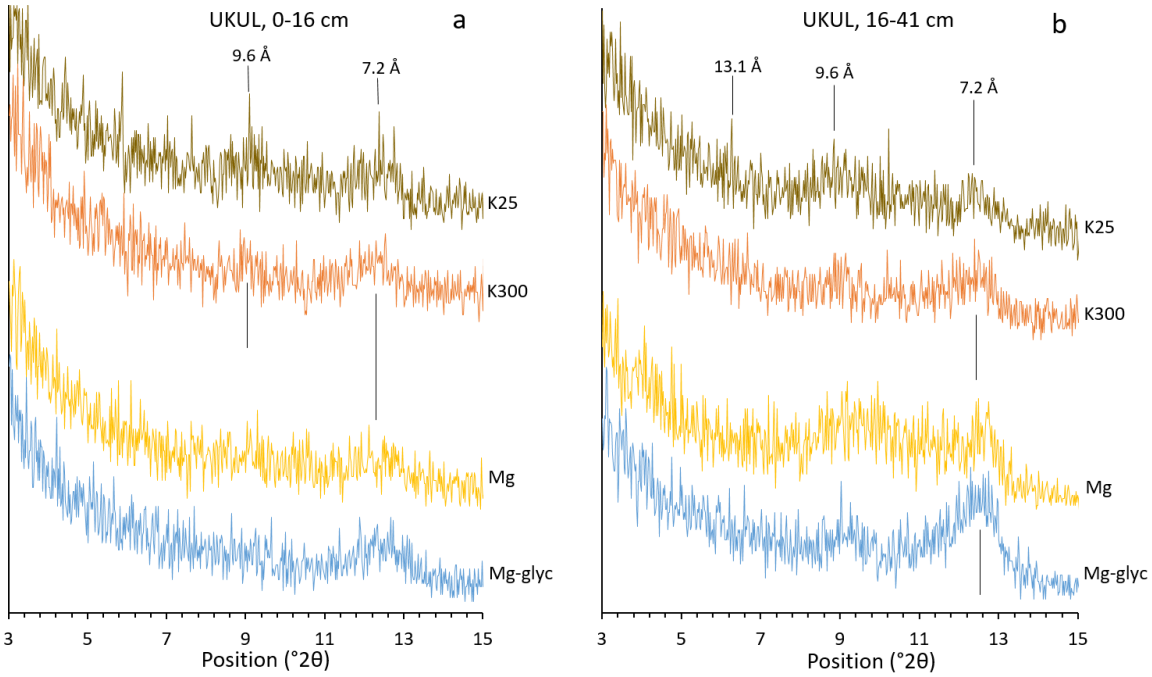

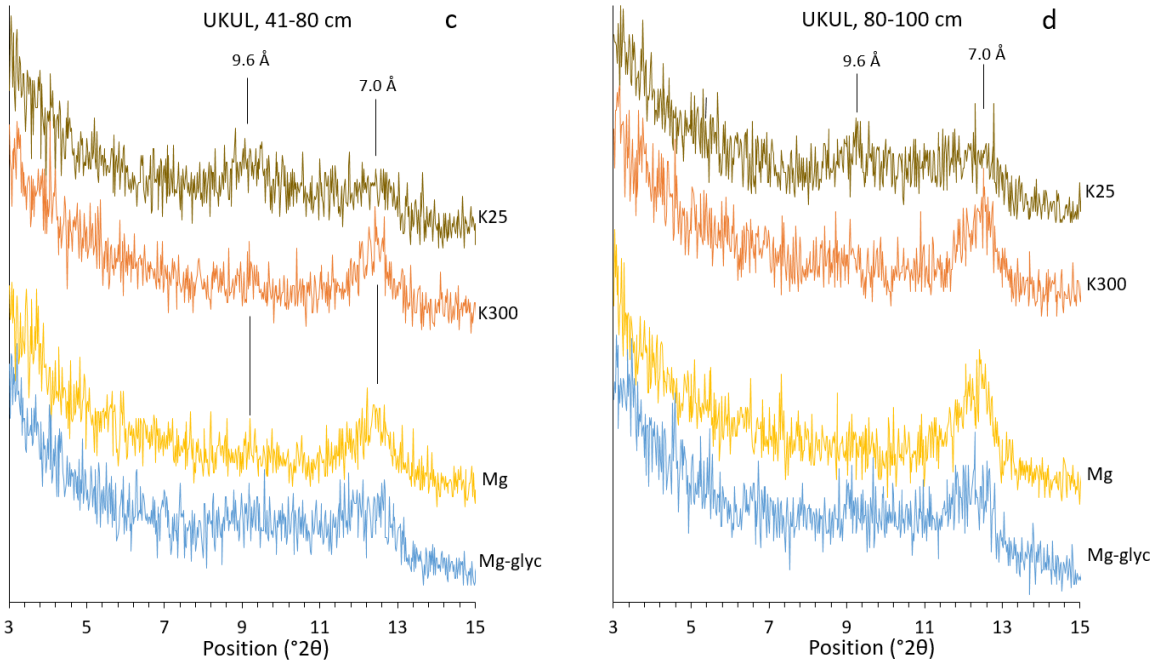

Figure 2-17. X-Ray Diffractogram data for pedon UKUL by genetic horizon (a-d). Peaks are marked with d-spacing. Å, angstrom; K25, K saturated sample at 25 °C; K300, K saturated sample at 300 °C; Mg, Mg saturated sample; Mg-glyc, Mg saturated sampled treated with glycerin.

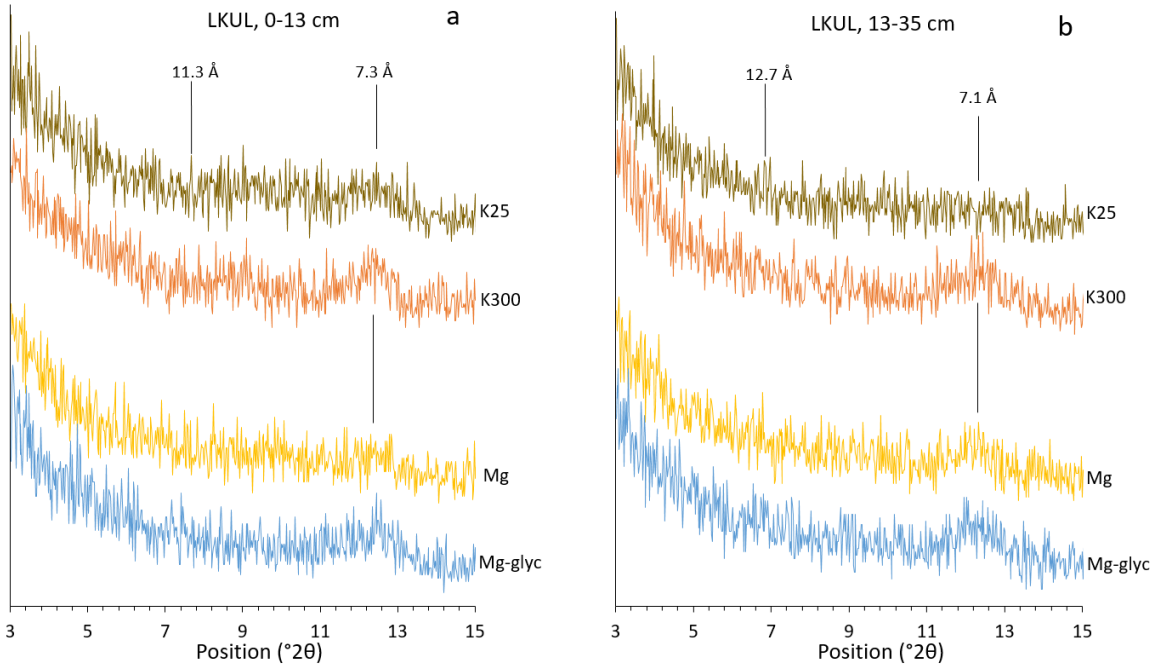

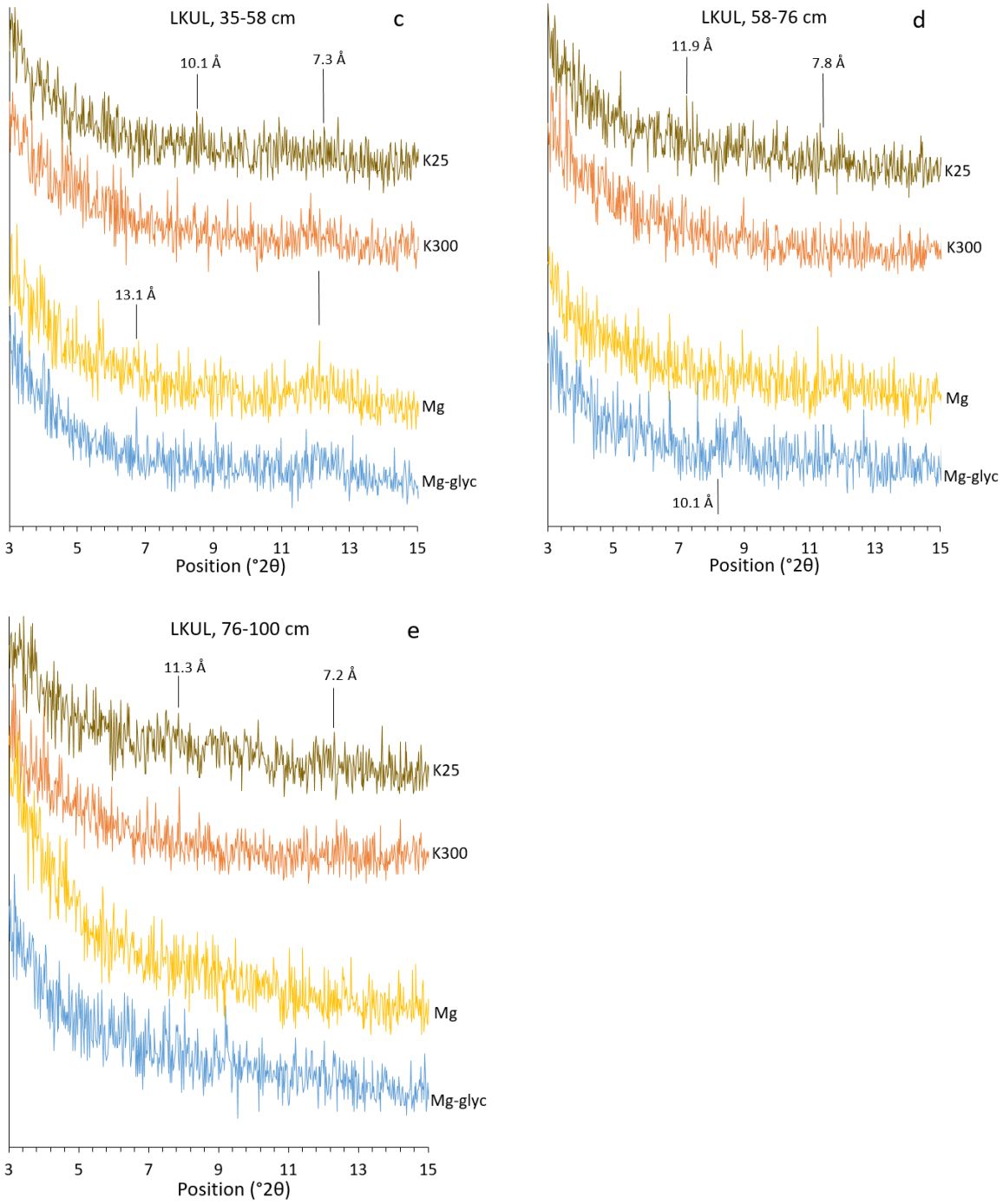

Figure 2-18. X-Ray Diffractogram data for pedon LKUL by genetic horizon (a-e). Peaks are marked with d-spacing. Å, angstrom; K25, K saturated sample at 25 °C; K300, K saturated sample at 300 °C; Mg, Mg saturated sample; Mg-glyc, Mg saturated sampled treated with glycerin.

Pedons OL and HALE both classify as Andisols (Table 2-1). Pedon HALE contains the highest Al + ½Fe (AO) in the study at 12.40% (depth-weighted average), and pedon OL contains a weighted average of 6.52% Al + ½Fe (AO) with over 15% in the deepest horizon. Both pedon OL (Figure 2-19) and HALE (Figure 2-20) are highly amorphous with pedon OL potentially showing a small amount of crystalline phyllosilicates (Figure 2-19), but this warrants further investigation. Pedon HALE lacks any indication for the presence of phyllosilicate minerals.

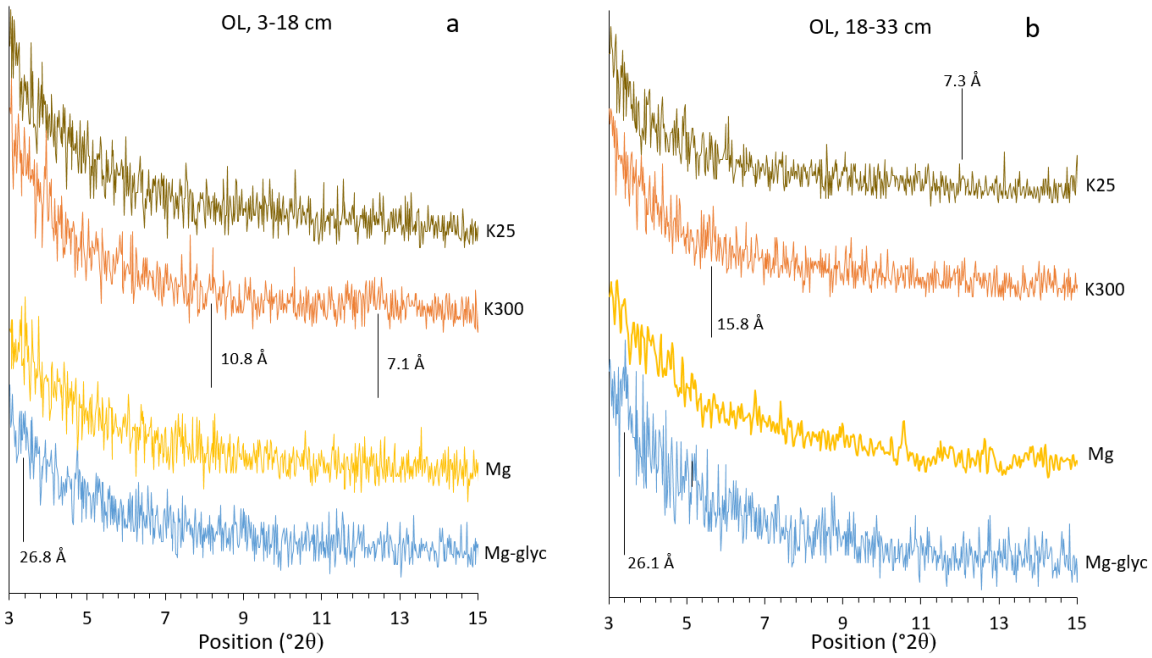

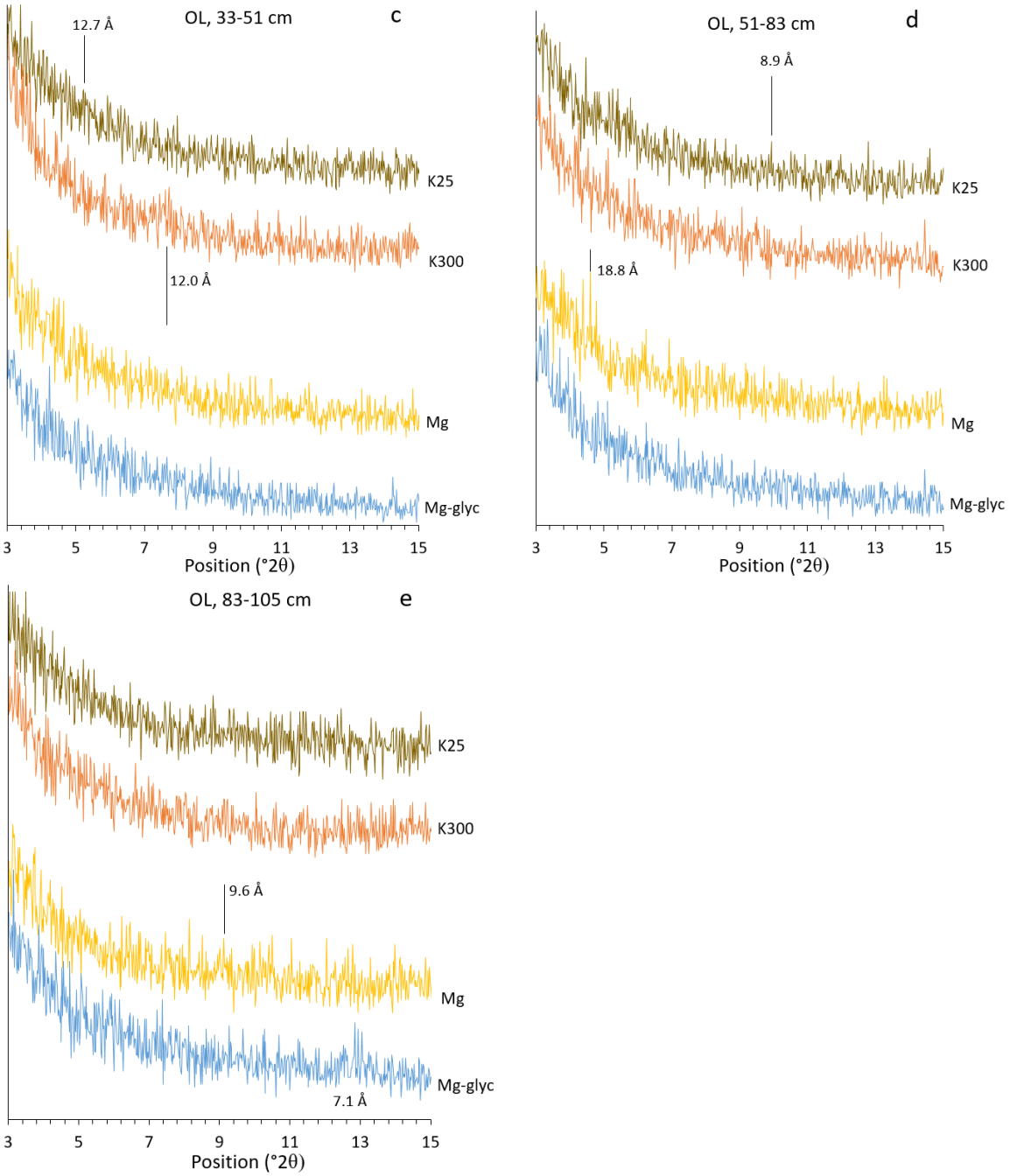

Figure 2-19. X-Ray Diffractogram data for pedon OL by genetic horizon (a-e). Peaks are marked with d-spacing. Å, angstrom; K25, K saturated sample at 25 °C; K300, K saturated sample at 300 °C; Mg, Mg saturated sample; Mg-glyc, Mg saturated sampled treated with glycerin.

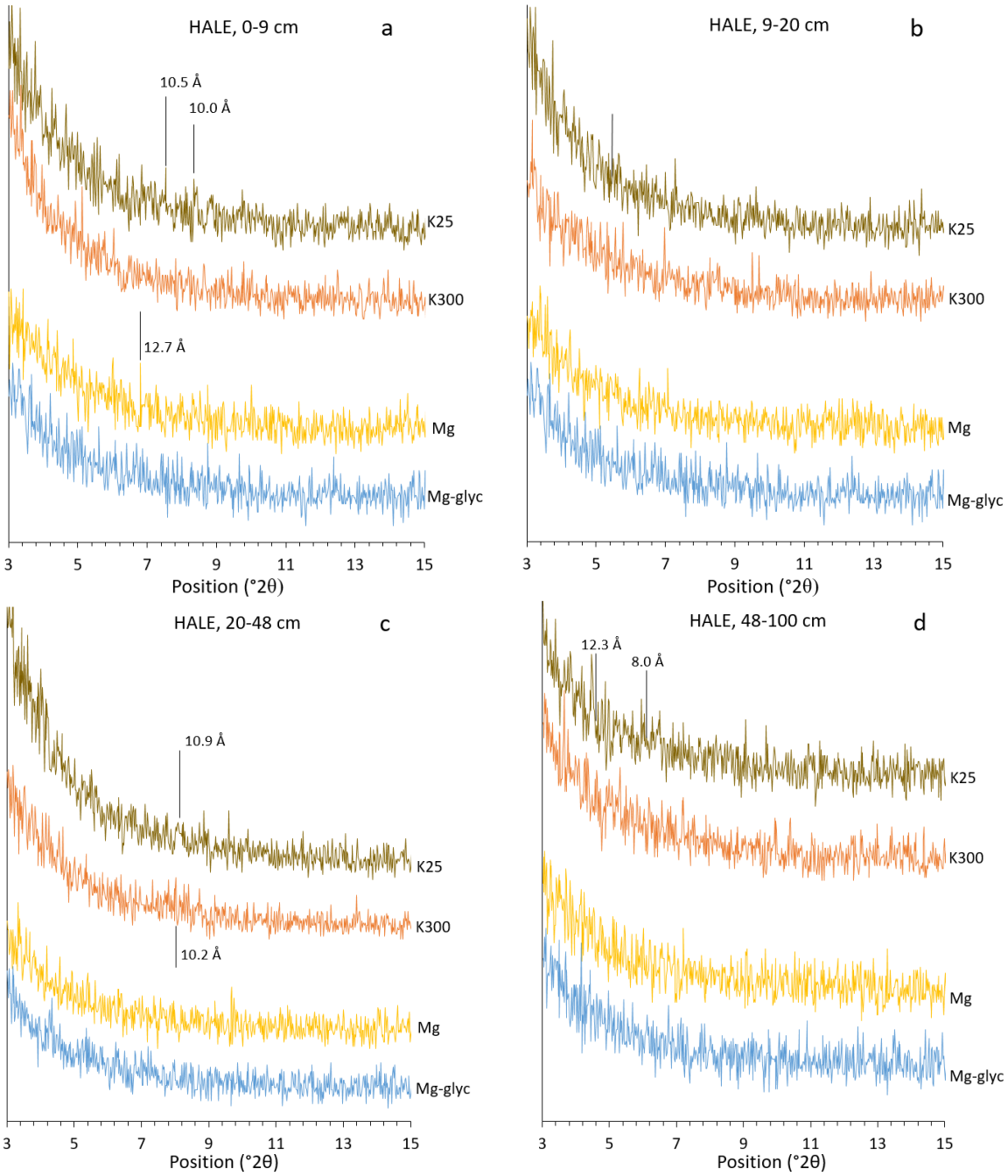

Figure 2-20. X-Ray Diffractogram data for pedon HALE by genetic horizon (a-d). Peaks are marked with d-spacing. Å, angstrom; K25, K saturated sample at 25 °C; K300, K saturated sample at 300 °C; Mg, Mg saturated sample; Mg-glyc, Mg saturated sampled treated with glycerin.

With the exception of pedons MAKA and OL, Fe (AO-HH) (Figure 2-21)

generally increased with increasing elevation, but mean pedon Fe (AO-HH), more clearly

increased with increasing precipitation (Figure 2-22). Iron (AO-HH) is more variable within a soil pedon with depth (Figure 2-21). Pedon MAKA had greater MAP than HALE and HR, and its surface horizons had higher Fe (AO-HH) than HALE and HR. The surface horizons of MAKA may simply be more weathered than its subsoil. The topsoil of MAKA also had the most amorphous Fe in this sequence (Figure 2-13a). Pedon OL, as described earlier, consisted of more weathered material that had buried an A horizon. Pedon OL occurs in a high precipitation environment, but was not persistently wet enough to cause reduction and leaching of Fe. Therefore, the eroded material in the middle three horizons had a relatively high Fe (AO-HH).

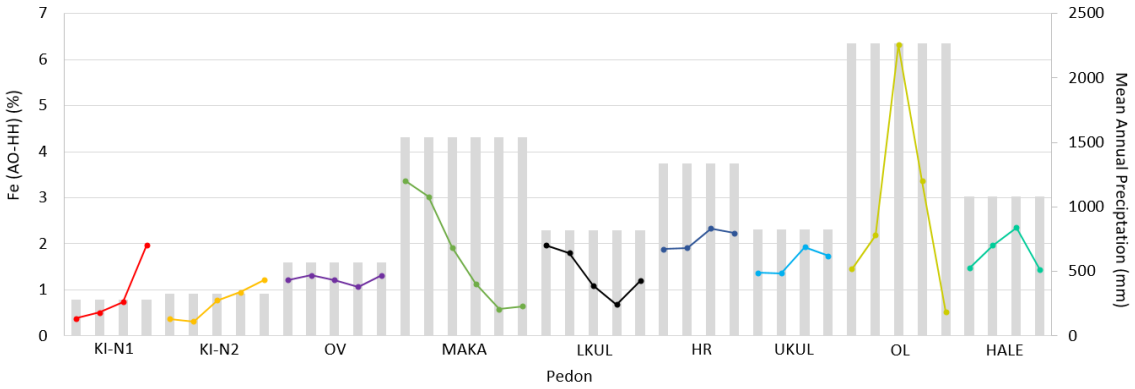

Figure 2-21. Iron (AO-HH) values of genetic horizons for select pedons of western Haleakalā, Maui. Pedons are arranged by increasing elevation from left to right. Soil horizon data are plotted from the surface downward from left to right. Secondary y-axis (grey bars) indicates mean annual precipitation for each pedon. AO, ammonium oxalate; HH, hydroxylamine hydrochloride hydrochloric acid.

Ammonium oxalate is known to dissolve magnetite, or at least a proportion of it, while HH dissolves virtually no magnetite (Chao and Zhou, 1983). Walker (1983) found the greatest percentage of magnetite in intermediate-age soils, and the decrease in their Fe ratios may be due to Fe being released from hematized magnetite during the citrate-

dithionite extraction. It is important to note that the Fe (AO) dissolved from magnetite was directly proportional to the concentration of magnetite in the soil (Walker, 1983).

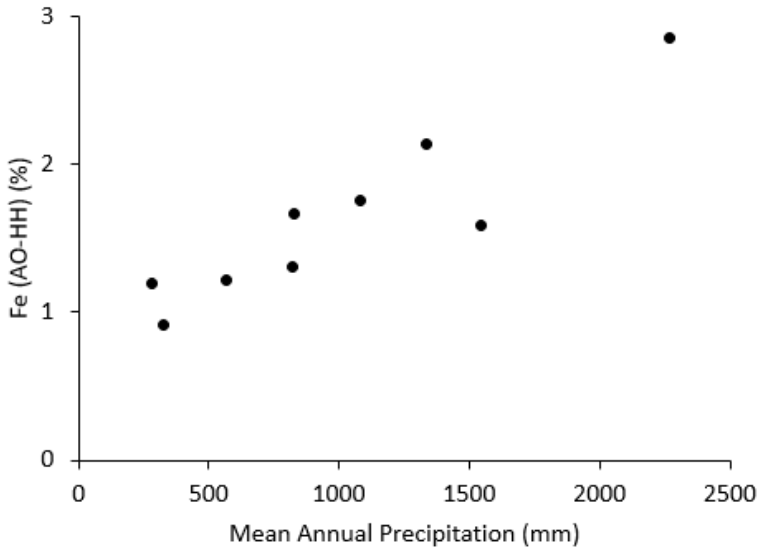

Figure 2-22. Depth-weighted pedon average (black circles) values of Fe (AO-HH) as functions of mean annual precipitation for pedons KI-N1, KI-N2, OV, LKUL, UKUL, HR, MAKA, OL, and HALE of western Haleakalā, Maui. AO, ammonium oxalate; HH, hydroxylamine hydrochloride hydrochloric acid.

Pedogenesis

The 1) dilation of amorphous Fe and Al and collapse of crystalline Fe in elevational climosequence pedons influenced by volcanic ash, and 2) higher crystalline Fe (CD-AO) of the coastal climosequence pedons, as well as pedons KI-N1 and KI-N2, indicate that lower elevation landforms and soils more distant from the summit across western Haleakalā are likely older than those of upcountry Maui.

The decrease of crystalline Fe (CD-AO) with increasing precipitation in the coastal climosequence not affected by more recent volcanic ash additions behaves

similarly to the decrease in crystalline Fe in Miller et al. (2001). However, the threshold where crystalline Fe decreased in Miller et al. (2001) occurred at a higher MAP (2750 mm) is influenced by the cooler MAT (16-17 °C) requiring more rainfall to cause the same thermodynamic reduction of Fe.

The climosequence on the Kohala Peninsula defined the position of pedogenic transitional thresholds in MAP where intense leaching occurs at about 1700 mm MAP (Vitousek and Chadwick, 2013), whereas in this study, it occurs at about 1500 mm MAP, and on the island of Kauai the threshold is much lower at 900 mm (Vitousek and Chadwick, 2013). The transition thresholds of the Kohala Peninsula of the Big Island and East Maui for these dynamic soil properties of Figure 4 differ by just 200 mm MAP, which can be expected due to their relatively close age in substrate and limited weathering of primary minerals. The variation in pedogenic thresholds between the Big Island, Maui, and Kauai may suggest a decreasing gradient in a transitional threshold for dynamic soil properties across the Hawaiian Islands due to increasing substrate and soil age.

REFERENCES

Alexander, E. B., Mallory, J. I., & Colwell, W. L. (1993). Soil-elevation relationships on a volcanic plateau in the southern Cascade Range, northern California, USA. *Catena*, *20*(1-2), 113-128.

Algoe, C., Stoops, G., Vandenberghe, R. E., & Van Ranst, E. (2012). Selective dissolution of Fe–Ti oxides—Extractable iron as a criterion for andic properties revisited. *Catena*, *92*, 49-54.

Bates, T. F. (1962). Halloysite and gibbsite formation in Hawaii. In *Clays and Clay Minerals* (pp. 315-328). Pergamon.

Buol, S. W., Southard, R. J., Graham, R. C., & McDaniel, P. A. (2011). *Soil genesis and classification*. John Wiley & Sons.

Chadwick, O.A., Gavenda, R. T., Kelly, E. F., Zeigler, K., Olson, C. G., Elliot, W. C., & Hendricks, D. M. (2003). The impact of climate on the biogeochemical functioning of volcanic soils. *Chemical Geology 202*, 195-223.

Chao, T. T., & Zhou, L. (1983). Extraction techniques for selective dissolution of amorphous iron oxides from soils and sediments. *Soil Science Society of America Journal*, *47*(2), 225-232.

Chen, C. Y., Frey, F. A., Garcia, M. O., Dalrymple, G. B., & Hart, S. R. (1991). The tholeiite to alkalic basalt transition at Haleakalā Volcano, Maui, Hawai'i. *Contributions to Mineralogy and Petrology 106*, 183–200.

Chorover, J., Amistadi, M. K., & Chadwick, O. A. (2004). Surface charge evolution of mineral-organic complexes during pedogenesis in Hawaiian basalt. *Geochimica Et Cosmochimica Acta 68*(23), 4859–4876.

Dahlgren, R. A., Boettinger, J. L., Huntington, G. L., & Amundson, R. G. (1997). Soil development along an elevational transect in the western Sierra Nevada, California. *Geoderma*, *78*(3-4), 207-236.

DIN (Deutsches Institut für Normung). (2002). Soil quality-Determination of particle size distribution in mineral soil material-Methods by sieving and sedimentation. DIN ISO 11277. Beuth Verlag, Berlin, Germany.

DIN (Deutsches Institut für Normung). (2011). Baugrund, Untersuchung von Bodenproben—Bestimmung der Korngroeßenverteilung. DIN ISO 18123. German Norm, Beuth Berlag, Berlin, Germany.

Dixon, J. L., Chadwick, O. A., & Vitousek, P. M. (2016). Climate-driven thresholds for chemical weathering in postglacial soils of New Zealand. *Journal of Geophysical Research: Earth Surface*, *121*(9), 1619-1634.

Gavenda, R. T. (1992). Hawaiian Quaternary paleoenvironments: A review of geological, pedological, and botanical evidence. *Pacific Science*. *46*, 295–307.

Gee, G. W., & Or, D. (2002). Particle-Size Analysis. In: *Methods of Soil Analysis: Part 4 Physical Methods*, 255-293. 4th ed., SSSA Book Series No. 5. Soil Science Society of America.

Giambelluca, T. W., & Schroeder, T. A. (1998). Climate. In: Juvik, S.P., Juvik, J.O., *Atlas of Hawaii*, 3rd Ed. University of Hawaii Press, Honolulu, pp. 49-59.

Giambelluca, T. W., Chen, Q., Frazier, A. G., Price, J. P., Chen, Y. L., Chu, P. S., Eischeid, J. K., & Delparte, D. M. (2013). Online Rainfall Atlas of Hawai'i. *Bulletin of the American Meteorological Society*. *94*, 313-316, doi: 10.1175/BAMS-D-11-00228.1.

Gillman, G. P. (1979). A proposed method for the measurement of exchange properties of highly weathered soils. *Australian Journal of Soil Research. 17*, 129-139.

Gillman, G. P., & Sumpter, E. A. (1986). Modification to the Compulsive Exchange Method for Measuring Exchange Characteristics of Soils. *Australian Journal of Soil Research*, *24*, 61–66.

Harris, W., & White, G.N. (2008). X-ray Diffraction Techniques for Soil Mineral Identification. *Methods of Soil Analysis, Part 5 – Mineralogical Methods*. Soil Science Society of America Journal, Madison. p 81.

Jenny, H. (1941). *Factors of Soil Formation: A System of Pedology*, McGraw-Hill book Company, Incorporated, New York.

Kleber, M., Schwendenmann, L., Veldkamp, E., Rößner, J., & Jahn, R. (2007). Halloysite versus gibbsite: silicon cycling as a pedogenetic process in two lowland neotropical rain forest soils of La Selva, Costa Rica. *Geoderma*, *138*(1-2), 1-11.

McKeague, J. A. (1967). An evaluation of 0.1 M pyrophosphate and pyrophosphate-dithionite in comparison with oxalate as extractants of the accumulation products in Podzols and some other soils. *Canadian Journal of Soil Science 47*, 95–99.

Miller, A.J., Schuur, E. A., & Chadwick, O. A. (2001). Redox control of phosphorus pools in Hawaiian montane forest soils. *Geoderma*, *102*(3-4), 219-237.

Minyard, W. P., Giambellucca, T. W., & Nullet, D. (1994). Elevation patterns of climate on the leeward slope of East Maui, Hawaii. Cooperative National Park Resources Studies Unit, University of Hawaii at Manoa. https://scholarspace.manoa.hawaii.edu/bitstream/10125/7246/1/092.pdf

Moore, J. G. (1987). Subsidence of the Hawaiian Ridge. Pp 85-100 *in* Decker, R.W., T.L. Wright, and P.H. Stauffer (eds). Volcanism in Hawaii. *U.S. Geological Survey. Professional Paper* 1350.

Nanzyo, M., Dahlgren, R., & Shoji, S. (1993). Chemical characteristics of volcanic ash soils. In *Developments in soil science* (Vol. 21, pp. 145-187). Elsevier.

Noshiroya, N. (1992). Changes in the soil properties of Andisols due to wetland rice farming. Master's thesis, Tohoku University.

Petterson, S. (1941). *Introduction to Meteorology.* New York, London: McGraw-Hills Book Company.

Price, J. P., & Elliot-Fisk, D. (2004). Topographic History of the Maui Nui Complex, Hawai'i, and Its Implications for Biogeography. *Pacific Science*. *58*(1), 27-45.

Rasmussen, C., Matsuyama, N., Dahlgren, R. A., Southard, R. J., & Brauer, N. (2007). Soil Genesis and Mineral Transformation Across an Environmental Gradient on Andesitic Lahar. *Soil Science Society of America Journal*, *71*(1), 225-237.

Rasmussen, C., Dahlgren, R. A., & Southard, R. J. (2010). Basalt weathering and pedogenesis across an environmental gradient in the southern Cascade Range, California, USA. *Geoderma*, *154*(3-4), 473-485.

Rennert, T. (2018). Wet-chemical extractions to characterise pedogenic Al and Fe species–a critical review. *Soil Research*, *57*(1), 1-16.

Rhoton, F. E., Bigham, J. M., Norton, L. D., & Smeck, N. E. (1981). Contribution of magnetite to oxalate-extractable iron in soils and sediments from the Maumee River basin of Ohio. *Soil Science Society of America Journal*, *45*(3), 645-649.

Riehl, H., Yeh, T. C., Malkus, J. J., & La Seur, N. E. (1951). The northeast trade of the Pacific Ocean. *Quarterly Journal of the Royal Meteorological Society*. *77*, 598-626.

Ross, G. J., Wang, C., & Schuppli, P.A. (1985). Hydroxylamine and ammonium oxalate solutions as extractants for iron and aluminum from soils. *Soil Science Society of America Journal*, *49*(3), 783-785.

Schoeneberger, P. J., Wysocki, D. A., & Benham, E. C. (Eds.). (2012). Field book for describing and sampling soils. Government Printing Office.

Shang, C., & Zelazny, L. W. (2008). Selective Dissolution Techniques for Mineral Analysis of Soils and Sediments. Methods of Soil Analysis, Part 5 – Mineralogical Methods. *Soil Science Society of America Journal*, Madison. p 33.

Sherrod, D. R., Nishimitsu, Y., & Tagami, T. (2003). New K-Ar ages and the geologic evidence against rejuvenated-stage volcanism at Haleakalā, East Maui, a postshield-stage volcano of the Hawaiian island chain. *GSA Bulletin*. *115*, 683–694.

Sherrod, D. R., Hagstrum, J. T., McGeehin, J. P., Champion, D. E., & Trusdell, F. A. (2006). Distribution, 14C chronology, and paleomagnetism of latest Pleistocene and Holocene lava flows at Haleakala volcano, Island of Maui, Hawai‘i: A revision of lava flow hazard zones, *Journal of Geophysical Research* ., *111*, B05205, doi:10.1029/2005JB003876.

Sherrod, D. R., Sinton, J. M., Watkins, S. E., & Blunt, K. M. (2007). *Geologic Map of the State of Hawaii*. US Department of the Interior. USGS.

Silva, J. H., Deenik, J. L., Yost, R. S., Bruland, G. L., & Crow, S. E. (2015). Improving clay content measurement in oxidic and volcanic ash soils of Hawaii by increasing dispersant concentration and ultrasonic energy levels. *Geoderma*, *237*, 211-223.

Soil Survey Staff. (2014a). *Keys to Soil Taxonomy, 12th Edition*. USDA, Natural Resources Conservation Service, Washington, DC.

Soil Survey Staff. (2014b). *Soil Survey Field and Laboratory Methods Manual*. Soil Survey Investigations Report No. 51, Version 2.0. R. Burt and Soil Survey Staff (ed.). U.S. Department of Agriculture, Natural Resources Conservation Service.

Soil Survey Staff. (2014c). *Kellogg Soil Survey Laboratory Methods Manual*. Soil Survey Investigations Report No. 42, Version 5.0. R. Burt and Soil Survey Staff (ed.). U.S. Department of Agriculture, Natural Resources Conservation Service.

Stearns, H. T., & MacDonald, G. A. (1942). Geology and groundwater resources of the island of Maui, Hawaii. *Advertiser Publishing Co., Ltd*., Honolulu, Hawaii.

Stewart, B. W., Capo, R. C., & Chadwick, O. A. (2001). Effects of rainfall on weathering rate, base cation provenance, and Sr isotope composition of Hawaiian soils. *Geochimica et Cosmochimica Acta*, *65*(7), 1087-1099.

Strawn, D. G., Bohn, H. L., & O'Connor, G.A. (2015). *Soil Chemistry*. John Wiley & Sons.

Thomas, W. L., Thomas, J. E., & Moody, L. E. (2008). Petrographic Microscope Techniques for Identifying Soil Minerals in Grain Mounts. p. 161 - 190. *In* Ulery, A.L. and L.R. Drees (ed.'s) *Methods of Soil Analysis*. SSSA Book Ser. 5. SSSA, Madison, WI.

Vitousek, P. M., Chadwick, O. A., Crews, T. E., Fownes, J. H., Hendricks, D. M., & Herbert, D. (1997). Soil and ecosystem development across the Hawaiian Islands. *GSA Today*, *7*(9), 1-8.

Vitousek, P. M., & Chadwick, O.A. (2013). Pedogenic thresholds and soil process domains in basalt-derived soils. *Ecosystems*, *16*(8), 1379-1395.

Walker, A. L. (1983). The effects of magnetite on oxalate-and dithionite-extractable iron. *Soil Science Society of America Journal*, *47*(5), 1022-1026.

Whittig, L. D., & W. R. Allardice. (1986). X-ray diffraction techniques. In Klute, A. (ed) *Methods of Soil Analysis, Physical and Mineralogical Methods, 2nd Edition*. SSSA, Madison, WI.

APPENDIX

Table 2-2a. Chemical property data of all study pedons and horizons with depth-weighted averages to 1-m, or root restricting layer, across the study area of western Haleakalā, Maui.

Pedon	**Horizon**	**Depth**	**OC**	**pH**		**EC**	**P-Ret.[a]**	**Al**
						1:5		**1N KCl**
		cm	%	1:5	$BaCl_2$	dS m^{-1}	%	$cmol_c$ kg^{-1}
KI-N1	A	0-10	1.39	6.1	6.3	0.28	41	--
	Bo1	10-21	0.79	7.1	6.3	0.03	46	--
	Bo2	21-31	0.68	6.8	6.4	0.03	50	--
	2Bw	31-57	0.86	6.4	6.3	0.07	72	--
		wt. avg.	0.91	6.6	6.3	0.09	58	--
KI-N2	A	0-8	1.51	6.6	6.0	0.07	40	--
	AB	8-21	0.81	7.0	6.2	0.04	45	--
	Bw1	21-40	0.60	7.1	6.3	0.04	51	--
	Bw2	40-65	0.53	7.0	6.2	0.05	68	--
	2Bw3	65-108	0.51	7.0	6.4	0.06	84	--
		wt. avg.	0.64	7.0	6.3	0.05	67	--
KI-S1	A	0-14	1.64	6.5	6.4	0.15	33	--
	Bw	14-34	0.65	6.9	6.6	0.04	35	--
	Bt1	34-46	0.64	7.0	6.8	0.04	39	--
	2Bt2	46-57	0.63	7.0	6.8	0.04	45	--
		wt. avg.	0.89	6.8	6.6	0.07	37	--
AIR	Ap1	0-15	0.92	7.6	8.4	0.43	73	--
	Ap2	15-24	1.04	7.8	8.5	0.14	76	--
	Bw1	24-33	0.90	7.9	8.4	0.15	69	--
	Bw2	33-72	0.50	8.1	8.1	0.15	73	--
	Bw3	72-91	0.59	8.1	7.9	0.16	70	--
	2Bw4	91-99	0.28	8.2	7.8	0.16	69	--
		wt. avg.	0.65	8.0	8.1	0.20	72	--
KI-S2	A	0-10	4.14	6.9	6.3	0.07	78	--
	Bw1	10-30	2.23	7.1	6.4	0.07	88	--
	2Bw2	30-36	0.85	7.6	6.8	0.07	83	--
		wt. avg.	2.53	7.1	6.5	0.07	85	--
OV	Ap	0-6	2.04	6.0	5.7	0.08	54	--
	A	6-16	1.01	6.7	6.3	0.05	66	--
	Bw1	16-40	1.29	6.8	6.2	0.05	61	--
	Bw2	40-60	1.36	6.7	6.4	0.10	58	--
	2Bw3	60-78	0.86	6.8	6.7	0.13	68	--
		wt. avg.	1.23	6.7	6.3	0.08	62	--

Pedon	Horizon	Depth	OC	pH		EC 1:5	P-Ret.[a]	Al 1N KCl
		cm	%	1:5	$BaCl_2$	dS m^{-1}	%	$cmol_c$ kg^{-1}
CEM	Ap	0-18	1.13	8.6	8.6	0.20	82	--
	Bo1	18-33	0.38	8.4	8.5	0.24	60	--
	Bo2	33-48	0.37	8.4	8.6	0.35	59	--
	Bo3	48-54	0.42	8.4	8.7	0.82	63	--
		wt. avg.	0.63	8.5	8.6	0.32	67	--
LKUL	Ap	0-13	5.14	6.3	5.9	0.21	95	--
	AB	13-35	4.96	6.4	5.9	0.11	99	--
	Bw1	35-58	6.08	6.7	6.0	0.08	100	--
	2Bw2	58-76	7.20	5.9	5.2	0.09	100	2.9
	2Bw3	76-100	6.10	5.5	4.8	0.10	100	3.6
		wt. avg.	5.92	6.1	5.5	0.11	99	1.4
UKUL	A	0-16	4.71	6.6	6.3	0.21	71	--
	Bt1	16-41	1.07	7.0	6.3	0.09	86	--
	Bt2	41-80	0.26	7.0	6.5	0.07	84	--
	Bw	80-100	0.25	7.3	6.6	0.07	83	--
		wt. avg.	1.17	7.0	6.4	0.10	82	--
HALE	A	0-9	19.23	6.5	5.9	0.16	96	--
	AB	9-20	15.67	6.5	5.8	0.11	99	--
	2Bw1	20-48	12.89	6.5	5.8	0.08	100	--
	2Bw2	48-100	11.17	6.3	5.5	0.05	100	2.3
		wt. avg.	12.87	6.4	5.6	0.07	100	1.2
PAIA	Ap	0-11	1.83	7.0	6.1	0.07	58	--
	A	11-21	1.71	7.2	6.3	0.07	60	--
	Bo1	21-44	1.42	7.3	6.4	0.05	63	--
	Bo2	44-71	0.90	6.8	5.9	0.06	63	--
	Bo3	71-100	0.39	6.6	5.5	0.06	65	2.0
		wt. avg.	1.06	6.9	5.9	0.06	63	0.6
HR	N/A	0-4	N/A	N/A	N/A	NA	N/A	N/A
	Ap	4-20	8.34	6.1	5.7	0.23	95	--
	2Bw1	20-40	2.54	6.5	5.8	0.07	98	--
	2Bw2	40-68	1.56	6.7	6.0	0.05	99	--
	2Bw3	68-100	1.26	6.7	6.1	0.05	99	--
		wt. avg.	2.68	6.3	5.7	0.08	94	--
MAKA	A	0-13	8.11	6.6	5.6	0.49	77	--
	AB	13-23	4.96	7.0	5.8	0.10	87	--
	Bw1	23-45	3.35	7.0	6.0	0.09	97	--
	2Bw2	45-63	2.26	6.9	6.1	0.09	96	--
	2Bw3	63-80	2.06	6.8	6.1	0.10	96	--
	2Cr	80-100	1.18	6.9	6.1	0.08	92	--

Pedon	Horizon	Depth	OC	pH		EC 1:5	P-Ret.[a]	Al 1N KCl
		cm	%	1:5	$BaCl_2$	dS m^{-1}	%	$cmol_c$ kg^{-1}
		wt. avg.	3.28	6.9	6.0	0.14	92	--
HAI-W	Ap1	0-15	3.06	5.1	4.5	0.11	61	3.2
	Ap2	15-37	1.82	4.7	4.4	0.04	51	5.0
	Bt1	37-54	1.52	4.6	4.3	0.04	51	5.2
	Bt2	54-68	2.05	4.7	4.3	0.04	61	4.5
	Bt3	68-91	2.21	4.8	4.3	0.04	58	4.6
	Bt4	91-100	2.25	4.7	4.1	0.03	71	2.7
		wt. avg.	2.12	4.8	4.3	0.05	57	4.4
OL	N/A	0-3	N/A	N/A	N/A	NA	N/A	N/A
	Ap	3-18	4.39	6.3	5.3	0.08	94	2.6
	AB	18-33	4.97	5.9	4.8	0.06	70	2.8
	Bw1	33-51	3.94	5.3	4.6	0.03	79	3.2
	Bw2	51-83	4.30	5.1	4.6	0.02	92	3.9
	2A	83-105	10.74	5.2	4.7	0.01	100	3.8
		wt. avg.	5.57	5.3	4.6	0.03	86	3.3
HAI-E	Ap	0-13	3.18	5.7	4.6	0.07	64	4.3
	AB	13-24	2.49	5.1	4.5	0.04	65	4.6
	Bt1	24-48	2.41	4.9	4.5	0.02	82	5.3
	Bt2	48-72	1.28	4.8	4.3	0.03	68	6.6
	Bt3	72-104	0.89	4.5	4.2	0.03	62	6.0
	Cr	104-120	0.85	4.4	4.1	0.03	64	N/A
		wt. avg.	1.66	4.8	4.3	0.03	68	5.6

Note. P-Ret., phosphate retention; OC, organic carbon; EC, electrical conductivity; --, not determined; N/A, not applicable (root mat).

Table 2-2b. NH_4OAc and $BaCl_2$ chemical property data of all study pedons and horizons with depth-weighted averages to 1-m, or root restricting layer, across the study area of western Haleakalā, Maui.

Pedon	Depth	$BaCl_2$						NH4OAc					
		Exchangeable Base Cations						Exchangeable Base Cations					
		Ca	Mg	Na	K	BS	CEC	Ca	Mg	Na	K	BS	CEC
	cm	----------$cmol_c\ kg^{-1}$----------				%	----------$cmol_c\ kg^{-1}$----------					%	$cmol_c\ kg^{-1}$
KI-N1	0-10	12.6	5.2	0.3	3.5	100	19.1	15.5	7.6	0.4	4.6	173.6	16.2
	10-21	10	4	0.2	1.9	100	12.6	6.5	3.1	0.4	1.9	85.6	13.9
	21-31	9.4	4	0.3	1.4	90.4	16.7	6.3	3.2	0.3	1.4	81.9	13.7
	31-57	6.5	3	0.6	0.7	92.2	11.7	4.1	2.3	0.4	0.7	62.8	11.9
	wt. avg.	8.8	3.7	0.4	1.5	100	14.0	6.9	3.5	0.4	1.7	90.0	13.3
KI-N2	0-8	12.7	4.7	0.2	3.2	94.0	22.0	12.8	5.8	0.5	4.8	139.4	17.2
	8-21	13.5	5.2	0.2	2.1	93.8	22.4	13.4	6.5	0.5	3.4	139.9	17.0
	21-40	12.4	5.0	0.2	1.1	94.0	20.0	12.3	6.1	0.5	1.7	132.2	15.6
	40-65	10.3	4.0	0.3	0.2	93.2	15.9	10.3	5.0	0.7	0.4	116.3	14.1
	65-108	5.9	2.2	0.6	0.1	96.5	9.1	6.4	2.8	0.9	0.1	118.0	8.7
	wt. avg.	9.5	3.6	0.4	0.8	94.8	15.1	9.9	4.7	0.7	1.3	124.8	13.1
KI-S1	0-14	24.0	6.5	0.2	4.6	99.8	35.4	19.4	7.1	0.2	6.2	163.5	20.1
	14-34	23.4	6.9	0.3	2.2	99.7	33.0	23.9	8.7	0.5	3.5	178.1	20.5
	34-46	24.1	7.1	0.4	1.3	86.1	38.1	14.9	5.2	0.2	1.3	103.9	20.7
	46-57	23.5	6.8	0.5	1.3	86.4	37.0	16.4	5.8	0.4	1.4	116.7	20.5
	wt. avg.	23.7	6.8	0.3	2.4	94.3	35.4	19.4	7.0	0.3	3.3	147.1	20.4
AIR	0-15	18.9	3.1	0.3	2.7	100	18.5	45.9	4.1	0.4	1.2	511.2	10.1
	15-24	18.9	2.9	0.5	0.5	100	18.5	42.7	3.8	0.6	0.4	446.4	10.6
	24-33	16.8	3.1	0.9	0.1	100	16.4	45.2	5.1	1.3	0.2	487.0	10.6
	33-72	11.7	2.4	4.4	0.1	100	13.7	10.3	2.1	2.9	0.1	112.0	13.7
	72-91	11.1	2.8	5	0.1	100	15.2	13.1	3.7	4.6	0.1	164.8	13.1

Pedon	Depth	$BaCl_2$						NH4OAc					
		Exchangeable Base Cations						Exchangeable Base Cations					
		Ca	Mg	Na	K	BS	CEC	Ca	Mg	Na	K	BS	CEC
	cm	----------$cmol_c\ kg^{-1}$----------				%	----------$cmol_c\ kg^{-1}$----------					%	$cmol_c\ kg^{-1}$
	91-99	10.2	2.9	5.3	0.1	100	14.1	11.5	3.8	5.2	0.1	148.3	13.9
	wt. avg.	13.7	2.7	3.3	0.5	100	15.4	22.5	3.3	2.7	0.3	310.6	12.0
KI-S2	0-10	25.3	7.4	0.4	2.4	88.6	40.1	24.6	9.9	0.9	4.0	183.7	21.4
	10-30	24.3	6.8	0.8	0.7	84.6	38.5	27.6	9.8	1.4	1.2	185.7	21.6
	30-36	24.3	5.9	2.1	0.4	100	28.8	26.6	8.0	3.0	0.6	186.3	20.4
	wt. avg.	24.6	6.8	0.9	1.1	90.5	37.3	26.6	9.5	1.5	1.9	185.3	21.3
OV	0-6	16.2	4.2	0.3	3.3	100	23.3	16.3	5.1	0.6	4.5	128.4	20.5
	6-16	18.8	4.1	0.8	1.7	100	25	16.6	4.6	1.0	2.3	131.4	18.7
	16-40	24.4	3.9	0.9	0.6	98.7	30.1	25.1	4.8	1.3	0.9	160.5	20.0
	40-60	27.6	5.1	0.9	0.4	97.8	34.7	23.7	5.7	1.1	0.7	149.5	20.8
	60-78	21.4	4.4	0.9	0.9	100	27.1	24.4	5.5	1.2	1.3	172.6	18.8
	wt. avg.	23.2	4.4	0.8	1.0	99.9	29.4	22.8	5.2	1.1	1.4	154.3	19.8
CEM	0-18	16.3	3.1	0.7	1.2	100	13.7	65.7	8.7	1.5	1.4	814.5	9.5
	18-33	12.1	3.3	1.1	2.3	100	12.1	32.4	6.2	1.6	3.2	320.7	13.5
	33-48	10.7	3.8	1.5	2.3	100	13.3	28.0	7.7	2.2	3.4	424.9	9.7
	48-54	9.7	5.8	3.9	2.3	100	13.1	31.0	13.7	4.8	3.2	622.3	8.5
	wt. avg.	12.8	3.7	1.4	1.9	100	13.1	42.1	8.3	2.1	2.7	547.7	10.6
LKUL	0-13	21.9	7.3	0.3	2.9	99.9	32.4	20.9	8.5	0.6	3.8	151.2	22.3
	13-35	24.3	8.0	0.4	1.2	99.5	34.2	24.6	9.5	0.8	1.8	160.7	22.9
	35-58	20.8	10.9	0.6	0.3	89.0	36.7	24.8	15.1	1.0	0.5	171.6	24.1
	58-76	8.8	7.8	0.3	0.2	92.8	18.3	8.4	10.1	0.6	0.2	77.8	24.8
	76-100	4.5	4.3	0.3	0.1	100	7.6	3.0	5.4	0.7	0.2	42.2	22.1
	wt. avg.	15.7	7.6	0.4	0.8	100	25.3	16.1	9.8	0.8	1.1	118.6	23.2

Pedon	Depth	$BaCl_2$						NH4OAc					
		Exchangeable Base Cations						Exchangeable Base Cations					
		Ca	Mg	Na	K	BS	CEC	Ca	Mg	Na	K	BS	CEC
	cm	----------$cmol_c\ kg^{-1}$----------				%	----------$cmol_c\ kg^{-1}$----------					%	$cmol_c\ kg^{-1}$
UKUL	0-16	22.3	8.4	0.2	4.9	98.8	36.4	23.8	10.1	0.4	6.9	191.7	21.5
	16-41	12.2	4.5	0.2	5.0	100	19.2	11.5	4.7	0.5	7.0	124.9	19.0
	41-80	10.6	4.1	0.4	3.4	100	14.3	10.8	4.7	0.7	4.8	123.1	17.0
	80-100	12	4.2	1.8	0.3	100	13.9	12.1	4.8	2.6	0.4	121.2	16.4
	wt. avg.	13.2	4.9	0.6	3.4	100	19	13.3	5.6	1.0	4.8	134.1	18.1
HALE	0-9	35.6	9.3	0.2	2.1	92.7	51.1	41.5	13.0	0.6	3.1	229.6	25.3
	9-20	37.7	5.7	0.2	2.2	96.1	47.7	41.4	7.8	0.6	3.2	210.5	25.1
	20-48	37.4	3.6	0.2	1.4	100	38.5	38.6	4.7	0.5	2.0	220.0	20.8
	48-100	24.8	2.2	0.2	0.5	100	21.5	25.7	2.9	0.6	0.7	117.6	25.4
	wt. avg.	30.7	3.6	0.2	1.1	100	31.8	32.5	4.8	0.5	1.6	166.6	24.1
PAIA	0-11	16.3	2.2	0.3	0.8	100	16.9	18.6	2.8	0.7	1.1	159.8	14.6
	11-21	16.3	1.8	0.3	0.4	100	16	19.9	2.5	0.6	0.7	164.7	14.4
	21-44	13	1.3	0.3	0.2	100	11.4	14.6	1.6	0.6	0.3	136.3	12.6
	44-71	8.6	1.2	0.5	0.1	100	7.7	9.1	1.4	0.9	0.2	94.8	12.2
	71-100	6.6	1.8	0.7	0.1	100	8.2	6.7	2.0	1.2	0.2	91.5	11.1
	wt. avg.	10.6	1.6	0.5	0.2	100	10.5	11.8	1.9	0.9	0.4	117.5	12.4
HR	0-4	N/A	N/A	N/A	N/A	N/A	N/A	N/A	N/A	N/A	N/A	N/A	N/A
	4-20	19.0	8.1	0.3	3.2	98.2	31	19.7	9.7	0.5	4.3	151.7	22.5
	20-40	12.0	3.3	0.3	3.3	100	18.2	12.3	3.7	0.6	4.5	109.0	19.3
	40-68	10.0	2.8	0.5	0.8	100	13.5	8.3	2.6	0.9	1.0	64.0	20.0
	68-100	7.4	2.3	0.4	0.1	98.3	10.4	7.7	2.6	0.6	0.2	68.3	16.3
	wt. avg.	10.6	3.5	0.4	1.4	100	15.7	10.8	4.0	0.7	2.0	89.4	19.04
MAKA	0-13	17.4	7.2	0.3	4.7	100	27.0	21.3	10.0	0.7	5.4	181.2	20.6

Pedon	Depth	$BaCl_2$						NH4OAc					
		Exchangeable Base Cations						Exchangeable Base Cations					
		Ca	Mg	Na	K	BS	CEC	Ca	Mg	Na	K	BS	CEC
	cm	----------$cmol_c\ kg^{-1}$----------				%	----------$cmol_c\ kg^{-1}$----------					%	$cmol_c\ kg^{-1}$
	13-23	14.6	6.2	0.2	3.4	98.0	25.0	17.1	8.3	0.6	4.8	148.5	20.8
	23-45	8.2	4.3	0.2	2.9	90.1	17.3	10.2	5.8	0.5	3.9	111.8	18.3
	45-63	7.2	2.8	0.2	2.6	97.2	13.1	9.2	3.8	0.5	3.7	97.9	17.6
	63-80	6.5	2.3	0.2	2.8	99.5	11.9	7.6	2.9	0.5	3.7	84.3	17.4
	80-100	4.7	1.5	0.2	3.8	100	9.8	5.6	2.0	0.5	5.4	83.5	16.1
	wt. avg.	8.9	3.7	0.2	3.3	99.0	16.1	10.8	5.0	0.5	4.4	111.6	18.1
HAI-W	0-15	1.5	1.3	0.3	0.5	70.2	5.2	1.2	1.5	0.5	0.4	26.3	14.0
	15-37	0.3	0.2	0.2	0.2	25.3	3.7	0.3	0.2	0.4	0.3	11.3	10.7
	37-54	0.3	0.1	0.2	0.2	23.3	3.3	0.2	0.1	0.5	0.2	6.6	15.5
	54-68	0.5	0.2	0.2	0.2	35.1	3.4	0.5	0.3	0.5	0.4	14.7	11.3
	68-91	0.8	0.3	0.2	0.2	44.0	3.4	0.5	0.3	0.5	0.3	9.0	17.9
	91-100	0.6	0.1	0.2	0.1	42.3	2.4	0.4	0.1	0.5	0.2	6.8	17.5
	wt. avg.	0.7	0.4	0.2	0.3	38.9	3.6	0.5	0.4	0.5	0.3	12.3	14.4
OL	0-3	N/A	N/A	N/A	N/A	N/A	N/A	N/A	N/A	N/A	N/A	N/A	N/A
	3-18	4.5	2.5	0.2	1.5	98.7	8.9	4.7	3.2	0.5	2.4	60.3	17.9
	18-33	3.9	1.4	0.2	0.3	83.0	6.9	3.0	1.7	0.4	0.5	35.9	15.6
	33-51	5.2	1.6	0.2	0.2	96.8	7.4	4.3	1.9	0.5	0.3	43.3	16.1
	51-83	2.3	0.5	0.2	0	69.9	4.3	2.1	0.6	0.5	0.1	21.4	15.3
	83-105	0.8	0.1	0.1	0	51.6	2.0	0.7	0.2	0.4	0	6.2	21.4
	wt. avg.	2.9	1	0.2	0.3	75.8	5.3	2.7	1.3	0.5	0.5	30.1	16.5
HAI-E	0-13	0.3	0.5	0.2	0.2	33.3	3.7	0.2	0.7	0.5	0.3	15.2	10.8
	13-24	0.1	0.2	0.1	0.1	21.3	2.6	0.1	0.3	0.4	0.2	10.2	9.8
	24-48	0.1	0.1	0.2	0.1	22.5	2.3	0.1	0.1	0.6	0.1	7.6	10.5

Pedon	Depth	$BaCl_2$						NH4OAc					
		Exchangeable Base Cations						Exchangeable Base Cations					
		Ca	Mg	Na	K	BS	CEC	Ca	Mg	Na	K	BS	CEC
	cm	----------$cmol_c\ kg^{-1}$----------				%	----------$cmol_c\ kg^{-1}$----------					%	$cmol_c\ kg^{-1}$
	48-72	0.1	0.1	0.6	0.2	38.8	2.3	0.0	0.1	1.1	0.2	7.8	18.1
	72-104	0	0	0.5	0.2	37.9	2	0.0	0.0	1.0	0.3	9.5	14.2
	104-120	0	0	0.4	0.2	37.5	1.8	--	--	--	--	--	--
	wt. avg.	0.1	0.1	0.4	0.1	32.0	2.3	0.1	0.2	0.8	0.2	9.5	13.3

Note. NH_4OAc, ammonium acetate; $BaCl_2$, barium chloride; BS, base saturation; CEC, cation exchange capacity; --, not determined; N/A, not applicable (root mat).

Table 2-3. Physical property data of all study pedons and horizons with depth-weighted averages to 1-m, or root restricting layer, across the study area of western Haleakalā, Maui.

Pedon	**Depth**	**Bulk density**	**Sand**	**Clay**	**Coarse fragments >2 mm**	**-1500 kPa water retention[a]**
	cm	g cm^{-3}	----------%----------			wt. %
KI-N1	0-10	1.22	4	48	5	16
	10-21	1.18	1	55	0	16
	21-31	--	1	65	55	16
	31-57	--	1	75	85	19
	wt. avg.	1.20	2	65	49	17
KI-N2	0-8	1.08	5	51	0	18
	8-21	1.26	5	54	0	18
	21-40	1.23	4	57	0	18
	40-65	1.12	7	53	0	19
	65-108	1.09	11	50	0	22
	wt. avg.	1.14	8	52	0	20
KI-S1	0-14	1.11	1	46	0	19
	14-34	1.27	3	52	3	17
	34-46	1.07	2	58	5	19
	46-57	--	2	60	80	20
	wt. avg.	1.17	2	53	18	18
AIR	0-15	1.24	9	63	0	18
	15-24	1.15	7	68	0	18
	24-33	1.00	6	69	0	18
	33-72	1.28	11	53	0	20
	72-91	1.23	14	46	5	21
	91-99	--	4	45	10	22
	wt. avg.	1.22	10	55	2	20
KI-S2	0-10	0.99	12	37	0	24
	10-30	1.00	7	58	15	27
	30-36	--	2	74	50	32
	wt. avg.	1.00	8	55	17	27
OV	0-6	--	6	61	10	21
	6-16	--	3	72	10	21
	16-40	--	2	59	15	19
	40-60	0.77	4	55	0	20
	60-78	--	2	67	30	22
	wt. avg.	0.77	3	62	14	20
CEM	0-18	--	51	42	0	12
	18-33	--	2	84	0	22

Pedon	Depth	Bulk density	Sand	Clay	Coarse fragments >2 mm	-1500 kPa water retention[a]
	cm	g cm^{-3}	----------%----------			wt. %
	33-48	--	2	84	15	43
	48-54	--	5	83	15	23
	wt. avg.	--	19	70	6	24
LKUL	0-13	--	10	42	5	26
	13-35	--	9	40	15	32
	35-58	--	9	19	20	41
	58-76	--	6	14	30	43
	76-100	--	11	16	50	41
	wt. avg.	--	9	25	26	37
UKUL	0-16	1.13	4	60	5	29
	16-41	1.03	1	81	10	31
	41-80	1.13	1	79	20	32
	80-100	1.01	0	76	20	30
	wt. avg.	1.08	1	76	15	31
HALE	0-9	--	14	40	2	60
	9-20	0.52	14	46	20	62
	20-48	0.48	14	28	50	79
	48-100	0.52	30	12	50	104
	wt. avg.	0.51	22	23	42	88
PAIA	0-11	1.31	2	78	0	24
	11-21	1.35	2	78	0	25
	21-44	1.37	2	77	0	24
	44-71	1.43	1	84	0	27
	71-100	1.42	1	75	0	28
	wt. avg.	1.39	1	79	0	26
HR	0-4	N/A	N/A	N/A	N/A	N/A
	4-20	0.81	33	25	0	35
	20-40	0.83	8	56	0	30
	40-68	0.97	3	58	0	28
	68-100	1.06	5	51	5	28
	wt. avg.	0.91	9	48	2	29
MAKA	0-13	0.94	13	40	1	34
	13-23	1.05	13	45	1	30
	23-45	0.71	4	51	2	42
	45-63	0.90	8	45	10	40
	63-80	--	10	45	20	41

Pedon	Depth	Bulk density	Sand	Clay	Coarse fragments >2 mm	-1500 kPa water retention[a]
	cm	g cm^{-3}	----------%----------			wt. %
	80-100	--	4	49	40	35
	wt. avg.	0.87	8	46	14	38
HAI-W	0-15	1.46	5	45	0	17
	15-37	1.60	5	41	0	14
	37-54	1.61	3	57	0	18
	54-68	1.64	2	77	0	23
	68-91	1.53	1	76	0	23
	91-100	1.13	0	92	0	24
	wt. avg.	1.53	3	62	0	19
OL	0-3	N/A	N/A	N/A	N/A	N/A
	3-18	0.90	18	31	1	15
	18-33	1.10	5	40	0	25
	33-51	1.07	3	60	0	29
	51-83	0.66	5	48	3	41
	83-105	--	9	51	40	80
	wt. avg.	0.85	7	46	9	40
HAI-E	0-13	1.23	6	34	1	18
	13-24	1.15	9	36	3	18
	24-48	1.14	7	54	3	24
	48-72	--	10	53	35	22
	72-104	--	9	39	40	20
	104-120	--	10	25	60	17
	wt. avg.	1.17	9	42	27	20

Note. --, not determined.
[a] kPa, kilopascal.

Table 2-4. Selective dissolution extraction data of all study pedons and horizons with depth-weighted averages to 1-m across the study area of western Haleakalā, Maui.

Pedon	Depth	AO			HH		CD		PY	
		Fe	Al	Si	Fe	Al	Fe	Al	Fe	Al
		mg g^{-1}								
KI-N1	0-10	10.61	4.39	6.35	6.79	4.37	82.94	3.48	0.14	0.56
	10-21	9.98	3.71	3.92	4.93	3.8	89.21	3.26	0.11	0.66
	21-31	11.92	4.31	3.76	4.55	4	90.07	3.52	0.12	0.71
	31-57	23.17	8.32	4.87	3.54	5.89	92.19	8.1	0.23	0.92
	wt. avg.	16.45	6.04	4.75	4.56	4.89	89.62	5.55	0.17	0.77
KI-N2	0-8	8.63	3.79	5.79	4.92	4.05	90.45	3.97	0.33	0.88
	8-21	7.56	3.59	4.89	4.43	3.86	98.17	3.66	0.17	1.06
	21-40	11.82	4.16	3.93	4.06	3.75	99.03	3.85	0.2	0.97
	40-65	12.62	5.52	2.71	3.14	4.15	100.04	5.06	0.17	0.9
	65-105	16.51	6.41	5.33	4.36	5.11	113.58	11.21	0.14	0.75
	wt. avg.	13.12	5.27	4.46	4.07	4.42	104.32	7.05	0.18	0.87
KI-S1	0-14	8.1	3.47	3.47	7.68	5.26	59	2.15	0.33	0.9
	14-34	6.77	3.23	4.14	5.97	4.5	68.03	2.07	0.37	1.27
	34-46	6.95	3.4	4.26	5.97	4.63	70.87	2.14	0.48	1.51
	46-57	8.04	4.15	5.3	6.03	5.16	74.08	2.37	0.29	1.27
	wt. avg.	7.38	3.5	4.22	6.4	4.84	67.58	2.16	0.37	1.23
AIR	0-15	7.73	4.02	4.97	3.79	4.07	88.53	5.1	0.05	0.16
	15-24	10.1	4.78	4.83	3.41	3.89	91.43	5.37	0.04	0.2
	24-33	7.44	4.64	4.22	2.75	4.32	93.71	5.95	0.04	0.26
	33-72	4.62	5.47	4.56	1.04	4.64	86.68	8.36	0.08	0.59
	72-91	4.3	4.89	3.72	0.98	4.29	83.02	7.88	0.16	0.69
	91-99	5.58	5.56	3.74	1.06	4.52	75	6.43	0.12	0.69
	wt. avg.	5.86	5.01	4.39	1.82	4.38	86.38	7.13	0.08	0.49

Pedon	Depth	AO			HH		CD		PY	
		Fe	Al	Si	Fe	Al	Fe	Al	Fe	Al
		----------mg g^{-1}----------								
KI-S2	0-10	60.08	17.54	13.51	31.06	15.8	82.22	7.96	0.98	1.87
	10-30	67.85	19.44	14.48	41.89	17.19	91.84	9.1	0.88	1.7
	30-36	60.49	9.85	12.2	46.63	10.2	92.65	6.41	0.95	1.26
	wt. avg.	64.47	17.31	13.83	39.67	15.64	89.3	8.33	0.92	1.67
OV	0-6	33.55	8.85	7.09	21.37	8.9	77.56	6.38	0.98	1.26
	6-16	38.07	9.36	6.98	24.93	9.69	82.34	6.53	0.46	0.76
	16-40	34.89	10.49	6.36	22.72	11.4	80.11	6.73	0.64	1.2
	40-60	33.24	10.85	5.72	22.53	12.21	78.47	6.35	0.56	1.01
	60-78	37.09	10.04	8.06	23.9	10.12	84.21	6.75	0.31	0.58
	wt. avg.	35.28	10.21	6.73	23.12	10.9	80.73	6.58	0.55	0.96
CEM	0-18	4.1	2.46	4.32	2.11	3.31	33.45	2.4	0.04	0.3
	18-33	12.94	3.81	5.07	4.07	3.28	88.05	5.1	0.02	0.15
	33-48	13.36	3.82	5.32	4.41	3.22	90.34	5.3	0.01	0.13
	48-54	13.99	4.1	4.77	3.8	3.39	85.34	5.39	0.02	0.14
	wt. avg.	10.23	3.4	4.86	3.48	3.29	70.19	4.29	0.02	0.19
LKUL	0-13	38.09	43.14	22.19	18.38	41.19	58.42	13.41	3.76	5.33
	13-35	39.16	56.26	27.36	21.09	55.29	58.45	18.36	4.58	6.66
	35-58	38.95	102.5	51.76	28.03	106.31	52.8	32.57	4.71	8.16
	58-76	37.19	132.9	66.69	30.39	141.71	46.02	43.16	7.81	12.19
	76-100	43.39	132.1	77.16	31.47	133.77	51.76	61.12	13.33	17.98
	wt. avg.	39.63	97.2	51.33	26.5	99.58	53.3	35.71	7.19	10.54
UKUL	0-16	31.39	11.29	9.11	17.7	11.59	74.87	9.07	1.75	1.58
	16-41	34.86	9.88	5.63	21.21	9.42	82.48	9.75	0.8	0.87

Pedon	Depth	AO			HH		CD		PY	
		Fe	Al	Si	Fe	Al	Fe	Al	Fe	Al
		----------mg g^{-1}----------								
	41-80	31.64	8.65	4.88	12.32	6.52	73.66	8.46	0.59	0.88
	80-100	27.44	7.93	6.01	10.09	5.75	69.53	8.21	0.92	0.99
	wt. avg.	31.56	9.24	5.97	14.95	7.9	75.23	8.83	0.89	1.01
HALE	0-9	45.59	41.24	11.34	30.91	41.92	59.98	26.41	16.69	19.72
	9-20	58.26	51.81	13.47	38.6	51.88	76.1	34.77	29.61	27.47
	20-48	73.33	76.31	21.09	49.78	78.65	93.43	53.09	57.2	38.94
	48-100	59.86	119.45	45.46	45.5	128.53	69.67	57.69	23.95	22.19
	wt. avg.	62.17	92.9	32.05	44.63	98.34	76.16	51.06	33.23	27.24
PAIA	0-11	9.64	3.91	2.3	4.83	3.94	93.16	9.3	1.44	0.97
	11-21	10.09	3.87	4.5	4.09	3.77	92.37	9.26	1.44	0.89
	21-44	9.8	4.02	1.46	3.3	4.04	93.19	9.75	1.87	1.13
	44-71	8.99	3.75	4.9	2.39	3.06	93.08	10.34	1.25	1.26
	71-100	8.67	3.6	4.45	2.11	2.65	89.16	10.22	0.18	0.72
	wt. avg.	9.26	3.8	3.65	2.96	3.33	91.9	9.95	1.12	1
HR	0-4	N/A	N/A	N/A	N/A	N/A	N/A	N/A	N/A	N/A
	4-20	39.44	49.69	20.38	20.57	48.44	68.96	20.19	3.06	6.83
	20-40	40.46	37.3	13.08	21.35	37.1	82.64	23.56	5.88	6.12
	40-68	42.13	37.96	17.42	18.79	34.4	90.74	30.36	4.22	6.18
	68-100	38.98	37.37	16.06	16.69	32.82	85.59	33.4	2.49	5.07
	wt. avg.	38.67	38	15.89	18.16	35.3	80.36	27.13	3.65	5.67
MAKA	0-13	59.04	38.08	14.99	25.28	34.74	80.55	16.98	7.29	7.11
	13-23	58.88	40.45	15.52	28.61	38.37	93.01	19.56	5.46	6.28
	23-45	46.78	67.42	27.19	27.58	66.97	83.21	23.57	3.37	4.9

Pedon	Depth	AO			HH		CD		PY	
		Fe	Al	Si	Fe	Al	Fe	Al	Fe	Al
		----------mg g^{-1}----------								
	45-63	30.63	71.32	30.15	19.32	75.22	70.27	22.14	1.42	4.16
	63-80	21.72	65.93	27.43	15.94	70.14	47.43	19.07	1.45	3.88
	80-100	16.91	43.6	17.96	10.49	38.47	39.57	14.5	2.21	3.49
	wt. avg.	36.45	56.59	23.16	20.5	56.25	66.71	19.48	3.18	4.74
HAI-W	0-15	15.15	4.29	2.9	6.07	3.16	160.23	17.27	29.67	5.19
	15-37	11.04	3.21	1.33	3.36	2.49	158.95	15.86	22.69	4.13
	37-54	31.34	5.11	3.08	2.22	2.25	196.98	18.75	46.03	6.09
	54-68	45.73	6.86	1.83	2.08	2.32	240.05	23.97	80.94	9.79
	68-91	42.12	6.2	3.46	2.28	2.17	245.65	23.32	80.59	9.29
	91-100	60.11	7.69	3.7	2.15	1.95	308.2	28.68	143.05	14.21
	wt. avg.	31.53	5.3	2.64	3.04	2.4	210.34	20.57	60.01	7.51
OL	0-3	N/A	N/A	N/A	N/A	N/A	N/A	N/A	N/A	N/A
	3-18	25.31	38.18	20.41	10.81	36.64	73.58	13.19	35.69	6.88
	18-33	30.49	9.19	2.54	8.59	7.32	180	12.88	19.69	5.49
	33-51	88.32	9.43	4.12	25.15	5.72	237.95	14.84	90.57	8.86
	51-83	67.3	24.6	6.64	33.65	21.5	229.83	25.99	71.42	14.8
	83-105	27.6	137.08	46.9	22.39	142.23	85.66	68.63	19.14	26.64
	wt. avg.	49.41	44.6	15.84	22.03	43.61	165.01	28.57	49.21	13.38
HAI-E	0-13	17.3	4.72	1.51	10.61	3.78	89.01	12	30.15	6.07
	13-24	17.95	5.71	1.62	9.14	4.43	103.97	13.91	37.91	7.54
	24-48	59.24	14.97	2.98	10.17	7.87	142.36	22.62	63.51	13.74
	48-72	59.69	13.33	1.74	3.61	4.57	122.37	17.05	51.57	9.29
	72-104	48.6	11.33	3.52	2.33	3.99	107.86	15.21	36.85	6.93

Pedon	Depth	AO			HH		CD		PY	
		Fe	Al	Si	Fe	Al	Fe	Al	Fe	Al
		----------mg g^{-1}----------								
	104-120	37.63	10.43	3.08	2.42	4.06	102.04	14.23	23.76	5.35
	wt. avg.	45.28	11.11	2.6	5.69	4.91	114.49	16.46	42.75	8.52

Note. AO, ammonium oxalate; CD, citrate dithionite; HH, hydroxylamine hydrochloride hydrochloric acid; PY, sodium pyrophosphate; N/A, not applicable (root mat).

Table 2-5. Iron (AO-HH), amorphous Fe and Al (AO-PY), and crystalline Fe (CD-AO) of all study pedons and horizons with depth-weighted averages to 1-m, or root restricting layer, across the study area of western Haleakalā, Maui.

Pedon	Depth	Fe (AO-HH)	Amorphous Fe (AO-PY)	Al + 1/2Fe (AO)	Amorphous Al (AO-PY)	Crystalline Fe (CD-AO)
	cm			%		
KI-N1	0-10	0.38	1.05	0.97	0.38	7.23
	10-21	0.51	0.99	0.87	0.31	7.92
	21-31	0.74	1.18	1.03	0.36	7.82
	31-57	1.96	2.29	1.99	0.74	6.90
	wt. avg.	1.19	1.63	1.43	0.53	7.32
KI-N2	0-8	0.37	0.83	0.81	0.29	8.18
	8-21	0.31	0.74	0.74	0.25	9.06
	21-40	0.78	1.16	1.01	0.32	8.72
	40-65	0.95	1.25	1.18	0.46	8.74
	65-108	1.22	1.64	1.47	0.57	9.71
	wt. avg.	0.91	1.29	1.18	0.44	9.12
KI-S1	0-14	0.04	0.78	0.75	0.26	5.09
	14-34	0.08	0.64	0.66	0.20	6.13
	34-46	0.10	0.65	0.69	0.19	6.39
	46-57	0.20	0.78	0.82	0.29	6.60
	wt. avg.	0.10	0.70	0.72	0.23	6.02
AIR	0-15	0.39	0.77	0.79	0.39	8.08
	15-24	0.67	1.01	0.98	0.46	8.13
	24-33	0.47	0.74	0.84	0.44	8.63
	33-72	0.36	0.45	0.78	0.49	8.21
	72-91	0.33	0.41	0.70	0.42	7.87
	91-99	0.45	0.55	0.84	0.49	6.94
	wt. avg.	0.40	0.58	0.79	0.45	8.05
KI-S2	0-10	2.90	5.91	4.76	1.57	2.21
	10-30	2.60	6.70	5.34	1.77	2.40
	30-36	1.39	5.95	4.01	0.86	3.22
	wt. avg.	2.48	6.36	4.95	1.56	2.48
OV	0-6	1.22	3.26	2.56	0.76	4.40
	6-16	1.31	3.76	2.84	0.86	4.43
	16-40	1.22	3.43	2.79	0.93	4.52
	40-60	1.07	3.27	2.75	0.98	4.52
	60-78	1.32	3.68	2.86	0.95	4.71
	wt. avg.	1.22	3.47	2.78	0.93	4.55
CEM	0-18	0.20	0.41	0.45	0.22	2.94
	18-33	0.89	1.29	1.03	0.37	7.51

Pedon	Depth	Fe (AO-HH)	Amorphous Fe (AO-PY)	Al + 1/2Fe (AO)	Amorphous Al (AO-PY)	Crystalline Fe (CD-AO)
	cm		----------%----------			
	33-48	0.90	1.34	1.05	0.37	7.70
	48-54	1.02	1.40	1.11	0.40	7.14
	wt. avg.	0.68	1.02	0.85	0.32	6.00
LKUL	0-13	1.97	3.43	6.22	3.78	2.03
	13-35	1.81	3.46	7.58	4.96	1.93
	35-58	1.09	3.42	12.20	9.43	1.39
	58-76	0.68	2.94	15.15	12.07	0.88
	76-100	1.19	3.01	15.38	11.41	0.84
	wt. avg.	1.31	3.24	11.70	8.67	1.37
UKUL	0-16	1.37	2.96	2.70	0.97	4.35
	16-41	1.37	3.41	2.73	0.90	4.76
	41-80	1.93	3.11	2.45	0.78	4.20
	80-100	1.74	2.65	2.17	0.69	4.21
	wt. avg.	1.66	3.07	2.50	0.82	4.37
HALE	0-9	1.47	2.89	6.40	2.15	1.44
	9-20	1.97	2.87	8.09	2.43	1.78
	20-48	2.36	1.61	11.30	3.74	2.01
	48-100	1.44	3.59	14.94	9.73	0.98
	wt. avg.	1.75	2.89	12.40	6.57	1.40
PAIA	0-11	0.48	0.82	0.87	0.29	8.35
	11-21	0.60	0.87	0.89	0.30	8.23
	21-44	0.65	0.79	0.89	0.29	8.34
	44-71	0.66	0.77	0.82	0.25	8.41
	71-100	0.66	0.85	0.79	0.29	8.05
	wt. avg.	0.63	0.81	0.84	0.28	8.26
HR	0-4	N/A	N/A	NA	N/A	N/A
	4-20	1.89	3.64	6.94	4.29	2.95
	20-40	1.91	3.46	5.75	3.12	4.22
	40-68	2.33	3.79	5.90	3.18	4.86
	68-100	2.23	3.65	5.69	3.23	4.66
	wt. avg.	2.05	3.50	5.97	3.23	4.17
MAKA	0-13	3.38	5.18	6.76	3.10	2.15
	13-23	3.03	5.34	6.99	3.42	3.41
	23-45	1.92	4.34	9.08	6.25	3.64
	45-63	1.13	2.92	8.66	6.72	3.96
	63-80	0.58	2.03	7.68	6.21	2.57
	80-100	0.64	1.47	5.21	4.01	2.27
	wt. avg.	1.60	3.33	7.48	5.19	3.03

Pedon	Depth	Fe (AO-HH)	Amorphous Fe (AO-PY)	Al + 1/2Fe (AO)	Amorphous Al (AO-PY)	Crystalline Fe (CD-AO)
	cm		----------%----------			
HAI-W	0-15	0.91	-1.45	1.19	-0.09	14.51
	15-37	0.77	-1.17	0.87	-0.09	14.79
	37-54	2.91	-1.47	2.08	-0.10	16.56
	54-68	4.37	-3.52	2.97	-0.29	19.43
	68-91	3.98	-3.85	2.73	-0.31	20.35
	91-100	5.80	-8.29	3.77	-0.65	24.81
	wt. avg.	2.85	-2.85	2.11	-0.22	17.88
OL	0-3	N/A	N/A	NA	N/A	N/A
	3-18	1.45	-1.04	5.08	3.13	4.83
	18-33	2.19	1.08	2.44	0.37	14.95
	33-51	6.32	-0.23	5.36	0.06	14.96
	51-83	3.37	-0.41	5.82	0.98	16.25
	83-105	0.52	0.85	15.09	11.04	5.81
	wt. avg.	2.74	0.02	6.52	3.12	11.56
HAI-E	0-13	0.67	-1.29	1.34	-0.14	7.17
	13-24	0.88	-2.00	1.47	-0.18	8.60
	24-48	4.91	-0.43	4.46	0.12	8.31
	48-72	5.61	0.81	4.32	0.40	6.27
	72-104	4.63	1.18	3.56	0.44	5.93
	104-120	3.52	1.39	2.92	0.51	6.44
	wt. avg.	3.96	0.25	3.44	0.26	6.92

Note. AO, ammonium oxalate; CD, citrate dithionite; HH, hydroxylamine hydrochloride hydrochloric acid; PY, sodium pyrophosphate; N/A, not applicable (root mat).

III. UNDERSTANDING THE INFLUENCE OF VOLCANIC ASH ON SOIL WEATHERING USING ELEMENTAL TRENDS ACROSS MAUI CLIMOSEQUENCES

ABSTRACT

The western slopes of Haleakalā, Maui are greatly affected by orographic climate effect, creating a massive precipitation gradient and a rain shadow effect. However, the presence of volcanic vents along East Maui's northwest rift have created irregularity in the deposition of volcanic ash across the landscape, making it difficult to determine a soil's relative age and degree of ash-influence. The main goals of this study were to 1) characterize and classify the basalt substrate of pedons sampled across a wide climatic gradient; 2) determine how elemental composition and soil chemical properties vary with precipitation and elevation; 3) identify pedogenic thresholds of western Haleakalā climosequences; and 4) determine if elemental indices can distinguish pedons and soil horizons that have been influenced by volcanic ash.

We sampled 16 soils across elevational and precipitation gradients formed in Kula Volcanics on northwest-facing slopes <5%. Soils were sampled and described to 1-m depth. Total elemental analysis was determined on rock samples and soil horizons by x-ray fluorescence, and various soil physical and chemical properties were measured in the laboratory. A total of 22 weathering indices were applied across non-ash influenced and ash influenced climosequences.

Soil pedon rock samples were alkalic basalt and predominantly classified as tephrite basanite with four samples classifying as foidite. Pedogenic thresholds for SiO_2/TiO_2 were identified at 500 mm and 1300 mm MAP for the coastal climosequence,

showing that although pedon AIR had lower MAP than pedons CEM and PAIA, it is more weathered. Crystalline Fe (CD-AO) for pedons KI-N1, KI-N2, and AIR was very high considering the low MAP, demonstrating that although KI-N1 and KI-N2 were rejuvenated by volcanic ash (with volcanic glass in the deepest horizon of AIR), these soils are likely much older than soils closer to the summit of Haleakalā. Soil SiO_2/TiO_2 and MnO/TiO_2 normalized to the pedon rock fragments may be a viable indicator for distinguishing ash-rejuvenated soil pedons and genetic horizons from those that are not.

INTRODUCTION

Weathering and formation of soils derived from basalts have been studied using climosequences (Chadwick et al., 2003; Gardiner, 1967), elevational sequences (Meijer and Buurman, 2003; Rasmussen et al., 2010), and chronosequences (He et al., 2008; Zhang et al., 2007). Soil, as a component of an open system, is subject to water input and associated chemical reactions of soil bases with atmospheric acidity (Chadwick and Chorover, 2001). Buffering capacity of a soil controls the extent of these reactions and is highly dependent on soil mineral composition and quantity. But as we see with climosequences with increasing rainfall, boundaries, or pedogenic thresholds, are created where primary minerals such as potassium feldspar transform to create kaolinite, halloysite, or montmorillonite, for example. Or, primary minerals weather completely, creating thresholds in pH and base saturation as bases and silica are lost and Al and Fe are enriched in a soil (Chadwick et al., 2003; Chadwick and Chorover, 2001; Gardiner, 1976; Vitousek et al., 2016). These processes are also observed in climosequences where increasing elevation causes a decrease in mean annual temperature and an increase in

mean annual precipitation to a winter snowline before decreasing. On a basalt elevational sequence of the Cascade Range, California (Rasmussen et al., 2010), maximum soil development occurred just below the winter snowline, where soil displayed high loss of base cations, high clay content, and were dominated by secondary minerals including halloysite, kaolinite, and Fe oxyhydroxides. Also, along chronosequences in the South China Sea, base cations and silica were strongly leached and Al and Fe were enriched (Zhang et al., 2007), and pH and cation exchange capacity (CEC) decreased (He et al., 2008), with increasing soil age.

The deposition and influence of volcanic ash on soil weathering has provided unique opportunities for sequence studies. Chrono- and climosequence studies (Candra et al., 2019; Candra et al., 2021) in the Galapagos have provided insight into the effects of volcanic ash additions on the chemical, physical, and mineralogical weathering on soils of varying age and climate (as a result of elevation). With increasing soil age, pH, organic carbon, and CEC decreased. Areas of low evapotranspiration favored the formation and accumulation of short-range-order (SRO) materials and organic carbon. Soils formed on cinder cones in a dry, cold environment of southern Idaho (Vaughan et al., 2018) showed an accumulation of SRO materials, eluviation of Fe, Al, and Ti from surface horizons, and an accumulation of crystalline materials with soil age. Along an elevation transect of the Equadorian Andes, Zehetner et al. (2003) determined that climate was the overriding factor contributing to soil weathering differences of pedons at varying elevations. Additionally, Zehetner et al. (2003) found that the increase in organic carbon with elevation is the due to the decrease in microbial decomposition of organic matter with decreasing temperature.

The weathering of volcanic ash-influenced soils across climatic and elevational gradients creates wide variations in pedogenic weathering sequences as well as mixed mineralogy systems unique to individual pedons. It is because of these mixed mineralogy systems that volcanic ash soils exhibit a spectrum of unique chemical properties that reflect their parent material and their degree of weathering, including organic matter, active Fe and Al, and variable charge surfaces (Nanzyo et al., 1993). Isolating soil forming factors has been the conventional and ideal approach in understanding soil forming factor-process-property relationships since the introduction of soil forming factors by Jenny (1941). However, the mantling of volcanic ash across landscapes that are at various stages of pedogenic weathering complicates the ability to interpret soil weathering pathways across various sequences. Volcanic ash is dominated by amorphous glass and is similar in chemical composition as the source parent rock, except volcanic glass has a higher silica content (Shoji et al., 1975). Volcanic glass also shows the least resistance to weathering due to its porous and fine particle size (Dahlgren et al., 1993), releasing base cations and silica into soil solution, and allowing for the rapid formation of SRO materials such as allophane and imogolite.

Operationally defined methods have been developed to quantify the various phases of Fe, Al, and/or Si—such as organo-bound Fe and Al (McKeague, 1967), noncrystalline phases (Shang and Zelanzy, 2008), and free Fe (Soil Survey Staff, 2014b). Other soil properties used to determine andic soils, or soils influenced by SRO materials, include Al + ½Fe extracted by ammonium oxalate (AO), bulk density, and phosphate retention (Soil Survey Staff, 2014c). However, these methods become inadequate for determining if a soil has been influenced by volcanic ash in poorly weathered, or mixed

mineralogy, soils. Glass count of the very fine sand and coarse silt fractions is used by the Natural Resources Conservation Service (NRCS) in classifying andic soil properties in poorly weathered soils.

In a chronosequence (0.4-3 Ma) of soils on terrace remnants dominated by granitic parent material from the Sierra Nevada, Harden (1988) found that Fe, Mn, Al and Ti were retained relative to the alkali and alkali-earth elements, and there was a significant shift of Ti and Fe into the fine fraction over time. Applying an immobile, stable or resistant element, such as Ti, as a reference element would help distinguish net losses and gains of elements of interest from relative changes to Ti (Harden, 1988). Percent loss of an element in this study was adapted from Merrill (1906). While Ti was immobile, clay was not and can mobilize through the soil profile (Harden, 1988).

A weathering sequence of soils formed in relatively young (hundreds to thousands of years old) andesitic ash parent material in Costa Rica (Meijer and Buurman, 2003) occurred across an elevational transect (40-3300 m) on the Turrialba volcano. With increasing elevation, rainfall increased to the cloud layer then decreased, while air temperature continued to decrease. Mean annual precipitation increased from 4000 mm yr^{-1} in the lowlands (26 °C mean annual temperature (MAT)), to 7000 mm yr^{-1} at 1000 m elevation (20 °C MAT), then decreased to 2500 mm yr^{-1} above the cloud layer at the volcano summit (3300 m, 9 °C MAT). Elemental loss of soils relies on comparing the concentration of a referenced immobile element, typically Ti, Al, or Zr to the parent material. An increase in Ti, Al, or Zr concentration in soil would indicate weathering and the loss of more mobile elements. Using a weathering index (WI) derived from Ti, V, and Zr contents by factor analysis, Meijer and Buurman (2003) observed a sharp increase in

WI values on andic soils with decreasing elevation below 1200 m, where rainfall was higher, and temperatures were warmer below the 1200 m cloud layer. Across four volcanic soils of increasing rainfall and age developed from deposits of the Gauro and Vico volcanoes in Italy, Cortizas et al. (2003) observed a slight enrichment of elements Mn, Zn, and As, mainly in organic-rich surface horizons, a relative collapse of K and Ti, and an increase in amorphous Al and Fe and phosphate retention.

An exhaustive list of 31 weathering indices was assessed against the soil weathering stage of pyroclastic rock in Hong Kong (Duzgoren-Aydin, 2002). The indices assessed are proposed elsewhere in the literature for various types of rock, including mafic, ultramafic, intermediate, acidic, volcanic, and granitic. Many of the indices are defined as ratios with some intended to assess the degree of weathering compared to an unweathered sample. Many of the indices calculate ratios of mobile elements or oxides (e.g., Na_2O, K_2O, SiO_2) to less mobile or non-mobile elements/oxides such as Al_2O_3, Fe_2O_3, and TiO_2. For example, the silica-titania index (STI) observes the behavior of silica (SiO_2) against less mobile elements (Ti, and Al) (Taboada et al., 2016).

Isla Santa Cruz in the Galapagos, Equador is covered in basaltic lava flows of the Shield Series ranging between 590 kya and 24 kya (Taboada et al., 2016; White et al., 1993). The weathering of 43 soils along a windward sequence from the coast (500 mm MAP) to above 500 m in elevation where MAP ranges between 1500 mm and 2000 mm were assessed using several weathering indices. There is a residual accumulation of Al and Fe due to loss of mobile elements such as Si. Taboada et al. (2016) utilized a SiO_2-Al_2O_3-Fe_2O_3 ternary diagram, proposed by Chesworth (1973), to observe these elemental changes across the toposequence. There was a depletion of Si and an enrichment of Al in

pedons which received greater than 1500 mm yr^{-1} rainfall (Taboada et al., 2016). Values of the STI index did not change gradually or predictably with soil depth, likely due to additions of younger materials or volcanic ash deposition. Additionally, STI decreased with elevation, likely due to the progressive increase in rainfall and weathering with increasing elevation. Other indices observed by Taboada et al. (2016) included weathering index of Parker (WIP) (also known as the Parker Index (PI)), chemical index of alteration (CIA), chemical index of weathering (CIW), and plagioclase index of alteration (PIA), and were well correlated with each other, with the exception of STI. High WIP and STI values were associated with young basalt flows, while low WIP values represented more weathered soils.

In 20 volcanic pedons across Europe, Taboada et al. (2007) showed the Normalized Chemical Index of Alteration (NCIA) (Nesbitt and Young, 1982) to be well correlated ($R^2 = 0.83$) with noncrystalline Al (extracted by ammonium oxalate). However, this correlation was weakened in two pedons that had relatively higher concentrations of halloysite and gibbsite. Therefore, NCIA and noncrystalline Al (extracted by ammonium oxalate) can be used as weathering indices to compare vitric versus andic soils to assess degree of weathering and development (Taboada et al., 2007).

On the Kohala Peninsula of the Big Island of Hawaii, (Chadwick et al., 2003; Stewart et al., 2001; Vitousek et al., 2016), a soil climosequence on a basalt substrate where mean annual precipitation (MAP) ranged from 160 mm to >3000 mm exhibited a sharp decrease in base cations, including silica and Al, at 1400 mm MAP. In terms of leaching and elemental loss, arid soils saw movement of bases and silica to shallow depths, while Al saw no movement at all; whereas, at the humid sites (>1400 mm MAP)

base cations and silica were depleted (Steward et al., 2001) with Al decreasing by as much as 60% relative to the parent rock (Chadwick et al., 2003). On a Kauai climosequence (Vitousek and Chadwick, 2013), Fe is high to around 1700 mm MAP before decreasing at wetter sites.

Five of the eight major Hawaiian Islands experience climosequences due to varying levels of precipitation. The soil climosequence studies of the Kohala area of the Hawai‘i Island belong to relatively young substrates and have not undergone substantial soil maturity. There are many volcanic vents across the Kohala Peninsula, and therefore, these soils may have been influenced by volcanic ash, but relevant studies (Chadwick et al., 2003; Vitousek and Chadwick, 2013) do not address ash as a second parent material in soil formation. The island of Maui, specifically, western Haleakalā, on the other hand, has eight mapped soil orders and consists of a broad climosequence spanning a mean annual precipitation gradient of roughly 2500 mm. Complicating the ability to understand soil weathering along climosequences of Maui is the presence of volcanic vents along the three major rift zones of Haleakalā. Because past vent activity in the area is unknown, the frequency, intensity, and duration of ash depositional events, including ash deposition quantity, are all unknown variables when considering the influence of ash as parent material of soil weathering in the area. Western Haleakalā, with its variable presence of volcanic ash, variability in precipitation, and soil maturity, provides an ideal opportunity to study the application of weathering indices on a soil climosequence formed in a tropical basalt environment.

The main goals of this study were to characterize elemental trends across a soil climosequence of western Haleakalā, Hawaii, to identify a set of elemental indices or

ratios that may assess the degree of weathering of soils. Acknowledging that some soils of western Haleakala have received more recent additions of volcanic ash, we also assess whether elemental indices could facilitate the identification of soil and soil horizons influenced by volcanic ash. To meet these goals, the objectives of this study were to 1) characterize and classify the basalt substrate of pedons sampled across a wide climatic gradient in East Maui; 2) determine how elemental composition and soil chemical properties vary with precipitation and elevation in East Maui; 3) identify pedogenic thresholds of East Maui's climosequences; and 4) determine if elemental indices can distinguish pedons and soil horizons that have been influenced by volcanic ash.

MATERIALS AND METHODS

Study Area

East Maui, specifically, the western slopes of Haleakalā, is predominantly comprised of the Pleistocene Kula Volcanics basalt substrate (0.78-0.15 Ma). Maui is one of five Hawaiian Islands that are subject to orographic climate effect which has a created a precipitation gradient that ranges between 271 mm and 10271 mm in mean annual precipitation (Figure 3-1). Therefore, as trade winds carry moisture from the north end of western Haleakalā towards Kihei, precipitation gradually decreases, creating a rain shadow effect. East Maui has three major rift zones that meet at the summit and are up to 2 miles in width. The formation of volcanic vents along the northwest rift zone has caused the deposition of non-uniform and variable amounts of ash across western Haleakalā as the southwest trade winds pass through central Maui.

Three predominant basalt substrates, ordered from youngest to oldest, occur on East Maui: Hāna, Kula, and Honomanū (Sherrod et al., 2007a). Across the three substrates, SiO_2 generally occurs between 40 and 54% (Hāna), with the Kula Volcanics having SiO_2 values between 41 and 58%, and the oldest, the Honomanū Basalt, with SiO_2 values between 45.5 and 52% (Sherrod et al., 2007b). Samples taken from East Maui classify primarily as basalt (Honomanū), tephrite basanite (Hāna), and anywhere between picro-basalt and trachyandesite (Kula) (Sherrod et al., 2007b).

Site Selection and Field Sampling

The intention of site selection for sampling pedons was to gain appropriate representation of the variation in precipitation and temperature across the study area. Transects across the precipitation gradient and with elevation captures differences in rainfall and temperature on soil formation. Pedon locations were selected based on similar aspect, limited slope (<5%), and the same substrate (Kula Volcanics). Sampling took place over the course of two research excursions in 2019 (7) and 2020 (9). Mapped soils that were relatively close in proximity to pedons sampled from the first excursion but differed in their soil taxonomy were taken into consideration when selecting locations to sample for the second excursion. Sixteen pedons were ultimately selected for sampling, most of which occurred on lands designated as pasture. Naming of sampled pedons is based on their general location: north Kihei (KI-N1 and KI-N2), south Kihei/Makena (KI-S1 and KI-S2), Ocean Vodka Organic Farm and Distillery (OV), lower Kula (LKUL) and upper Kula (UKUL), the closest pedon to Haleakalā summit (HALE), Haleakalā Ranch (HR), Olinda (OL), Makawao (MAKA), Kahului Airport

(AIR), Paia cemetery (CEM), Paia area (PAIA), west Haiku (HAI-W), and east Haiku (HAI-E) (Figure 3-1). Two climosequences were created: 1) a coastal climosequence, and 2) an elevational climosequence. The coastal climosequence consists of pedons AIR, CEM, PAIA, HAI-W, and HAI-E. The elevational climosequence consists of pedons KI-N1, KI-N2, OV, LKUL, UKUL, HR, MAKA, HALE, and OL.

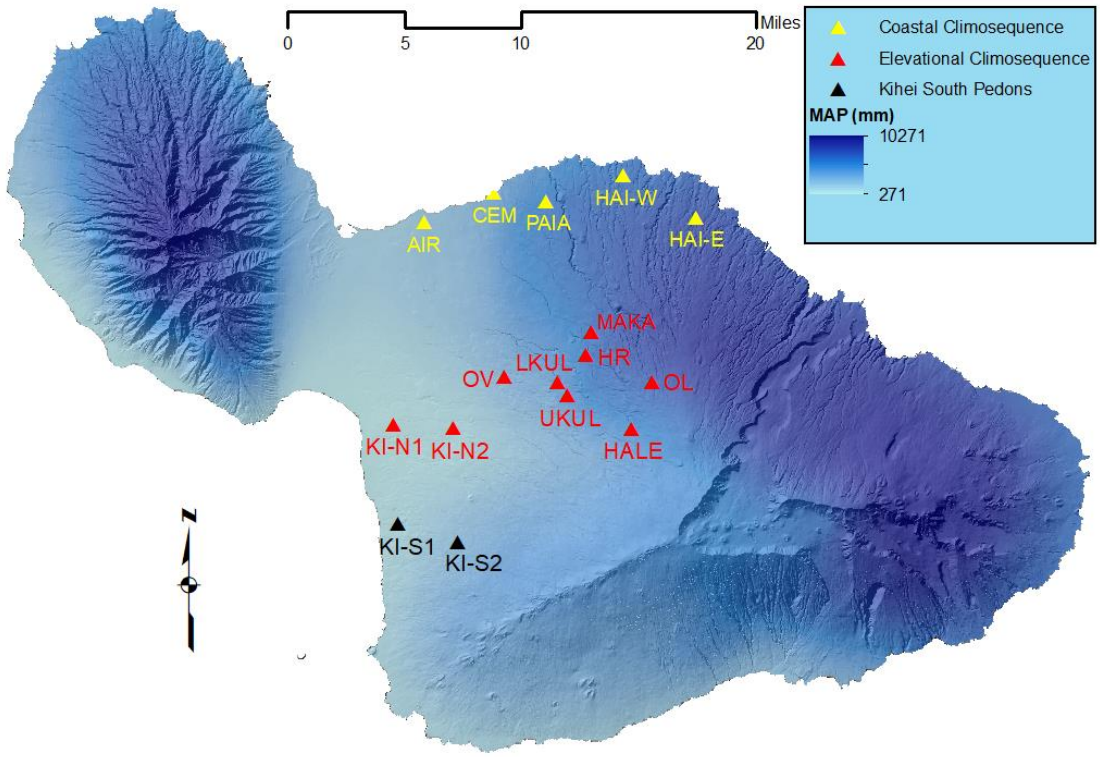

Figure 3-1. Mean annual precipitation (MAP) map of the island of Maui with labeled sampled pedons. MAP data source: Giambelluca et al., 2013.

Pedons were sampled by genetic horizon to at least 1-m depth or to a root-restricting layer, if shallower. Bulk density samples were taken for each horizon using the hammer-driven corer (ring excavation) method (Soil Survey Staff, 2014a), unless high coarse fragment content prevented us from doing so. Rock fragments at the base of each soil pit were sampled.

Laboratory Methods

All lab analyses were performed on the air-dried fine-earth fraction (<2 mm) of samples from each genetic horizon of all pedons, unless otherwise noted. Soil properties contributing to the classification of andic soil properties according to *Soil Taxonomy* (Soil Survey Staff 2014c) include: organic carbon, Al + ½Fe (by ammonium oxalate), bulk density, and phosphate retention. Oven dry bulk density was measured using the hammer-driven core samples (Soil Survey Staff, 2014a). Total (TC) and inorganic carbon (IC) were analyzed using the Skalar Carbon Analyzer, and organic carbon (OC) was determined by difference (TC – IC = OC). Phosphate retention was measured using the New Zealand method (Soil Survey Staff, 2014a).

Extraction of noncrystalline inorganic and organically complexed Fe, Al, and Si was performed with acid ammonium oxalate (AO) at pH 3 using a modified method of Shang and Zelanzy (2008), and by hydroxylamine hydrochloride-hydrochloric acid (HH) (Ross et al., 1985). Extraction of organo-bound Fe and Al was performed using sodium pyrophosphate (PY) (McKeague, 1967). Free Fe was extracted in the dark by citrate-dithionite (CD) using a modified method for free Fe in Soil Survey Staff (2014b).

Weathered rinds were broken away from the rock fragments sampled at the base of each pedon until reaching unweathered cores, which were then ground in a tungsten ball mill. All < 2-mm soil samples to be analyzed for total elemental analysis were further ground to pass a 150-µm sieve and both soil and rock samples were oven-dried at 110 °C for 24 hours. Total elemental analysis (SiO_2, TiO_2, Al_2O_3, Fe_2O_3, MnO, MgO, CaO, Na_2O, K_2O, P_2O_5, and Loss-on-ignition (LOI)) of calcined soil and rock samples was

performed by x-ray fluorescence (XRF) at Brigham Young University – Provo using the fused disk method (Dailey, 2016).

Weathering Indices/Elemental Loss

Total elemental analysis data from all genetic soil horizon samples and rock fragment samples from each pedon were used to create weathering indices and elemental ratios. Weathering indices surveyed by Duzgoren-Aydin (2002) and Taboada (2016) that are specific to basic rocks are listed in Table 1. These indices (Table 3-1) were assessed using total elemental analysis of rock samples and soil horizons of the study pedons. The list is broad due to the indices ease of validation including their use in other studies as functions of elevation (Meijer and Buurman, 2003; Taboada et al., 2016). Additionally, the indices LOI and SA were combined to create the index (LOI + SiO_2)/Al_2O_3. Total elemental analysis of rock samples and soil horizons were referenced to the immobile oxide TiO_2 to create elemental ratios. In this study, weathering indices of Table 1 and elemental ratios were evaluated by measuring their relationship and correlation between each other and with specific soil properties to determine which indices can be best used to assess degree of weathering. Soil properties that were correlated with weathering indices of Table 3-1 include: Al + ½Fe (AO), phosphate retention, Al (AO-PY)/Si (AO),

Table 3-1. Elemental indices from Duzgoren-Aydin (2002) and Taboada et al. (2016) assessed using rock samples and soil horizons of study pedons across western Haleakalā, Maui.

Index	Formula	Notes	Reference
SA	SiO_2/Al_2O_3		Harrassowitz, 1926 in Rocha-Filho et al., 1985
Ba	$(K_2O + Na_2O + CaO)/Al_2O_3$	bases	Harrassowitz, 1926 in Rocha-Filho et al., 1985
Ba_1	$(K_2O + Na_2O)/Al_2O_3$	bases	Harrassowitz, 1926 in Rocha-Filho et al., 1985
Ba_2	$(CaO + MgO)/Al_2O_3$	bases	Harrassowitz, 1926 in Rocha-Filho et al., 1985
B	$(I_{weathered}/I_{parent\ material})$ $I = (K_2O + Na_2O + CaO)/Al_2O_3$	parent normalized ba ratio	Harrassowitz, 1926 in Rocha-Filho et al., 1985
β	$(I_{weathered}/I_{parent\ material})$ $I = (K_2O + Na_2O)/Al_2O_3$	parent normalized lixiviation index	Harrassowitz, 1926 in Rocha-Filho et al., 1985
SF	SiO_2/Fe_2O_3		Jenny, 1941
Silica:R_2O_3	$SiO_2/(Al_2O_3 + Fe_2O_3 + TiO_2)$		Jenny, 1941
PI	$100 * [SiO_2/(SiO_2 + TiO_2 + Fe_2O_3 + Al_2O_3)]$	weathering direction = Product Index	modified from Reiche, 1943
WI	$100 * (I_{weathered}/I_{parent\ material})$ $I = [(K_2O + Na_2 + CaO)/(SiO_2 + Al_2O_3 + Fe_2O_3 + TiO_2 + CaO + MgO + Na_2O + K_2O)]$	parent normalized weathering index	modified from Short, 1961
Parkers Index	$100 * [(Na/0.35) + (Mg/0.9) + (K/0.25) + (Ca/0.7)]$		Parker, 1970
CIA	$100 * Al_2O_3/(Al_2O_3 + CaO + Na_2O + K_2O)$	chemical index of alteration	Nesbitt and Young, 1982
bases:alumina	$(K_2O + Na_2O + CaO + MgO)/Al_2O_3$		Colman, 1982
bases:R_2O_3	$(K_2O + Na_2O + CaO + MgO)/(Al_2O_3 + Fe_2O_3 + TiO_2)$		Colman, 1982
LOI	H_2O (+ and -)	loss-on-ignition	Sueoka et al., 1985
ALK RATIO	$100 * K_2O/(K_2O + Na_2O)$	alkaline ratio	Harnois and Moore, 1988
CWI	$(Al_2O_3 + Fe_2O_3 + TiO_2 +$ LOI)/all chemical oxides	chemical weathering index	Sueoka et al., 1985
STI	$100 * (SiO_2/TiO_2)/[(SiO_2/TiO_2) + (SiO_2/Al_2O_3) + (Al_2O_3/TiO_2)]$	silica-titania index	Jayawardena and Izawa, 1994

crystalline Fe (CD-AO), and organic carbon. Because we are most interested in total change between a soil and its parent material, elemental analysis was performed on the fine-earth fraction versus just the clay fraction. Correlation statistics were performed using R Statistical Software (v4.0.5; R Core Team, 2021) and utilized the Pearson method, which is a linear regression analysis. The Kendall correlation method was also

applied to determine if there were any significant differences in results between the different methods.

RESULTS AND DISCUSSION

Sampled Pedon Classification

Of the 16 sampled pedons classified according to *Soil Taxonomy* (Soil Survey Staff, 2014c), there were nine Mollisols, two Inceptisols, two Ultisols, and three Andisols (Table 3-2). Additionally, there were three sampled pedons classifying into andic intergrades of Mollisols and an Inceptisol, with another five pedons expressing andic characteristics. Of the sampled Mollisols, subgroups include Torroxic, Aridic, Aridic Lithic, Oxic, and Andic. Interestingly, one pedon sampled from an Oxic Dystrustepts map unit (Haliimaile Series) was classified as a Humic Haplustand.

Table 3-2. Site identification, Soil Series and subgroup classification (Soil Survey Staff, 2014c) of the map unit, and the subgroup classification of the sampled pedons in western Haleakalā, Maui.

Pedon	NRCS		Revised
	Soil Series	Subgroup classification of mapped soil series	Subgroup classification of sampled pedons
KI-N1	Waiakoa	Torroxic Haplustolls	Torroxic Haplustolls
KI-N2	Waiakoa (90%)/ Keahua (10%)	Torroxic Haplustolls (90%)/ Ustic Haplocambids (10%)	Aridic Haplustolls
KI-S1	Makena	Typic Haplotorrands	Aridic Argiustolls
AIR	Molokai	Typic Eutrotorroxes	Typic Haplustolls
KI-S2	Waiakoa	Torroxic Haplustolls	Aridic Lithic Haplustolls
OV	Keahua	Ustic Haplocambids	Andic Haplustolls
CEM	Pane	Torroxic Haplustolls	Oxic Haplustepts
LKUL	Kamaole	Aridic Haplustolls	Andic Haplustolls
UKUL	Pane	Typic Haplustands	Typic Argiustolls
HALE	Kaipoipoi	Humic Haplustands	Pachic Haplustands
PAIA	Paia	Torroxic Haplustolls	Oxic Haplustolls
HR	Pane	Typic Haplustands	Humic Haplustands
MAKA	Haliimaile	Oxic Dystrustepts	Humic Haplustands
HAI-W	Haiku	Ustic Palehumults	Typic Sombrihumults
OL	Olinda	Dystric Haplustands	Andic Dystrustepts
HAI-E	Pauwela	Ustic Kanhaplohumults	Typic Haplohumults

Rock Samples

Pedons from this study all occurred on what has been mapped as Kula Volcanics. Based on MacDonald and Katsura's (1964) figure, which distinguishes alkalic from tholeiitic basalts, all rock samples classified as alkalic, most likely of the Upper Kula alkalic cap. However, there was differentiation among our samples, creating three distinct groupings. Rocks sampled from pedons HR, MAKA, HAI-W, and OL had SiO_2 values between 30% and 36%, and classified as the ultrabasic basalt, foidite (Figure 3-2). This is unusual as the only other rock samples classified as foidite in Hawaii occur on Oʻahu (Koʻolau volcano)—from the Honolulu Volcanics, with some samples containing as low as 26% SiO_2 (Sherrod et al., 2007). The Kula Volcanics formation (0.78-0.15 Ma) likely

comprises tens of thousands of individual eruptive units (personal communication with John Sinton, University of Hawaii, Mānoa), and the Honolulu Volcanics range anywhere from about 0.80 Ma to younger than 0.1 Ma (Ozawa et al., 2005). Considering the similarity in age range between these two volcanic substrates, and the dynamic and variable flows of the Kula Volcanics, it is possible that eruptive flows were occurring from the Honolulu Volcanics on O‘ahu and the Kula Volcanics on Maui during relatively similar time periods. The four rock samples classified as foidite had, on average, about 4% more Al_2O_3 and Fe_2O_3 than the mean of all pedon rock samples.

Rock samples from pedons HALE and UKUL had relatively high alkali and silica concentrations, and classified on the border of basic and intermediate basalt. Pedon UKUL is virtually 5 km “downhill” from pedon HALE. There is a flow unit (30-50 kya) belonging to the Hāna Volcanics that is adjacent to the HALE pedon. The downslope extent of this flow unit is unknown (Sherrod et al., 2007). It is possible that while the HALE and UKUL pedons technically occur within the mapped Kula Volcanics, they may occur on the

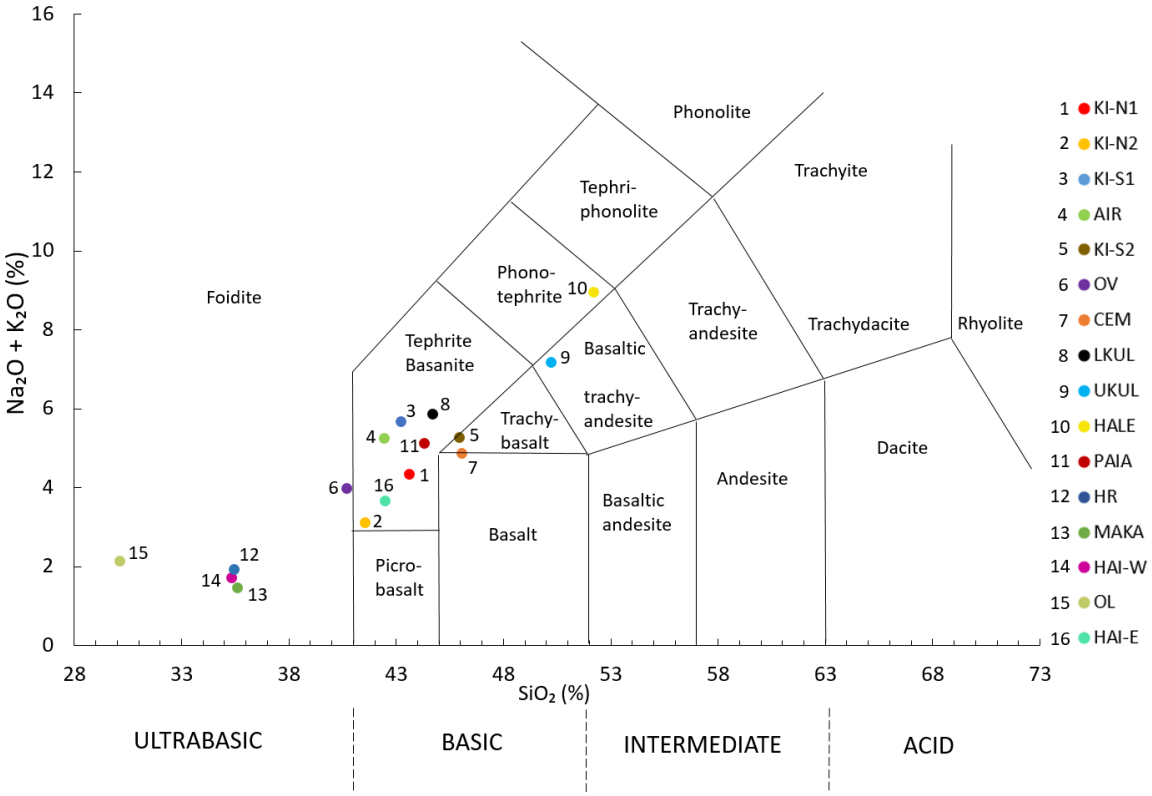

Figure 3-2. Chemical classification of rock fragments sampled at the base of each pedon across western Haleakalā, Maui, based on total alkali and silica. Pedon legend (colored circles) is arranged, top to bottom, by mean annual precipitation. Diagram source: Le Bas et al. (1986).

younger, more alkalic flow unit of the Hāna Volcanics. However, samples taken from the Kula Volcanics have shown to be very diverse in chemical composition (Sherrod et al., 2007), classifying anywhere from tephrite basanite, along the tephri-trachy boundary, to trachyite.

Application of common elemental ratios

Correlation between elemental indices and ratios with soil properties

Of the vetted weathering indices in Table 3-1, soil properties Al + ½Fe (AO), phosphate retention, and organic carbon were best correlated with indices LOI, LOI +

SA, and SA (Table 3-3). Loss-on-ignition, however, is often used as a means to measure organic carbon (Hoogsteen, 2015; Schulte and Hopkins, 1996; Soil Survey Staff, 2014b), and organic carbon is well associated with SRO aluminosilicates. Additionally, the process of measuring LOI affects other SRO materials such as Fe oxyhydroxides. Therefore, LOI cannot be used as a reliable index for the occurrence of an ash depositional event. The remaining indices of Table 3-1 were not well correlated with andic soil properties. Knowing that soil Si is lost and Ti is conserved in other sequences described in the literature (Duzgoren-Aydin, 2002; Taboada et al., 2016), SiO_2/TiO_2 was calculated for each genetic soil horizon and rock samples, and the soil index normalized to its respective rock sample index, to create a new index ratio that was plotted along the coastal climosequence. In the same way, MnO was used to create an index ratio to TiO_2 for each soil/rock sample. While MnO/TiO_2 was not well correlated with soil properties used to classify andic soil properties, it showed interesting trends with soils and pedons that are influenced by volcanic ash.

Al (AO-PY)/Si (AO), a formula used to measure the ratio needed for the formation of SRO aluminosilicates, was well correlated with three indices: MnO/TiO_2 (corr. = 0.87, p-value = 8.36E-13), SiO_2/TiO_2 (corr. = 0.75 p-value = 5.68E-8), and crystalline Fe (CD-AO) (corr. = -0.96, p-value = 0). These three indices are included in Table 3-3.

Table 3-3. Correlation values and p-values between elemental weathering indices and soil properties relevant to andic soil characteristics. Data used from genetic horizons (n = 77) of study pedons across western Haleakalā, Maui.

Elemental Indices[a]	Al + ½Fe (AO)[b]		phosphate retention		organic carbon	
	corr[c]	p-value	corr[c]	p-value	corr[c]	p-value
LOI	0.95	2.40E-14***	0.89	7.22E-10***	0.96	0***
LOI + SA	0.84	4.90E-8***	0.77	2.11E-6***	0.85	1.66E-10***
WI	0.44	0.02*	0.4	0.04*	0.57	3.51E-04***
CWI	0.4	0.04*	0.4	0.04*	0.31	0.07†
B	0.32	0.11	0.25	0.2	0.47	4.08E-03**
ba_2	0.07	0.74	-0.02	0.94	0.42	0.01**
bases:R2O3	0.06	0.75	0	1	0.31	0.07†
Parkers Index	0.04	0.86	-0.03	0.88	0.27	0.12
CIA	0.03	0.87	0.13	0.53	-0.29	0.09†
Ba	-0.02	0.91	-0.11	0.57	0.30	0.08†
ALK RATIO	-0.04	0.85	-0.02	0.94	-0.14	0.43
bases:alumina	-0.07	0.72	-0.17	0.41	0.26	0.13
β	-0.08	0.7	-0.11	0.57	-0.03	0.86
SF	-0.25	0.22	-0.25	0.2	-0.19	0.27
PI	-0.25	0.21	-0.26	0.19	-0.18	0.30
silica:R_2O_3	-0.31	0.12	-0.32	0.10†	-0.22	0.20
ba_1	-0.35	0.08†	-0.41	0.03*	-0.18	0.29
SA	-0.69	5.89E-5***	-0.78	1.74E-6***	-0.44	8.96E-03**
MnO/TiO_2	0.29	8.20E-2	0.34	3.59E-2	0.13	4.37E-1
SiO_2/TiO_2	-0.06	7.05E-1	-0.04	8.20E-1	-0.17	3.16E-1
Fe (CD-AO)	-0.37	2.26E-2	-0.39	1.50E-2	-0.30	6.39E-2

Note. Grey highlighting indicates correlation values between -1 and -0.60, and 0.60 and 1.

[a] ALK RATIO, alkaline ratio; B, parent normalized ba ratio; ba_1, potassium-sodium to aluminum ratio; ba_2, calcium-magnesium to aluminum ratio; β, parent normalized lixiviation index; CIA, chemical index of alteration; Ba, potassium-sodium-calcium to aluminum ratio; CWI, chemical weathering index; LOI, loss on ignition; PI, product index; SA, SiO_2/Al_2O_3; SF, silica to iron ratio; WI, parent normalized weathering index.

[b] AO, ammonium oxalate

[c] corr., correlation.

†Significant at the .1 probability level. *Significant at the .05 probability level. **Significant at the .01 probability level. ***Significant at the .001 probability level.

Coastal Climosequence

Five soil pedons that occur along the windward coast of East Maui, from Kahului to Haiku, form a climosequence (Figure 3-3). The pedons were low in elevation (< 224

m), had about the same MAT (22-24 °C), and ranged in MAP from 461 mm to 2768 mm. These pedons generally occurred upwind of volcanic vents of Haleakalā's northwest rift zone, and, therefore, were little influenced by volcanic ash. Generally, there are two clear pedogenic thresholds in SiO_2/TiO_2 between pedons AIR and CEM, and between pedons PAIA and HAI-W (Figure 3-3). As the loss of silica from a soil is often considered an indicator for the degree of soil weathering (Uehara and Gillman, 1981), the low SiO_2/TiO_2 of AIR compared to CEM and PAIA indicates greater weathering of AIR. Given AIR had lower MAP, it is likely an older soil on an older landform. The deepest horizon of AIR had a significant amount of Si, Mg, Ca, and K, and a relatively high amount of volcanic glass, contributing to the dilation of SiO_2 relative to TiO_2 (Figure 3-3). Pedon CEM was adjacent to the beach and is exposed to wind-blown sand deposition, resulting in the dilation of SiO_2 in the surface horizon. With the exception of the surface horizon of CEM, SiO_2/TiO_2 was uniform throughout the horizons of CEM and PAIA, which demonstrate relatively uniform weathering with depth. Pedons HAI-W and HAI-E, both Ultisols (Table 3-2) with argillic (clay-rich) subsoil horizons and higher MAP, have lower SiO_2/TiO_2, indicating greater weathering than CEM and PAIA. The SiO_2/TiO_2 was relatively uniform with depth in HAI-W, whereas it was higher in the deeper horizons of HAI-E. The partially weathered rock fragments in the deepest two horizons of HAI-E—some of which could not be removed from the fine-earth fraction—likely contributed to the slight dilation of SiO_2 with depth.

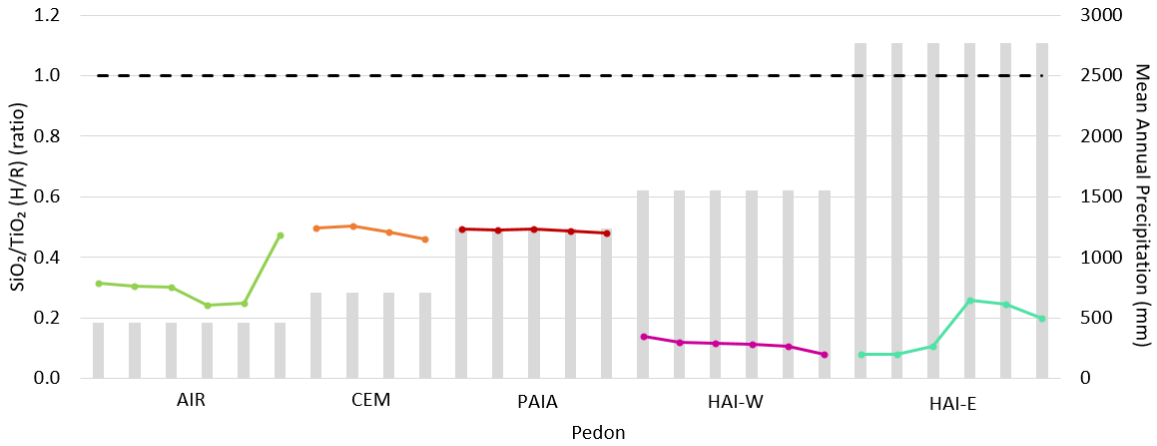

Figure 3-3. SiO_2/TiO_2 ratio by horizon for pedons AIR, CEM, PAIA, HAI-W, and HAI-E of western Haleakalā, Maui. Soil horizon data is normalized to rock fragments from base of each pedon. Soil horizon data are plotted from surface downward from left to right. Black dotted line is the SiO_2/TiO_2 value of rock fragments at the base of each pedon normalized to 1. Secondary y-axis (grey bars) indicates mean annual precipitation for each pedon. H = horizon, R = rock fragments.

The pedogenic threshold for a dramatic decrease in pH and base saturation was above 1500 mm MAP (Chapter 2) and corresponds to the drop in SiO_2/TiO_2 in HAI-W and HAI-E. Pedons HAI-W and HAI-E both had substrate rock fragments with less SiO_2 (Figure 3-2) than that of the other pedons of this sequence. However, the SiO_2/TiO_2 in soils was normalized to the rock fragments. Therefore, the greater loss of silica in HAI-W and HAI-E can be attributed to weathering.

Crystalline Fe (CD-AO) in the coastal climosequence ranged between 5 and 10%, except for pedon HAI-W and the surface horizon of CEM (Figure 3-4). The surface of CEM had a high content of wind-blown and unweathered sand (51%), causing a collapse in crystalline Fe. Pedon HAI-W, with a clay content of 45% in the surface that increased to 92% in the deepest sampled horizon, had much higher crystalline Fe, indicating advanced weathering. Crystalline Fe decreased dramatically in HAI-E above 2500 mm MAP. In a wet montane forest soil of upcountry Maui with MAT of 16-17 °C, Miller et

al. (2001) reported an increase in crystalline Fe with increasing MAP to ~2700 mm before decreasing, which was attributed to the reduction and mobilization of Fe in persistently wet soils. Reduction and leaching loss of Fe would explain the much lower crystalline Fe (CD-AO) content of HAI-E, with warmer MAT facilitating the reduction of Fe at lower MAP.

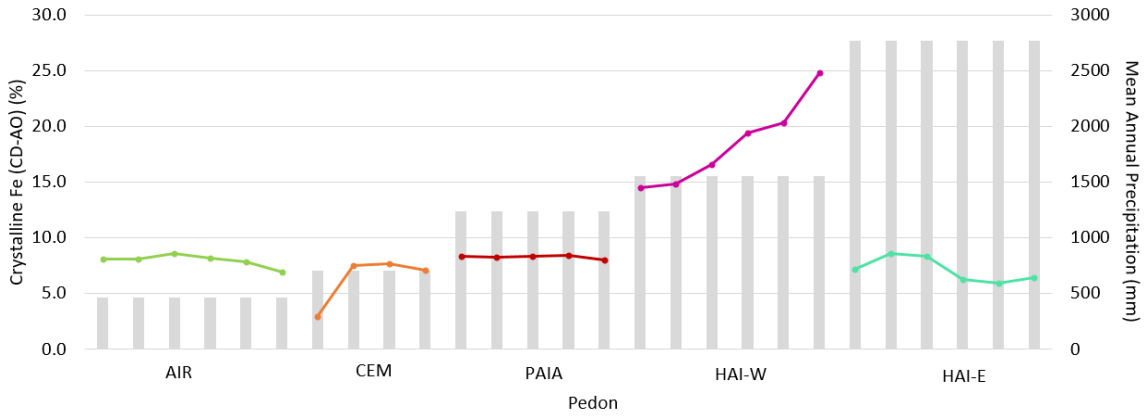

Figure 3-4. Crystalline Fe (CD-AO) by horizon for pedons AIR, CEM, PAIA, HAI-W, and HAI-E of western Haleakalā, Maui. Soil horizon data is normalized to rock fragments from base of each pedon. Soil horizon data are plotted from surface downward from left to right. Secondary y-axis (grey bars) indicates mean annual precipitation for each pedon.

All Pedons

Figures 3-5 through 3-8 plot selected elemental indices and MAP for all pedons with increasing MAP from left to right. Values of SiO_2/TiO_2 generally decreased with soil depth, but whole pedon values of SiO_2/TiO_2 were highly variable with increasing precipitation (Figure 3-5). The SiO_2/TiO_2 was low at high MAP (HAI-W, OL, HAI-E), indicative of the influence of rainfall on the degree of weathering and leaching, resulting in loss of Si. However, 1) the surface and deepest horizons (buried A) of pedon OL and 2) pedons MAKA and HR had relatively high SiO_2/TiO_2, indicating the influence of more recently deposited volcanic ash. At lower elevations, KI-S1 had relatively high SiO_2/TiO_2

in most horizons, indicating the influence of ash. The increase in SiO_2/TiO_2 in the deepest horizons of KI-S1 and AIR indicate the relatively high volcanic glass content.

The soil from HALE, an Andisol, had much lower SiO_2/TiO_2 than the rock sample taken from the bottom of the soil pit. This demonstrates that either increased silica leaching has taken place, or the soil is unrelated to the underlying rock fragments. While the MAP of pedon HALE is intermediate, persistent moisture due to its position within the cloud layer may have decreased overall SiO_2 content relative to TiO_2.

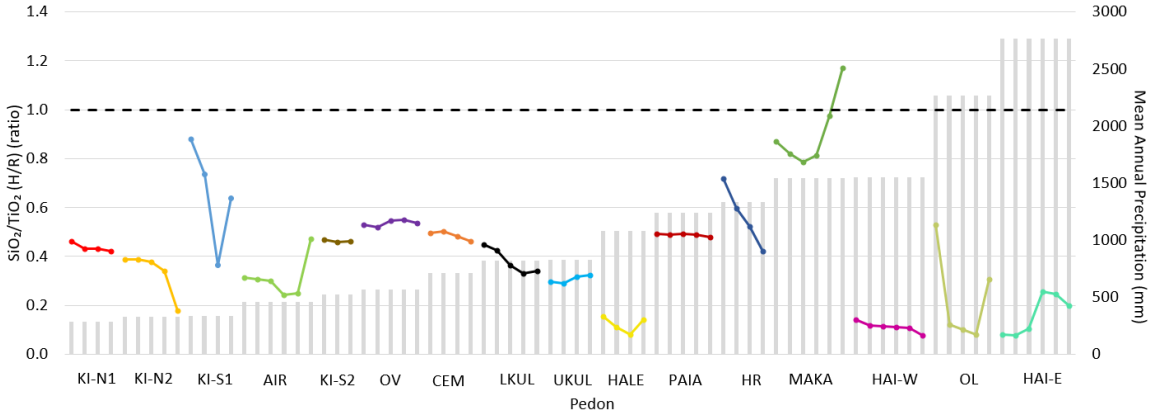

Figure 3-5. SiO_2/TiO_2 ratio by horizon for all sampled pedons of western Haleakalā, Maui. Soil horizon data is normalized to rock fragments from base of each pedon. Soil horizon data are plotted from surface downward from left to right. Black dotted line is the SiO_2/TiO_2 value of rock fragments at the base of each pedon normalized to 1. Secondary y-axis (grey bars) indicates mean annual precipitation for each pedon. H = horizon, R = rock fragments.

The index that most resembles the SiO_2/TiO_2 ratio is the STI. The STI values on the Isla Santa Cruz were well correlated with elevation (Taboada et al., 2016). Soils in the lowest elevation arid zone had the highest values of STI, moderate values of STI were at mid elevations and mid-MAP, and the STI at the highest elevation and higher MAP were the lowest. However, in East Maui, unlike the Isla Santa Cruz (Taboada et al., 2016), Costa Rica (Meijer and Buurman, 2003), and the Sierra Nevada (Dahlgren et al., 1997;

Rasmussen et al., 2007), while there is a decrease in temperature with elevation, the amount of rainfall depends on the windward/leeward position of a soil relative to Haleakalā.

Crystalline Fe (CD-AO) was highly variable across all pedons as well as with increasing depth in a pedon (Figure 3-6). In the coastal climosequence—where pedons were assumed to be uninfluenced by volcanic ash—AIR, CEM, and PAIA (MAP 461-1240 mm) had crystalline Fe (CD-AO) values around 7.5% uniformly with soil depth (with the exception of the sandy surface horizon of CEM). Pedons KI-N1, KI-N2, and KI-S1 had crystalline Fe values greater than or equal to AIR, CEM, and PAIA, although the MAP is ≤ 335 mm. Crystalline Fe accumulation is often considered an index for soil weathering, where higher amounts of crystalline iron are typically associated with increasing soil age (Walker, 1983). On fluvial deposits (Lair et al., 2009), the degree of

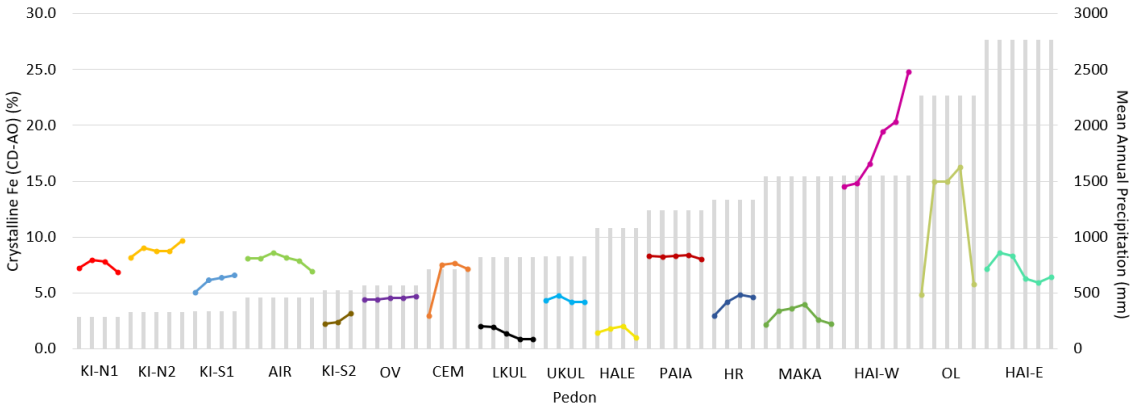

Figure 3-6. Crystalline Fe (CD-AO) by horizon for all sampled pedons of western Haleakalā, Maui. Soil horizon data is normalized to rock fragments from base of each pedon. Soil horizon data are plotted from surface downward from left to right. Secondary y-axis (grey bars) indicates mean annual precipitation for each pedon.

Fe oxide crystallinity (Fe (AO/CD)) was a reliable indicator of soil maturity. High crystalline Fe (CD-AO) of pedons KI-N1, KI-N2, and KI-S1 could indicate an older

landform compared to upcountry Maui where sample pedons occur much closer to Haleakalā summit. Even prior to the subsidence of the Maui Nui complex, the area of Kihei would still have been affected by the rain shadow of Haleakalā, creating a low precipitation environment (Price and Elliot-Fisk, 2004).

The pedons of upcountry Maui, KI-S2, OV, LKUL, UKUL, HALE, HR, MAKA, and the surface and deepest horizons of OL all had lower crystalline Fe (CD-AO) than the coastal sequence pedons and those of Kihei (KI-N1, KI-N2). This supports the possibility that soils closer to the summit of Haleakalā are younger than those more distant from the summit. LKUL, classified into an Andic supgroup, had about 2.5% less crystalline Fe than UKUL, which was only 1 km away and had nearly identical elevation and MAP. This indicates that, while ash deposition affects soils closer to the summit, the deposition of ash is not uniform and can disrupt weathering.

Figure 3-7 demonstrates the variability in MnO/TiO_2 across all pedons. Many pedons had high phosphate retention and/or high Al + 1/2Fe (AO) but did not meet the thickness requirements to classify as andic soil properties. These pedons including KI-N1, KI-N2, KI-S1, KI-S2, and UKUL, showed a slight collapse or dilation in MnO/TiO_2 relative to the associated rock material (Figure 3-7). Considering that KI-N1 and KI-N2 may be as old, or older, than AIR, the pedons of Kihei were more influenced by volcanic ash than AIR and had generally higher MnO/TiO_2 values. The highest value of MnO/TiO_2 in AIR (deepest horizon) matched the lowest values of MnO/TiO_2 in the Kihei pedons. Pedon KI-S1, like KI-N1 and KI-N2, had high crystalline Fe (CD-AO), and a well-formed argillic horizon in horizon 3. The dilation of MnO/TiO_2 in the upper two and deepest horizons of KI-S1 reflects the influence of ash on this well-developed soil. All

horizons in HR and MAKA, both Andisols, and pedon OV, an Andic Haplustoll (Table 3-2), had horizons that expressed a dilation of MnO/TiO_2. While pedons OL and HALE both expressed andic soil properties with the highest Al + ½Fe (AO) among any pedon, their persistent moisture—high precipitation in the case of pedon OL, and the occurrence of pedon HALE in the cloud layer (assuming HALE soil material in related to the rock fragments)—caused a collapse of MnO/TiO_2 in both pedons. It is possible that the high

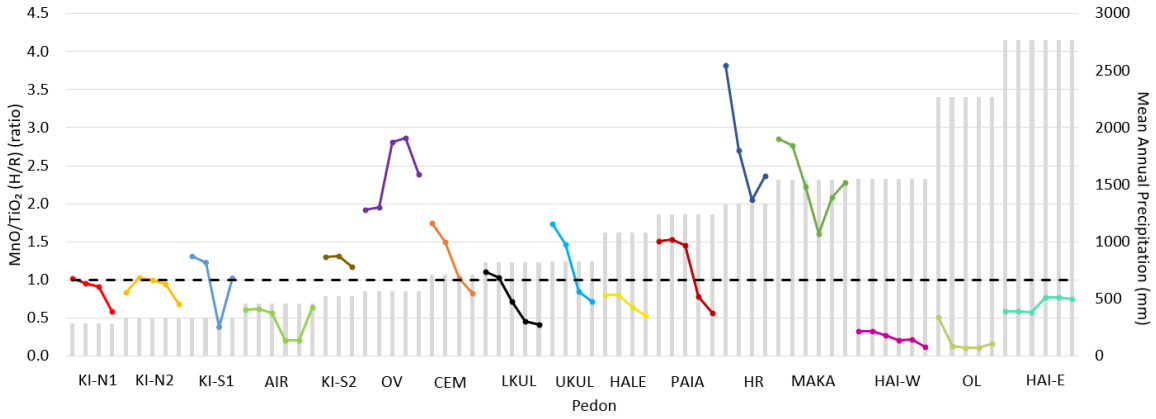

Figure 3-7. MnO/TiO_2 ratio by horizon for pedons AIR, CEM, PAIA, HAI-W, and HAI-E of western Haleakalā, Maui. Soil horizon data is normalized to rock fragments from base of each pedon. Soil horizon data are plotted from surface downward from left to right. Black dotted line is the MnO/TiO_2 value of rock fragments at the base of each pedon normalized to 1. Secondary y-axis (grey bars) indicates mean annual precipitation for each pedon. H = horizon, R = rock fragments.

MnO/TiO_2 values of the surface horizons of pedons CEM and PAIA, which occur downwind of and in close proximity to the ocean, are caused by wind-blown additions of sea spray/water. Oceanic manganese mostly originates from dust and hydrothermal vents, and hydrothermal vents and sediment are the greatest source of manganese to the Pacific Ocean than any other ocean in the world (van Hulten et al., 2016).

The trend in the SiO_2/Al_2O_3 (SA) index across all pedons (Figure 3-8) somewhat resembled the SiO_2/TiO_2 index in Figure 3-5 except for the higher MAP pedons MAKA,

HAI-W, OL, and HAI-E. The increase in SA in the second horizon of pedon OL may result from: 1) the eluviation of silica from the surface horizon enhanced by the high rainfall, 2) the lower concentration of Al due higher solubility and leaching in the low pH (<5.5) surface horizon, and/or 3) a highly mafic rock source (SiO_2 = 30.15%) (Figure 3-2). Aluminum has very low solubility over a wide pH range (see Figure 12.6 of Faure,

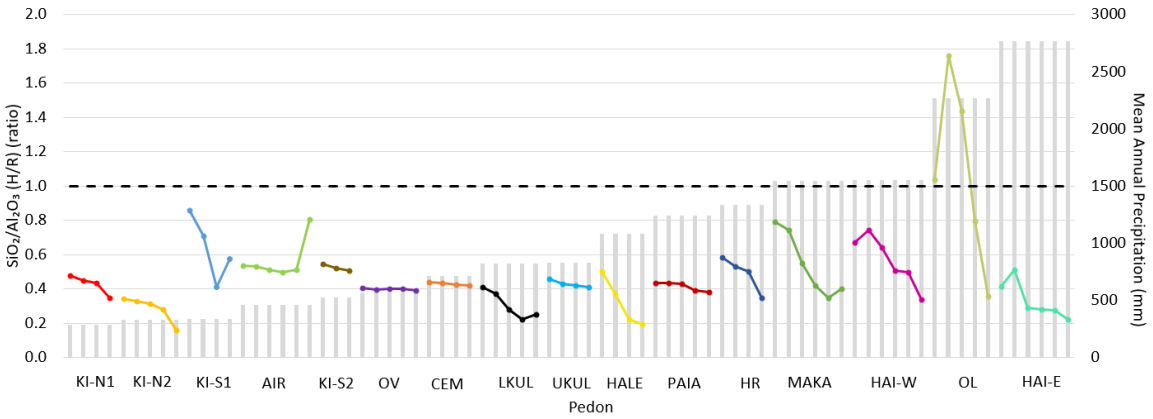

Figure 3-8. SiO_2/Al_2O_3 (SA) ratio by horizon for all sampled pedons of western Haleakalā, Maui. Soil horizon data is normalized to rock fragments from base of each pedon. Soil horizon data are plotted from surface downward from left to right. Black dotted line is the SiO_2/Al_2O_3 value of rock fragments at the base of each pedon normalized to 1. Secondary y-axis (grey bars) indicates mean annual precipitation for each pedon. H = horizon, R = rock fragments.

1997) but is soluble in strongly acid or strongly alkaline soil conditions (Birkeland, 1999). However, alkaline conditions are not typically compatible with a leaching environment; whereas, acid conditions are. Pedons HAI-W and HAI-E both have pH values between 4 and 5, indicative of Al mobilization. The mobilization of both silica and Al are causing low SA values relative to the rock fragments of pedon HAI-E, and therefore, utilizing SA to highlight soil horizons with ash additions may not be practical in strongly acid soils.

On Isla Santa Cruz in the Galapagos, as pedon elevation increased, silica depletion and Al enrichment occurred (Taboada et al., 2016), although only one pedon occurred above 500 m elevation. The soils of the Isla Santa Cruz may have weathered from tephritic materials and/or tholeiitic basalt, which are more silica-rich than the Kula Volcanics (alkalic basalt). Additionally, the pedons in this study could have weathered for a longer period of time (the Shield Series of Isla Santa Cruz has a much younger maximum age (590 kya) than the Kula Volcanics) and/or received higher rainfall and had better drainage than the soils in the Isla Santa Cruz (Taboada et al., 2016).

The K_2O content of pedons farther from Haleakalā summit that had less than 1400 mm MAP and occurred between Kihei and Kahului decreased linearly with distance from a volcanic vent (Figure 3-9). The K_2O content of pedons much closer to the summit and wetter also decreased with distance from the vent, but at a much steeper slope (Figure 3-9). In a high-alumina, aphyric basalt of Japan, potassium concentration in volcanic ash varied greatly depending on distance from its source (Kuno, 1960). Kuno's (1960) observation of decreasing potassium content as a function of increasing distance from ash sources is also observed in the soils of western Haleakalā, where parent rock is predominantly alkalic basalt.

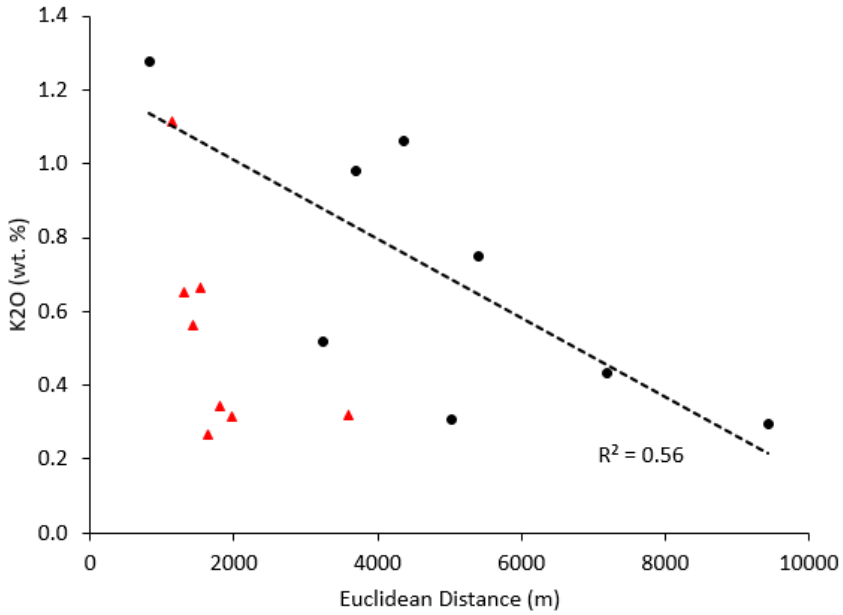

Figure 3-9. Depth-weighted averages of K_2O content as a function of Euclidean distance (m) from volcanic vents and Haleakalā summit for low elevation + low precipitation pedons (black circles; pedons KI-N1, KI-N2, KI-S1, KI-S2, AIR, OV, CEM, PAIA), and high elevation + high precipitation pedons (red triangles; all other pedons). Dashed line is the linear regression for just the black circles.

Summary

In this study, we applied various elemental indices used to gauge degree of soil weathering and identify pedogenic thresholds in an ash-influenced climosequence of Maui. Rock fragments from the base of all pedons classified as alkalic basalts and were visibly arranged into three groups: HR, MAKA, and HAI-W classifying as ultrabasic foidite with the lowest bases and silica contents; OL and UKUL classifying as intermediate basalts with the highest bases and silica; and the rocks of the rest of the pedons classifying together as basic basalts. Pedogenic thresholds for SiO_2/TiO_2 were identified at 500 mm and 1300 mm MAP for the coastal sequence, showing that pedon AIR is older than pedons CEM and PAIA. Crystalline Fe (CD-AO) for Kihei pedons KI-N1 and KI-N2 were higher than any in the coastal climosequence with precipitation

below 1240 mm, demonstrating that although these soils were rejuvenated by volcanic ash, they likely occur on the oldest landforms and soil in the study. Lastly, soil indices SiO_2/TiO_2 and MnO/TiO_2 normalized to the pedon rock fragments may be viable indicators for distinguishing ash-rejuvenated soil pedons and genetic horizons from those that are not.

REFERENCES

Birkeland, P. W. (1999). Soils and Geomorphology. 3rd edition. Oxford University Press, Inc.

Candra, I. N., Gerzabek, M. H., Ottner, F., Tintner, J., Wriessnig, K., & Zehetner, F. (2019). Weathering and soil formation in rhyolitic tephra along a moisture gradient on Alcedo Volcano, Galápagos. *Geoderma*, *343*, 215-225.

Candra, I. N., Gerzabek, M. H., Ottner, F., Wriessnig, K., Tintner, J., Schmidt, G., ... & Zehetner, F. (2021). Soil development and mineral transformations along a one-million-year chronosequence on the Galápagos Islands. *Soil Science Society of America Journal*, *85*(6), 2077-2099.

Chadwick, O. A., Gavenda, R. T., Kelly, E. F., Zeigler, K., Olson, C. G., Elliot, W. C., & Hendricks, D. M. (2003). The impact of climate on the biogeochemical functioning of volcanic soils. *Chemical Geology*, *202*, 195-223.

Chesworth, W. (1973). The residua system of chemical weathering: a model for the chemical breakdown of silicate rocks at the surface of the earth. *Journal of Soil Science*, *24*(1), 69-81.

Colman, S. M. (1982). Chemical weathering of basalts and andesites: evidence from weathering rinds. *US Geological Survey Professional Paper*, no.1246, 51 p.

Cortizas, A. M., Gayoso, E. G. R., Muñoz, J. N., Pombal, X. P., Buurman, P., & Terribile, F. (2003). Distribution of some selected major and trace elements in four Italian soils developed from the deposits of the Gauro and Vico volcanoes. *Geoderma*, *117*(3-4), 215-224.

Dahlgren, R., Shoji, S., & Nanzyo, M. (1993). Mineralogical characteristics of volcanic ash soils. In *Developments in Soil Science* (Vol. 21, pp. 101-143). Elsevier.

Dahlgren, R. A., Boettinger, J. L., Huntington, G. L., & Amundson, R. G. (1997). Soil development along an elevational transect in the western Sierra Nevada, California. *Geoderma*, *78*(3-4), 207-236.

Dailey, S. R. (2016). *Geochemistry of the flourine- and beryllium-rich Spor Mountain rhyolite, Western Utah*: M.S. thesis, Brigham Young University, Provo, Utah.

Duzgoren-Aydin, N. S., Aydin, A., & Malpas, J. (2002). Re-assessment of chemical weathering indices: case study on pyroclastic rocks of Hong Kong. *Engineering Geology*, *63*(1-2), 99-119.

Faure, G. (1997). *Principles and Applications of Geochemistry* (Vol. 625). Upper Saddle River, NJ: Prentice Hall.

Gardiner, H. C. (1967). Genesis of a climosequence of soils in the Kohala region.

Harden, J. W. (1988). Genetic interpretations of elemental and chemical differences in a soil chronosequence, California. *Geoderma*, *43*(2-3), 179-193.

Harnois, L. (1988). The CIW index: a new chemical index of weathering. *Sedimentary Geology*, *55*(3), 319-322.

Harrassowitz, H. (1926). Laterit: Material und Versuch erdgeschichtlicher Auswertung. Verlag von Gebrüder Borntraeger.

He, Y., Li, D. C., Velde, B., Yang, Y. F., Huang, C. M., Gong, Z. T., & Zhang, G. L. (2008). Clay minerals in a soil chronosequence derived from basalt on Hainan Island, China and its implication for pedogenesis. *Geoderma*, *148*(2), 206-212.

Hoogsteen, M. J., Lantinga, E. A., Bakker, E. J., Groot, J. C., & Tittonell, P. A. (2015). Estimating soil organic carbon through loss on ignition: effects of ignition conditions and structural water loss. *European Journal of Soil Science*, *66*(2), 320-328.

Jayawardena, U. D. S., & Izawa, E. (1994). A new chemical index of weathering for metamorphic silicate rocks in tropical regions: A study from Sri Lanka. *Engineering Geology*, *36*(3-4), 303-310.

Jenny, H. (1941). *Factors of Soil Formation: A System of Pedology*, McGraw-Hill book Company, Incorporated, New York.

Kuno, H. (1960). High alumina basalt. *Journal of Petrology*, *1*, 121-145.

Lair, G. J., Zehetner, F., Hrachowitz, M., Franz, N., Maringer, F. J., & Gerzabek, M. H. (2009). Dating of soil layers in a young floodplain using iron oxide crystallinity. *Quaternary Geochronology*, *4*(3), 260-266.

Le Bas, M. J., Le Maitre, R. W., Streckeisen, A., Zanettin, B., & IUGS Subcommission on the Systematics of Igneous Rocks. (1986). A chemical classification of volcanic rocks based on the total alkali-silica diagram. *Journal of Petrology*, *27*(3), 745-750.

MacDonald, G. A., & Katsura, T. (1964). Chemical composition of Hawaiian lavas. *Journal of Petrology*, *5*(1), 82-133.

McKeague, J. A. (1967). An evaluation of 0.1 M pyrophosphate and pyrophosphate-dithionite in comparison with oxalate as extractants of the accumulation products in Podzols and some other soils. *Canadian Journal of Soil Science, 47,* 95–99.

Meijer, E. L., & Buurman, P. (2003). Chemical trends in a perhumid soil catena on the Turrialba volcano (Costa Rica). *Geoderma*, *117*(3-4), 185-201.

Merrill, G. P. (1906). *A Treatise on Rocks, Rock Weathering and Soils*. Macmillan, New York, N.Y., 400 pp.

Nanzyo, M., Dahlgren, R., & Shoji, S. (1993). Chemical characteristics of volcanic ash soils. In *Developments in Soil Science* (Vol. 21, pp. 145-187). Elsevier.

Nesbitt, H., & Young, G. M. (1982). Early Proterozoic climates and plate motions inferred from major element chemistry of lutites. *Nature*, *299*(5885), 715-717.

Ozawa, A., Tagami, T., & Garcia, M. O. (2005). Unspiked K–Ar dating of the Honolulu rejuvenated and Koolau shield volcanism on Oahu, Hawaii. *Earth and Planetary Science Letters*, *232*, 1–11.

Parker, A. (1970). An index of weathering for silicate rocks. *Geological Magazine*, *107*(6), 501-504.

R Core Team (2021). R: A language and environment for statistical computing. R Foundation for Statistical Computing, Vienna, Austria. URL https://www.R-project.org/.

Rasmussen, C., Matsuyama, N., Dahlgren, R. A., Southard, R. J., & Brauer, N. (2007). Soil genesis and mineral transformation across an environmental gradient on andesitic lahar. *Soil Science Society of America Journal*, *71*(1), 225-237.

Rasmussen, C., Dahlgren, R. A., & Southard, R. J. (2010). Basalt weathering and pedogenesis across an environmental gradient in the southern Cascade Range, California, USA. *Geoderma*, *154*(3-4), 473-485.

Rocha-Filho, P., Antunes, F. S., & Falcao, M. F. G. (1985). Quantitative influence of the weathering degree upon the mechanical properties of a young gneiss residual soil. In *Proceedings of the First International Conference on Geomechanics in Tropical Lateritic and Saprolitic Soils, Brasilia* (Vol. 1, pp. 281-294).

Ross, G. J., Wang, C., & Schuppli, P. A. (1985). Hydroxylamine and ammonium oxalate solutions as extractants for iron and aluminum from soils. *Soil Science Society of America Journal*, *49*(3), 783-785.

Schulte, E. E., & Hopkins, B. G. (1996). Estimation of soil organic matter by weight loss-on-ignition. *Soil organic matter: Analysis and interpretation*, *46*, 21-31.

Shang, C., & Zelazny, L. W. (2008). Selective Dissolution Techniques for Mineral Analysis of Soils. *Methods of Soil Analysis: Mineralogical Methods. Part 5*, *9*, 33.

Sherrod, D. R., Nishimitsu, Y., & Tagami, T. (2003). New K-Ar ages and the geologic evidence against rejuvenated-stage volcanism at Haleakala, East Maui, a postshield-stage volcano of the Hawaiian island chain. *Geological Society of America Bulletin*, *115*(6), 683-694.

Sherrod, D. R., Sinton, J. M., Watkins, S. E., & Blunt, K. M. (2007a). *Geologic Map of the State of Hawaii.* US Department of the Interior. USGS.

Sherrod, D. R., Sinton, J. M., Watkins, S. E., & Brunt, K. M. (2007b). Geologic map of the State of Hawaii. *US Geological Survey open-file report*, *1089*(8).

Shoji, S., Kodayashi, S., Yamada, I., & Masui, J. I. (1975). Chemical and mineralogical studies on volcanic ashes I. Chemical composition of volcanic ashes and their classification. *Soil Science and Plant Nutrition*, *21*(4), 311-318.

Shoji, S., Dahlgren, R., & Nanzyo, M. (1993). Genesis of volcanic ash soils. In *Developments in Soil Science* (Vol. 21, pp. 37-71). Elsevier.

Short, N. M. (1961). Geochemical variations in four residual soils. *The Journal of Geology*, *69*(5), 534-571.

Soil Survey Staff. (2014a). *Soil Survey Field and Laboratory Methods Manual*. Soil Survey Investigations Report No. 51, Version 2.0. R. Burt and Soil Survey Staff (ed.). U.S. Department of Agriculture, Natural Resources Conservation Service.

Soil Survey Staff. (2014b). *Kellogg Soil Survey Laboratory Methods Manual*. Soil Survey Investigations Report No. 42, Version 5.0. R. Burt and Soil Survey Staff (ed.). U.S. Department of Agriculture, Natural Resources Conservation Service.

Soil Survey Staff. (2014c). *Keys to Soil Taxonomy, 12th Edition*. USDA, Natural Resources Conservation Service, Washington, DC.

Stewart, B. W., Capo, R. C., & Chadwick, O. A. (2001). Effects of rainfall on weathering rate, base cation provenance, and Sr isotope composition of Hawaiian soils. *Geochimica et Cosmochimica Acta*, *65*(7), 1087-1099.

Sueoka, T. I. K. L., Lee, I. K., Muramatsu, M., & Imamura, S. (1985). Geomechanical properties and engineering classification for decomposed granite soils in Kaduna

district, Nigeria. In *Proceedings of the First International Conference on Geomechanics in Tropical Lateritic and Saprolitic Soils, Brasilia* (Vol. 1, pp. 175-186).

Taboada, T., García, C., Martínez-Cortizas, A., Nóvoa, J. C., Pontevedra, X., & García-Rodeja, E. (2007). Chemical weathering of reference European volcanic soils. In *Soils of volcanic regions in Europe* (pp. 307-323). Springer, Berlin, Heidelberg.

Taboada, T., Rodríguez-Lado, L., Ferro-Vázquez, C., Stoops, G., & Cortizas, A. M. (2016). Chemical weathering in the volcanic soils of Isla Santa Cruz (Galápagos Islands, Ecuador). *Geoderma*, *261*, 160-168.

Uehara, G., & Gillman, G. (1981). *The mineralogy, chemistry, and physics of tropical soils with variable charge clays*. Westview Press, Inc.

van Hulten, M., Dutay, J. C., Middag, R., de Baar, H., Roy-Barman, M., Gehlen, M., ... & Sterl, A. (2016). Manganese in the world ocean: A first global model. *Biogeosciences Discuss*, *14*, 1-38.

Vaughan, K. L., McDaniel, P., Strawn, D., & Blecker, S. (2018). Soil Evolution and Mass Flux of Basaltic Cinder Cones in a Cool, Semi-Arid Climate. *Soil Science Society of America Journal*, *82*(5), 1177-1190.

Vitousek, P. M., & Chadwick, O. A. (2013). Pedogenic thresholds and soil process domains in basalt-derived soils. *Ecosystems*, *16*(8), 1379-1395.

Vitousek, P., Dixon, J. L., & Chadwick, O. A. (2016). Parent material and pedogenic thresholds: observations and a simple model. *Biogeochemistry*, *130*(1), 147-157.

Walker, A. L. (1983). The effects of magnetite on oxalate-and dithionite-extractable iron. *Soil Science Society of America Journal*, *47*(5), 1022-1026.

White, W. M., McBirney, A. R., & Duncan, R. A. (1993). Petrology and geochemistry of the Galápagos Islands: Portrait of a pathological mantle plume. *Journal of Geophysical Research: Solid Earth*, *98*(B11), 19533-19563.

Zehetner, F., Miller, W. P., & West, L. T. (2003). Pedogenesis of volcanic ash soils in Andean Ecuador. *Soil Science Society of America Journal*, *67*(6), 1797-1809.

Zhang, G. L., Pan, J. H., Huang, C. M., & Gong, Z. T. (2007). Geochemical features of a soil chronosequence developed on basalt in Hainan Island, China. *Revista mexicana de ciencias geológicas*, *24*(2), 261-269.

APPENDIX

Table 3-4. Major elemental data of the sampled pedons across western Haleakalā, Maui. Averages are depth-weighted to 1 meter (grey).

Pedon	Depth	Si	Ti	Al	Fe	Mn	Mg	Ca	Na	K	P	O
	cm	wt. %										
KI-N1	0-10	14.08	3.27	9.40	30.45	0.25	0.63	0.49	0.13	0.51	0.11	40.66
	10-21	13.62	3.40	9.67	31.14	0.24	0.51	0.27	0.10	0.47	0.08	40.51
	21-31	13.57	3.37	9.96	30.97	0.23	0.48	0.23	0.08	0.44	0.08	40.59
	31-57	12.61	3.21	11.63	30.75	0.14	0.41	0.16	0.06	0.21	0.13	40.68
	wt. avg.	13.23	3.29	10.57	30.81	0.19	0.48	0.25	0.09	0.35	0.11	40.63
	R	18.40	1.98	5.88	18.77	0.15	3.19	6.88	2.22	0.75	0.17	41.61
KI-N2	0-8	13.80	3.29	9.65	30.69	0.24	0.57	0.48	0.11	0.43	0.13	40.62
	8-21	13.67	3.26	9.88	31.00	0.29	0.47	0.33	0.05	0.37	0.09	40.59
	21-40	13.35	3.29	10.21	31.18	0.28	0.45	0.27	0.03	0.31	0.08	40.55
	40-65	12.40	3.37	10.52	32.26	0.27	0.42	0.21	0.04	0.22	0.08	40.20
	65-108	7.57	3.95	11.48	37.62	0.23	0.46	0.13	0.05	0.15	0.11	38.25
	wt. avg.	11.16	3.54	10.65	33.64	0.26	0.46	0.23	0.05	0.25	0.09	39.67
	R	17.59	1.63	4.20	17.95	0.14	7.35	7.58	1.54	0.60	0.13	41.30
KI-S1	0-14	19.84	2.62	7.55	23.87	0.26	0.83	1.01	0.20	0.87	0.15	42.80
	14-34	18.00	2.84	8.27	25.90	0.26	0.78	0.79	0.16	0.78	0.08	42.12
	34-46	12.66	4.04	10.07	32.10	0.12	0.24	0.24	0.17	0.02	0.05	40.29
	46-57	16.37	2.98	9.33	27.18	0.23	0.72	0.65	0.10	0.69	0.07	41.69
	wt. avg.	17.01	3.07	8.68	26.95	0.22	0.67	0.70	0.16	0.63	0.09	41.82
	R	18.67	2.17	6.10	17.12	0.16	3.03	6.73	2.79	1.21	0.25	41.77
AIR	0-15	12.73	3.32	9.88	28.83	0.27	0.44	3.80	0.13	0.49	0.08	40.03
	15-24	12.60	3.36	9.86	29.22	0.28	0.41	3.63	0.15	0.45	0.07	39.97
	24-33	12.51	3.41	10.10	29.75	0.26	0.39	2.94	0.14	0.43	0.07	40.02
	33-72	12.14	4.11	10.15	32.56	0.12	0.22	0.37	0.14	0.07	0.06	40.07
	72-91	12.47	4.09	10.08	32.29	0.11	0.22	0.28	0.16	0.03	0.06	40.21
	91-99	17.00	2.94	8.74	26.87	0.26	0.75	0.71	0.14	0.73	0.07	41.79
	wt. avg.	12.76	3.76	9.95	30.93	0.18	0.33	1.43	0.14	0.25	0.07	40.22
	R	20.38	1.67	8.44	16.85	0.22	1.75	2.78	2.25	1.93	0.50	43.23
KI-S2	0-10	14.74	2.84	8.99	27.68	0.32	1.85	1.37	0.26	0.60	0.30	41.05
	10-30	14.66	2.88	9.39	28.09	0.33	1.55	1.11	0.23	0.42	0.25	41.09

Pedon	Depth	Si	Ti	Al	Fe	Mn	Mg	Ca	Na	K	P	O
	cm	----------wt. %----------										
	30-36	15.20	2.97	10.00	28.12	0.30	0.75	0.70	0.15	0.31	0.11	41.39
	wt. avg.	14.77	2.88	9.38	27.98	0.32	1.50	1.11	0.23	0.45	0.24	41.13
	R	20.35	1.83	6.78	15.78	0.16	2.56	5.73	2.69	1.10	0.28	42.75
OV	0-6	13.88	3.15	9.33	28.99	0.41	1.08	1.05	0.13	0.80	0.45	40.72
	6-16	13.78	3.19	9.52	29.45	0.42	0.90	0.84	0.12	0.77	0.34	40.65
	16-40	13.85	3.04	9.44	28.78	0.58	0.88	1.08	0.15	0.85	0.60	40.75
	40-60	13.82	3.02	9.41	28.50	0.59	0.93	1.32	0.15	0.86	0.66	40.76
	60-78	13.87	3.11	9.65	29.39	0.50	0.78	0.76	0.13	0.79	0.33	40.69
	wt. avg.	13.84	3.08	9.48	28.95	0.53	0.89	1.03	0.14	0.82	0.51	40.72
	R	17.21	2.07	4.67	18.38	0.14	4.86	8.89	1.85	0.89	0.17	40.87
CEM	0-18	8.35	1.57	6.20	16.03	0.26	1.85	28.59	0.31	0.64	0.14	36.08
	18-33	14.52	2.68	10.94	27.18	0.38	0.52	1.20	0.19	1.14	0.11	41.13
	33-48	14.24	2.74	10.88	27.60	0.26	0.61	1.24	0.21	1.10	0.11	41.01
	48-54	13.42	2.70	10.46	26.95	0.21	1.33	3.02	0.25	1.00	0.11	40.55
	wt. avg.	12.26	2.33	9.29	23.55	0.29	1.08	10.54	0.24	0.95	0.12	39.35
	R	20.34	1.89	6.63	16.65	0.18	2.36	5.46	2.16	1.38	0.29	42.67
LKUL	0-13	13.82	3.05	11.35	26.93	0.27	1.09	1.09	0.12	0.55	0.39	41.34
	13-35	13.28	3.10	12.02	26.97	0.26	1.03	1.07	0.10	0.43	0.40	41.32
	35-58	11.76	3.22	14.09	26.43	0.19	1.07	1.07	0.05	0.25	0.51	41.35
	58-76	11.10	3.32	16.80	24.59	0.12	0.82	0.49	0.00	0.15	0.63	41.99
	76-100	11.34	3.33	15.24	26.69	0.11	0.75	0.30	0.00	0.10	0.57	41.57
	wt. avg.	12.14	3.22	14.04	26.35	0.18	0.94	0.78	0.05	0.27	0.50	41.51
	R	19.66	1.96	6.60	15.97	0.16	2.66	6.11	2.88	1.33	0.32	42.36
UKUL	0-16	15.34	2.66	10.71	26.33	0.72	0.66	0.69	0.14	0.82	0.31	41.63
	16-41	15.17	2.67	11.36	26.64	0.61	0.51	0.31	0.12	0.76	0.18	41.68
	41-80	15.66	2.53	12.07	25.82	0.33	0.45	0.24	0.07	0.52	0.14	42.17
	80-100	15.62	2.48	12.30	25.85	0.28	0.42	0.26	0.11	0.26	0.16	42.26
	wt. avg.	15.48	2.58	11.72	26.11	0.45	0.49	0.34	0.10	0.57	0.18	41.98
	R	23.04	1.18	7.41	13.79	0.18	1.29	3.42	3.49	1.91	0.37	43.91
HALE	0-9	12.83	3.04	7.86	29.00	0.54	1.45	3.24	0.39	0.49	1.05	40.10
	9-20	10.12	3.38	8.37	32.90	0.60	1.15	2.85	0.29	0.47	0.99	38.90
	20-48	7.36	3.39	10.29	36.61	0.48	0.68	1.83	0.19	0.44	0.76	37.98
	48-100	9.53	2.52	15.11	28.91	0.30	0.70	1.32	0.20	0.33	0.63	40.44
	wt. avg.	9.28	2.91	12.37	31.51	0.40	0.81	1.81	0.23	0.39	0.74	39.55

Pedon	Depth	Si	Ti	Al	Fe	Mn	Mg	Ca	Na	K	P	O
	cm	----------wt. %----------										
	R	23.34	0.87	7.18	13.00	0.19	1.09	3.73	4.42	2.14	0.30	43.76
PAIA	0-11	13.55	3.04	9.55	30.62	0.37	0.62	0.42	0.07	1.22	0.21	40.34
	11-21	13.51	3.04	9.53	30.73	0.38	0.61	0.40	0.07	1.20	0.21	40.32
	21-44	13.52	3.03	9.62	30.77	0.36	0.58	0.30	0.07	1.21	0.20	40.34
	44-71	13.21	2.99	10.34	30.88	0.19	0.54	0.19	0.06	0.95	0.19	40.46
	71-100	13.11	3.02	10.50	30.94	0.14	0.54	0.15	0.04	0.86	0.20	40.49
	wt. avg.	13.32	3.02	10.05	30.83	0.25	0.56	0.25	0.06	1.04	0.20	40.42
	R	18.70	2.07	5.74	18.58	0.17	2.81	6.55	2.61	0.90	0.21	41.66
HR	4-20	12.55	2.97	11.17	28.87	0.79	0.83	0.74	0.05	0.75	0.62	40.67
	20-40	11.58	3.30	11.32	30.99	0.62	0.64	0.34	0.03	0.63	0.39	40.17
	40-68	10.76	3.50	11.12	32.63	0.50	0.59	0.25	0.02	0.47	0.39	39.76
	68-100	8.80	3.54	13.24	32.89	0.59	0.55	0.18	0.01	0.35	0.38	39.47
	wt. avg.	10.57	3.38	11.88	31.75	0.60	0.63	0.33	0.02	0.51	0.43	39.90
	R	16.24	2.76	8.43	23.27	0.19	2.38	3.31	0.68	0.78	0.33	41.62
MAKA	0-13	12.07	3.16	8.64	32.34	0.46	0.74	0.78	0.02	0.97	0.98	39.84
	13-23	11.62	3.23	8.82	33.43	0.45	0.69	0.55	0.01	0.92	0.73	39.55
	23-45	10.78	3.13	11.13	32.54	0.35	0.61	0.34	0.00	0.76	0.57	39.79
	45-63	10.38	2.90	14.05	30.05	0.24	0.55	0.27	0.01	0.53	0.51	40.50
	63-80	10.69	2.50	17.39	25.57	0.26	0.65	0.25	0.01	0.41	0.55	41.71
	80-100	12.16	2.36	17.27	23.85	0.27	0.77	0.20	0.04	0.41	0.37	42.29
	wt. avg.	11.22	2.84	13.39	29.23	0.32	0.66	0.36	0.01	0.63	0.59	40.73
	R	15.55	3.54	8.79	28.03	0.18	0.93	0.56	0.54	0.51	0.09	41.26
HAI-W	0-15	5.21	6.28	3.70	48.20	0.15	0.61	0.04	0.02	0.67	0.17	34.96
	15-37	4.86	6.87	3.11	48.85	0.16	0.66	0.01	0.02	0.62	0.15	34.69
	37-54	4.37	6.43	3.25	49.81	0.13	0.60	0.01	0.02	0.84	0.16	34.39
	54-68	3.75	5.64	3.53	51.50	0.08	0.43	0.01	0.02	0.83	0.17	34.03
	68-91	3.53	5.58	3.37	52.11	0.09	0.42	0.02	0.01	0.79	0.20	33.87
	91-100	2.41	5.19	3.39	54.39	0.05	0.21	0.01	0.00	0.63	0.36	33.36
	wt. avg.	4.15	6.09	3.37	50.53	0.12	0.51	0.02	0.02	0.74	0.19	34.28
	R	16.27	2.75	7.73	23.26	0.20	3.07	3.68	0.56	0.76	0.27	41.47
OL	3-18	12.73	3.48	8.89	31.29	0.23	0.94	0.85	0.54	0.68	0.37	40.01
	18-33	5.56	6.59	2.29	49.59	0.11	0.43	0.15	0.02	0.33	0.17	34.76
	33-51	4.05	5.86	2.04	53.32	0.08	0.32	0.12	0.00	0.26	0.16	33.80
	51-83	3.17	5.66	2.87	53.94	0.08	0.27	0.07	0.00	0.14	0.18	33.62

Pedon	Depth	Si	Ti	Al	Fe	Mn	Mg	Ca	Na	K	P	O
	cm	----------wt. %----------										
	83-105	7.09	3.35	14.46	34.77	0.07	0.27	0.11	0.00	0.10	0.60	39.17
	wt. avg.	5.91	5.05	5.86	45.94	0.11	0.40	0.21	0.08	0.26	0.29	35.89
	R	15.25	2.21	11.02	22.15	0.29	2.45	2.11	0.90	0.89	0.66	42.06
HAI-E	0-13	4.14	7.79	3.85	47.78	0.22	1.04	0.02	0.01	0.31	0.06	34.78
	13-24	4.43	8.51	3.34	47.04	0.24	1.14	0.03	0.02	0.31	0.06	34.89
	24-48	4.16	6.00	5.59	47.86	0.17	0.81	0.01	0.01	0.33	0.06	35.01
	48-72	6.89	4.05	9.50	41.09	0.15	0.76	0.01	0.01	0.15	0.07	37.33
	72-104	6.87	4.25	9.62	40.69	0.16	0.78	0.01	0.01	0.14	0.07	37.40
	104-120	6.03	4.63	10.60	40.23	0.16	0.74	0.01	0.00	0.11	0.10	37.38
	wt. avg.	5.60	5.55	7.18	44.13	0.17	0.86	0.01	0.01	0.23	0.06	36.19
	R	19.97	3.03	7.72	15.57	0.15	1.99	5.45	1.90	0.90	0.27	43.05

Note. R, rock fragments.

Table 3-5. Major elemental oxide data of the sampled pedons across western Haleakalā, Maui. Averages are depth-weighted to 1 meter (grey).

Pedon	Depth	SiO_2	TiO_2	Al_2O_3	Fe_2O_3	MnO	MgO	CaO	Na_2O	K_2O	P_2O_5	LOI
	cm	----------wt. %----------										
KI-N1	0-10	30.71	5.58	22.94	23.94	0.33	1.07	0.70	0.18	0.63	0.27	13.48
	10-21	30.17	5.88	23.96	24.87	0.32	0.88	0.39	0.14	0.59	0.19	12.46
	21-31	29.90	5.80	24.54	24.58	0.31	0.82	0.33	0.11	0.54	0.20	12.72
	31-57	26.61	5.29	27.45	23.38	0.18	0.68	0.22	0.08	0.25	0.29	15.42
	wt. avg.	28.59	5.55	25.47	23.98	0.25	0.81	0.36	0.12	0.43	0.25	14.04
	R	43.66	3.66	15.61	16.05	0.21	5.87	10.69	3.32	1.01	0.42	-0.67
KI-N2	0-8	29.97	5.59	23.46	24.03	0.31	0.96	0.68	0.15	0.53	0.29	13.88
	8-21	30.01	5.60	24.27	24.54	0.38	0.80	0.48	0.07	0.45	0.21	13.04
	21-40	29.30	5.63	25.07	24.67	0.37	0.77	0.39	0.04	0.38	0.19	13.04
	40-65	27.30	5.79	25.91	25.60	0.36	0.72	0.30	0.06	0.28	0.19	13.34
	65-108	16.65	6.79	28.27	29.84	0.31	0.79	0.19	0.07	0.18	0.25	16.51
	wt. avg.	24.52	6.07	26.17	26.64	0.34	0.78	0.33	0.07	0.31	0.22	14.40
	R	41.60	3.01	11.11	15.30	0.20	13.49	11.74	2.29	0.80	0.32	-0.16
KI-S1	0-14	41.72	4.30	17.76	18.09	0.33	1.35	1.40	0.26	1.03	0.34	13.23
	14-34	38.45	4.74	19.77	19.95	0.34	1.30	1.11	0.22	0.94	0.19	12.79

Pedon	Depth	SiO_2	TiO_2	Al_2O_3	Fe_2O_3	MnO	MgO	CaO	Na_2O	K_2O	P_2O_5	LOI
	cm	wt. %										
	34-46	27.91	6.95	24.83	25.50	0.16	0.42	0.35	0.23	0.03	0.13	13.28
	46-57	34.76	4.95	22.16	20.80	0.29	1.18	0.90	0.13	0.83	0.16	13.64
	wt. avg.	36.32	5.14	20.80	20.83	0.29	1.10	0.98	0.21	0.75	0.21	13.17
	R	43.26	3.93	15.80	14.29	0.23	5.45	10.21	4.08	1.58	0.62	0.26
AIR	0-15	26.47	5.40	23.00	21.61	0.34	0.70	5.17	0.18	0.57	0.17	16.12
	15-24	26.37	5.50	23.10	22.05	0.35	0.66	4.97	0.20	0.53	0.16	15.84
	24-33	26.46	5.64	23.89	22.68	0.33	0.64	4.07	0.19	0.51	0.15	15.21
	33-72	26.76	7.07	25.01	25.86	0.16	0.37	0.53	0.19	0.09	0.15	13.60
	72-91	27.39	7.01	24.76	25.57	0.15	0.37	0.40	0.22	0.04	0.15	13.71
	91-99	36.26	4.90	20.85	20.66	0.33	1.24	0.99	0.18	0.88	0.16	13.37
	wt. avg.	27.54	6.36	24.05	24.10	0.23	0.54	1.97	0.19	0.29	0.15	14.34
	R	42.48	2.71	19.68	12.66	0.28	2.83	3.80	2.97	2.27	1.12	8.97
KI-S2	0-10	29.20	4.40	19.91	19.76	0.38	2.84	1.77	0.33	0.67	0.64	19.72
	10-30	30.11	4.62	21.59	20.81	0.41	2.48	1.50	0.30	0.49	0.54	16.85
	30-36	31.60	4.82	23.25	21.08	0.38	1.21	0.95	0.19	0.36	0.24	15.61
	wt. avg.	30.11	4.59	21.40	20.56	0.40	2.37	1.48	0.29	0.52	0.52	17.44
	R	46.00	3.24	17.14	12.86	0.22	4.48	8.48	3.84	1.40	0.67	1.26
OV	0-6	29.20	5.18	21.96	21.98	0.52	1.76	1.44	0.18	0.95	1.00	15.55
	6-16	29.35	5.31	22.67	22.61	0.55	1.49	1.18	0.16	0.92	0.78	14.72
	16-40	29.17	5.00	22.24	21.84	0.74	1.44	1.48	0.20	1.01	1.36	15.18
	40-60	28.92	4.94	22.03	21.50	0.74	1.51	1.81	0.19	1.01	1.48	15.56
	60-78	29.55	5.18	23.01	22.57	0.65	1.29	1.07	0.18	0.95	0.75	14.57
	wt. avg.	29.22	5.08	22.40	22.03	0.68	1.46	1.43	0.19	0.98	1.15	15.11
	R	40.72	3.82	12.37	15.68	0.20	8.92	13.79	2.77	1.18	0.43	-0.27
CEM	0-18	12.84	1.88	10.66	8.89	0.24	2.20	28.81	0.30	0.56	0.23	32.83
	18-33	30.77	4.44	25.92	20.76	0.49	0.86	1.67	0.25	1.37	0.26	12.96
	33-48	30.30	4.55	25.91	21.17	0.34	1.00	1.73	0.28	1.32	0.26	12.92
	48-54	27.63	4.35	24.09	20.00	0.26	2.12	4.07	0.33	1.17	0.25	15.49
	wt. avg.	24.31	3.61	20.63	16.83	0.34	1.49	11.00	0.28	1.06	0.25	19.85
	R	46.10	3.35	16.82	13.61	0.25	4.16	8.10	3.08	1.76	0.70	1.76
LKUL	0-13	25.39	4.38	23.33	17.83	0.30	1.56	1.31	0.14	0.57	0.77	24.18
	13-35	23.76	4.34	24.05	17.39	0.28	1.44	1.26	0.12	0.43	0.77	25.93
	35-58	19.32	4.13	25.91	15.66	0.19	1.37	1.15	0.05	0.23	0.89	30.91
	58-76	16.40	3.83	27.77	13.09	0.11	0.94	0.47	0.00	0.12	1.00	36.16

Pedon	Depth	SiO_2	TiO_2	Al_2O_3	Fe_2O_3	MnO	MgO	CaO	Na_2O	K_2O	P_2O_5	LOI
	cm	wt. %										
	76-100	17.90	4.10	26.91	15.18	0.11	0.92	0.31	0.00	0.09	0.96	33.41
	wt. avg.	20.22	4.15	25.74	15.75	0.19	1.22	0.87	0.05	0.26	0.88	30.48
	R	44.74	3.48	16.80	13.09	0.22	4.71	9.10	4.13	1.70	0.77	0.94
UKUL	0-16	29.22	3.96	22.83	18.08	0.83	0.98	0.87	0.17	0.88	0.63	21.19
	16-41	31.00	4.27	25.97	19.63	0.75	0.80	0.41	0.15	0.87	0.40	15.38
	41-80	32.25	4.07	27.81	19.17	0.41	0.71	0.33	0.09	0.60	0.31	13.92
	80-100	32.01	3.97	28.20	19.09	0.34	0.67	0.35	0.14	0.30	0.35	14.26
	wt. avg.	31.41	4.08	26.63	19.09	0.55	0.77	0.44	0.13	0.65	0.39	15.52
	R	50.26	2.01	18.08	10.84	0.24	2.19	4.89	4.81	2.35	0.86	3.20
HALE	0-9	17.21	3.19	11.79	14.02	0.44	1.51	2.85	0.33	0.37	1.51	46.45
	9-20	14.83	3.87	13.72	17.39	0.53	1.31	2.74	0.27	0.39	1.55	43.07
	20-48	11.18	4.02	17.50	20.05	0.44	0.80	1.82	0.18	0.38	1.24	42.16
	48-100	13.07	2.70	23.17	14.28	0.24	0.74	1.19	0.18	0.26	0.93	43.02
	wt. avg.	13.10	3.24	19.52	16.22	0.35	0.89	1.68	0.20	0.32	1.14	43.10
	R	52.24	1.52	17.97	10.49	0.26	1.89	5.46	6.24	2.70	0.73	0.11
PAIA	0-11	29.24	5.12	23.04	23.81	0.49	1.04	0.59	0.09	1.48	0.48	14.42
	11-21	29.31	5.16	23.13	24.03	0.50	1.03	0.57	0.09	1.47	0.48	14.03
	21-44	29.52	5.17	23.50	24.22	0.48	0.98	0.43	0.10	1.49	0.47	13.44
	44-71	28.71	5.08	25.13	24.19	0.25	0.91	0.28	0.08	1.17	0.44	13.59
	71-100	28.73	5.18	25.73	24.44	0.18	0.91	0.22	0.06	1.06	0.46	12.85
	wt. avg.	29.02	5.14	24.50	24.21	0.33	0.95	0.36	0.08	1.28	0.46	13.48
	R	44.36	3.83	15.23	15.88	0.24	5.17	10.18	3.91	1.20	0.54	-0.77
HR	4-20	21.53	3.98	21.44	17.86	0.82	1.10	0.84	0.05	0.72	1.15	30.20
	20-40	23.17	5.15	25.34	22.35	0.75	0.99	0.44	0.03	0.71	0.84	19.92
	40-68	22.31	5.67	25.80	24.39	0.63	0.95	0.34	0.02	0.55	0.87	18.20
	68-100	17.63	5.55	29.69	23.76	0.71	0.86	0.24	0.01	0.40	0.81	20.14
	wt. avg.	20.80	5.24	26.28	22.67	0.71	0.95	0.41	0.02	0.56	0.89	21.20
	R	35.47	4.71	20.60	18.32	0.25	4.03	4.74	0.94	0.96	0.78	8.97
MAKA	0-13	22.04	4.50	17.64	21.28	0.50	1.05	0.93	0.02	1.00	1.91	28.84
	13-23	22.90	4.97	19.44	23.74	0.54	1.05	0.71	0.01	1.03	1.54	23.81
	23-45	20.67	4.68	23.87	22.48	0.41	0.91	0.42	0.00	0.82	1.17	24.36
	45-63	19.14	4.18	28.98	19.97	0.26	0.79	0.33	0.01	0.55	1.02	24.59
	63-80	18.41	3.36	33.50	15.87	0.27	0.87	0.28	0.01	0.40	1.01	25.88
	80-100	21.65	3.29	34.37	15.30	0.29	1.06	0.23	0.05	0.41	0.71	22.45

Pedon	Depth	SiO_2	TiO_2	Al_2O_3	Fe_2O_3	MnO	MgO	CaO	Na_2O	K_2O	P_2O_5	LOI
	cm	----------wt. %----------										
	wt. avg.	20.61	4.09	27.27	19.44	0.36	0.94	0.44	0.02	0.66	1.16	24.81
	R	35.64	6.34	22.54	23.15	0.25	1.66	0.84	0.78	0.66	0.22	7.68
HAI-W	0-15	13.46	12.66	10.69	44.87	0.23	1.21	0.07	0.03	0.98	0.47	15.18
	15-37	13.21	14.60	9.45	47.89	0.27	1.39	0.03	0.04	0.95	0.42	11.60
	37-54	11.91	13.68	9.91	48.93	0.21	1.27	0.03	0.04	1.29	0.46	12.12
	54-68	10.06	11.81	10.59	49.74	0.14	0.89	0.03	0.03	1.25	0.49	14.82
	68-91	9.49	11.74	10.15	50.56	0.14	0.88	0.03	0.03	1.21	0.57	15.01
	91-100	6.44	10.83	10.12	52.36	0.07	0.44	0.02	0.00	0.95	1.04	17.54
	wt. avg.	11.12	12.77	10.10	48.89	0.19	1.07	0.03	0.03	1.11	0.54	13.99
	R	35.39	4.66	18.81	18.24	0.26	5.18	5.24	0.77	0.93	0.62	9.76
OL	3-18	25.46	5.44	19.89	22.55	0.28	1.46	1.11	0.68	0.76	0.79	21.39
	18-33	14.67	13.58	6.75	47.14	0.18	0.87	0.26	0.03	0.49	0.49	15.40
	33-51	10.93	12.35	6.15	51.87	0.13	0.67	0.21	0.00	0.39	0.47	16.70
	51-83	8.43	11.76	8.55	51.70	0.12	0.56	0.11	0.00	0.21	0.52	17.91
	83-105	10.40	3.84	23.72	18.38	0.06	0.31	0.10	0.00	0.08	0.95	41.99
	wt. avg.	12.76	9.61	12.58	40.01	0.15	0.71	0.30	0.11	0.34	0.63	22.65
	R	30.15	3.41	24.38	15.78	0.35	3.77	2.74	1.13	0.99	1.40	15.74
HAI-E	0-13	10.81	15.87	11.24	44.93	0.34	2.10	0.03	0.02	0.46	0.15	13.89
	13-24	11.51	17.27	9.70	44.06	0.38	2.31	0.04	0.03	0.46	0.15	13.93
	24-48	10.32	11.63	15.53	42.85	0.25	1.57	0.02	0.02	0.46	0.15	17.06
	48-72	15.63	7.18	24.10	33.60	0.21	1.34	0.01	0.01	0.20	0.17	17.42
	72-104	15.64	7.56	24.50	33.39	0.22	1.37	0.01	0.02	0.18	0.17	16.81
	104-120	13.38	8.02	26.32	32.16	0.22	1.28	0.02	0.00	0.14	0.25	18.10
	wt. avg.	13.28	10.59	18.90	38.38	0.26	1.61	0.02	0.02	0.32	0.16	16.32
	R	42.52	5.03	18.39	11.95	0.19	3.29	7.60	2.56	1.08	0.61	6.59

Note. R, rock fragments; LOI, loss on ignition.

Table 3-6. Chemical and physical property data of all sampled pedons and horizons with depth-weighted averages to 1-m, or root restricting layer, across the study area of western Haleakalā, Maui.

Pedon	Horizon	Depth	OC	P-Ret.	Sand	Clay
		cm	%	%	%	%
KI-N1	A	0-10	1.39	41	4	48
	Bo1	10-21	0.79	46	1	55
	Bo2	21-31	0.68	50	1	65
	2Bw	31-57	0.86	72	1	75
		wt. avg.	0.91	58	2	65
KI-N2	A	0-8	1.51	40	5	51
	AB	8-21	0.81	45	5	54
	Bw1	21-40	0.60	51	4	57
	Bw2	40-65	0.53	68	7	53
	2Bw3	65-108	0.51	84	11	50
		wt. avg.	0.64	67	8	52
KI-S1	A	0-14	1.64	33	1	46
	Bw	14-34	0.65	35	3	52
	Bt1	34-46	0.64	39	2	58
	2Bt2	46-57	0.63	45	2	60
		wt. avg.	0.89	37	2	53
AIR	Ap1	0-15	0.92	73	9	63
	Ap2	15-24	1.04	76	7	68
	Bw1	24-33	0.90	69	6	69
	Bw2	33-72	0.50	73	11	53
	Bw3	72-91	0.59	70	14	46
	2Bw4	91-99	0.28	69	4	45
		wt. avg.	0.65	72	10	55
KI-S2	A	0-10	4.14	78	12	37
	Bw1	10-30	2.23	88	7	58
	2Bw2	30-36	0.85	83	2	74
		wt. avg.	2.53	85	8	55
OV	Ap	0-6	2.04	54	6	61
	A	6-16	1.01	66	3	72
	Bw1	16-40	1.29	61	2	59
	Bw2	40-60	1.36	58	4	55
	2Bw3	60-78	0.86	68	2	67
		wt. avg.	1.23	62	3	62
CEM	Ap	0-18	1.13	82	51	42
	Bo1	18-33	0.38	60	2	84
	Bo2	33-48	0.37	59	2	84

Pedon	Horizon	Depth	OC	P-Ret.	Sand	Clay
		cm	%	%	%	%
	Bo3	48-54	0.42	63	5	83
		wt. avg.	0.63	67	19	70
LKUL	Ap	0-13	5.14	95	10	42
	AB	13-35	4.96	99	9	40
	Bw1	35-58	6.08	100	9	19
	2Bw2	58-76	7.20	100	6	14
	2Bw3	76-100	6.10	100	11	16
		wt. avg.	5.92	99	9	25
UKUL	A	0-16	4.71	71	4	60
	Bt1	16-41	1.07	86	1	81
	Bt2	41-80	0.26	84	1	79
	Bw	80-100	0.25	83	0	76
		wt. avg.	1.17	82	1	76
HALE	A	0-9	19.23	96	14	40
	AB	9-20	15.67	99	14	46
	2Bw1	20-48	12.89	100	14	28
	2Bw2	48-100	11.17	100	30	12
		wt. avg.	12.87	100	22	23
PAIA	Ap	0-11	1.83	58	2	78
	A	11-21	1.71	60	2	78
	Bo1	21-44	1.42	63	2	77
	Bo2	44-71	0.90	63	1	84
	Bo3	71-100	0.39	65	1	75
		wt. avg.	1.06	63	1	79
HR	N/A	0-4	N/A	N/A	N/A	N/A
	Ap	4-20	8.34	95	33	25
	2Bw1	20-40	2.54	98	8	56
	2Bw2	40-68	1.56	99	3	58
	2Bw3	68-100	1.26	99	5	51
		wt. avg.	2.68	94	10	50
MAKA	A	0-13	8.11	77	13	40
	AB	13-23	4.96	87	13	45
	Bw1	23-45	3.35	97	4	51
	2Bw2	45-63	2.26	96	8	45
	2Bw3	63-80	2.06	96	10	45
	2Cr	80-100	1.18	92	4	49
		wt. avg.	3.28	92	8	46
HAI-W	Ap1	0-15	3.06	61	5	45
	Ap2	15-37	1.82	51	5	41

Pedon	Horizon	Depth	OC	P-Ret.	Sand	Clay
		cm	%	%	%	%
	Bt1	37-54	1.52	51	3	57
	Bt2	54-68	2.05	61	2	77
	Bt3	68-91	2.21	58	1	76
	Bt4	91-100	2.25	71	0	92
		wt. avg.	2.12	57	3	62
OL	N/A	0-3	N/A	N/A	N/A	N/A
	Ap	3-18	4.39	94	18	31
	AB	18-33	4.97	70	5	40
	Bw1	33-51	3.94	79	3	60
	Bw2	51-83	4.30	92	5	48
	2A	83-105	10.74	100	9	51
		wt. avg.	5.57	86	7	45
HAI-E	Ap	0-13	3.18	64	6	34
	AB	13-24	2.49	65	9	36
	Bt1	24-48	2.41	82	7	54
	Bt2	48-72	1.28	68	10	53
	Bt3	72-104	0.89	62	9	39
	Cr	104-120	0.85	64	10	25
		wt. avg.	1.66	68	8	45

Note. P-Ret., phosphate retention; OC, organic carbon; EC, electrical conductivity; --, not determined; N/A, not applicable (root mat).

Table 3-7. Selective dissolution extraction data of all sampled pedons and horizons with depth-weighted averages to 1-m across the study area of western Haleakalā, Maui.

Pedon	Depth	AO			HH		CD		PY	
		Fe	Al	Si	Fe	Al	Fe	Al	Fe	Al
		----------mg g^{-1}----------								
KI-N1	0-10	10.61	4.39	6.35	6.79	4.37	82.94	3.48	0.14	0.56
	10-21	9.98	3.71	3.92	4.93	3.80	89.21	3.26	0.11	0.66
	21-31	11.92	4.31	3.76	4.55	4.00	90.07	3.52	0.12	0.71
	31-57	23.17	8.32	4.87	3.54	5.89	92.19	8.10	0.23	0.92
	wt. avg.	16.45	6.04	4.75	4.56	4.89	89.62	5.55	0.17	0.77
KI-N2	0-8	8.63	3.79	5.79	4.92	4.05	90.45	3.97	0.33	0.88
	8-21	7.56	3.59	4.89	4.43	3.86	98.17	3.66	0.17	1.06
	21-40	11.82	4.16	3.93	4.06	3.75	99.03	3.85	0.20	0.97
	40-65	12.62	5.52	2.71	3.14	4.15	100.04	5.06	0.17	0.90

Pedon	Depth	AO			HH		CD		PY	
		Fe	Al	Si	Fe	Al	Fe	Al	Fe	Al
		----------mg g^{-1}----------								
	65-105	16.51	6.41	5.33	4.36	5.11	113.58	11.21	0.14	0.75
	wt. avg.	13.12	5.27	4.46	4.07	4.42	104.32	7.05	0.18	0.87
KI-S1	0-14	8.10	3.47	3.47	7.68	5.26	59.00	2.15	0.33	0.90
	14-34	6.77	3.23	4.14	5.97	4.50	68.03	2.07	0.37	1.27
	34-46	6.95	3.40	4.26	5.97	4.63	70.87	2.14	0.48	1.51
	46-57	8.04	4.15	5.30	6.03	5.16	74.08	2.37	0.29	1.27
	wt. avg.	7.38	3.50	4.22	6.40	4.84	67.58	2.16	0.37	1.23
AIR	0-15	7.73	4.02	4.97	3.79	4.07	88.53	5.10	0.05	0.16
	15-24	10.10	4.78	4.83	3.41	3.89	91.43	5.37	0.04	0.20
	24-33	7.44	4.64	4.22	2.75	4.32	93.71	5.95	0.04	0.26
	33-72	4.62	5.47	4.56	1.04	4.64	86.68	8.36	0.08	0.59
	72-91	4.30	4.89	3.72	0.98	4.29	83.02	7.88	0.16	0.69
	91-99	5.58	5.56	3.74	1.06	4.52	75.00	6.43	0.12	0.69
	wt. avg.	5.86	5.01	4.39	1.82	4.38	86.38	7.13	0.08	0.49
KI-S2	0-10	60.08	17.54	13.51	31.06	15.80	82.22	7.96	0.98	1.87
	10-30	67.85	19.44	14.48	41.89	17.19	91.84	9.10	0.88	1.70
	30-36	60.49	9.85	12.20	46.63	10.20	92.65	6.41	0.95	1.26
	wt. avg.	64.47	17.31	13.83	39.67	15.64	89.30	8.33	0.92	1.67
OV	0-6	33.55	8.85	7.09	21.37	8.90	77.56	6.38	0.98	1.26
	6-16	38.07	9.36	6.98	24.93	9.69	82.34	6.53	0.46	0.76
	16-40	34.89	10.49	6.36	22.72	11.40	80.11	6.73	0.64	1.20
	40-60	33.24	10.85	5.72	22.53	12.21	78.47	6.35	0.56	1.01
	60-78	37.09	10.04	8.06	23.90	10.12	84.21	6.75	0.31	0.58
	wt. avg.	35.28	10.21	6.73	23.12	10.90	80.73	6.58	0.55	0.96
CEM	0-18	4.10	2.46	4.32	2.11	3.31	33.45	2.40	0.04	0.30
	18-33	12.94	3.81	5.07	4.07	3.28	88.05	5.10	0.02	0.15
	33-48	13.36	3.82	5.32	4.41	3.22	90.34	5.30	0.01	0.13
	48-54	13.99	4.10	4.77	3.80	3.39	85.34	5.39	0.02	0.14
	wt. avg.	10.23	3.40	4.86	3.48	3.29	70.19	4.29	0.02	0.19
LKUL	0-13	38.09	43.14	22.19	18.38	41.19	58.42	13.41	3.76	5.33
	13-35	39.16	56.26	27.36	21.09	55.29	58.45	18.36	4.58	6.66
	35-58	38.95	102.50	51.76	28.03	106.31	52.80	32.57	4.71	8.16
	58-76	37.19	132.90	66.69	30.39	141.71	46.02	43.16	7.81	12.19
	76-100	43.39	132.10	77.16	31.47	133.77	51.76	61.12	13.33	17.98
	wt. avg.	39.63	97.20	51.33	26.50	99.58	53.30	35.71	7.19	10.54
UKUL	0-16	31.39	11.29	9.11	17.70	11.59	74.87	9.07	1.75	1.58
	16-41	34.86	9.88	5.63	21.21	9.42	82.48	9.75	0.80	0.87
	41-80	31.64	8.65	4.88	12.32	6.52	73.66	8.46	0.59	0.88

Pedon	Depth	AO			HH		CD		PY	
		Fe	Al	Si	Fe	Al	Fe	Al	Fe	Al
		----------mg g^{-1}----------								
	80-100	27.44	7.93	6.01	10.09	5.75	69.53	8.21	0.92	0.99
	wt. avg.	31.56	9.24	5.97	14.95	7.90	75.23	8.83	0.89	1.01
HALE	0-9	45.59	41.24	11.34	30.91	41.92	59.98	26.41	16.69	19.72
	9-20	58.26	51.81	13.47	38.60	51.88	76.10	34.77	29.61	27.47
	20-48	73.33	76.31	21.09	49.78	78.65	93.43	53.09	57.20	38.94
	48-100	59.86	119.45	45.46	45.50	128.53	69.67	57.69	23.95	22.19
	wt. avg.	62.17	92.90	32.05	44.63	98.34	76.16	51.06	33.23	27.24
PAIA	0-11	9.64	3.91	2.30	4.83	3.94	93.16	9.30	1.44	0.97
	11-21	10.09	3.87	4.50	4.09	3.77	92.37	9.26	1.44	0.89
	21-44	9.80	4.02	1.46	3.30	4.04	93.19	9.75	1.87	1.13
	44-71	8.99	3.75	4.90	2.39	3.06	93.08	10.34	1.25	1.26
	71-100	8.67	3.60	4.45	2.11	2.65	89.16	10.22	0.18	0.72
	wt. avg.	9.26	3.80	3.65	2.96	3.33	91.90	9.95	1.12	1.00
HR	0-4	N/A	N/A	N/A	N/A	N/A	N/A	N/A	N/A	N/A
	4-20	39.44	49.69	20.38	20.57	48.44	68.96	20.19	3.06	6.83
	20-40	40.46	37.30	13.08	21.35	37.10	82.64	23.56	5.88	6.12
	40-68	42.13	37.96	17.42	18.79	34.40	90.74	30.36	4.22	6.18
	68-100	38.98	37.37	16.06	16.69	32.82	85.59	33.40	2.49	5.07
	wt. avg.	38.67	38.00	15.89	18.16	35.30	80.36	27.13	3.65	5.67
MAKA	0-13	59.04	38.08	14.99	25.28	34.74	80.55	16.98	7.29	7.11
	13-23	58.88	40.45	15.52	28.61	38.37	93.01	19.56	5.46	6.28
	23-45	46.78	67.42	27.19	27.58	66.97	83.21	23.57	3.37	4.90
	45-63	30.63	71.32	30.15	19.32	75.22	70.27	22.14	1.42	4.16
	63-80	21.72	65.93	27.43	15.94	70.14	47.43	19.07	1.45	3.88
	80-100	16.91	43.60	17.96	10.49	38.47	39.57	14.50	2.21	3.49
	wt. avg.	36.45	56.59	23.16	20.50	56.25	66.71	19.48	3.18	4.74
HAI-W	0-15	15.15	4.29	2.90	6.07	3.16	160.23	17.27	29.67	5.19
	15-37	11.04	3.21	1.33	3.36	2.49	158.95	15.86	22.69	4.13
	37-54	31.34	5.11	3.08	2.22	2.25	196.98	18.75	46.03	6.09
	54-68	45.73	6.86	1.83	2.08	2.32	240.05	23.97	80.94	9.79
	68-91	42.12	6.20	3.46	2.28	2.17	245.65	23.32	80.59	9.29
	91-100	60.11	7.69	3.70	2.15	1.95	308.20	28.68	143.05	14.21
	wt. avg.	31.53	5.30	2.64	3.04	2.40	210.34	20.57	60.01	7.51
OL	0-3	N/A	N/A	N/A	N/A	N/A	N/A	N/A	N/A	N/A
	3-18	25.31	38.18	20.41	10.81	36.64	73.58	13.19	35.69	6.88
	18-33	30.49	9.19	2.54	8.59	7.32	180.00	12.88	19.69	5.49
	33-51	88.32	9.43	4.12	25.15	5.72	237.95	14.84	90.57	8.86
	51-83	67.30	24.60	6.64	33.65	21.50	229.83	25.99	71.42	14.80

Pedon	Depth	AO			HH		CD		PY	
		Fe	Al	Si	Fe	Al	Fe	Al	Fe	Al
		mg g^{-1}								
	83-105	27.60	137.08	46.90	22.39	142.23	85.66	68.63	19.14	26.64
	wt. avg.	49.41	44.60	15.84	22.03	43.61	165.01	28.57	49.21	13.38
HAI-E	0-13	17.30	4.72	1.51	10.61	3.78	89.01	12.00	30.15	6.07
	13-24	17.95	5.71	1.62	9.14	4.43	103.97	13.91	37.91	7.54
	24-48	59.24	14.97	2.98	10.17	7.87	142.36	22.62	63.51	13.74
	48-72	59.69	13.33	1.74	3.61	4.57	122.37	17.05	51.57	9.29
	72-104	48.60	11.33	3.52	2.33	3.99	107.86	15.21	36.85	6.93
	104-120	37.63	10.43	3.08	2.42	4.06	102.04	14.23	23.76	5.35
	wt. avg.	45.28	11.11	2.60	5.69	4.91	114.49	16.46	42.75	8.52

Note. AO, ammonium oxalate; CD, citrate dithionite; HH, hydroxylamine hydrochloride hydrochloric acid; PY, sodium pyrophosphate; N/A, not applicable (root mat).

Table 3-8. Magnetite sourced iron (AO-HH), amorphous iron and aluminum (AO-PY), and crystalline iron (CD-AO) of all sampled pedons and horizons with depth-weighted averages to 1-m, or root restricting layer, across the study area of western Haleakalā, Maui.

Pedon	Depth	Fe (AO-HH)	Amorphous Fe (AO-PY)	Al + 1/2Fe (AO)	Amorphous Al (AO-PY)	Crystalline Fe (CD-AO)
	cm	%--------				
KI-N1	0-10	0.38	1.05	0.97	0.38	7.23
	10-21	0.51	0.99	0.87	0.31	7.92
	21-31	0.74	1.18	1.03	0.36	7.82
	31-57	1.96	2.29	1.99	0.74	6.90
	wt. avg.	1.19	1.63	1.43	0.53	7.32
KI-N2	0-8	0.37	0.83	0.81	0.29	8.18
	8-21	0.31	0.74	0.74	0.25	9.06
	21-40	0.78	1.16	1.01	0.32	8.72
	40-65	0.95	1.25	1.18	0.46	8.74
	65-108	1.22	1.64	1.47	0.57	9.71
	wt. avg.	0.91	1.29	1.18	0.44	9.12
KI-S1	0-14	0.04	0.78	0.75	0.26	5.09
	14-34	0.08	0.64	0.66	0.20	6.13
	34-46	0.10	0.65	0.69	0.19	6.39
	46-57	0.20	0.78	0.82	0.29	6.60
	wt. avg.	0.10	0.70	0.72	0.23	6.02
AIR	0-15	0.39	0.77	0.79	0.39	8.08

Pedon	Depth	Fe (AO-HH)	Amorphous Fe (AO-PY)	Al + 1/2Fe (AO)	Amorphous Al (AO-PY)	Crystalline Fe (CD-AO)
	cm		----------%----------			
	15-24	0.67	1.01	0.98	0.46	8.13
	24-33	0.47	0.74	0.84	0.44	8.63
	33-72	0.36	0.45	0.78	0.49	8.21
	72-91	0.33	0.41	0.70	0.42	7.87
	91-99	0.45	0.55	0.84	0.49	6.94
	wt. avg.	0.40	0.58	0.79	0.45	8.05
KI-S2	0-10	2.90	5.91	4.76	1.57	2.21
	10-30	2.60	6.70	5.34	1.77	2.40
	30-36	1.39	5.95	4.01	0.86	3.22
	wt. avg.	2.48	6.36	4.95	1.56	2.48
OV	0-6	1.22	3.26	2.56	0.76	4.40
	6-16	1.31	3.76	2.84	0.86	4.43
	16-40	1.22	3.43	2.79	0.93	4.52
	40-60	1.07	3.27	2.75	0.98	4.52
	60-78	1.32	3.68	2.86	0.95	4.71
	wt. avg.	1.22	3.47	2.78	0.93	4.55
CEM	0-18	0.20	0.41	0.45	0.22	2.94
	18-33	0.89	1.29	1.03	0.37	7.51
	33-48	0.90	1.34	1.05	0.37	7.70
	48-54	1.02	1.40	1.11	0.40	7.14
	wt. avg.	0.68	1.02	0.85	0.32	6.00
LKUL	0-13	1.97	3.43	6.22	3.78	2.03
	13-35	1.81	3.46	7.58	4.96	1.93
	35-58	1.09	3.42	12.20	9.43	1.39
	58-76	0.68	2.94	15.15	12.07	0.88
	76-100	1.19	3.01	15.38	11.41	0.84
	wt. avg.	1.31	3.24	11.70	8.67	1.37
UKUL	0-16	1.37	2.96	2.70	0.97	4.35
	16-41	1.37	3.41	2.73	0.90	4.76
	41-80	1.93	3.11	2.45	0.78	4.20
	80-100	1.74	2.65	2.17	0.69	4.21
	wt. avg.	1.66	3.07	2.50	0.82	4.37
HALE	0-9	1.47	2.89	6.40	2.15	1.44
	9-20	1.97	2.87	8.09	2.43	1.78
	20-48	2.36	1.61	11.30	3.74	2.01
	48-100	1.44	3.59	14.94	9.73	0.98
	wt. avg.	1.75	2.89	12.40	6.57	1.40
PAIA	0-11	0.48	0.82	0.87	0.29	8.35

Pedon	Depth	Fe (AO-HH)	Amorphous Fe (AO-PY)	Al + 1/2Fe (AO)	Amorphous Al (AO-PY)	Crystalline Fe (CD-AO)
	cm		----------%----------			
	11-21	0.60	0.87	0.89	0.30	8.23
	21-44	0.65	0.79	0.89	0.29	8.34
	44-71	0.66	0.77	0.82	0.25	8.41
	71-100	0.66	0.85	0.79	0.29	8.05
	wt. avg.	0.63	0.81	0.84	0.28	8.26
HR	0-4	N/A	N/A	NA	N/A	N/A
	4-20	1.89	3.64	6.94	4.29	2.95
	20-40	1.91	3.46	5.75	3.12	4.22
	40-68	2.33	3.79	5.90	3.18	4.86
	68-100	2.23	3.65	5.69	3.23	4.66
	wt. avg.	2.05	3.50	5.97	3.23	4.17
MAKA	0-13	3.38	5.18	6.76	3.10	2.15
	13-23	3.03	5.34	6.99	3.42	3.41
	23-45	1.92	4.34	9.08	6.25	3.64
	45-63	1.13	2.92	8.66	6.72	3.96
	63-80	0.58	2.03	7.68	6.21	2.57
	80-100	0.64	1.47	5.21	4.01	2.27
	wt. avg.	1.60	3.33	7.48	5.19	3.03
HAI-W	0-15	0.91	-1.45	1.19	-0.09	14.51
	15-37	0.77	-1.17	0.87	-0.09	14.79
	37-54	2.91	-1.47	2.08	-0.10	16.56
	54-68	4.37	-3.52	2.97	-0.29	19.43
	68-91	3.98	-3.85	2.73	-0.31	20.35
	91-100	5.80	-8.29	3.77	-0.65	24.81
	wt. avg.	2.85	-2.85	2.11	-0.22	17.88
OL	0-3	N/A	N/A	NA	N/A	N/A
	3-18	1.45	-1.04	5.08	3.13	4.83
	18-33	2.19	1.08	2.44	0.37	14.95
	33-51	6.32	-0.23	5.36	0.06	14.96
	51-83	3.37	-0.41	5.82	0.98	16.25
	83-105	0.52	0.85	15.09	11.04	5.81
	wt. avg.	2.74	0.02	6.52	3.12	11.56
HAI-E	0-13	0.67	-1.29	1.34	-0.14	7.17
	13-24	0.88	-2.00	1.47	-0.18	8.60
	24-48	4.91	-0.43	4.46	0.12	8.31
	48-72	5.61	0.81	4.32	0.40	6.27
	72-104	4.63	1.18	3.56	0.44	5.93
	104-120	3.52	1.39	2.92	0.51	6.44

Pedon	Depth	Fe (AO-HH)	Amorphous Fe (AO-PY)	Al + 1/2Fe (AO)	Amorphous Al (AO-PY)	Crystalline Fe (CD-AO)
	cm		----------%----------			
	wt. avg.	3.96	0.25	3.44	0.26	6.92

Note. AO, ammonium oxalate; CD, citrate dithionite; HH, hydroxylamine hydrochloride hydrochloric acid; PY, sodium pyrophosphate; N/A, not applicable (root mat).

IV. PREDICTING THE EXTENT OF ANDIC SOILS ACROSS WESTERN HALEAKALĀ, MAUI

ABSTRACT

Maui is one of five Hawaiian Islands affected by orographic climate effect, exhibiting a massive precipitation gradient across western Haleakalā. However, high variability of volcanic ash deposits as a parent material across the study area not only complicates the ability to isolate the influence of climate on soil formation, but little is documented about the spatial extent of ash deposition, frequency and intensity of volcanic ejecta events, and composition of ash. Therefore, andic soils, which contain short-range-order (SRO) aluminosilicates and iron oxides resulting in unique soil chemical and physical properties, are challenging to map.

Using climate and andic soil property data from 16 pedons sampled in the study area—bulk density, phosphate retention, and aluminum plus ½ iron extracted by ammonium oxalate—we applied multiple linear regression to create spatial prediction models of these three soil properties.

The mean prediction for Natural Resources Conservation Service (NRCS) pedons showed a soil classification accuracy of 50% in the study area for Andisols (data to 60-cm), andic intergrades (data to 75-cm), and non-andic soils. Soil property predictions using depth-weighted average data to 1 meter, on the other hand, increased soil classification accuracy of Andisols to 87.5%, of andic-intergrades to 100%, and of non-andic soils to 83.3%. Whether a soil exhibits andic soil properties within 60 or 75-cm is irrelevant when considering prior or current presence of ash in a soil. Accounting for all

available pedon data with depth improves prediction accuracy when attempting to predict andic soils.

INTRODUCTION

Andisols are soils that typically form in loose volcanic ejecta (tephra) such as volcanic ash, cinders, or pumice (McDaniel et al., 2012; Soil Survey Staff, 2014a) and make up less than 1% of the ice-free soil area globally. While Andisols cover less land area than any other soil order, they support high human population densities (~10% globally) (Ping, 2000). In Europe, they occur in Iceland, France, Spain, Germany, Romania, Italy (Buol et al., 2011; IUSS Working Group WRB, 2015). In Africa, Andisols are found in Ethiopia, Kenya, Rwanda, Cameroon and Madagascar. Andisols are concentrated in the "ring of fire" around the Pacific Ocean contributes to the dominating presence of Andisols (Hillel and Hatfield, 2005; McDaniel et al., 2012) due to their close association with areas that are currently, or were once, volcanically active and include Japan, the Philippines, Indonesia, Papua New Guinea, New Zealand (IUSS Working Group WRB, 2015; Takahashi and Shoji, 2002), and the western United States; California, Oregon, and Washington (Weil and Brady, 2008). Additionally, the majority of mapped Andisols occur in high rainfall areas, with roughly 60% of the world's Andisols occurring in the tropics (Takahashi and Shoji, 2002; Wilding, 2000), including the Pacific: Fiji, Vanuatu, New Caledonia, Samoa, and Hawai‘i (IUSS Working Group WRB, 2015). Andisols are common in the Hawaiian Islands, which were formed due to hot spot magmatism.

Andic soils are characterized by unique soil properties that are attributed to short-range-order (SRO) minerals—allophane, imogolite, ferrihydrite, or metal-humus complexes—formed from the weathering of volcanic tephra, including volcanic glass. Among the various components of volcanic ash, volcanic glass is the most weatherable (Dahlgren et al., 1993). During any volcanic eruption, heavier ash particles will fall to the ground much closer to its source than smaller ash particles, and as ash particle size decreases, the proportion of volcanic glass increases. However, there is only a small difference in the chemical composition of the bulk ash component and the volcanic glass component of basaltic ash (Dahlgren et al., 1993). Temperature and precipitation both influence soil mineral weathering rates (Ito et al., 1991; Nanzyo et al., 1993a). As weathering of glass proceeds, silica concentrations decrease, and aluminum, titanium, and iron accumulate steadily due to their immobility (Nanzyo et al., 1993a). Because allophane and imogolite are kinetically favored, SRO materials preferentially form over long-range-order crystalline materials by the synthesis of soluble Al and Si (Ugolini and Dahlgren, 2002). Whether smectite, kaolinite, halloysite, or SRO materials form, or dissolved ions leach out of the soil entirely, depends greatly on mean annual precipitation (Sieffermann and Millot, 1969; Rasmussen et al., 2007; Dahlgren et al., 1997).

Noncrystalline materials of allophane and imogolite—due to their high specific surface, nanoscale size (3.5-5 nm and 1-2 nm, respectively), and high electronegativity—exhibit low bulk density and high phosphate retention (Nanzyo et al., 1993a and 1993b; Strawn et al., 2015). Ammonium oxalate (AO) is commonly used in the dissolution of noncrystalline iron and aluminum for the quantification of allophane, imogolite, and other SRO materials (Shang and Zelanzy, 2008). *Soil Taxonomy* defines andic soil

materials as having less than 25% organic C and either 1) bulk density < 0.90 g cm^{-3} measured at 0.33 kPa water retention, ≥ 85% phosphate retention, and ≥ 2.0% Al plus ½Fe extracted by ammonium oxalate; or 2) ≥ 30% of the fine-earth fraction between 0.02 and 2.0 mm in diameter, ≥ 25% phosphate retention, ≥ 0.4% Al plus ½ Fe extracted by ammonium oxalate, ≥ 5% volcanic glass, and [(Al plus ½Fe %) times (15.625)] + [volcanic glass %] ≥ 36.25 (Soil Survey Staff, 2014a). Andisols typically have andic soil materials in at least 60% of the upper 60 cm of the mineral soil, whereas Andic intergrades in other soil orders have bulk density < 1.0 g cm^{-3} measured at 0.33 kPa water retention and ≥ 1.0% Al plus ½Fe extracted by ammonium oxalate in at least 24% of the upper 75 cm of mineral soil (Soil Survey Staff, 2014a).

The distinct and unique nature of andic soils, defined as Andisols and Andic intergrades in soils of other orders, present both advantages and challenges. Advantages include 1) high inherent fertility, especially when frequent additions of tephra create fresh sources of plant nutrients, 2) low bulk density and unique consistence (Ugolini and Dahlgren, 2002), which makes the soil easy to till due to high porosity, low plasticity and stickiness, and weak rupture resistance (Nanzyo et al., 1993b), and 3) typically high organic matter contents, which provides cation exchange capacity and stores plant-available nutrients. These properties make andic soils well suited for agricultural use. Disadvantages of andic soils that are typically associated with SRO mineralogy include low bulk density, which creates weight-bearing limitations, and high fixation and immobility of phosphate (Nanzyo et al., 2013a), which creates plant nutrient deficiencies that are challenging to overcome. Maui is the second youngest island in the volcanic Hawaiian Island chain. Seven mineral soil orders, including Andisols, are mapped on the

western slope of Haleakalā, the volcano that dominates East Maui. From sea level to Haleakalā's peak (3,055 m), mean annual precipitation (MAP) ranges from about 300 to 6000 mm (Giambelluca et al., 2013). While climate is a clear factor influencing soil variability across East Maui, the presence of surficial volcanic ash over basic igneous rock likely affected mineral weathering and soil development. The rejuvenating effects of volcanic ash may have disrupted pedogenesis, eventually forming dissimilar soils adjacent to one another. The variable extent of ash deposition across western Haleakalā, influenced by the intensity, composition, and frequency of past ejecta events, makes mapping soils using conventional techniques extremely challenging.

Conventional soil maps rely on point sampling in the field by soil mappers. Some of the challenges associated with conventional soil maps are that they are static and are generally based on obsolete data, are difficult to reproduce, and the methodology used in map drawing is not well documented (Arrouays et al., 2020). With rapid advancement in computer software, technology, and geostatistics, rapid data production and increased access to existing data known as the "data deluge" has created the Digital Soil Mapping (DSM) concept (Roudier et al., 2015). Digital Soil Mapping leverages soil property data—typically obtained from soil surveys—to make predictions of a soil class or attribute with the support of other spatially referenced factors. Typical environmental covariates used to quantitatively predict a soil class or attribute in DSM include spatially explicit data used to represent soil (s), climate (c), organisms (o), relief (r), parent material (p), age (a), and spatial location(n), or a "*scorpan*" model (McBratney et al., 2003). Some benefits of DSM include a quantitative prediction of soil attributes and estimates of uncertainty. Digital soil maps are reproducible, adaptable, and easy to

update. They are cost-efficient and can be rapidly produced, and they may allow for the ranking of controlling factors on specific soil attribute distribution (Arrouays et al., 2020). Advances in DSM over the past 20 years include the implementation of modern computational methods including machine learning, data mining, and the availability of more covariates and environmental data (Arrouays et al., 2020; Minasny and McBratney, 2016). It is important, however, to integrate new and emerging data, along with already existing data collected from conventional soil mapping surveys, in order to propagate more robust digital mapping techniques.

Digital soil mapping was used to predict the distribution of soil properties in volcanic ash soils of Guatamala's Atitlán Lake Basin (Búcaro-González et al., 2022). Multiple linear regression (MLR) and random forest (RF) modeling of environmental covariates representing climate and relief was used to spatially predict cation exchange capacity (CEC) and phosphorus content, which are directly influenced by volcanic ash. Not only was MLR more effective in predicting CEC and P content, but MAP was an important predictor.

Volcanic vent location, wind field (direction and intensity; Folch et al, 2009; Hurst and Turner, 1999; Hurst and Davis, 2017; Shoji et al., 1993), elevation, and temperature (Folch et al., 2009) have been used to model potential volcanic ash air travel and deposition patterns for currently active volcanoes. Factors that contribute to the weathering of volcanic ash and the formation of andic properties are temperature and precipitation (Ito et al., 1991; Nanzyo et al., 1993a), soil evaporation, and evapotranspiration. These factors are all potential environmental covariates for predicting soil properties required for classification of Andisols and Andic intergrades of other soil

orders. The objective of this study was to use open-source climate and environmental raster data, point-sampled soil data, and multiple linear regression modeling to predict the areal extent of andic soils on the western slopes of Haleakalā, Maui.

MATERIALS AND METHODS

Study Area and Soil Sampling

The study area of western Haleakalā is approximately 550,200 m^2, spans a precipitation gradient of 5,874 mm MAP (272-6,146 mm) (Figure 4-1), and spans an elevation gradient from sea level to 1722 m. The predominant substrate is the Kula Volcanics basalt formation, which ranges in age from 0.15 to 0.78 Ma (Sherrod et al., 2007). Sites for soil sampling were selected to represent a broad range in precipitation and elevation, with pedon locations ranging from 283 to 2768 mm in MAP, and 7 to 1362 m in elevation. Using ArcMap, soil pedon locations were restricted to soils within the boundary of the Kula Volcanics substrate on slopes less than 5%. Areas prone to or that showed evidence of accelerated erosion were avoided. Soil sampling was stratified across all mapped mineral soil orders (Figure 4-2).

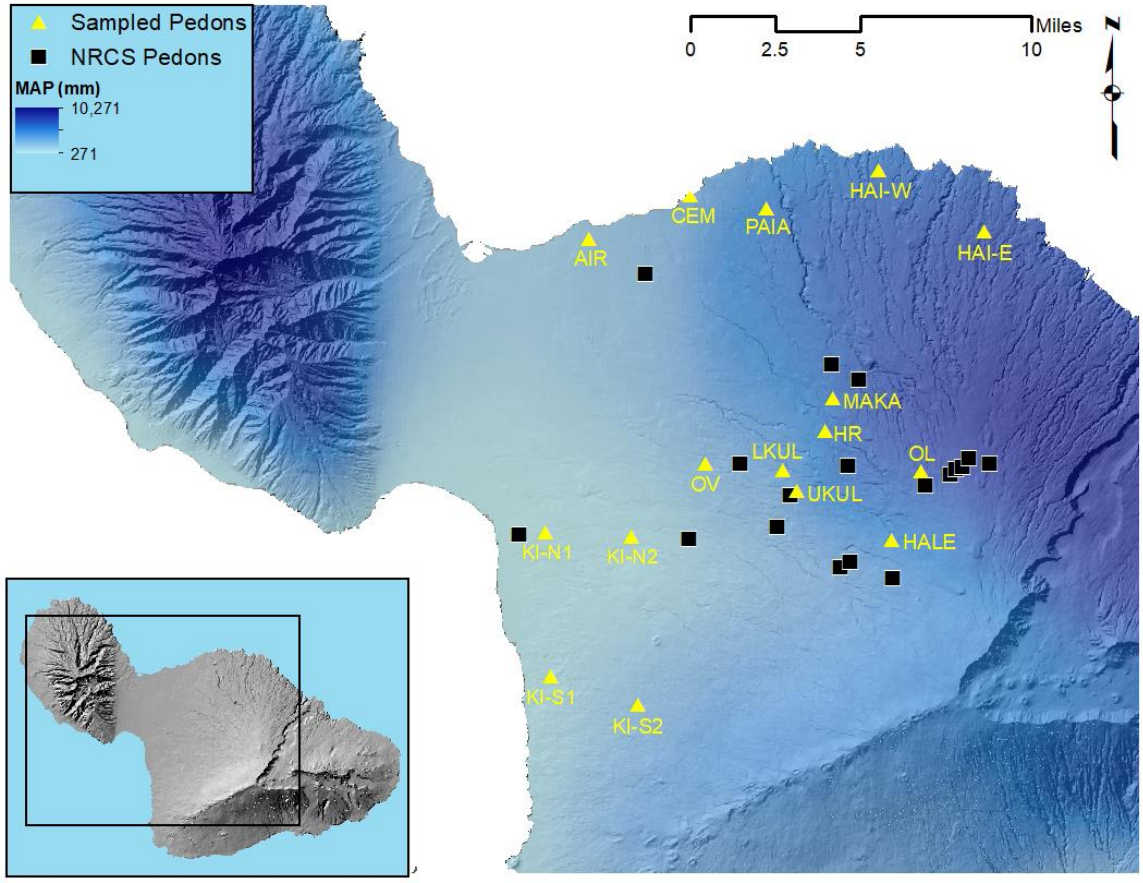

Figure 4-1. Sampled and NRCS study pedons across western Haleakalā's precipitation gradient. MAP data source: Giambelluca et al. (2013). MAP = mean annual precipitation.

Sixteen soils were manually excavated to a depth of at least 1-m or to a root limiting layer, if shallower. Soils were described and sampled by genetic horizon according to Schoeneberger et al. (2012). Bulk density samples were extracted using a hammer-driven corer unless restricted by high coarse fragment volume. Pedons were named based on their general location: north Kihei (KI-N1 and KI-N2), south Kihei/Makena (KI-S1 and KI-S2), Ocean Vodka Organic Farm and Distillery (OV), lower Kula (LKUL) and upper Kula (UKUL), the closest pedon to Haleakalā summit (HALE), Haleakalā Ranch (HR), Olinda (OL), Makawao (MAKA), Kahului Airport

(AIR), Paia cemetery (CEM), Paia area (PAIA), west Haiku (HAI-W), and east Haiku (HAI-E).

Laboratory Analyses

Soil samples were air-dried, and sieved to < 2 mm. All laboratory analyses were performed on the fine-earth fraction (< 2 mm) of samples from each genetic horizon of all pedons. Oven-dry bulk density was measured on the hammer-driven core samples, and phosphate retention was measured using the New Zealand method (Soil Survey Staff, 2014b). Acid ammonium oxalate (AO) at pH 3 extracted SRO and noncrystalline inorganic and organically complexed iron and aluminum according to a modified method of Shang and Zelanzy (2008. Soils were classified to family based on Keys to Soil Taxonomy (Soil Survey Staff, 2014a).

Legacy Soil Data

There have been 31 soils sampled by the U.S. Department of Agriculture Natural Resources Conservation Service (NRCS) in the study area since 1962. However, only soils sampled since 1998 have data required for the classification of Andisols and Andic intergrades of other soil orders. Therefore, only 18 of the 31 NRCS pedons were used in this study (Figures 4-1 and 4-2).

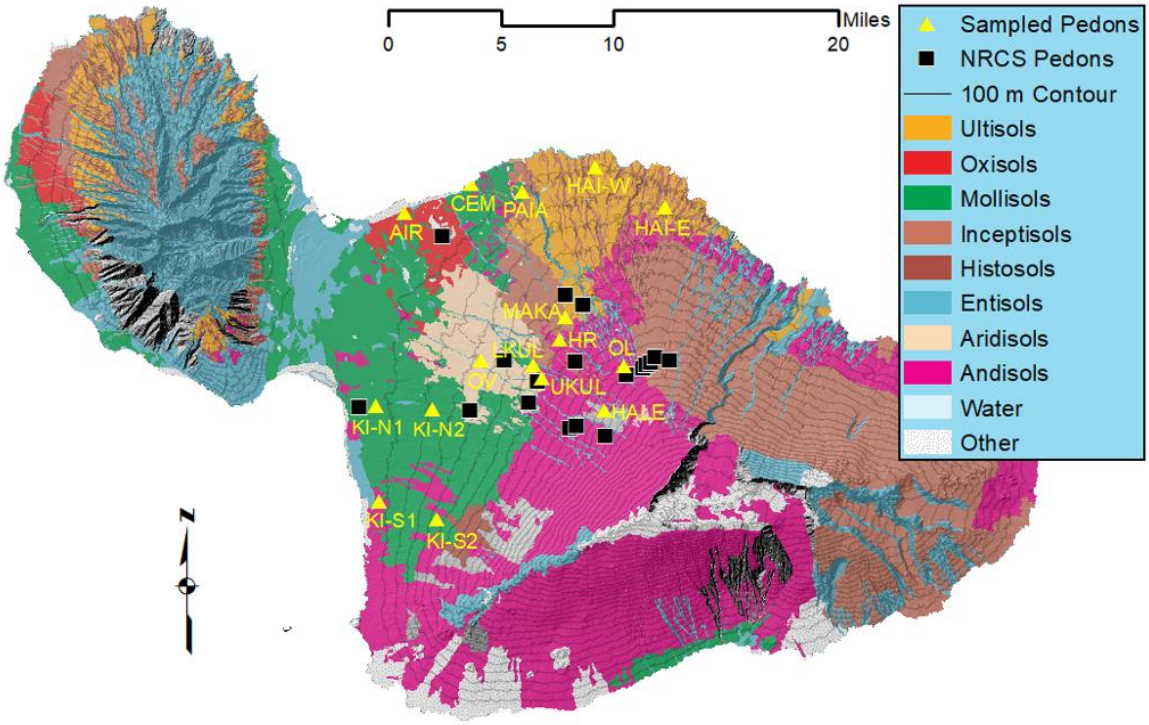

Figure 4-2. Locations of sampled and NRCS study pedons on the map of soil orders of the Hawaiian Island of Maui. Soil order data source: Soil Survey Staff, 2020.

Soil Data Preparation

In consideration of the taxonomic requirements for Andisols and andic intergrades, average soil property data used in the prediction of the three soil properties for Andisols (non-vitric) were depth-weighted to 60-cm, and average soil property data used for andic intergrades (non-vitric) were depth-weighted to 75-cm (Table 4-1). Additionally, to maintain consistency with other data analyses of the study, a third dataset was prepared for model analysis containing the depth-weighted average of the three soil properties to 1 meter or a root limiting layer. Of the 31 NRCS pedons sampled within the study area since 1962, 18 pedons (sampled between 1983 and 1998) contain soil property data used in the classification of Andisols and andic intergrades. Data preparation methods used for our study pedon data were applied to the NRCS pedon data.

Digital Data

Vent locations of the Kula Volcanics (red polygons) where tephra may have originated across the study area are shown in Figure 4-3. Environmental rasters were obtained from the University of Hawai‘i’s Evapotranspiration of Hawai‘i (Giambelluca et al., 2014) and Online Rainfall Atlas of Hawai‘i (Giambelluca et al., 2013) websites. These include mean annual air temperature (°C) and mean annual precipitation (1978-2007) (mm), Penman-Monteith potential evapotranspiration (mm), soil evaporation (mm), clear sky radiation with terrain shading (W/m^2), and net radiation (W/m^2) (Figure 4-4 a-f, respectively), which are data potentially influencing the development of andic soil properties. The remaining rasters from Giambelluca et al. (2014) are annual means and were not developed using a base period due to costs involved with evapotranspiration measurements. Raster data potentially influencing volcanic ash deposition included Euclidean distance from volcanic vents, elevation (m), wind speed (m/s), and wind direction effect (Figures 4-4 h, g, i, and j). Euclidean distance (m) from volcanic vents within and surrounding the study area was calculated in RStudio using the “distanceFromPoints” function (Figure 4-4h; Hijmans, 2020). Wind effect (windward/leeward index) was calculated in SAGA GIS (v2.3.2; Conrad et al., 2015) using the wind effect tool with the wind speed raster as an input grid system (Figure 4-4j). All rasters have a resolution of 250 m (0.00225 x 0.00225 cell size) and use geographic coordinates, WGS84 datum.

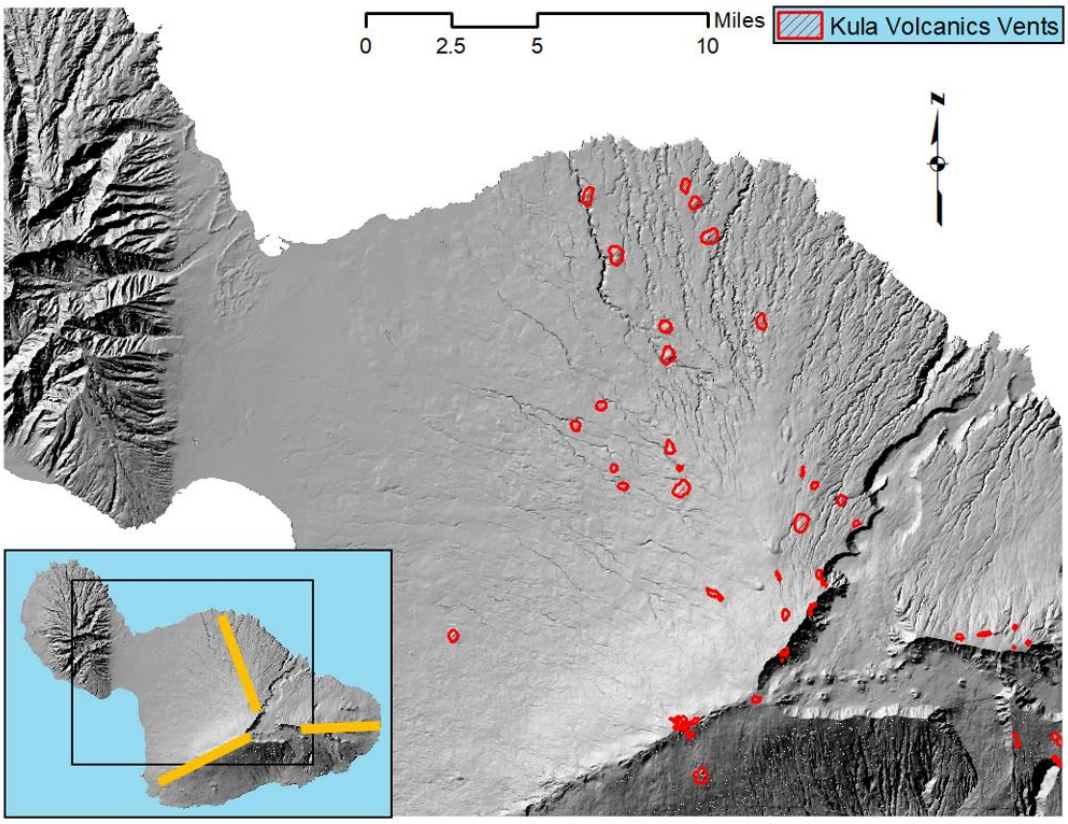

Figure 4-3. Hillshade topographic map of Maui with red polygons identifying vents of Kula Volcanics geologic material (Sherrod et al., 2007). Orange bars in inset map mark the three major fault lines of Haleakalā.

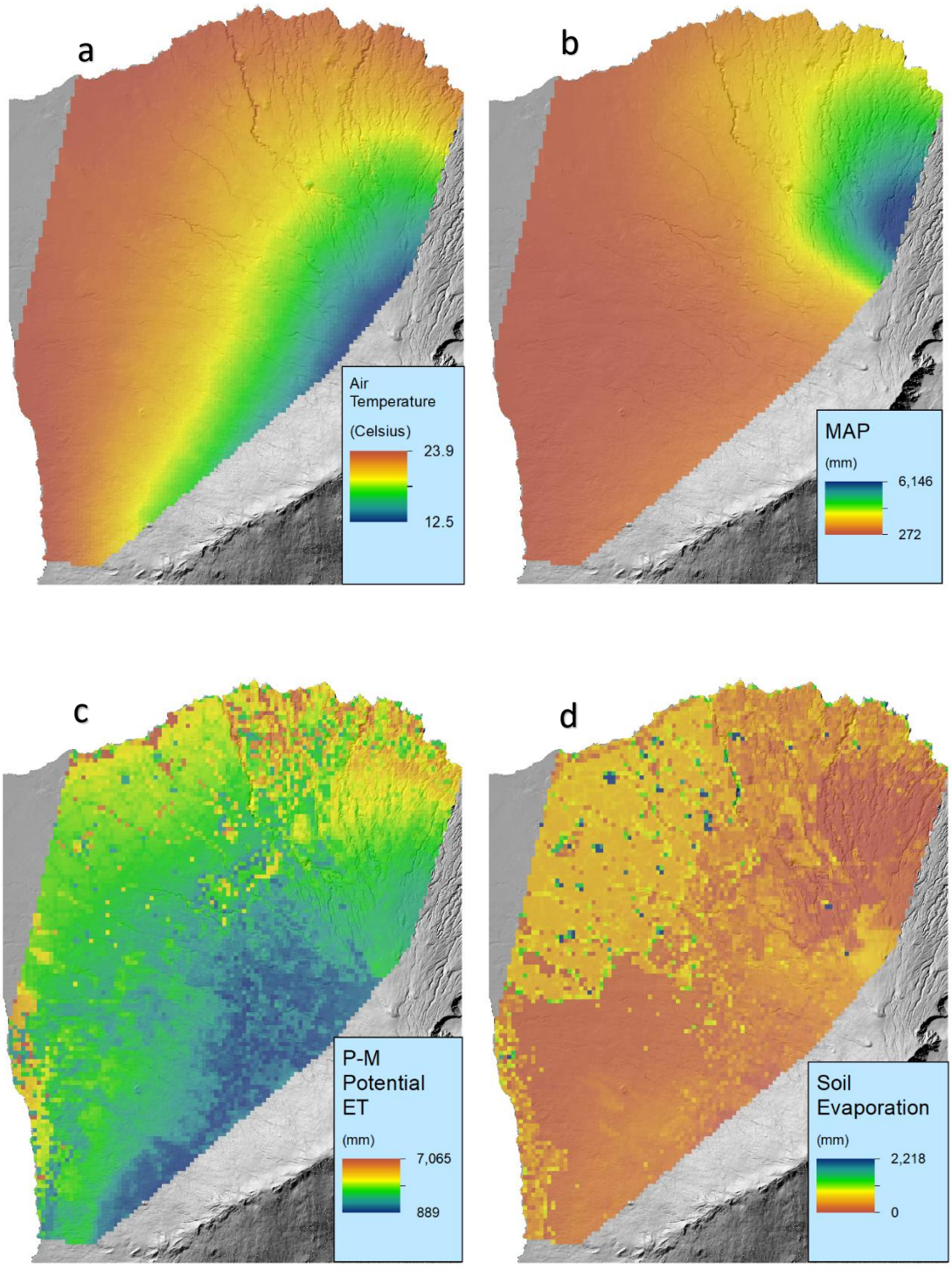
a
Air Temperature
(Celsius)
23.9
12.5
b
MAP
(mm)
6,146
272
c
P-M Potential ET
(mm)
7,065
889
d
Soil Evaporation
(mm)
2,218
0

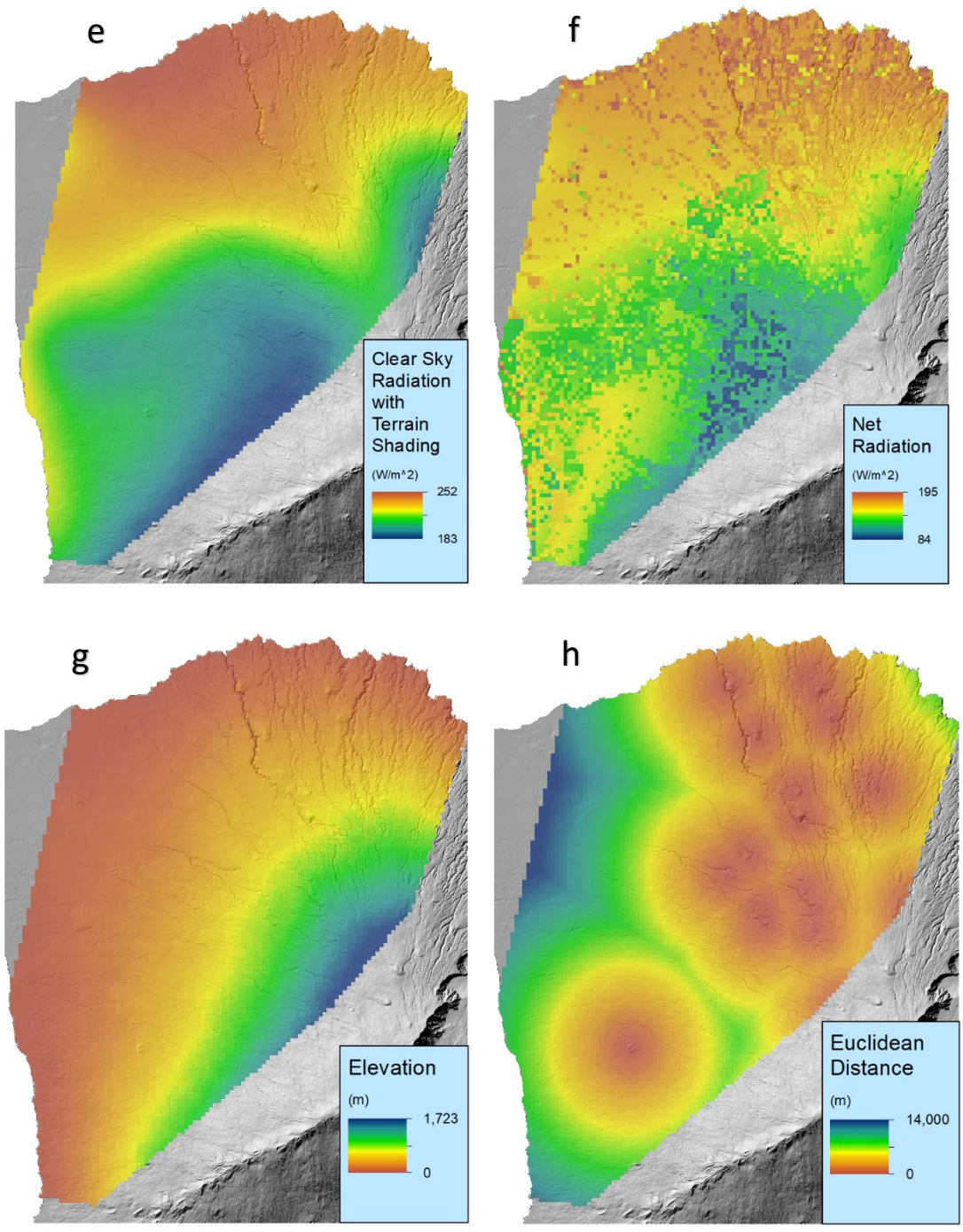
e
Clear Sky Radiation with Terrain Shading
(W/m^2)
252
183
f
Net Radiation
(W/m^2)
195
84
g
Elevation
(m)
1,723
0
h
Euclidean Distance
(m)
14,000
0

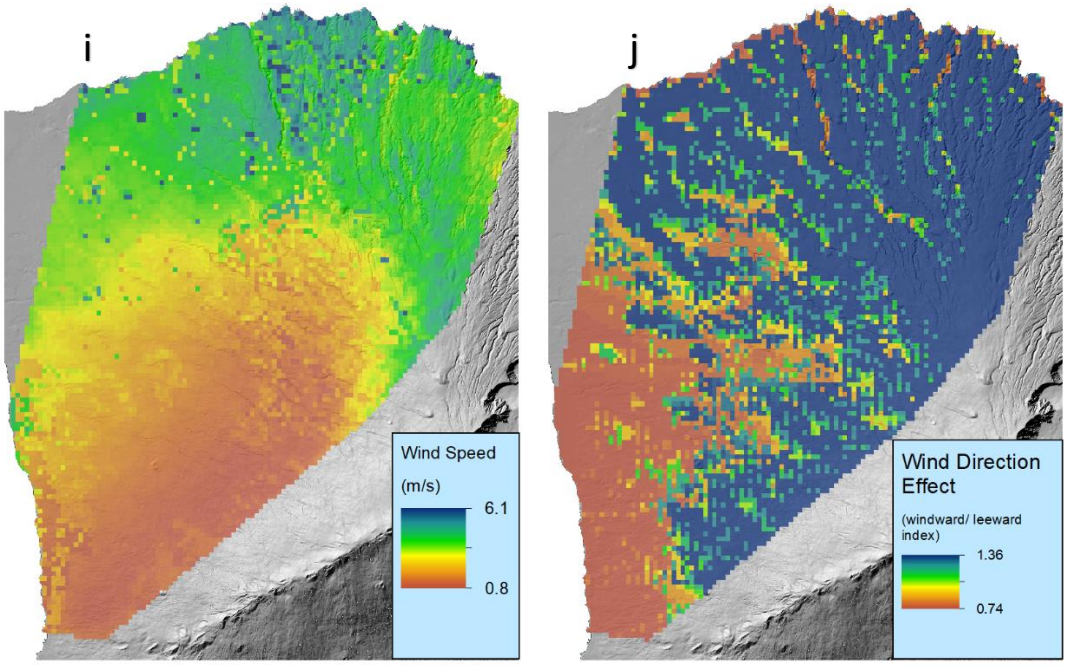

Figure 4-4. Raster covariates used in multiple linear regression models for the spatial prediction of soil properties across the study area of western Haleakalā, Maui. a-f: covariates that influence the formation of andic properties, g-j: covariates that influence the deposition of volcanic ash. MAP = mean annual precipitation, P-M = Penman-Monteith.

Statistical Analyses

All spatial data were extracted and all statistical analyses were performed using R Statistical Software (v4.0.5; R Core Team, 2021). In RStudio, covariate rasters were first clipped to the study area, which is the outer boundary of all study and NRCS pedons, prior to statistical analysis. Using the "crop" function, clipped covariate rasters were cropped to the exact extent in order to ensure proper alignment of raster cells. Cropped rasters were then used in the "stack" function to create a single raster stack. At each of the 16 sampled pedon location, raster data were extracted. Multiple linear regression models of soil properties (Al + ½Fe (AO), bulk density, and phosphorus retention) and raster covariate data (see Figure 4-4) were determined using the Best Subsets function

called “regsubsets” (Lumley, 2020). Variance Inflation Factor (VIF) was used to satisfy the condition of multicollinearity by using the “vif” function (Fox and Weisberg, 2019). VIF values equal to 0 indicate no multicollinearity, VIF values equal to 5 indicate some multicollinearity, and VIF values 10 and above indicate multicollinearity. Selected model for each soil property was based on highest Adjusted R^2 and contained covariates with VIF values less than 5. Study pedon data and locations were used as the training/calibration data to apply and assess model goodness-of-fit.

An independent assessment of goodness-of-fit was performed using the NRCS pedon data and locations (not used for calibration). Spatial predictions for each of the three soil properties were performed using the “predict” function following the requirement that Andisols possess andic properties for the upper 60-cm (averaged data depth-weighted to 60-cm). Spatial predictions for bulk density and Al + 1/2Fe (AO) were done again for andic-intergrades but followed the requirement that soil properties be observed in the upper 75-cm in assessing andic properties (averaged data depth-weighted to 75-cm). Mean, upper, and lower (90% confidence interval (CI)) predictions were made for averaged soil property data that had been depth-weighted to 60 and 75-cm, and mean predictions were made for averaged soil property data that had been depth-weighted to 1-m.

Following model predictions in RStudio for each respective soil property using depth-weighted average data to 60-cm, 75-cm, and 1-m, prediction rasters were imported into ArcMap to produce Andisol and andic-intergrade areal extent polygons. Predicted rasters were modified using the “Con” and “Set Null” tools to exclude raster cells that did not meet the minimum value requirements for each soil property. For mean, upper CI,

and lower CI Andisol polygons, Al + ½Fe (AO) predictions were modified to only contain cells with values ≥ 2%, bulk density predictions were modified to only contain cells with values ≤ 0.90 g/cm^3, and phosphate retention predictions were modified to only contain cells with values ≥ 85%. For mean, upper CI, and lower CI andic-intergrade rasters, Al + 1/2Fe (AO) predictions were modified to only contain cells with values ≥ 1%, bulk density predictions were modified to only contain cells with values ≤ 1.0 g/cm^3. Rasters were then converted to polygons. Using the "clip" function, a polygon was created to express the minimum extent of all three soil properties for Andisols. The same method was done to create a polygon to express the minimum extent of andic-intergrades using polygons of Al + ½Fe (AO) and bulk density. Soil classification accuracy was assessed for study and NRCS pedons within the study area.

RESULTS AND DISCUSSION

Data results for the three soil properties used in classifying andic soils are in Table 4-1. Results include depth-weighted average data to 60-cm, 75-cm, and 1-m for both the point-sampled pedons and the 18 NRCS pedons that included soil property data used in classifying andic soils.

Table 4-1. Soil property data for all sampled pedons and NRCS pedons within the study area of western Haleakalā, Maui that were used as predictors in multiple linear regression modeling.

Pedon	Depth-weighted average analyses								
	0-60 cm			0-75 cm			0-1 m		
	Al + ½Fe (AO)[a]	Bulk density	P-Ret.[b]	Al + ½Fe (AO)[a]	Bulk density	P-Ret.[b]	Al + ½Fe (AO)[a]	Bulk density	P-Ret.[b]
	%	g cm^{-3}	%	%	g/cm^{-3}	%	%	g cm^{-3}	%
KI-N1	1.43	1.20	58	1.40	1.20	58	1.43	1.20	58
KI-N2	0.98	1.18	54	1.06	1.16	59	1.18	1.14	67
KI-S1	0.72	1.17	37	0.72	1.17	37	0.72	1.17	37
AIR	0.84	1.13	72	0.82	1.16	72	0.79	1.22	72
KI-S2	4.95	1.00	85	4.95	1.00	85	4.95	1.00	85
OV	2.76	0.77	60	2.78	0.77	61	2.78	0.77	62
CEM	0.85	N/A	67	0.90	N/A	67	0.85	N/A	67
LKUL	9.31	N/A	99	10.48	N/A	99	11.70	N/A	99
UKUL	2.63	1.09	82	2.60	1.10	82	2.50	1.08	82
HALE	10.70	0.50	99	11.55	0.65	99	12.40	0.51	100
PAIA	0.87	1.37	62	0.86	1.38	62	0.84	1.39	63
HR	6.15	0.87	98	6.07	0.90	98	5.97	0.94	98
MAKA	8.13	0.86	91	8.08	0.73	92	7.48	0.87	92
HAI-W	1.50	1.57	55	1.77	1.58	56	2.11	1.53	57
OL	4.59	0.97	83	4.85	0.90	85	6.52	0.85	85
HAI-E	3.21	1.17	72	3.40	1.17	71	3.44	1.17	69
83HI009001	0.52	1.30	53	0.52	1.30	53	0.53	1.29	54
83HI009002	0.98	1.25	N/A	1.04	1.26	N/A	1.12	1.27	71
83HI009003	2.17	1.14	72	1.89	1.16	70	1.69	1.15	68
83HI009004	7.78	0.75	99	7.88	0.98	99	8.28	1.05	99
83HI009005	8.50	1.12	100	8.42	1.14	100	8.33	1.16	100

Pedon	Depth-weighted average analyses								
	0-60 cm			0-75 cm			0-1 m		
	Al + ½Fe (AO)[a]	Bulk density	P-Ret.[b]	Al + ½Fe (AO)[a]	Bulk density	P-Ret.[b]	Al + ½Fe (AO)[a]	Bulk density	P-Ret.[b]
	%	g cm^{-3}	%	%	g/cm^{-}3	%	%	g cm^{-3}	%
83HI009006	9.81	0.89	100	9.96	0.93	99	13.91	1.00	98
83HI009007	0.69	1.31	52	0.69	1.32	55	0.68	1.35	59
83HI009011	5.84	1.12	94	7.07	1.12	95	11.56	1.13	96
83HI009012	1.36	1.56	56	1.15	1.24	43	1.52	1.66	56
83HI009013	0.72	1.52	56	0.72	1.45	58	0.76	1.47	60
89HI009001	5.76	N/A	93	6.36	N/A	94	6.84	N/A	95
97HI009001	2.83	1.22	69	2.90	1.49	75	2.23	1.49	81
97HI009002	2.30	1.06	56	3.36	1.06	76	4.35	1.06	82
97HI009003	2.42	1.29	72	2.42	1.29	72	2.42	1.29	72
97HI009004	3.23	0.44	94	2.84	0.44	94	2.84	0.44	94
97HI009005	2.07	1.22	82	2.85	1.22	86	4.60	1.22	89
98HI009001	12.38	N/A	94	12.55	N/A	95	12.68	N/A	96
98HI009002	6.49	N/A	82	7.02	N/A	85	7.64	N/A	88

[a] AO, ammonium oxalate; [b] P-ret., phosphate retention.

Spatial prediction of Andisols and andic intergrades

Tables 4-2 to 4-4 show the results and statistics of multiple linear regression models used for the spatial prediction of Al + ½Fe (AO), bulk density, and phosphate retention soil properties. While wind strength had less effect on ash distribution (Hurst and Turner, 1999), wind speed is a main predictor for all bulk density models (Tables 4-2 to 4-4). However, wind speed was only significant when using depth-weighted average data to 75-cm. Wind Effect—which accounts for topographic elevation to produce a windward/leeward index raster—was, however, a statistically significant factor in the prediction of all three soil properties for the 0-60 cm study pedon dataset (Table 2). Model goodness-of-fit plots for each prediction model are shown in Figures 4-5 to 4-7.

The presence of Euclidean distance and wind effect as covariates in all models (Tables 4-2 to 4-4) show the importance of volcanic vent location from which ash is sourced, as well as the effects of meteorological conditions on the disbursement of ash and ashfall location. The significance of Euclidean distance and wind effect rasters as model covariates may also be attributed to the isolation of the Hawaiian Islands. Hawaii's distance from any other potential sources of volcanic ash, including the prevailing wind pattern across East Maui, have likely contributed to the success of our models. Using wind effect, wind speed, and Euclidean distance in modeling soil properties as a result of historical ash deposition events may be of interest in continental areas, but may be better suited for other volcanic islands or locations which are minimally influenced by variable wind patterns, and have defined, local ash sources.

All three soil properties using the 0-60 cm data (Table 4-2) include covariates that affect both ash distribution (Euclidean distance, wind effect, wind speed) and ash weathering (PET, MAT, MAP). All models were highly statistically significant, and most covariates using 0-60 cm data were statistically significant with the exception of Euclidean distance (Al + ½Fe (AO)), and MAP and wind speed (Bulk Density).

Goodness-of-fit for prediction models using 0-60 cm depth-weighted average data were all statistically significant with high correlation coefficient values for both training and validation datasets (Figure 4-5). Validation set goodness-of-fit for all dataset models are generally weaker than the training datasets (Figures 4-5 to 4-7). Typically, the training set for this approach in model fitting consists of a random, and larger, subset (70%) of all available data, with the training set consisting of the remaining 30% of the dataset. However, the NRCS pedons dataset has a slightly larger sample size (n = 18) than the sampled pedon dataset of the training set (n = 16), which may have led to the weakened validation model goodness-of-fit. Data from sampled soils and NRCS soils were not combined into one dataset for various reasons. Bulk density of sampled soils was done by the hammer-driven corer method, whereas the NRCS generally uses bulk density values at -33 kPa water content. While the same methods were used for Al + ½Fe (AO) and phosphate retention, execution of analytical methods varies by laboratory worker, potentially creating variation in accuracy and precision. Because study and NRCS sample sizes are small, and the author was not involved in the field sampling or laboratory analyses of NRCS sampled soils, combining sampled and NRCS soil data into one dataset may have weakened initial soil property prediction models.

Table 4-2. Statistical results for Al + ½Fe (AO), bulk density, and phosphate retention models using depth-weighted average data 0-60 cm.

Soil Property	Coefficients	Estimate	Std. Error	t value	p-value	VIF	Model		
							Multiple R^2	Adjusted R^2	p-value
Al + ½Fe (AO)	(Intercept)	-0.19	3.31	-0.06	0.95	--	0.71	0.63	0.003**
	Euclidean Distance	4.58E-04	3.38E-04	1.36	0.20	2.50			
	Wind Effect	8.64	2.69	3.22	0.008**	1.79			
	PET	-2.87E-03	7.15E-04	-4.01	0.002**	1.91			
Bulk Density	(Intercept)	-1.41	5.49E-01	-2.57	0.04*	--	0.85	0.71	0.01**
	MAT	0.10	2.38E-02	4.20	0.004**	2.84			
	MAP	1.08E-04	9.68E-05	1.12	0.30	3.56			
	Euclidean Distance	-4.09E-05	2.09E-05	-1.96	0.09†	1.88			
	Wind Speed	0.10	7.02E-02	1.38	0.21	2.25			
	Wind Effect	0.49	2.38E-01	2.06	0.08†	2.76			
	Soil Evaporation	-3.81E-03	1.52E-03	-2.51	0.04*	3.63			
Phosphate Retention	(Intercept)	14.06	13.03	1.08	0.30	--	0.86	0.83	4.52E-05***
	Euclidean Distance	3.97E-03	1.33E-03	2.98	0.01**	2.50			
	Wind Effect	73.98	10.59	6.98	0.00002***	1.79			
	PET	-0.02	2.82E-03	-5.50	0.0002***	1.91			

Note. AO, ammonium oxalate; MAP, mean annual precipitation; MAT, mean annual temperature; PET, potential evapotranspiration; VIF, variance inflation factor.

†Significant at the .1 probability level. *Significant at the .05 probability level. **Significant at the .01probability level. ***Significant at the .001 probability level.

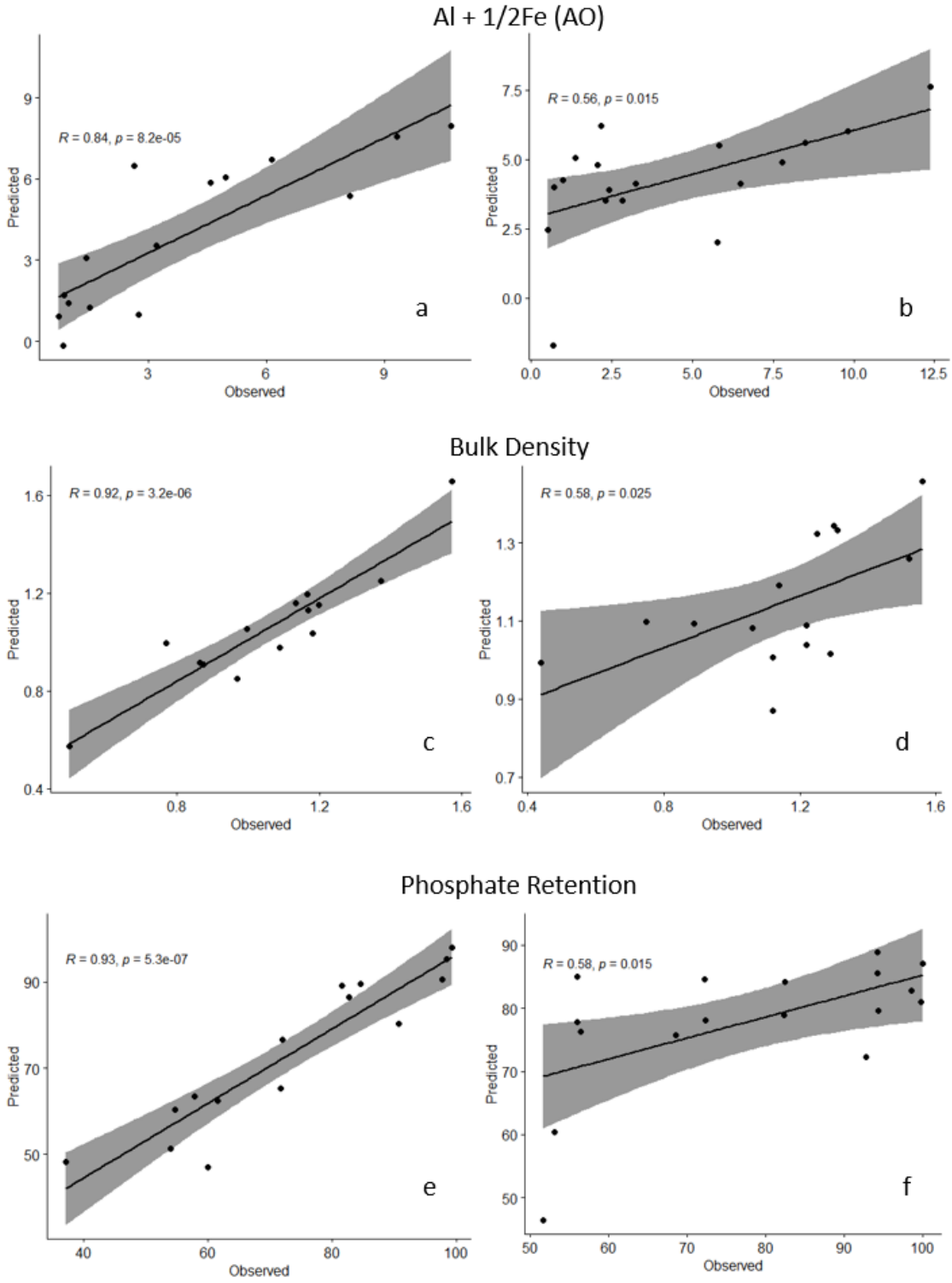

Figure 4-5. Goodness-of-fit for Al + ½Fe (AO), bulk density, and phosphate retention prediction models (0-60 cm data). Training (a, c, d) used the sampled pedon dataset, and validation (b, d, f) used the NRCS pedon dataset. Grey area indicates 90% confidence interval. AO = ammonium oxalate; p = probability value; R = correlation coefficient.

Model statistics for Al + ½Fe (AO) using 0-75 cm data (Table 4-3) looks nearly identical to model statistics using the shallower 0-60 cm dataset from Table 4-2. The covariates used are the same and model significance and correlation coefficient have not worsened much. Because data used are depth-weighted averages, much of the model data (60/75 cm) in Tables 4-2 and 4-3 are shared, explaining their similarities. Covariates MAT and MAP do not contribute to the bulk density model when including data between 60 and 75-cm (Table 4-3) and primarily consists of covariates that affect ash deposition, of which all are significant. While the bulk density model p-value—including its covariates and the validation goodness-of-fit (Figure 4-6c)—are all significant with high correlation coefficients, the training set's goodness-of-fit model was marginally significant with a low correlation coefficient (Figure 4-6d), the weakest in the study. Phosphate retention is not a soil property considered when determining andic-intergrades of non-Andisol soil orders (Soil Survey Staff, 2014a).

Table 4-3. Statistical results for Al + ½Fe (AO) and Bulk Density models using depth-weighted average data 0-75 cm. AO = ammonium oxalate.

Soil Property	Coefficients	Estimate	Std. Error	t value	p-value	VIF	Model		
							Multiple R^2	Adjusted R^2	p-value
Al + 1/2Fe (AO)	(Intercept)	-0.36	3.65	-0.10	0.92	--	0.69	0.61	0.004**
	Euclidean Distance	4.86E-04	3.72E-04	1.31	0.22	2.50			
	Wind Effect	9.24	2.96	3.12	0.01**	1.79			
	PET	-3.04E-03	7.89E-04	-3.85	0.003**	1.91			
Bulk Density	(Intercept)	0.85	0.24	3.57	0.007**	--	0.83	0.73	0.006**
	Elevation	-5.36E-04	1.28E-04	-4.20	0.003**	2.12			
	Euclidean Distance	-3.78E-05	1.97E-05	-1.92	0.09†	1.84			
	Wind Speed	0.13	0.06	2.29	0.05*	1.64			
	Wind Effect	0.54	0.23	2.38	0.04*	2.74			
	Soil Evaporation	0.00	0.00	-2.76	0.02*	2.93			

Note. AO, ammonium oxalate; PET, potential evapotranspiration; VIF, variance inflation factor.

†Significant at the .1 probability level. *Significant at the .05 probability level. **Significant at the .01probability level. ***Significant at the .001 probability level.

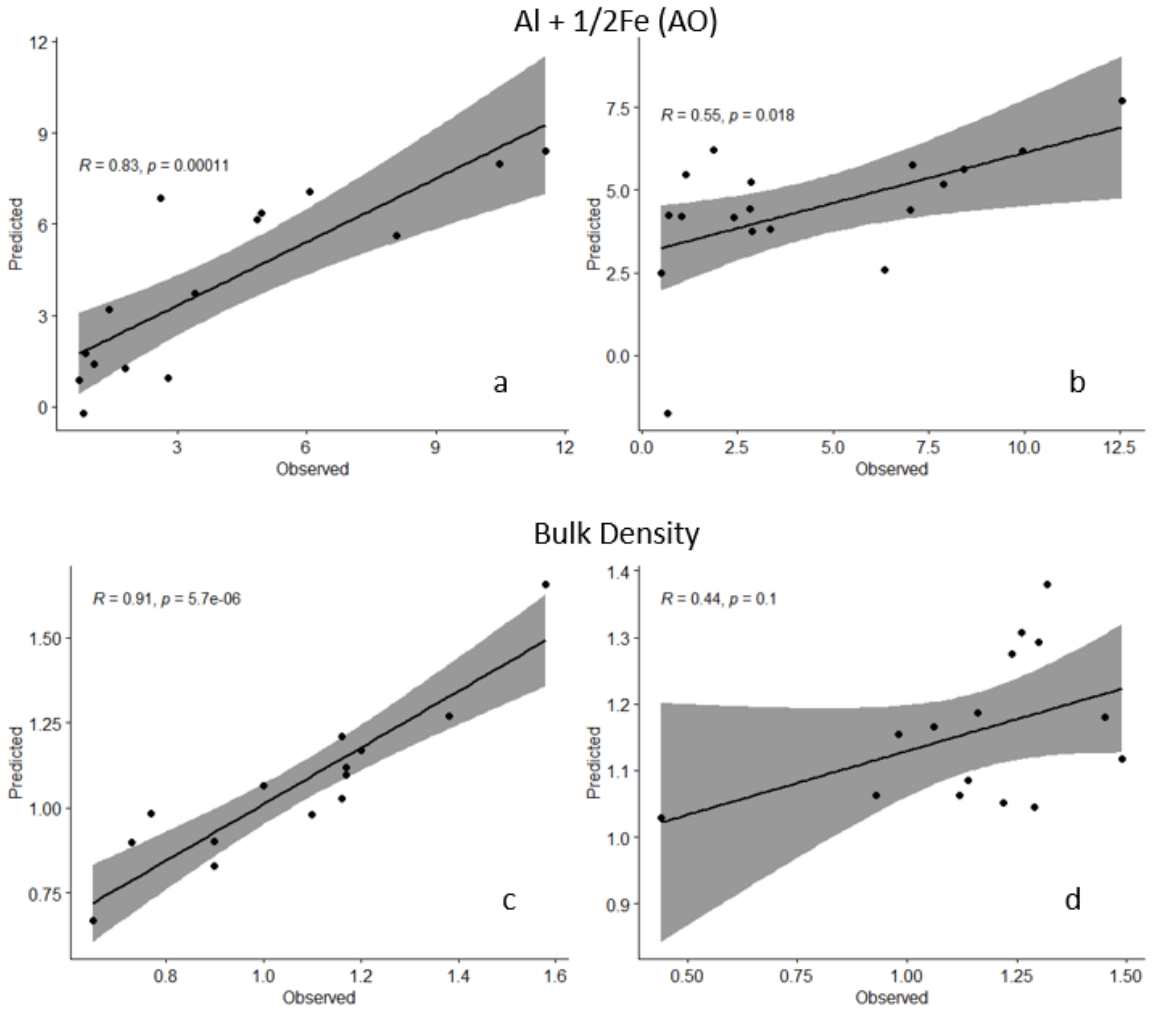

Figure 4-6. Goodness-of-fit for Al + ½Fe (AO) and bulk density prediction models (0-75 cm data). Training (a, c) used the sampled pedon dataset, and validation (b, d) used the NRCS pedon dataset. Grey area indicates 90% confidence interval. AO = ammonium oxalate; p = probability value; R = correlation coefficient.

Considering soil data to 1-m versus 60 or 75-cm did not negatively affect model significance for Al + 1/2Fe (AO), but it weakened the significance of model covariates (Table 4-4). None are statistically significant with the exception of PET. Soil weathering and the formation of Al + ½Fe (AO) may be less prevalent deep within a pedon, explaining the lack of covariate significance with this soil property model, unless we observe a buried horizon, such as with pedon OL at 83 cm. The presence of the same

covariates for the bulk density and phosphate retention models are little affected with the changing dataset depths between 60 and 100 cm, as well as their validation goodness-of-fit (Figure 4-7).

Table 4-4. Statistical results for Al + ½Fe (AO), bulk density, and phosphate retention models using depth-weighted average data 0-1 m.

Soil Property	Coefficients	Estimate	Std. Error	t value	p-value	VIF	Model		
							Multiple R^2	Adjusted R^2	p-value
Al + ½Fe (AO)	(Intercept)	11.14	10.46	1.064	0.31	--	0.73	0.62	0.007**
	MAT	-0.50	0.41	-1.21	0.25	3.12			
	Euclidean Distance	4.26E-04	4.03E-04	1.059	0.31	2.67			
	Wind Effect	6.85	4.10	1.671	0.13	2.99			
	PET	-2.23E-03	1.19E-03	-1.884	0.09†	4.09			
Bulk Density	(Intercept)	-1.38	0.42	-3.31	0.01**	--	0.87	0.79	0.002**
	MAT	0.09	0.02	5.47	5.97E-04***	2.09			
	Euclidean Distance	-3.4E-05	1.749E-05	-1.94	0.09†	1.85			
	Wind Speed	0.11	0.05	2.21	0.06†	1.57			
	Wind Effect	0.50	0.20	2.50	0.04*	2.73			
	Soil Evaporation	-2.38E-03	1.14E-03	-2.09	0.07†	2.88			
Phosphate Retention	(Intercept)	24.56	15.35	1.60	0.14	--	0.80	0.74	3.81E-04***
	Euclidean Distance	3.51E-03	1.57E-03	2.24	0.05*	2.50			
	Wind Effect	66.29	12.47	5.31	2.47E-04***	1.79			
	PET	-0.01	3.32E-03	-4.49	9.22E-04***	1.91			

Note. AO, ammonium oxalate; MAT, mean annual temperature; PET, potential evapotranspiration; VIF, variance inflation factor.
†Significant at the .1 probability level. *Significant at the .05 probability level. **Significant at the .01probability level. ***Significant at the .001 probability level.

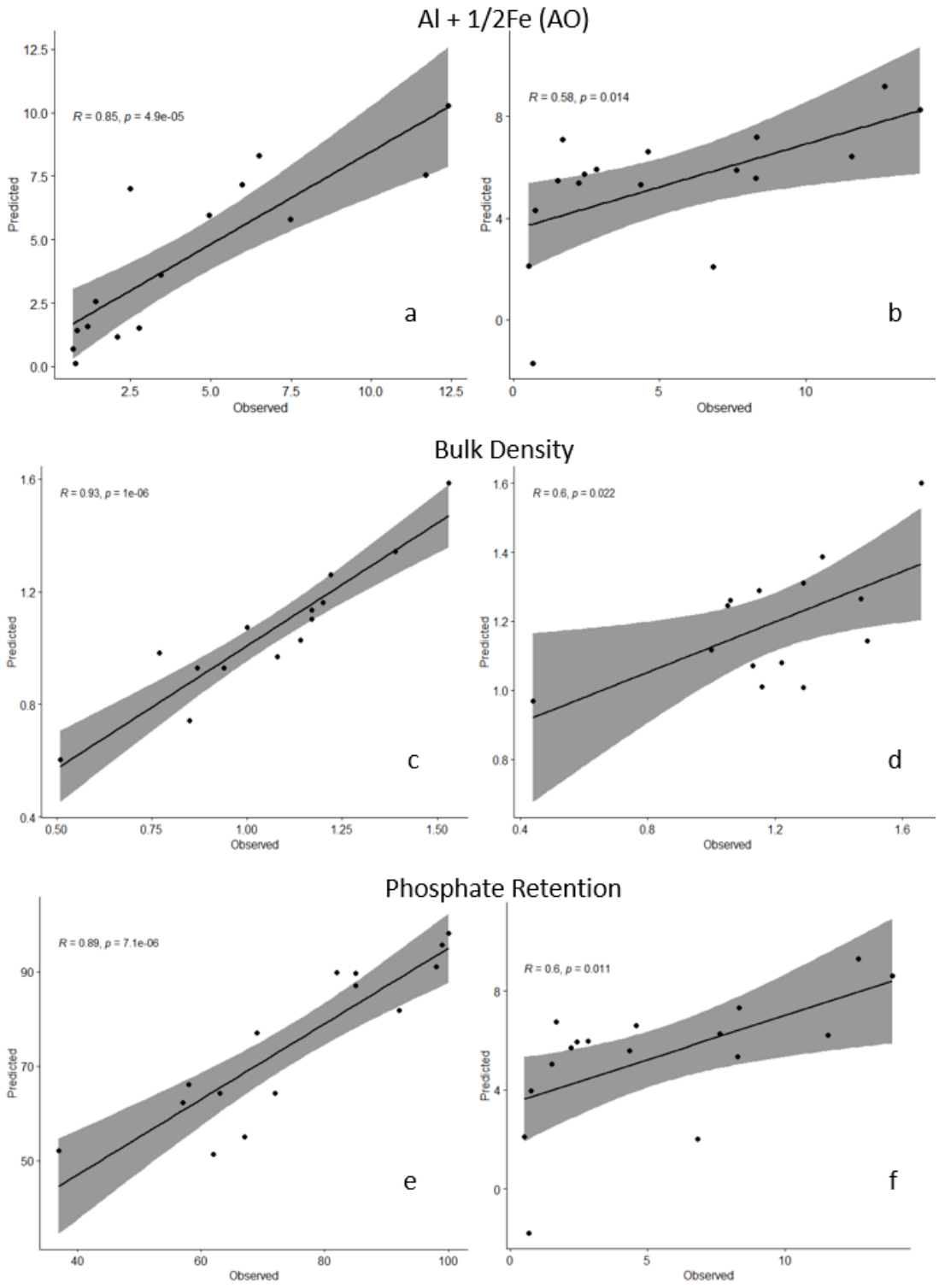

Figure 4-7. Goodness-of-fit for Al + ½Fe (AO), bulk density, and phosphate retention prediction models (0-1 m data). Training (a, c, d) used the sampled pedon dataset, and validation (b, d, f) used the NRCS pedon dataset. Grey area indicates 90% confidence interval. AO = ammonium oxalate; p = probability value; R = correlation coefficient.

Figure 4-8 shows the mean prediction raster results of all three soil property models used to determine the areal extent of Andisols across the study area using depth-weighted average data to 1 meter. As elevation increases (towards the summit of Haleakalā), there is an increase in Al + ½Fe (AO) and phosphate retention, and a decrease in bulk density.

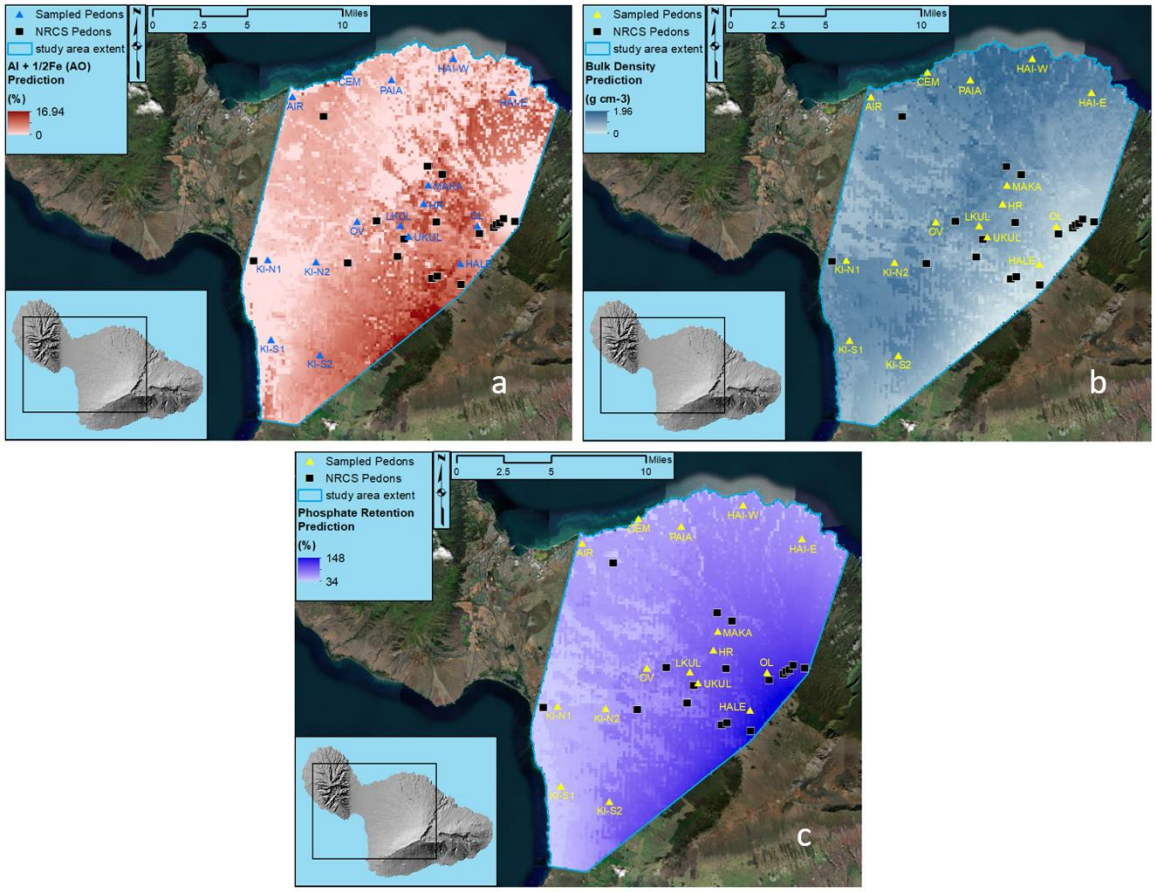

Figure 4-8. Mean spatial predictions for Al + ½Fe (AO; a), bulk density (g cm^{-3}; b), and phosphate retention (%; c) across western Haleakalā, Maui. Depth-weighted average data to 1 m were used for each soil property. AO = ammonium oxalate.

Prior to converting rasters of Figure 4-8 to polygons, raster cells that did not meet the minimum requirement for each respective soil property for andic and andic-intergrades characteristics were set to null. The minimal extent of each soil property

prediction could then be synthesized. Figure 4-9 below shows the mean areal extent of Andisols and andic-intergrades across the study area using depth-weighted average data to 1-m. By displaying non-vitric Andisols and andic-intergrades that have been mapped

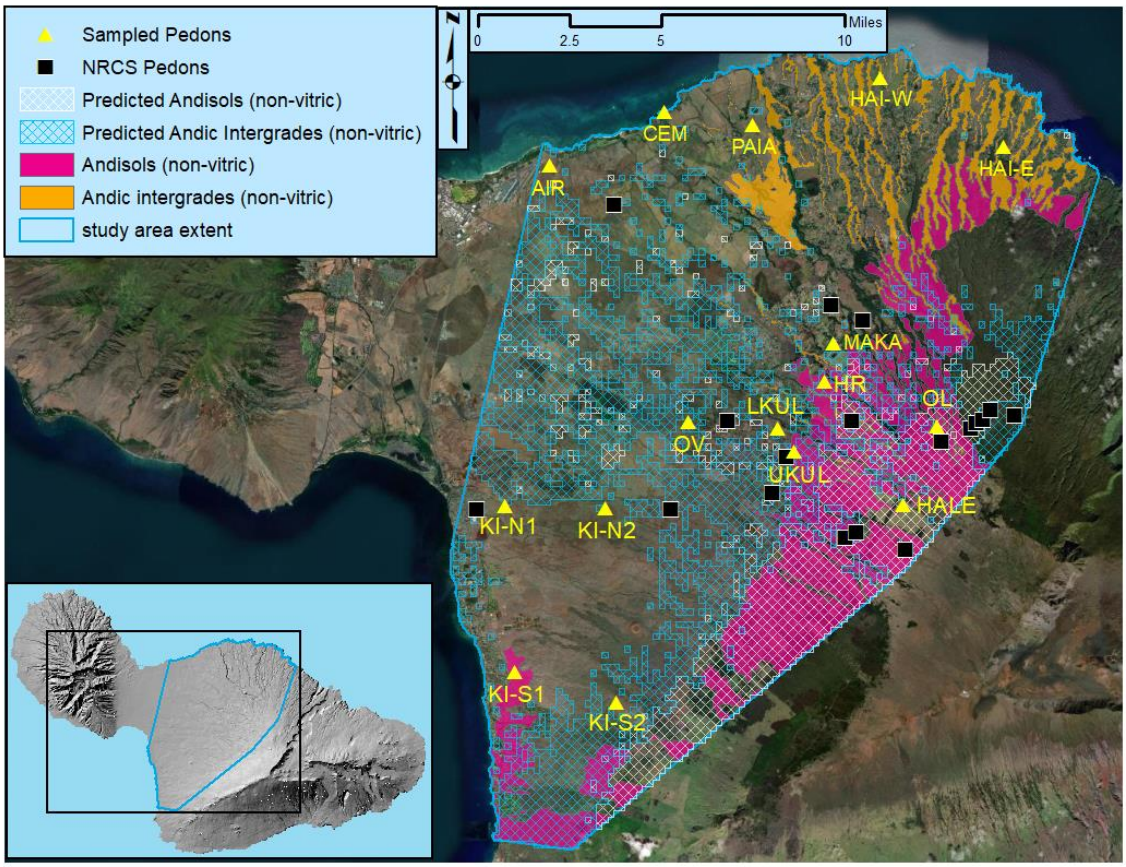

Figure 4-9. Minimum areal extent of the stacked soil property spatial predictions (Figure 8) for Andisols (white cross hatch) and andic intergrades (blue cross hatch) across western Haleakalā, Maui. Soil property data for spatial predictions was depth-weighted averaged to 1-m. Soil properties used are based on the requirements for non-vitric Andisols and andic intergrades according to Keys to Soil Taxonomy (Soil Survey Staff, 2014).

by the NRCS (Figure 4-9), we get an idea of just how our predictions compare visually, and where, perhaps, additional soil sampling and classification can be done to better map these soils. The predicted extent of Andisols occurs over much of the same area that is mapped as Andisols (Figure 4-9). However, most of the area predicted as andic

intergrades does not occur where it is mapped. Andic intergrades can have greater agronomic potential than those that are not, and the fact that predicted andic intergrades occur over much of undeveloped central Maui could threaten how these landscapes are utilized in the future.

Using soil property data to 60-cm for Andisols and 75-cm for andic intergrades, the mean prediction accuracy of the models in correctly classifying a soil pedon is 50% for NRCS pedons in the study area and 62.5% for our study pedons (Table 4-5). When looking at just the Andisols and andic-intergrades, NRCS pedons were predicted correctly at 50%, while the study pedons had a classification accuracy of just 16.7%. The areal extents of Andisols and andic intergrades are unaltered from the raster predictions. Upon closer observation of Figure 4-9, many pedons that were inaccurately predicted fall just outside of a pixel which would accurately classify them. Lower and upper limit prediction accuracy boundaries (90% CI) is shown in Table 4-5. For the lower limit, the prediction accuracy naturally increases across the board for Andisols and andic-intergrades for both study and NRCS pedon classification. However, overall accuracy, when considering non-andic pedon classification, decreases. This can be expected as the minimum requirements for soil properties to be considered andic is more liberal spatially. The opposite is seen for upper limit prediction accuracy. As there are more study pedons that are classified as non-andic, their expectation to be classified as Andisols or andic-intergrades increases, and therefore decreases the overall prediction accuracy.

Table 4-5. Lower and Upper limit (90% Confidence Interval) prediction accuracies of soil property models (depth-weighted average data to 60 and 75-cm, Tables 4-2 and 4-3), and the classification of study and NRCS pedons across western Haleakalā, Maui.

Sampled				**NRCS**			
Pedon	**Classification**	**Predicted as[a]**		**Pedon**	**Classification**	**Predicted as[a]**	
		Lower	**Upper**			**Lower**	**Upper**
MAKA	Humic Haplustands	And	Non	83HI009004	Humic Haplustands	And	Non
HALE	Pachic Haplustands	And	Int	83HI009005	Typic Haplustands	And	Int
HR	Humic Haplustands	And	Non	83HI009006	Humic Haplustands	And	Int
OV	Andic Haplustolls	Int	Non	83HI009011	Dystric Haplustands	And	Non
OL	Andic Dystrustepts	And	Non	89HI009001	Ultic Hapludands	Int	Non
LKUL	Andic Haplustolls	And	Non	97HI009004	Acrudoxic Hydrudands	And	Non
KI-N1	Torroxic Haplustolls	Int	Non	98HI009001	Pachic Haplustands	And	Int
KI-S1	Aridic Argiustolls	Int	Non	98HI009002	Typic Hydrudands	And	Non
AIR	Typic Haplustolls	Int	Non	83HI009003	Andic Haplustolls	And	And
CEM	Oxic Haplustepts	Non	Non	97HI009001	Andic Dystrudepts	And	Non
HAI-W	Typic Sombrihumults	Non	Non	97HI009002	Andic Dystrudepts	And	Non
HAI-E	Typic Haplohumults	And	Non	97HI009003	Andic Dystrudepts	And	Non
KI-S2	Aridic Lithic Haplustolls	And	Non	83HI009001	Typic Haplocambids	Non	Non
KI-N2	Aridic Haplustolls	Int	Non	83HI009007	Rhodic Eutrustoxes	And	Non
UKUL	Typic Argiustolls	And	Non	83HI009012	Oxic Dystrudepts	Non	Non
PAIA	Oxic Haplustolls	Int	Non	83HI009013	Pachic Haplustolls	And	Non
				97HI009005	Fluvaquentic Humaquepts	And	Non
				83HI009002	Torroxic Haplustolls	And	Non
Classification Accuracy							
Andisols		100%	0%			87.5%	0%
Andic intergrades		33.3%	0%			0%	0%
Other		20%	100%			33%	100%
All pedons		37.5%	62.5%			50%	33.3%

Note. dark gray = Andisols, light gray = andic intergrades, white = non-andic soils.

[a] And, Andisol; Int, andic intergrade; Non, non-andic.

Using depth-weighted average data to 1-m for model predictions had surprising results in terms of accuracy in pedon classification. Soil property models show 88.9%, 87.5%, and 100% accuracy for all NRCS pedons, Andisols, and andic-intergrades, respectively (Table 4-6). This is an increase of 38.9% in accuracy (all NRCS pedons) from predictions which used data that was restricted to 60 cm and 75 cm. Classification

of soils always takes into consideration land use and management. Soil beneath 60-cm is less likely to affect land use and management, and therefore is not considered when

Table 4-6. Prediction accuracies of soil property models (depth-weighted average data to 60 and 75-cm, and 1-m) using Figures 4-6 and 4-7a, and the pedon classification of study and NRCS pedons across western Haleakalā, Maui.

Sampled				**NRCS**			
Pedon	**Classification**	**Predicted as[a]**		**Pedon**	**Classification**	**Predicted as[a]**	
		60/75-cm	**1-m**			**60/75-cm**	**1-m**
MAKA	Humic Haplustands	Int	And	83HI009004	Humic Haplustands	Int	And
HALE	Pachic Haplustands	And	And	83HI009005	Typic Haplustands	And	And
HR	Humic Haplustands	Int	And	83HI009006	Humic Haplustands	And	And
OV	Andic Haplustolls	Non	Int	83HI009011	Dystric Haplustands	And	And
OL	Andic Dystrustepts	And	And	89HI009001	Ultic Hapludands	Non	Non
LKUL	Andic Haplustolls	Non	Non	97HI009004	Acrudoxic Hydrudands	Int	And
KI-N1	Torroxic Haplustolls	Non	Non	98HI009001	Pachic Haplustands	Int	And
KI-S1	Aridic Argiustolls	Non	Non	98HI009002	Typic Hydrudands	And	And
AIR	Typic Haplustolls	Non	Non	83HI009003	Andic Haplustolls	Int	Int
CEM	Oxic Haplustepts	Non	Non	97HI009001	Andic Dystrudepts	And	Int
HAI-W	Typic Sombrihumults	Non	Non	97HI009002	Andic Dystrudepts	Int	Int
HAI-E	Typic Haplohumults	Non	Non	97HI009003	Andic Dystrudepts	And	Int
KI-S2	Aridic Lithic Haplustolls	Non	Non	83HI009001	Typic Haplocambids	Non	Non
KI-N2	Aridic Haplustolls	Non	Non	83HI009007	Rhodic Eutrustoxes	And	Non
UKUL	Typic Argiustolls	Non	And	83HI009012	Oxic Dystrudepts	Non	Non
PAIA	Oxic Haplustolls	Int	Non	83HI009013	Pachic Haplustolls	Int	Non
				97HI009005	Fluvaquentic Humaquepts	Int	And
				83HI009002	Torroxic Haplustolls	Non	Non
Classification Accuracy							
Andisols		33.3%	100%			50%	87.5%
Andic intergrades		0%	33.3%			50%	100%
Other		90%	90%			50%	83.3%
All pedons		62.5%	81.3%			50%	88.9%

Note. dark gray = Andisols, light gray = andic intergrades, white = non-andic soils.
[a] And, Andisol; Int, andic intergrade; Non, non-andic.

classifying Andisols. For example, Study Pedon LKUL is classified as an Andic Dystrustept, and that is because this soil does not meet the minimum criteria for andic properties, in terms of thickness, in the upper 60-cm of the soil. However, below 60-cm,

andic properties and organic carbon content are highly expressed, likely because it is a horizon that once contained a high volume of volcanic ash. This horizon may have once been located at the surface of the soil during an ash-depositing volcanic event(s) prior to being buried. Because depth-weighted average data to 1 m factored in higher Al + ½Fe (AO) and lower bulk density values, Pedon LKUL was misclassified as an Andisol.

While not relevant in terms of land use and management for the purpose of taxonomic classification, using data that had been depth-weighted to 1-m versus 60-cm took into account an ash depositional event that would have otherwise been ignored. The purpose of this modeling approach is to consider the possibility of a soil being exposed to the deposition of ash, which over time, leads to the formation of soil properties unique to andic soils. To do this, all available data with depth needs to be considered and represented in Andisol and andic intergrade prediction models. Accounting for the record of volcanic ash origin appears to matter most in our spatial prediction modeling, regardless of whether soils are classified as Andisols or andic intergrades.

This method of spatially predicting the extent of Andisols, andic intergrades, and non-andic soils, while relatively accurate at 88.9% (87.5% for Andisols and 100% andic intergrades), should not be relied on in determining the reach of andic soils, but rather serve as a suggestion as to where funding for future sampling and analysis should be directed. Considering the significance of the prediction models, their relative accuracy, and how little the mapped andic intergrades coincide with predicted andic intergrades, these findings should encourage further investigation as to where andic intergrades truly extend. The soils of western Haleakalā are diverse, inherently fertile, and limited in extent. Improving soil mapping of some of these soils would ideally preserve limited

prime farmland and range land for what they are most suited for. This may create opportunity to increase Hawaii's self-sustainability—reducing food costs and the state's reliance on imported goods—as well as reevaluate areas that may have been considered for urban development, preserving them for range management and agriculture.

REFERENCES

Arrouays, D., McBratney, A., Bouma, J., Libohova, Z., Richer-de-Forges, A. C., Morgan, C. L., ... & Mulder, V. L. (2020). Impressions of digital soil maps: The good, the not so good, and making them ever better. *Geoderma Regional*, *20*, e00255.

Brady, N. C., Weil, R. R., & Weil, R. R. (2008). *The Nature and Properties of Soils* (Vol. 13, pp. 662-710). Upper Saddle River, NJ: Prentice Hall.

Búcaro-González, A., Mata, R. A., Alemán-Montes, B., Fernandez-Moya, J., Algeet-Abarquero, N., Tobías, H., Henríquez-Henríquez, C., & Camacho, M. E. (2022). Soil Digital Mapping of Chemical Properties in Volcanic Ash Soils: A Case of Study in Atitlán Lake Basin, Guatemala. Available at SSRN: https://ssrn.com/abstract=4041741 or http://dx.doi.org/10.2139/ssrn.4041741

Buol, S. W., Southard, R. J., Graham, R. C., & McDaniel, P. A. (2011). *Soil Genesis and Classification*. John Wiley & Sons.

Conrad, O., Bechtel, B., Bock, M., Dietrich, H., Fischer, E., Gerlitz, L., Wehberg, J., Wichmann, V., & Böhner, J. (2015). System for Automated Geoscientific Analyses (SAGA) v. 2.1.4, *Geoscientific Model Development*, *8*, 1991-2007, doi:10.5194/gmd-8-1991-2015.

Dahlgren, R., Shoji, S., & Nanzyo, M. (1993). Mineralogical characteristics of volcanic ash soils. In *Developments in Soil Science* (Vol. 21, pp. 101-143). Elsevier.

Dahlgren, R. A., Boettinger, J. L., Huntington, G. L., & Amundson, R. G. (1997). Soil development along an elevational transect in the western Sierra Nevada, California. *Geoderma*, *78*(3-4), 207-236.

Folch, A., Costa, A., & Macedonio, G. (2009). FALL3D: A computational model for transport and deposition of volcanic ash. *Computers & Geosciences*, *35*(6), 1334-1342.

Fox, J., & Weisberg, S. (2019). An {R} Companion to Applied Regression, Third Edition. Thousand Oaks, CA: Sage. URL: https://socialsciences.mcmaster.ca/jfox/Books/Companion/

Giambelluca, T. W., Q. Chen, A. G. Frazier, J. P. Price, Y. L. Chen, P. S. Chu, J. K. Eischeid, and D.M. Delparte. (2013). Online Rainfall Atlas of Hawai‘i. *Bulletin of the American Meteorological Society*, *94*, 313-316, doi: 10.1175/BAMS-D-11-00228.1.

Giambelluca, T. W., Shuai, X., Barnes, M. L., Alliss, R. J., Longman, R. J., Miura, T., Chen, Q., Frazier, A. G., Mudd, R. G., Cuo, L., & Businger, A. D. (2014). Evapotranspiration of Hawai‘i. Final report submitted to the U.S. Army Corps of Engineers—Honolulu District, and the Commission on Water Resource Management, State of Hawai‘i.

Hijmans, R.J. (2020). raster: Geographic Data Analysis and Modeling. R package version 3.4-5. https://CRAN.R-project.org/package=raster

Hillel, D., & Hatfield, J. L. (Eds.). (2005). *Encyclopedia of Soils in the Environment* (Vol. 3). Amsterdam: Elsevier.

Hurst, T., & Davis, C. (2017). Forecasting volcanic ash deposition using HYSPLIT. *Journal of Applied Volcanology*, *6*(1), 1-8.

Hurst, A. W., & Turner, R. (1999). Performance of the program ASHFALL for forecasting ashfall during the 1995 and 1996 eruptions of Ruapehu volcano. *New Zealand Journal of Geology and Geophysics*, *42*(4), 615-622.

Ito, T., Shoji, S., & Saigusa, M. (1991). Classification of volcanic ash soils from Konsen district, Hokkaido [Japan], according to the last keys to soil taxonomy (1990). *Japanese Journal of Soil Science and Plant Nutrition (Japan)*.

IUSS Working Group WRB. (2015). World Reference Base for Soil Resources 2014, update 2015 International soil classification system for naming soils and creating legends for soil maps. *World Soil Resources Reports No. 106*. FAO, Rome.

Lumley, T. based on Fortran code by Alan Miller (2020). leaps: Regression Subset Selection. R package version 3.1. https://CRAN.R-project.org/package=leaps.

McBratney, A. B., Santos, M. M., & Minasny, B. (2003). On digital soil mapping. *Geoderma*, *117*(1-2), 3-52.

McDaniel, P. A., Lowe, D. J., Arnalds, O., & Ping, C. L. (2012). Andisols. In ‘*Handbook of Soil Sciences. Vol. 1: Properties and Processes’* (eds. PM Huang, Y Li, ME Sumner) pp. 33.29-33.48.

Minasny, B., & McBratney, A. B. (2016). Digital soil mapping: A brief history and some lessons. *Geoderma*, *264*, 301-311.

Nanzyo, M., Dahlgren, R., & Shoji, S. (1993a). Chemical characteristics of volcanic ash soils. In *Developments in Soil Science* (Vol. 21, pp. 145-187). Elsevier.

Nanzyo, M., Shoji, S., & Dahlgren, R. (1993b). Physical characteristics of volcanic ash soils. In *Developments in Soil Science* (Vol. 21, pp. 189-207). Elsevier.

Ping, C. L. (2000). Volcanic soils. *Encyclopedia of Volcanoes. Academic Press, London*, 1259-1270.

R Core Team (2021). R: A language and environment for statistical computing. R Foundation for Statistical Computing, Vienna, Austria. URL https://www.R-project.org/.

Rasmussen, C., Matsuyama, N., Dahlgren, R. A., Southard, R. J., & Brauer, N. (2007). Soil genesis and mineral transformation across an environmental gradient on andesitic lahar. *Soil Science Society of America Journal*, *71*(1), 225-237.

Roudier, P., Ritchie, A., Hedley, C., & Medyckyj-Scott, D. (2015). The rise of information science: a changing landscape for soil science. In *IOP Conference Series: Earth and Environmental Science* (Vol. 25, No. 1, p. 012023). IOP Publishing.

Schoeneberger, P. J., Wysocki, D. A., & Benham, E. C. (Eds.). (2012). *Field Book for Describing and Sampling Soils*. Government Printing Office.

Shang, C., & Zelazny, L. W. (2008). Selective Dissolution Techniques for Mineral Analysis of Soils. *Methods of Soil Analysis: Mineralogical methods. Part 5*, *9*, 33.

Sherrod, D. R., Sinton, J. M., Watkins, S. E., & Blunt, K. M. (2007). *Geologic Map of the State of Hawaii*. US Department of the Interior. USGS.

Shoji, S., Dahlgren, R., & Nanzyo, M. (1993). Genesis of volcanic ash soils. In *Developments in Soil Science* (Vol. 21, pp. 37-71). Elsevier.

Sieffermann, G., & Millot, G. (1969). Equatorial and tropical weathering of recent basalts from Cameroon: allophanes, halloysite, metahalloysite, kaolinite and gibbsite. In *Proceedings International Clay Conference, Tokyo, Japan* (Vol. 1, pp. 417-430).

Soil Survey Staff. (2014a). *Keys to Soil Taxonomy, 12th Edition*. USDA, Natural Resources Conservation Service, Washington, DC.

Soil Survey Staff. (2014b). *Kellogg Soil Survey Laboratory Methods Manual*. Soil Survey Investigations Report No. 42, Version 5.0. R. Burt and Soil Survey Staff (ed.). U.S. Department of Agriculture, Natural Resources Conservation Service.

Soil Survey Staff. (2020). Gridded Soil Survey Geographic (gSSURGO) Database for Hawaii. United States Department of Agriculture, Natural Resources Conservation Service. Available online at https://gdg.sc.egov.usda.gov/. September, 28, 2020 (2020 official release).

Strawn, D. G., Bohn, H. L., & O'Connor, G. A. (2015). *Soil Chemistry*. John Wiley & Sons.

Takahashi, T., & Shoji, S. (2002). Distribution and classification of volcanic ash soils. *Global Environmental Research-English Edition*, *6*(2), 83-98.

Ugolini, F. C., & Dahlgren, R. A. (2002). Soil development in volcanic ash. *Global Environmental Research-English Edition*, *6*(2), 69-82.

Wilding, L. P. (2000). Introduction: General characteristics of soil orders and global distribution. In M. E. Sumner, ed. *Handbook of Soil Science*. CRC Press, Boca Raton, FL, pp. E175-183.

V. CONCLUSIONS

This dissertation took a series of conventional techniques and applied them in unconventional ways to better understand how spatially variable depositions of volcanic ash affect the weathering processes of tropical basalt soils across climosequences. In an attempt to provide clarity to such complicated processes, Chapter II put emphasis on observing soil properties across two precipitation gradients. The first being a coastal sequence that, due to its relative position upwind from volcanic vents, is uninfluenced by volcanic ash. The second is the study-wide climosequence which includes pedons that have been variably influenced by volcanic ash. Chapter II examined soil property trends and pedogenic thresholds of chemical and physical soil properties across these two precipitation gradients of East Maui. Along the coastal climosequence, base saturation and pH remained high before reaching a pedogenic threshold at 1500 mean annual precipitation (MAP) where they begin to decrease. Iron (AO-HH) had a positive linear relationship with precipitation. Using Fe (AO-HH) as a proxy for soil age was considered, however, sampled pedons which receive low levels of rainfall are likely to be older than some pedons at higher rainfall. Crystalline Fe (CD-AO) was shown to increase with increasing MAP to 2000 mm before decreasing due to reduction and mobilization of Fe at higher rainfalls.

Chapter 3 reported the effectiveness of well-established weathering indices in determining pedogenic thresholds across climosequences that are both comprised of various basalt flows, as well as soils at various stages of weathering with variable inputs of volcanic ash over their lifetimes. Additionally, the chapter explored other weathering indices, including SiO_2/TiO_2 and MnO_2/TiO_2. In observing SiO_2/TiO_2 across the coastal

climosequence with increasing precipitation, a pedogenic threshold occurred between pedons AIR and CEM, indicating that the soil of pedon AIR is likely on an older landform than those of pedons CEM and PAIA. A second pedogenic threshold occurred between pedons PAIA and HAI-W, supporting increased soil weathering due to precipitation above 1500 mm MAP, which was the pedogenic threshold defined in Chapter II for dynamic soil properties. Crystalline Fe (CD-AO) for pedons KI-N1 and KI-N2 were higher than any pedon in the coastal climosequence less than 1240 mm in MAP, demonstrating that although they have been rejuvenated by volcanic ash, this area is likely the oldest landform in the study, and that lowland soils of western Haleakalā are older than soils closer to the summit. The MnO_2/TiO_2 index demonstrated similar patterns to Al + ½Fe (AO) by genetic horizon, increasing in horizons determined to have been influenced by ash, and decreasing in horizons that are not influenced by ash. Pedons classified as Andisols or andic intergrades of other soil orders also showed higher pedon averaged SiO_2/TiO_2 and MnO_2/TiO_2 ratios than non-andic soils.

Due to the high variability of volcanic ash across western Haleakalā, its dynamic influence on soil properties, and the limited data of NRCS sampled pedons, Chapter IV explored the application of digital soil mapping using multiple linear regression techniques in estimating the areal extent of andic soils. Of the data rasters used in predicting the extent of phosphate retention, bulk density, and Al + ½Fe (AO), Euclidean distance form a volcanic vent and wind effect were used as covariates for all three soil property models. The shield formation and elevation (10,023 ft; 3,055 m) of Haleakalā forces wind to follow predictable paths around the mountain and across its western flank and through Maui's central valley, carrying ash originating from vents along the

northwest rift and depositing it across the landscape. All three models used in predicting the extent of the three soil properties of interest were statistically significant. Using taxonomic classifications of sampled and NRCS pedons according to *Soil Taxonomy* (Soil Survey Staff, 2014), the predicted extent of andic soils was most accurate when soil property models utilized soil data to 1-m depth versus 60 cm (for Andisols) and 75 cm (for andic intergrades). While using data to 60 and 75 cm is required for properly classifying andic soils in terms of land use and management, we find that doing so does not account for the potential for soil to accumulate ash based on its relative location downwind of volcanic vents. Chapter IV shows that climate and environmental rasters can be used to assist soil surveyors in determining future sampling locations and land management decisions, and demonstrates that there are various ways to approach digital soil mapping depending on the soil property of interest.

The effects of volcanic ash on soil processes and properties including pH, base saturation, and OC, which is clear between pedons like UKUL and LKUL, were not observes on the Kohala Peninsula (Chadwick et al., 2003; Vitousek and Chadwick, 2013; Vitousek et al., 2016), or elsewhere, where pedogenic thresholds are studied along climosequences constrained to a single parent material. The increase in pedogenic thresholds with dynamic soil properties of the elevational climosequence demonstrate the soil rejuvenating effect of ash as a parent material. These factors, along with incongruent patterns of amorphous Fe and Al (AO-PY) as functions of precipitation, show how the influence of volcanic ash disrupts the genesis and weathering direction of Maui's soils.

Smaller and more constrained climosequence studies in the area, geologic substrate dating of the Kula Volcanics across the lower slopes of Haleakalā, and

additional climosequence studies with increasing substrate age would all support a better understanding of pedogenic thresholds, elemental trends with weathering, and the effect of climate on soil property-process-factor relationships of Hawaii's soils.

REFERENCES

Chadwick, O.A., Gavenda, R. T., Kelly, E. F., Zeigler, K., Olson, C. G., Elliot, W. C., & Hendricks, D. M. (2003). The impact of climate on the biogeochemical functioning of volcanic soils. *Chemical Geology, 202*, 195-223.

Soil Survey Staff. (2014). *Keys to Soil Taxonomy, 12th Edition*. USDA, Natural Resources Conservation Service, Washington, DC.

Vitousek, P. M., & Chadwick, O.A. (2013). Pedogenic thresholds and soil process domains in basalt-derived soils. *Ecosystems, 16*(8), 1379-1395.

Vitousek, P., Dixon, J. L., & Chadwick, O. A. (2016). Parent material and pedogenic thresholds: observations and a simple model. *Biogeochemistry, 130*(1), 147-157.

APPENDIX

CHEMICAL, PHYSICAL, AND MINERALOGICAL COMPARISONS OF SELECT PEDONS

MATERIALS AND METHODS

The clay fraction of selected samples was analyzed with X-ray diffraction (XRD) according to Harris and White (2008). Four small-scale paired pedons provide direct comparisons of MAT, MAP, and parent material between sampled pedons and is detailed in Table A-1.

Table A-1. Pairs of sampled pedons with relevant physiographic data and taxonomic family classification of the mapped soil series.

Pedon	**Elevation**	**MAP**	**MAAT**	**Soil Series**	**Taxonomic soil classification of mapped Series**
	m	mm	°C		
KI-N2	224	329	24	Waiakoa	Fine, kaolinitic, isohyperthermic Torroxic Haplustoll
KI-S1	56	335	24	Makena*	Medial, amorphic, isohyperthermic Typic Haplotorrand
UKUL	715	826	19	Pane	Medial, amorphic, isothermic Typic Haplustand
LKUL	624	821	21	Kamaole*	Clayey over fragmental, mixed, semiactive, isothermic Aridic Haplustoll
OL	1226	2267	14	Olinda	Medial, ferrihydritic, isothermic Dystric Haplustand
HALE	1362	1082	13	Kaipoipoi	Medial, amorphic, isomesic Humic Haplustand

* no NRCS lab data.

Figure A-1 illustrates two sampled pedons which present a unique opportunity to measure the influence of surficial ash deposits on soil development. Pedon KI-N2 is on a soil classified as a Torroxic Haplustoll, and pedon KI-S1 is on a soil classified as a Typic Haplotorrand. Both sites are in the same arid soil temperature regime (STR) and soil moisture regime (SMR) (isohyperthermic) and are at similar elevations. According to the

NRCS, KI-S1 is located on the Makena Series, which was established in 1949. As one of four Series of East Maui with no reported lab data, sampling from this site also presents a unique opportunity for the first reported lab data of the Series. The exact location of the site used to describe the Makena Series by the NRCS is unknown due to coarse coordinates available. The Official Series Description (OSD) for the Makena Series describes it as having formed in material weathered from volcanic ash overlying ʻaʻā lava with no further horizon information indicating the presence of volcanic glass or ash (Soil Survey Staff, 2000a). If KI-S1 is influenced by ash, comparing data between these two

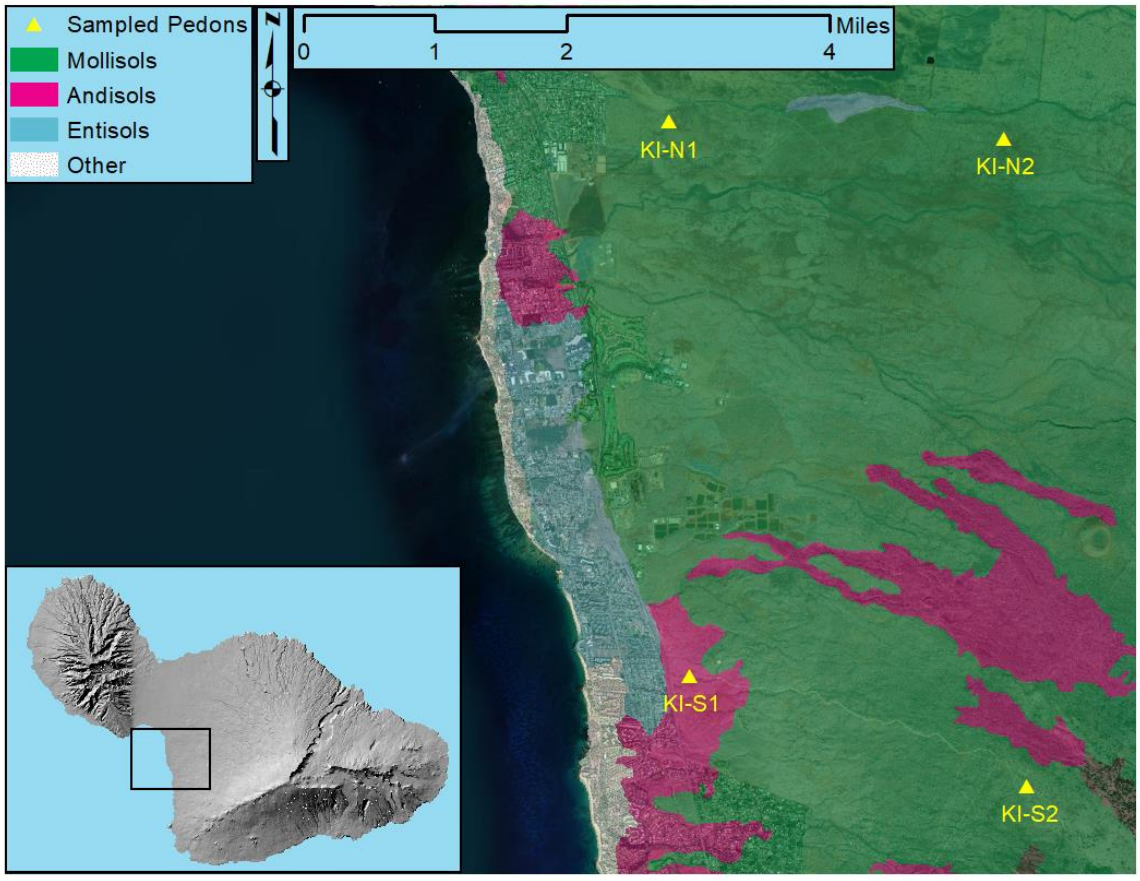

Figure A-1. Soil order map over an aerial image of pedon pair KI-N2 and KI-S1.

pedons will show the effects of ash and its weathering trajectory in an arid climate of leeward Maui which receives the majority of its precipitation as short, intense seasonal rainstorms. Here, leaching potential is low due to low MAP and high evapotranspiration potential, as well as the lack of consistent rainfall throughout the year.

In Figure A-2, a second sequence pair is shown; pedons UKUL and LKUL. Pedon UKUL is on a soil classified as a Typic Haplustand (Pane Series) while LKUL is on a soil classified as an Aridic Haplustoll (Kamaole Series) and are just 0.72 miles apart. The Kamaole Series was established in 1971 and is the third Series addressed which does not have any recorded lab data, presenting a unique opportunity to be the first to quantify various soil properties of this Series. The Kamaole Series OSD is said to have formed in material weathered from ash over ʻaʻā lava with no further horizon information indicating the presence of volcanic glass or ash (Soil Survey Staff, 2000b). Both Series are reported as having formed in material weathered from volcanic ash overlying basalt. What makes this sequence interesting for investigation is that fact that (1) there is a lack of lab data at for this Series, which means it could potentially be reclassified, and (2) if the soils of pedon LKUL remains an Aridic Haplustoll, the lower values of Al + ½Fe (AO) and/or volcanic glass of UKUL could tell a story of soil rejuvenation at LKUL, since this soil should meet the criteria for andic properties (Soil Survey Staff, 2014).

In Figure A-2, pedons LKUL, UKUL, and HR were sampled from a Typic Haplustand (Pane Series) and an Aridic Haplustoll (Kamaole Series). They lie at an elevation of 609 – 730 m (2000 – 2400 ft) and receive a MAP of 806 – 866 mm. The pedons located in the purple polygons are given the same classification: Pane Series. Where this sequence differs is in its MAP (~550 mm or 21 in dryer) and the inclusion of

a site on a soil classified as the Kamaole Series (Mollisol). Pedon KI-S2, above the town of Makena, is also located on the Kamaole Series. It is at a lower elevation (440 m; 1450 ft) and has a much dryer MAT (527 mm; 20 in) than pedons in Figure A-2.

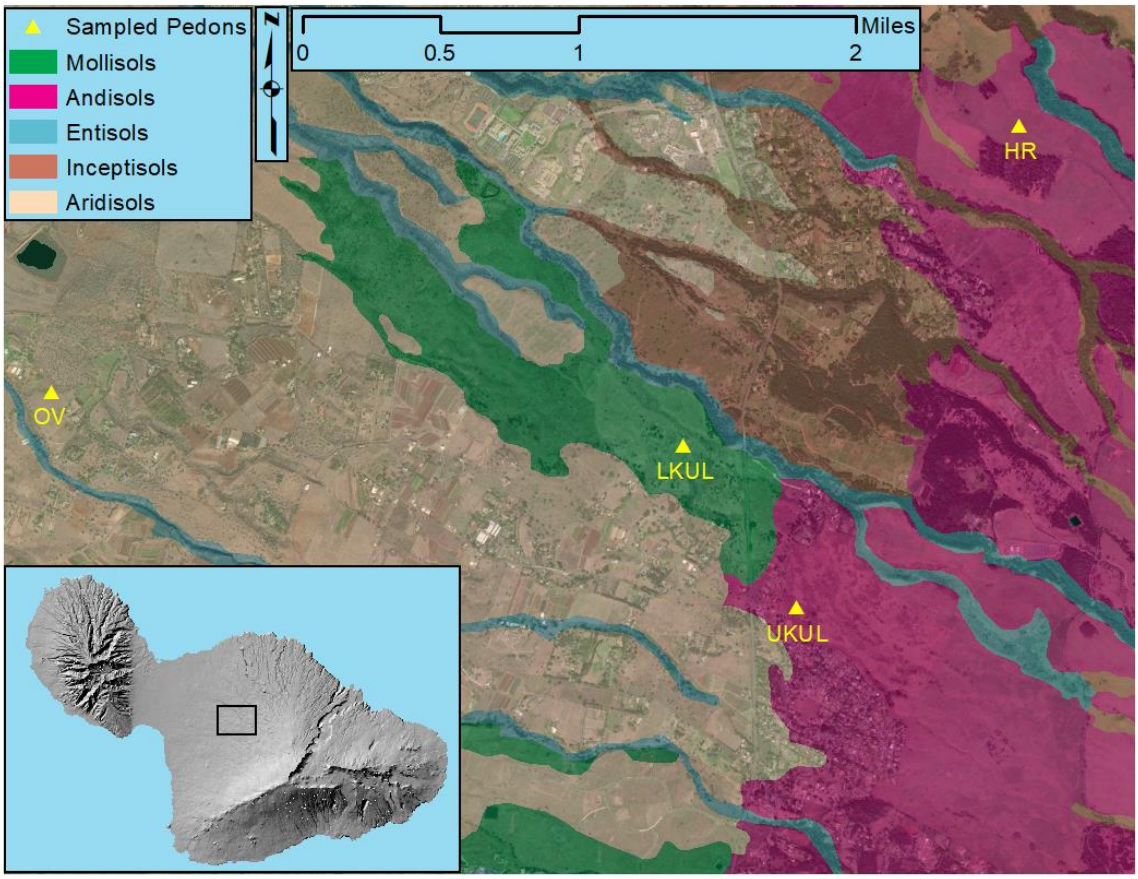

Figure A-2. Soil order map over an aerial image of pedon pair UKUL and LKUL sample site locations.

Looking at Figure A-3 below, pedon HALE is located in a rock outcrop, according to the NRCS. When HALE was originally planned for sampling, the area was classified as an Andisol. During the 2020 sampling excursion, it was noted that the area surrounding HALE had a surface rock cover of 10% and the pedon (surface to 100 cm) had a coarse fragment content of 42% (weighted average). In reality, this pedon will

likely later be classified as an Andisol. Pedon OL is on a soil classified as a Dystric Haplustand (Olinda Series) and HALE is on a soil that was classified as a Humic Haplustand (Kaipoioi Series). Both sites are at similar elevations (similar MAT) but differ in MAP by over 1,000 mm. This difference presents an opportunity to look at a climosequence of two very young Andisols.

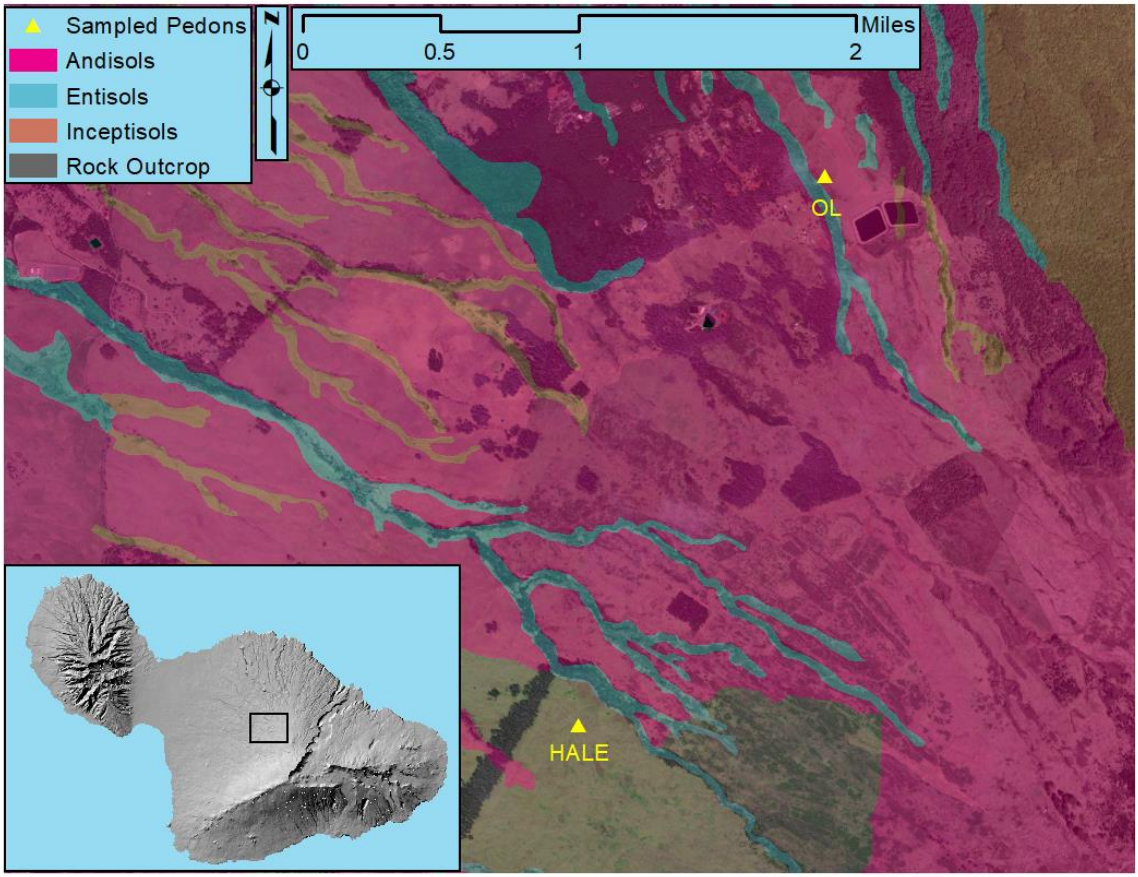

Figure A-3. Soil order map over an aerial image of pedon pair OL and HALE sample site locations.

RESULTS

Figures A-4 through A-6 provide a comparison of selected data with depth including pH (1:5), CEC by NH_4OAc (pH 7), organic carbon, P retention, CEC

[cmolc(+)/kg clay] (%), water retention at 1500 kPa (%), an estimate of SRO material (Al_{AO-PY}/Si_{AO}), crystalline iron (Fe_{CD-AO}) (%), and non-crystalline Al-oxides (Al_{AO-PY}) (%). The data summarized are between the small scale transects proposed and include sites KI-N2 vs. KI-S1 (Figure A-4), UKUL vs. LKUL (Figure A-5), and OL vs. HALE (Figure A-6). Maps of these site transects are provided in Figures A-1through A-3.

Pedons KI-N2 and KI-S1 were sampled in areas mapped as Torroxic Haplustolls (Waiakoa Series) and Typic Haplotorrands (Makena), respectively. Both pedons have the same weighted average clay content, yet KI-N2 receives higher MAP. Greater values in phosphate retention, SRO aluminosilicates, and Al (AO-PY) with depth for KI-N2 suggests early ash deposition in the genesis of these soils. This data, including the higher MAP of KI-N2, suggests it may be an older soil. Additionally, KI-S1 has nearly twice the volcanic glass content (22%) in the surface horizon than the surface horizon of KI-N2 (14%). Higher MAP and/or time are necessary for the formation of these SRO aluminosilicates from weathered ash deposits. Lower phosphate retention values and SRO aluminosilicates with depth of pedon 2 could also support the possibility that it is a rejuvenated landform of younger ash deposits where limited MAP and high evapotranspiration prevented the weathering of volcanic glass to allophane/imogolite. XRD analysis of these sites could support the relative older age of KI-N2 to KI-S1. This can also determine the presence of weathering products such as halloysite, indicating effects of increased weathering on an arid site receiving short, yet intense, seasonal rainfall, including the weathering trajectory of rejuvenated ash soils of leeward East Maui.

Pedons UKUL and LKUL (Figure A-5) were sampled in areas mapped as Typic Haplustand (Pane Series) and Aridic Haplustolls (Kamaole Series), respectively, with both sites having developed in volcanic ash over ʻaʻā lava, according to the NRCS. These sites are 0.72 miles apart and are at similar elevations, therefore, temperature and MAP are constrained, yet the majority of the soil properties of Figure A-5 are very different. LKUL has far less clay content (25%) compared to pedon 14 (76%) and generally has higher levels of phosphate retention, allophane, ferrihydrite, CEC, and OC with depth. Producing a complete picture with mineralogical data would help us understand what may have happened in the past at LKUL and if these differences are caused by an ash deposition event or more simply buried genetic horizons.

Pedons OL and HALE were sampled in areas mapped as Dystric Haplustands (Olinda Series) and Humic Haplustand (Kaipoioi Series), respectively. Like pedons UKUL and LKUL, elevation and temperature of both sites are very similar, therefore, these factors are constrained. This allows focus towards the effects of MAP and ash depositional events. First off, the bottom horizon of pedon OL (83-105 cm) seems to be a buried genetic horizon (Figure A-6). In this horizon, there is a substantial increase in OC, -1500 kPa water retention, allophane, and a slight increase in pH. Therefore, not only is this a buried horizon, but its parent material is dominated by volcanic ash. Generally, these soil properties demonstrate the effects of a wetter environment (pedon OL) on two andisols. Pedon HALE has a much higher concentration of base cations, CEC, pH, allophane, non-crystalline iron, and -1500 kPa water, yet lower organo-bound aluminum.

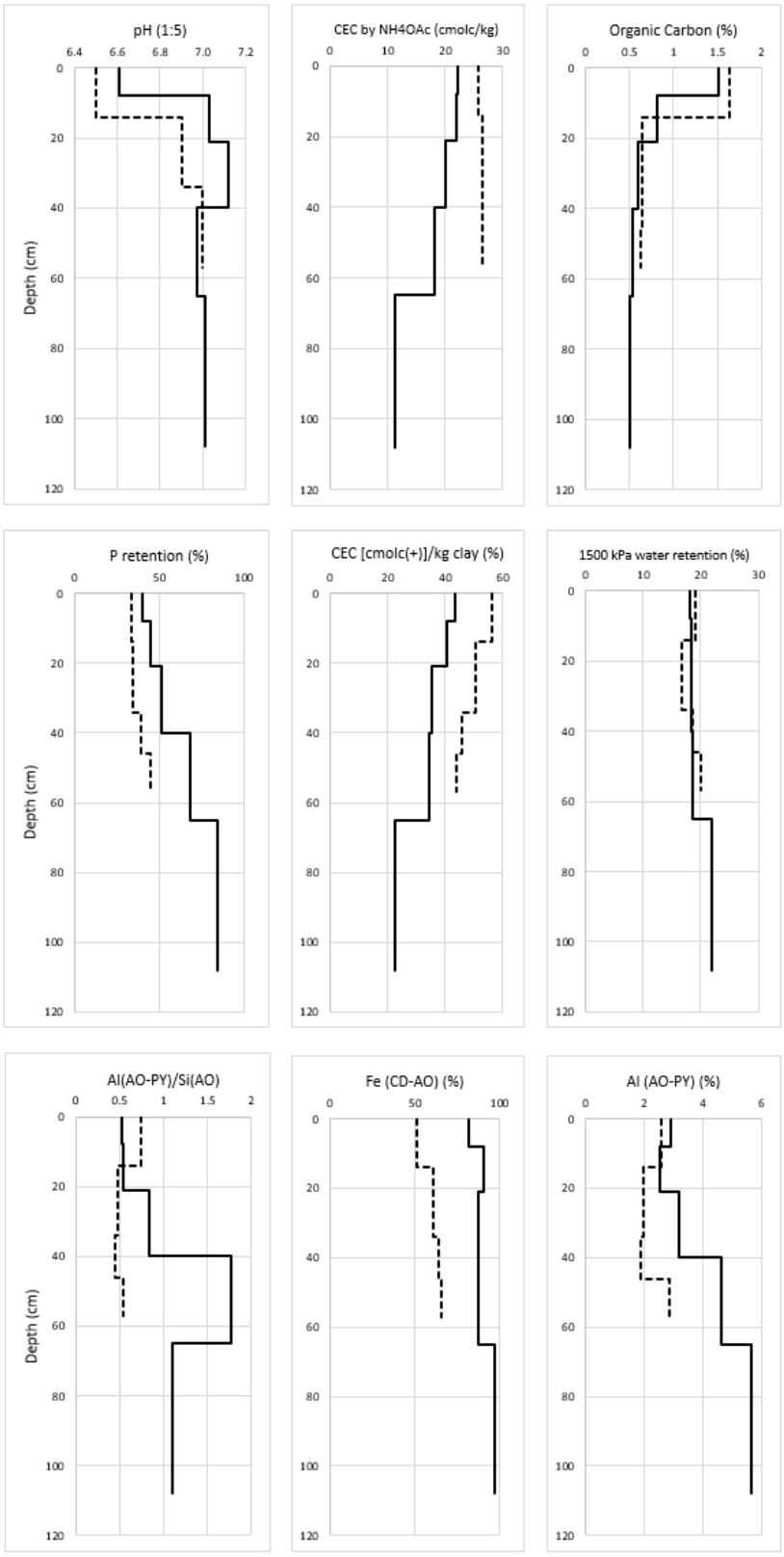

Figure A-4. Chemical, physical, and mineralogical comparisons between pedons KI-N2 (solid line) and KI-S1 (dashed line).

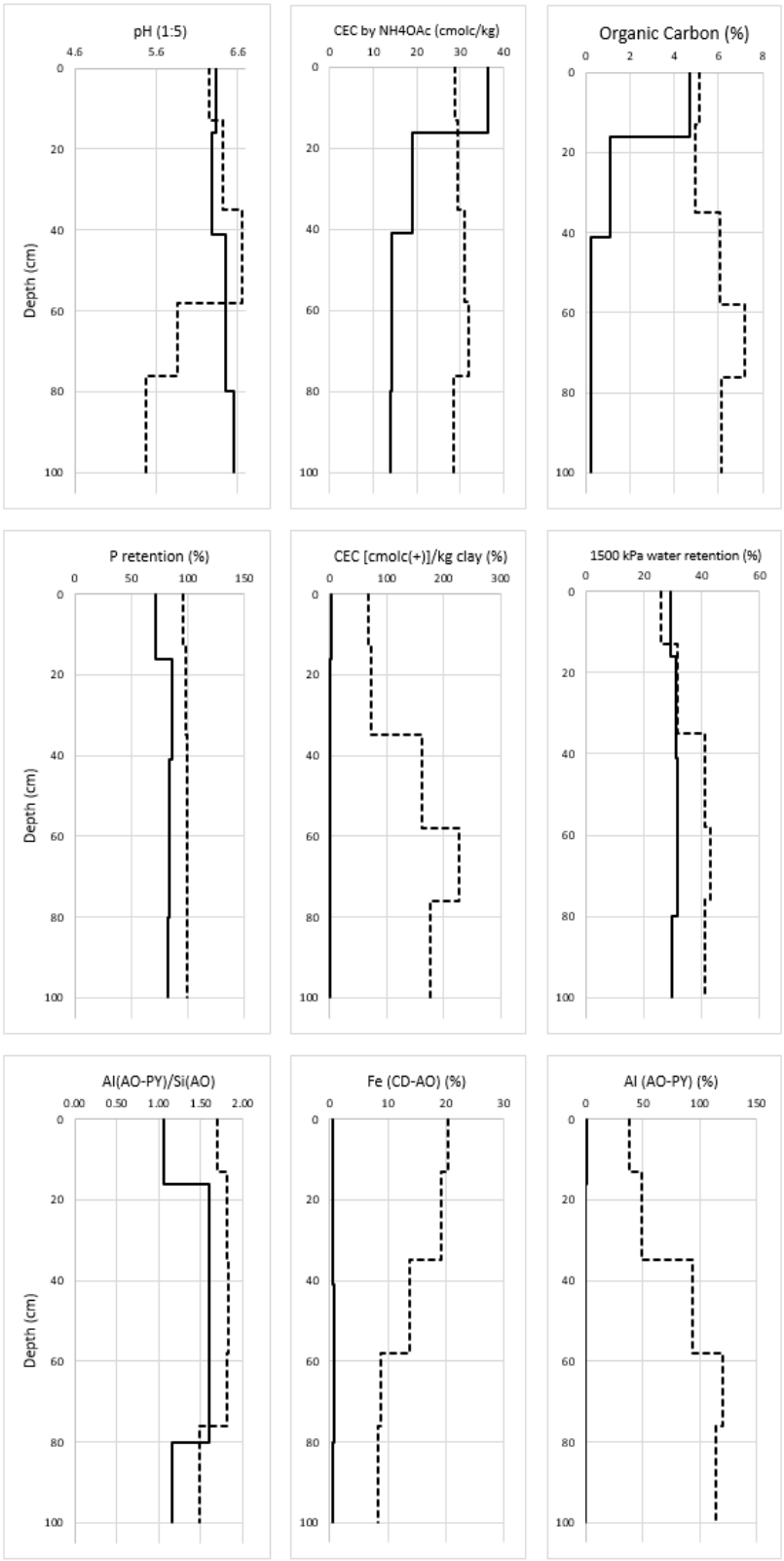

Figure A-5. Chemical, physical, and mineralogical comparisons between pedons UKUL (solid line) and LKUL (dashed line).

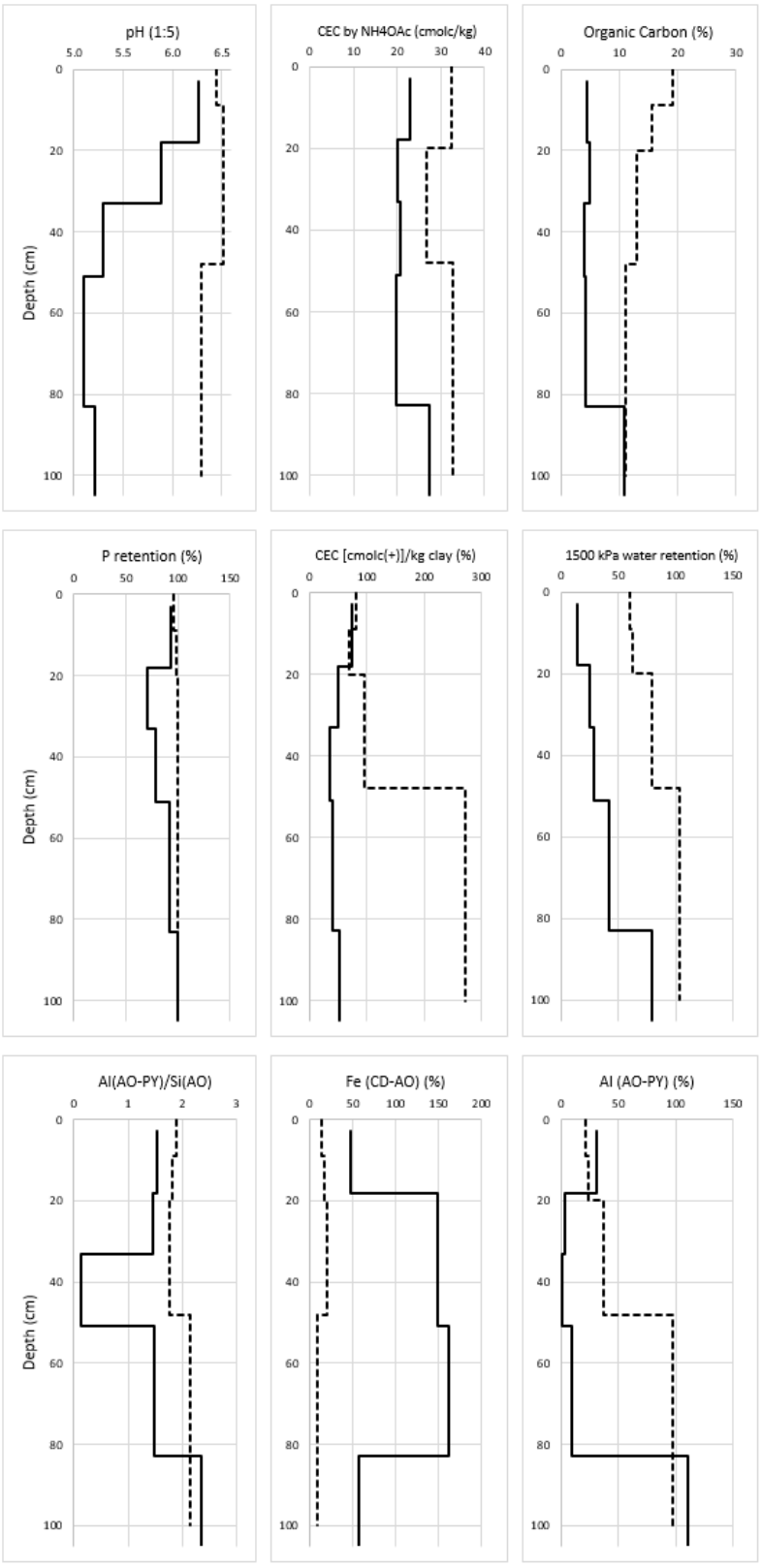

Figure A-6. Chemical, physical, and mineralogical comparisons between pedons OL (solid line) and HALE (dashed line).

Clay Mineralogy Data

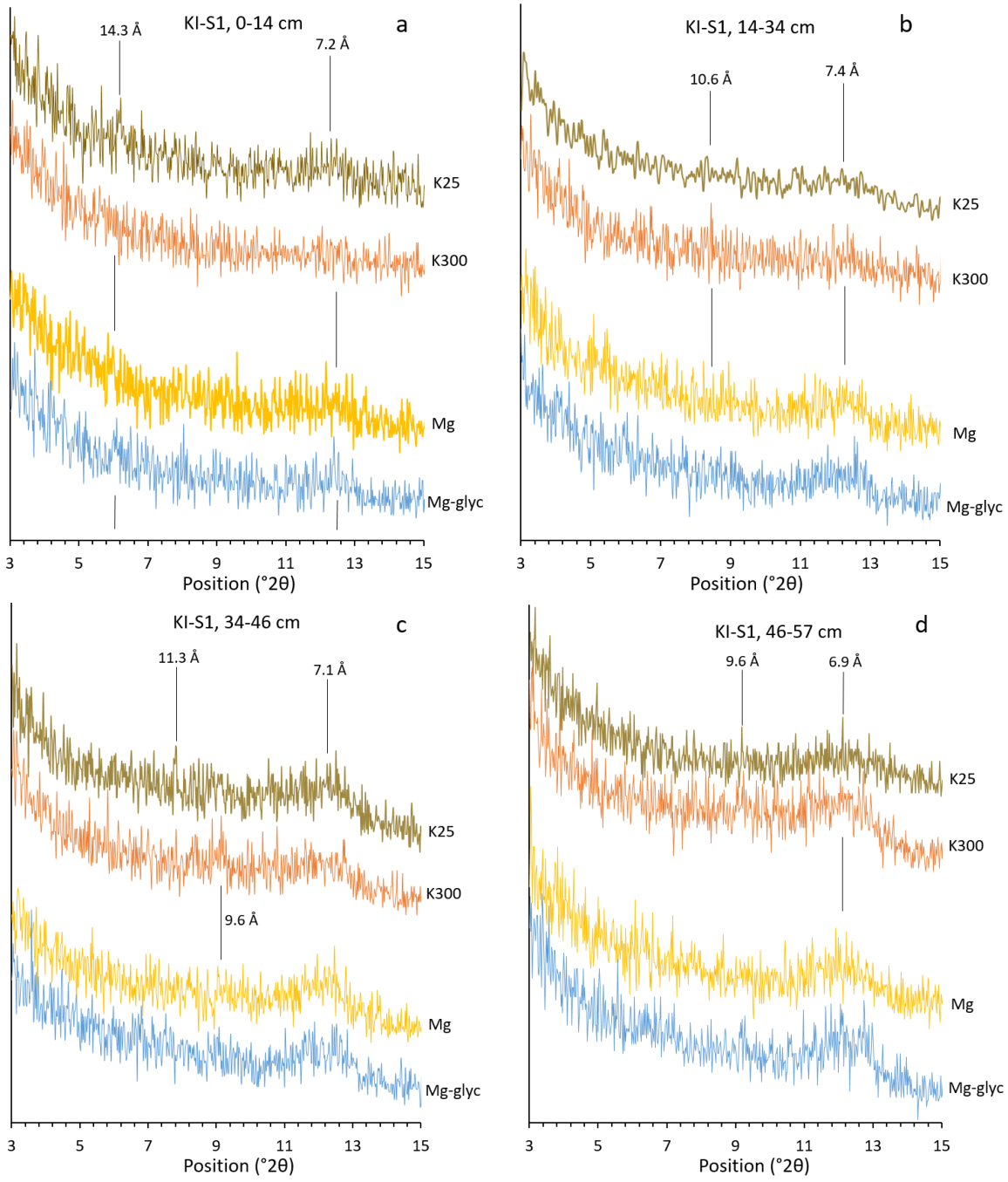

Figure A-7. X-Ray Diffractogram data for pedon KI-S1 by genetic horizon (a-d). Peaks are marked with d-spacing. Å, angstrom; K25, K saturated sample at 25 °C; K300, K saturated sample at 300 °C; Mg, Mg saturated sample; Mg-glyc, Mg saturated sampled treated with glycerin.

REFERENCES

Harris, W., & White, G.N. (2008). X-ray Diffraction Techniques for Soil Mineral Identification. *Methods of Soil Analysis, Part 5 – Mineralogical Methods*. Soil Science Society of America Journal, Madison. p 81.

Soil Survey Staff. (2000a). Official Series Description-Makena Series. USDA, NRCS. https://soilseries.sc.egov.usda.gov/OSD_Docs/M/MAKENA.html. (accessed Dec 16, 2020).

Soil Survey Staff. (2000b). Official Series Description-Kamaole Series. USDA, NRCS. https://soilseries.sc.egov.usda.gov/OSD_Docs/K/KAMAOLE.html. (accessed Dec 16, 2020).

Soil Survey Staff. (2014). *Keys to Soil Taxonomy, 12th Edition*. USDA, Natural Resources Conservation Service, Washington, DC.

CURRICULUM VITAE – RYAN C. HODGES

Phone: (808)304-0003 email: ryan.hodges@usu.edu

EDUCATION

Utah State University Logan, UT

Ph.D., Soil Science, (Expected NLT Aug 12, 2022)

- Dissertation Title: Soil Genesis Across a Climo-lithosequence of Western Haleakalā, Maui
- Advisor: Dr. Janis L. Boettinger
- Area of Study: Pedology, Digital Soil Mapping, Taxonomy

Graduate Certificate, Geographic Information Science, May 2021

M.S., Soil Science, March 2019

- Thesis Title: Phosphorus Rate Effects with and without AVAIL® on Dryland Winter Wheat in an Eroded Calcareous Soil
- Advisor: Dr. Grant E. Cardon
- Area of Study: Soil Fertility

University of Hawai‘i at Mānoa Honolulu, HI

B.S., Tropical Plant and Soil Sciences, Dec 2008

PROFESSIONAL EXPERIENCE

Graduate Research Assistant
Dept. of Plants, Soils, and Climate, USU Jan 2019 to present

- 0.5 FTE (20 hrs/week)
- **Doctoral research**
  - Developed and carried out research project from inception to completion.
  - Field work preplanning required site selection based on limiting various soil forming factors using GIS, and gaining access to desired sites by land owners and managers through outreach and networking—all done remotely. Required in-situ flexibility and adaptability for backup sampling sites when access to desired sites was not permitted.

- Field work included refining pedon location, manual excavation to 1 meter, describing site and soil characteristics/morphology by genetic horizon, and sampling by genetic horizon using standard methods.
- Laboratory experience:
  - Mineralogical: X-Ray Diffraction of the fine-earth clay fraction, glass count of the very fine sand fraction, and selective dissolution of the fine-earth fraction for organo-bound iron and aluminum (by sodium pyrophosphate), short-range order aluminosilicates and iron oxyhydroxides (by ammonium oxalate & by hydroxylamine hydrochloride hydrochloric acid), and free iron (by citrate-dithionite).
  - Physical: particle size analysis and sand fractionation, bulk density, -1500 kPa water retention
  - Chemical: total elemental analysis of soil and parent rock samples, total and inorganic carbon (for organic carbon), cation exchange capacity and base saturation (by barium chloride & by ammonium acetate), extractable aluminum (by 1N KCl), phosphate retention, pH, and electrical conductivity.
- Soil taxonomic classification and soil descriptions of research pedons using field and laboratory data.
- Used spatial statistics and modeling in the R programming language and ArcGIS to produce spatial predictions of soils of western Haleakala, Maui that classify as having andic properties.

- **Teaching Assistant**
  - Soils, Waters, and the Environment (PSC 2010)
    - Graded assignments and taught lectures as needed,
  - Soil Genesis, Morphology, and Classification (PSC 5130/6130).
    - Assisted with labs, maintained and dug soil pits, prepared field kits, graded assignments, and taught lectures as needed.
  - Lectures Taught:
    - PSC 5130/6130 (Nov 1, 2021) - Navigating and using Web Soil Survey
    - PSC 2010 (Apr 7, 2021) – Ion Exchange, Acid & Base Cations and Base Saturation, Specific Adsorption in Soil
    - PSC 2010 (Mar 3, 2021) – Soil texture
    - PSC 2010 (Feb 28, 2020) – Navigating and using Web Soil Survey
    - PSC 2010 (Feb 26, 2020) – Soil orders and classification
    - PSC 2010 (Feb 24, 2020) – Soil color, structure, and soil orders
    - PSC 5130/6130 (Oct 21, 2019) – Navigating and using Web Soil Survey
    - PSC 2010 (Feb 20, 2019) – Soil texture

Alaska and Arctic Soils Field Tour July 2021
University of Alaska Fairbanks

- Spent two weeks (56 hrs/week) examining cold region, permafrost-affected, and arctic soils and ecology of central Alaska—from Anchorage to Prudhoe Bay. We observed and studied 20 soils, all 8 soil orders of Alaska, and how they're affected by a changing climate, Matanuska glacier and its morphology, visited three research sites, a permafrost tunnel, Alyeska pipeline, patterned ground, sorted and unsorted polygons, and tundra rehabilitation.

Research Technician
Dept. of Plants, Soils, and Climate, USU Jan 2017 to Dec 2018

- 0.5 FTE (20 hrs/week)
- Assisted in laboratory and field research associated with soil fertility projects.
- Soil sampling to include hand tools and hydraulic sampling truck methods. Drying, grinding, and extraction for measuring pH, electrical conductivity, and other soil analyses.
- Operation of Skalar Soil Carbon Analyzer
- Soil and plant nitric acid digestion using the EPA3050 method for complete soil/plant elemental analyses

Laboratory/Field Technician Volunteer Sep 2016 to Dec 2016
Dept. of Tropical Plant and Soil Sciences, UH Mānoa

- 1.0 FTE (40 hrs/week)
- Sampled, processed, and analyzed soil samples from a Hawaiian Oxisol for nitrate content through the growing season of various vegetable crops.

Tactical Helicopter Aircrewman/Aviation Rescue Swimmer (AWR1/E-6)
US Navy Dec 2010 to Dec 2018

- Active Duty: 6 years, 1.0 FTE (40 hrs/week); Reserves: 2 years (4 hrs/week)
- Maintained proficiency and performed duties as a Sensor Operator, Utility Crewman, Search and Rescue Swimmer, and Aerial Door Gunner aboard the MH-60R Seahawk helicopter – 751 hours in airframe.
- Employed the aircraft's anti-submarine detection system, RADAR and Inverse Synthetic Aperture RADAR, Forward Looking Infrared (FLIR), onboard missile system, and Electronic Surveillance system.
- Assisted in vertical replenishment (VERTREP) between warships, ships in distress, and supply ships at sea, and also operated the personnel recovery hoist from the aircraft used for human rescues or in-flight refueling.
- Effected rescues at sea, and maintained the required training to do so at sea and on land.
- Deployed from OCT 2014 to MAY 2015 aboard the USS MICHAEL MURPHY Naval warship to South East Asia.

- **Search and Rescue Program Manager**
  Helicopter Maritime Strike Squadron 37, HI May 2015 to May 2016

  - Utilized time and personnel management to ensure 30 fellow Aircrewmen were proficient and qualified as Rescue Swimmers, including maintenance of all relevant records.
  - Organized and managed weekly pool training evolutions which included evaluation of swimmers and their satisfactory rescue techniques for their completion of quarterly, semi-annual, annual requirements, and helicopter-to-ocean jumps.
  - Training culminated to an annual evaluation of our organization conducted by pacific-wide evaluators. As program leader, our 2015 and 2016 evaluations resulted in "On Track" ratings.

Research Assistant
Trait Integration Department, Monsanto Co., Kunia, HI Jan 2009 to Dec 2010

- 1.0 FTE (40 hrs/week)
- Managed different field operations including planting, crossing, self-pollinating, data collection, and harvest of cross-breeding nurseries.
- Utilized research equipment such as planters and computers for in field record keeping and analysis.
- Provided guidance and support for day-to-day conversion nursery activities for post-harvest such as operation of shelling systems, seed counters, seed packaging, and shipping of hybrid testing materials.
- Assisted and contributed to safety training and guidance to field personnel.
- Trained new full-time crew and temporary employees in all the above.

Laboratory Assistant
Anthurium Breeding Program, UH Mānoa
Jan 2007 to Dec 2008

- 0.5 FTE (20 hrs/week)
- Micropropagated (tissue culture) advanced selections of anthurium for field-testing and evaluation with cooperators on the Big Island of Hawaii. Performed molecular analysis on transgenic anthuriums, including RNA extraction to understand transgene expression for bacterial resistance under different stress stimulus.

PROFESSIONAL PRESENTATIONS

Invited Presentations
NASA JSC "Mars Group" (Feb 9, 2022), title: *Soil genesis across a climo-lithosequence of western Haleakalā, Maui*

Volunteered Presentations

2021 SSSA conference poster presentation (Pedology division winner): *Predicting the Extent of Andic Soils Across Western Haleakalā, Maui*

2021 SSSA conference oral presentation (Pedology division): *Predicting the Extent of Andic Soils Across Western Haleakalā, Maui*

Spring 2021 PSC Department seminar oral presentation (05 Apr): *Soil chemical and physical variability across a climo-lithosequence of East Maui*

2020 SSSA conference poster presentation (Pedology division): *Soil chemical and physical variability across a climo-lithosequence of western Haleakalā, Maui*

2020 Western Region Cooperative Soil Survey rapid-fire presentation: *Soil genesis across a climo-lithosequence of western Haleakalā, Maui*

Fall 2019 PSC Department seminar oral presentation (02 Dec): *Soil genesis across a climo-lithosequence of western Haleakalā, Maui*

2019 (Oct) SSSA conference poster presentation (Pedology division): *Soil genesis across a climo-lithosequence of western Haleakalā, Maui*

2019 Western Nutrient Management Conference poster presentation and 2-minute rapid oral: *Phosphorus rate effects with and without AVAIL® on dryland winter wheat in an eroded calcareous soil.*

2019 (Jan) SSSA conference poster presentation (Soil Fertility division): *Phosphorus rate effects with and without AVAIL® on dryland winter wheat in an eroded calcareous soil.*

Spring 2018 PSC Seminar poster presentation on 19 Mar 2017 and oral presentation on 16 Apr 201: *Phosphorus rate effects with and without AVAIL® on dryland winter wheat in an eroded calcareous soil*.

Fall 2017 PSC Seminar poster presentation on 16 Oct 2017 and oral presentation on 11 Dec 2017 titled *Phosphorus rate effects with and without AVAIL® on dryland winter wheat in an eroded calcareous soil*.

PUBLICATIONS

Hodges, R.C. 2019. *Phosphorus rate effects with and without AVAIL® on dryland winter wheat in an eroded calcareous soil*. All Graduate Theses and Dissertations. 7461. http://digitalcommons.usu.edu/etd/7461.

Hodges, R.C., G.E. Cardon, and R. Clawson. 2017. *Soil Series: Elevation and Agricultural Soil Test Survey of the Godfrey Dryland Experimental Farm, Clarkston, Utah.* Utah State University. Available at: http://digitalcommons.usu.edu/cgi/viewcontent.cgi?article=2813&context=extension_curall.

3+ articles in production from doctoral research. Expected to publish summer/fall 2022.

AWARDS & ACHIEVEMENTS

National

- **Soil Science Society of America:** Pedology Division poster competition winner (2021), title: *Predicting the Extent of Andic Soils Across Western Haleakalā, Maui*
- **Federal:** Class of 2022 Presidential Management Fellow Finalist
- **METER Group:** Grant. A. Harris Award recipient, $10,000 in instrumentation (2020)

Utah State University

- Apogee Instruments/Campbell Scientific Fellowship (2010, 2020, 2021)
- Bastian Family Graduate Fellowship (2019, 2020)
- Robert N. Love Scholarship (2018, 2019, 2020, 2021)
- DeVere McAllister Scholarship (2018)

US Navy

- Navy and Marine Corps Commendation Medal (2016)
- Navy and Marine Corps Achievement Medal (2x) (2014, 2016)
- Helicopter Maritime Strike Squadron (HSM) 37 Aircrewman of the Year (2016)

Personal

- Private Pilot's License (Jan 2020) - 67 hours (Single-engine, fixed wing, land)
- IRONMAN World Championship 2005 finisher - youngest competitor (19 y.o.), time: 10hrs 13min.
- IRONMAN Lanzarote, Spain 2008 finisher - time: 13hrs 19min.
- Honu Half-IRONMAN finisher (2x) - Kona, HI (2005, 2006)
- Eagle Scout – Boy Scouts of America (2003)

LANGUAGES

Hawaiian – Beginner

- Born and raised in Hawaii. Self-taught.

Russian – Beginner/Intermediate
- Completed university Level 1 (two semesters; 2017/2018), and Level 2 (two semesters; 2018/2019)

Spanish – Beginner
- Middle school (2 years), high school (2 years)
- Completed 2 semesters at the university level

RELEVANT COURSEWORK

UH Mānoa (undergraduate)
- Tropical Crop Science
- Tropical Production Systems
- Plant Propagation
- Tissue Culture/Transformation

- Fundamentals of Soil Science
- Nutrient Management of Soils and Plants

- Statistics in Agriculture

Utah State University (graduate)
- Soil Chemistry
- Soil Genesis, Morphology, and Classification
- Soil Nutrient Management
- Soil Physics
- Soil Microbiology

- Design of Experiments (SAS)
- Modern Regression Methods (SAS)
- Applied Spatial Statistics (R)
- Introduction to R

- Geomorphology
- Geochemistry

- GIS for Natural Resources Applications (ArcGIS)
- Applied Remote Sensing (ArcGIS and Google Earth Engine)
- Advanced GIS and Spatial Statistics (ArcGIS)
- Geospatial Analysis (R)